Genetic divergence in two NOD^{k} mice strains with varied diabetes penetrance

Tenzin Dolma Dagpo

May 2021

A thesis submitted for the degree of Doctor of Philosophy of the

Australian National University

Statement of Originality

Bioinformatics analysis for the whole genome sequencing and RNA sequencing studies were performed by Dr. Zhi-Ping Feng, Mr Cameron Jack and Dr. Matt Field. With these exceptions, this declaration certifies that the following work is the author's original work and complies with the Australian National University Research Award Rules. It has not been previously accepted for award of a degree or diploma to any other university or institution of higher learning. The research presented in this thesis was supported by an Australian Government Research Training Program (RTP) scholarship.

Tenzin Dolma Dagpo

May 2021

Acknowledgements

I would first like to thank the Australian National University and the Australian government Research Training Program (RTP) scheme for awarding me a scholarship (the award formerly known as the Australian Postgraduate award: APA) throughout the course of my PhD program.

This project was a challenge from the beginning, since it ventured into the field of genetics and genome sequencing. This was new frontiers for our lab which has extensive expertise in cell biology and metabolism. However, the enthusiasm and optimism of Prof Chris Nolan to drive the project forward motivated me to continue and not give up. Not only did I benefit from his vast knowledge and expertise in this field, but was also able to work with a great team of geneticists, bioinformaticians, molecular biologists and embryologists obtain new perspectives and insights into the project. Thank you for always being supportive of new (expensive!) experiments for my project and for always encouraging me to present my work to my peers at national and international conferences.

My primary supervisor, Dr Viviane Delghingaro-Augusto has been my guide and mentor throughout my research life from my MPhil onwards. Everything I know about the lab has been under her tutelage. I have not only learned her values of perfectionism and quality research, but after 7 years I have unconsciously mirrored your dressing style and allergies. You have not only been an understanding and supportive supervisor, but also a great mentor and friend (I was going to say mom, but you are way too young). Thank you for feeding me with all the cakes over the years and for listening to my weird stories.

My research dream team: A/Prof Ruth Arkell who I was lucky to meet when I was lost in all the genetics of the project. Thank you for all your suggestions and for guiding me in the right direction. Dr Matt Field and Dr Dan Andrews for being the experts at untangling the web of genome sequence data that I had generated. Dr Zhi-Ping Feng, bioinformatician extraordinaire

and saviour who went above and beyond to help me make sense of my data. I am also grateful to Prof Jane Dahlstrom for her expert guidance with the histological analysis and advice for writing my thesis. I thank you all for being a part of my PhD project and always making time to see me to discuss my project.

My fellow PhD candidate Matt for lending your ears and being an understanding mate sailing on the same boat. Our past PhD student, now Dr Ainy Khan who worked very hard through her PhD, from which Matt and my PhD projects were borne. My lab neighbour from the Type 1 diabetes lab, also now Dr Sarita Dhounchak, who has always offered to listen and cheer me up whenever I looked down. Thank you for letting me eat all your Easter chocolates; as a fellow diabetes researcher, I appreciate it. I am also grateful to the animal technicians at the Australian Phenomics Facility and The Canberra Hospital (Ayumi, Ken, Dianna) for making sure our mice were happy and healthy. I have had one of the most fun but educational years with Dr Juliey Beckman and my fellow teaching associates at the Research school of Biology (RSB). Besides making me feel old, the undergrad students that I taught also made me see my project in a different light every time I explained it to them. A huge shout-out to all the senior exam invigilators I have worked with over the years. Thank you for always talking about my project like it was ground-breaking life-saving Nobel Prize-winning research.

Finally, I want to thank my friends and family for their support throughout these years. My PhD life would not have been the same if it were not for their love and friendship. I am lucky to have such a strong support network among my community, I have never felt like I was alone even though I was continents away from home. My family have been extremely supportive of my quest for research, and I was able to charge forward because I knew they always had my back no matter what. Last but not the least, eternal gratitude to His Holiness The Dalai Lama, for always encouraging us to pursue higher education. I hope I make you proud. This is for all of you.

Abstract

Diabetes mellitus is a chronic metabolic disorder characterized by persistent hyperglycaemia due to inadequate insulin secretion (β-cell dysfunction) and/or impaired insulin action (insulin resistance). While T1D is caused by autoimmune destruction of islet β-cells, islet β-cell dysfunction often with progressive decline in β-cell mass contributes to pathogenesis of T2D. Recent evidence of clinical convergence of T1D and T2D phenotypes in a proportion of people with diabetes suggests possible shared non-immune islet susceptibility factors.

The T1D-resistant O-NOD^{k} mouse sub-strain (created from the T1D-prone NOD mice through replacement of the Idd1-H2^{g7} with Idd-H2^{k}) develops impaired glucose tolerance, hyperinsulinaemia and T2D when fed a high fat (HF) diet. Through routine colony refreshment, our laboratory developed another sub-strain of NOD^{k} mice, the RF-NOD^{k} mice, which are resistant to HF diet-induced T2D. Since both O-NOD^{k} and RF-NOD^{k} mice colonies were maintained in the same animal facility under similar environmental conditions, we hypothesised that T2D predisposition in the O-NOD^{k} mice is of genetic origin. Thus, the aim of this project was to characterize the phenotype and genotype of both NOD^{k} mice sub-strains to determine the genetic factor(s) causing T2D susceptibility in O-NOD^{k} mice.

A long-term study (from 4-24 weeks of age) in these two mice sub-strains fed normal chow (NC) or HF diet monitored body weight, blood glucose and plasma insulin fortnightly and pancreatic histological alterations were evaluated at the end of the study. Assessments of β-cell function were performed *in vivo* and *in vitro* through intraperitoneal glucose tolerance tests (ipGTT) and isolated islet static insulin secretion, respectively. A cross-breeding study was designed to determine the allelic frequency and segregation of the diabetes susceptibility genetic factor(s) in the O-NOD^{k} mice. Whole genome sequencing (WGS) and RNA sequencing

(RNA-seq) were performed to identify genetic variants in the exome and transcriptomic profiles of these two mice sub-strains, respectively.

HF-fed O-NOD^{k} mice developed accelerated weight gain, impaired glucose tolerance, severe hyperinsulinaemia and T2D, whereas RF-NOD^{k} mice maintained normoglycaemia. Pancreas histological analysis revealed increased exocrine pancreas fat infiltration, mildly increased peri-ductal inflammation, and a similar mild peri-islet inflammation compared to RF-NOD^{k} mice. Reduced β-cell mass was observed in diabetic HF-fed O-NOD^{k} mice. *In vitro* studies revealed that pancreatic islets of HF-fed O-NOD^{k} mice secreted more insulin in response to glucose and fatty acids, and the insulin secretagogue IBMX. Cross-breeding studies showed that the diabetes trait in the O-NOD^{k} mice segregated as a simple Mendelian homozygous recessive trait. WGS identified 6 candidate genes with single nucleotide polymorphisms (*Atp13a3, Kcnh7, Gpr125, Ncor1, Myh4* and *Olfr954)* and over 1200 insertions and deletions in O-NOD^{k} mice only. RNA-seq highlighted the up-regulation of *Sdc2, Suclg2* and *Cbr3* genes, and down-regulation of *Pcp4* in O-NOD^{k} mice.

In conclusion, the phenotype of the diabetes-prone HF-fed O-NOD^{k} compared to diabetes resistant HF-fed RF-NOD^{k} mice, includes accelerated weight gain, severe hyperinsulinaemia, enhanced *in-vitro* insulin secretion, dysfunctional *in-vivo* insulin secretion and late loss of β-cell mass. Genetic studies suggest Mendelian homozygous recessive inheritance. Several candidate genes have been elucidated which warrant further validation and mechanistic studies.

Abbreviations

AATK	Apoptosis associated tyrosine kinase
ABCC8	ATP-binding cassette transporter sub family C member 8
AC	Adenylyl cyclase
ACRF	Australian Cancer Research Foundation
ADGRA3	Adhesion G protein-coupled receptor A3
ADP	Adenosine diphosphate
ANOVA	Analysis of variance
ANU	Australian National University
APC	Antigen presenting cells
ATF6	Activating transcription factor-6
ATGL	Adipose triglyceride lipase
ATP	Adenosine triphosphate
ATP13A3	ATPase type 13A3
AUC	Area under the curve
BAT	Brown adipose tissue
BGL	Blood glucose levels
BH	Benjamin-Hockberg
BIP	Binding immunoglobulin protein
BMI	Body mass index
BP	Base pairs
BRF	Biomolecular Resource Facility
BSA	Bovine serum albumin
BWA	Burrows-Wheeler Aligner
$CaCl_2$	Calcium Chloride
CaM	Calmodulin
CaMKII	Ca^{2+}-Calmodulin-dependent kinase II
cAMP	Cyclic adenosine monophosphate
CAPN10	Calpain-10
CAS9	CRISPR associated protein 9
CBR3	Carbonyl reductase 3
CDC	Centre for Disease Control and Prevention
CDKN2B	Cyclin dependent kinase inhibitor 2B

CFTR	Cystic fibrosis transmembrane conductance regulator
cGMP	Cyclic guanosine monophosphate
CHOP	C/EBP homologous protein
CPT-1	Carnitine palmitoyl transferase 1
CRISPR	Clustered regularly interspaced short palindromic repeats
CT	Computed tomography
CTLA4	Cytotoxic T-lymphocyte associated protein 4
CTS	Cataract Shionogi mouse
CUL4B	Cullin 4B
CV	Coefficient of variation
DAB	3,3'-Diaminobenzidine
DAG	Diacylglycerol
DAPL1	Death associated protein like 1
DAVID	Database for annotation, visualization and integrated discovery
dbSNP	Single nucleotide polymorphism database
DEG	Differential expressed gene
DEPP1	Decidual protein induced by progesterone autophagy regulator
DIO	Diet-induced obesity
EAG	Ether-a-go-go
EDTA	Ethylenediaminotetracetic acid
EPAC	Exchange protein directly activated by cAMP
ER	Endoplasmic reticulum
ERG3	Eag-related protein 3
FA	Fatty acids
FABP	Fatty acid binding protein
FAF1	Fas-associated factor 1
FBS	Fetal bovine serum
FDR	False discovery rates
FFA	Free fatty acids
FFAR1	Free fatty acid receptor 1
FOXO1	Forkhead box protein O1
FPG	Fasting plasma glucose
FPKM	Fragment Per Kilo-base Per Million

FRET	Fluorescence Resonance Energy Transfer
FYCO1	FYVE and coiled-coil domain autophagy adaptor 1
G-6-P	Glucose-6-phosphate
GAD	Glutamic acid decarboxylase
GATA3	GATA binding protein 3
GATK	Genome analysis tool kit
GDP	Guanosine-5'-Diphosphate
GIP	Glucose-dependent insulinotropic polypeptide
GK	Goto Kakizaki
GLP-1	Glucagon-like peptide-1
GLP-1R	Glucagon-like peptide-1 receptor
GLUT	Glucose transporter
Gly3P	Glycerol-3-phosphate
GO	Gene ontology
GPCR	G protein-coupled receptor
GPR125	G protein-coupled receptor 125
GSIS	Glucose stimulated insulin secretion
GTP	Guanosine-5'-Triphosphate
GUCY2C	Guanylate cyclase 2
GWAS	Genome-wide association studies
H_2O_2	Hydrogen peroxide
H&E	Haematoxylin & eosin
HBSS	Hanks Balanced Salt Solution
HDAC3	Histone deacetylase 3
HEB	Hugh Ennor building
HEL	Hen egg lysozyme
HEPES	4-*(2-hydroxyethyl)-1*-piperazineethanesulfonic acid
HF	High fat
HLA	Human leukocyte antigen
HNF1	Hepatic nucleotide factor 1
HO-1	Heme oxygenase 1
HOMA-IR	Homeostatic model assessment of insulin resistance
HSL	Hormone sensitive lipase

HSPG1	Heparan sulfate proteoglycan 1
HTRF	Homogeneous time resolved fluorescence
IAPP	Islet amyloid polypeptide
IBMX	3-isobutylmethylxanthine
IDD1	Insulin dependent diabetes locus 1
IDDM	Insulin dependent diabetes mellitus
IFI27	Interferon alpha inducible protein 27
IFN-γ	Interferon- gamma
IGT	Impaired glucose tolerance
IGV	Interactive genomics viewer
IHC	Immunohistochemistry
IL-22	Interleukin-22
IMTG	Intramuscular triglyceride
INDEL	Insertion deletion
iNOS	Inducible nitric oxide synthase
INS	Insulin
IP3	Inositol 1,4,5-triphosphate
ipGTT	Intraperitoneal glucose tolerance test
IR	Insulin resistance
IRE1-α	Inositol-requiring ER to nucleus signal kinase-1-alpha
IRS-1	Insulin receptor substrate 1
IVC	Individually ventilated cages
JCSMR	John Curtin School of Medical Research
JNK	Jun N-terminal kinase
K^+_{ATP}	ATP-sensitive K^+
KCl	Potassium Chloride
KCNH7	Potassium voltage-gated channel, subfamily H (eag-related), member 7
KCNJ11	Potassium inwardly rectifying channel subfamily J member 11
KEGG	Kyoto encyclopaedia of genes and genomes
KOH	Potassium Hydroxide
KRB	Krebs Ringer bicarbonate buffer
KRBH	KRB + HEPES
LC-CoA	Long chain acyl-coenzyme A

Lep	Leptin
Lepr	Leptin receptor
LoD	Limit of detection
Log FC	Log fold change
MafA	V-maf musculoaponeurotic fibrosarcoma oncogene homolog A
MAPK	Mitogen-activated protein kinase
MCF	Metabolic coupling factor
MCP-1	Monocyte chemoattractant protein 1
MDS	Multidimensional scaling
MetS	Metabolic syndrome
$MgCl_2$	Magnesium Chloride
MGP	Matrix Gla protein
$MgSO_4$	Magnesium Sulphate
MHC	Major histocompatibility complex
MIP-1α	Macrophage inflammatory protein-1α
MODY	Maturity onset diabetes of the young
MSigDB	Molecular signatures database
MTF1	Metal regulatory transcription factor 1
mTORC1	Mammalian target of rapamycin complex 1
MYH4	Myosin heavy polypeptide 4, skeletal muscle
NaCl	Sodium chloride
NAD	Nicotinamide adenine dinucleotide
NAFLD	Non-alcoholic fatty liver disease
NAFPD	Non-alcoholic fatty pancreas disease
NaH_2PO_4	Sodium phosphate
$NaHCO_3$	Sodium bicarbonate
NASH	Non-alcoholic steatohepatitis
NC	Normal chow
NCOR1	Nuclear receptor co-repressor 1
NEFA	Non-esterified fatty acids
NeuroD1	Neurogenic differentiation-1
NF-κB	Nuclear factor kappa-light-chain-enhancer of activated B cells
NGS	Next generation sequencing

NHMRC	National Health and Medical Research Council
NLRP3	NOD-, LRR- and pyrin domain-containing-3
NO	Nitric oxide
NOD	Non-obese diabetic
NRF2	Nuclear factor-erythroid 2 related factor 2
NZO	New Zealand Obese
OA	Oxaloacetate
OGTT	Oral glucose tolerance test
OLFR954	Olfactory receptor 954
O-NOD^{k}	Original NOD^{k} mice
P2RX4	P2X purinoreceptor 4
PAH	Pulmonary arterial hypertension
PAX	Paired box
PBS	Phosphate buffer solution
PC2	Prohormone convertase 2
PCA	Principal component analysis
PCP	Planar cell polarity
PCP4	Purkinje cell protein 4
PCP4L1	Pcp4-like protein 1
PCR	Polymerase chain reaction
PDE	Phosphodiesterase
PDX-1	Pancreatic and duodenal homeobox-1
PEG	Polyethylene glycol
PEP19	Polypeptide 19
PERK	Protein kinase RNA-like ER kinase
PI3K	Phosphatidylinositide-3-kinase
PIANP	PILR alpha associated neural protein
PILRA	Paired immunoglobulin-like type 2 receptor alpha
PKA	Protein kinase A
PL	Phospholipid
POLR2D	DNA-directed RNA polymerase II subunit RPB4
PP	Pancreatic polypeptide
PPAR-γ	Peroxisome proliferator-activated receptor-gamma

PPP4R3B	Serine/threonine-protein phosphatase 4 regulatory subunit 3B
Rap1	Ras-related protein 1
RF-NOD^{k}	Refreshed NOD^{k} mice
RGB	Red green blue
RIA	Radioimmunoassay
RIN	RNA integrity number
RNA-seq	Ribonucleic acid (RNA) sequencing
RNS	Reactive nitrogen species
ROI	Region of interest
ROS	Reactive oxygen species
RPMI	Roswell Park Memorial Institute
RPS6KA2	Ribosomal Protein S6 Kinase A2
RRP	Readily releasable pool
RSPH3B	RNA Polymerase II, radial spoke head protein 3 homolog B
SAT	Subcutaneous adipose tissue
SCGN	Secretagogin
SDC2	Syndecan 2
SDS	Sodium dodecyl sulfate
SEM	Standard error of the mean
SIFT	Sorts Intolerant from Tolerant
SLC2A2	Solute carrier family 2 member 2
SLC30A8	Solute carrier family 30 member 8
SNAP-25	Synaptosome-associated protein 25
SNARE	Soluble N-ethylmaleimide sensitive factor attachment protein receptor
SNP	Single nucleotide polymorphisms
SNV	Single nucleotide variants
SPSS	Statistical package of the social sciences
SRP	Signal recognition particles
STIM1	Stromal interaction molecule 1
SUCLG2	Succinate-CoA ligase GDP-forming subunit beta
T1D	Type 1 diabetes
T2D	Type 2 diabetes
TAAR1	Trace amine-associated receptor-1

T-bet	T box transcription factor
TCF7L2	Transcription factor 7-like 2
TCH	The Canberra Hospital
TG	Triacylglycerol
TIC	Total insulin content
TLR	Toll-like receptor
TMB	3,3',5,5'-Tetramethylbenzidine
TMM	Trimmed mean of M values
TNF-α	Tumour necrosis factor- alpha
TRIB3	Tribbles homolog 3
UCLA	University of California at Los Angeles
UCP2	Uncoupling protein 2
UPR	Unfolded protein response
VAT	Visceral adipose tissue
VLDL	Very low density lipoprotein
WAT	White adipose tissue
WGS	Whole genome sequencing
Wnt	Wingless-related integration site
ZRANB3	Zinc finger RANBP2-type containing 3

Table of contents

Chapter 1

Introduction

1. Introduction

The history of diabetes dates back to 1500 BC where Egyptian manuscripts described it as a disease of excessive urination (Lakhtakia, 2013). Araetus of Cappodocia coined the term "diabetes" (Greek: to pass through) to describe this disorder in 81-133 AD, while the term "mellitus" (Latin: sweet like honey) was coined by John Rollo in 1798, post-observation of the sweet taste of urine of people with diabetes (Lakhtakia, 2013). However, its experimental characterization began in 1889 when von Mering and Minkowski discovered that the removal of the pancreas in dogs led to diabetes (von Mering and Minkowski, 1890). Later, Banting, Best and Collip established insulin deficiency as the cause of diabetes in 1921 (Banting et al., 1922).

Diabetes mellitus is defined as a complex disease encompassing multiple metabolic disorders associated with disturbances in glucose homeostasis. The hallmark characteristic of diabetes mellitus is hyperglycaemia caused by defects in insulin secretion and/or insulin action on peripheral tissues (insulin resistance), leading to altered fuel metabolism (American Diabetes, 2011). Initial symptoms of diabetes mellitus include polyuria, polydipsia and polyphagia. Inability to maintain blood glucose levels at normal physiological range, leads to spilling of glucose into the urine (glycosuria), stimulating excretion of extra water in urine by the kidney for osmoregulation (Ahloulay et al., 1999). The consequent loss of water and calories through polyuria creates excessive thirst and weight loss, leading to increased hunger (Hernandez and Briese, 1972).

Hyperglycaemia also reduces vasodilator nitric oxide levels in blood vessels, thereby causing hypertension and promoting vasoconstriction (Hoshiyama et al., 2003). This restricts blood flow to peripheral tissues and can cause long-term complications and even organ failure. Diabetes-induced blood flow restriction to the brain and heart can potentially cause strokes and heart attacks, respectively (Aziz et al., 2019, Einarson et al., 2018). Similarly, it can also cause

retinopathy (Jackson et al., 2012), nephropathy and peripheral neuropathy, which can progress to blindness, chronic kidney disease, foot ulcers and limb amputation, respectively (Juster-Switlyk and Smith, 2016, Jackson et al., 2012, Schrier et al., 2002). Diabetes also affects the immune cells, causing slower wound healing and increasing susceptibility to bacterial and fungal infections (Muller et al., 2005, Geerlings and Hoepelman, 1999).

The current criteria for the diagnosis of diabetes is based on the 8 hours fasting plasma glucose (FPG) levels, or the 2-hours plasma glucose levels obtained after a 75 gram oral glucose tolerance test (OGTT), or a glycated haemoglobulin (HbA_1C) test, which indicates glycaemic trends over 2 months (Table 1) (World Health Organization, 2019, International Diabetes Federation, 2017, Bunn et al., 1976). Individuals diagnosed with prediabetes have impaired fasting blood glucose levels or impaired glucose tolerance, and are at risk to develop diabetes. These criteria are used to diagnose the two major types of diabetes mellitus: Type 1 diabetes (T1D) and Type 2 diabetes (T2D).

Table 1: Criteria for diagnosis of diabetes and pre-diabetes as per the International Diabetes Federation and World Health Organization guidelines.

Diagnostic tests	Diabetes	Prediabetes
8 hours fasted plasma glucose	≥ 7 mmol	6.1 – 6.9 mmol
OGTT 2 hours plasma glucose	≥ 11.1 mmol	7.8- 11.0 mmol
HbA_1c	≥ 6.5%	5.7- 6.4%

1.1 Type 1 diabetes (T1D)

T1D, formerly known as insulin-dependent diabetes mellitus, is a chronic autoimmune disorder caused by the immune destruction of insulin-secreting pancreatic β-cells, resulting in absolute insulin deficiency and subsequent dependence on exogenous insulin (Atkinson et al., 2014).

T1D accounts for 5-10% of all diabetes mellitus cases, and is commonly diagnosed in children and adolescents (American Diabetes, 2011), with 1.1 million adolescents below 20 years of age diagnosed globally (International Diabetes Federation, 2019). However, diagnosis of T1D at an older age has also been documented (Thunander et al., 2008). Its incidence is globally variable, with Finland and Sardinia displaying the highest incidence, while countries like China, India and Venezuela having the lowest incidence (Karvonen et al., 2000). This suggests that variation in T1D incidence may be attributed not only to inherited genetic predisposition factors, but may also be influenced by environmental risk factors. Experimental studies have suggested that viral infections, vitamin D deficiency and exposure to gluten or cow's milk during infancy and childhood may trigger T1D, although the latter is still under investigation (Knip et al., 2010, Stene et al., 2010). Nonetheless, genetics plays a major role in T1D risk.

T1D is a heritable polygenic disorder with multiple genes associated with disease development, the most important being the human leukocyte antigen (HLA) region on chromosome 6 (IDDM1 locus), particularly HLA Class II, which provides around 50% of the genetic susceptibility (Noble et al., 2010, Erlich et al., 2008). T1D has strong familial clustering, 40% of which is attributed to allelic variations in the HLA Class II alleles DR3, DR4 and DQ8 regions (Concannon et al., 2005). However, various non-HLA regions have also been associated with T1D risk such as the insulin (*INS*) and cytotoxic T-lymphocyte associated protein 4 (*CTLA4*) genes (Concannon et al., 2009). Nevertheless, most loci with linkages to T1D are involved with immune response (Nyaga et al., 2018).

T1D pathogenesis is accompanied by antibody and T-cell immune responses to antigens in the β-cells, with T-cell mediated effects being most important (Figure 1). Although the triggering mechanisms have not yet been established, autoantibodies against pancreatic islet antigens such as insulin, glutamic acid decarboxylase (GAD), zinc transport 8 or insulinoma associated antigen 2 have been identified in association with T1D (Kimpimaki et al., 2001, Steck et al., 2011, Rewers and Ludvigsson, 2016, von Herrath et al., 2007). Activation of naïve CD4+ T-cells resident in secondary lymphoid organs leads to differentiation into effector helper T-cells (Th1 or Th2) under the expression of transcription factors *T-bet* and *GATA3*, and secretion of pro-inflammatory cytokines (Kanhere et al., 2012). Concurrently, activation of CD8+ T-cells and subsequent differentiation into Th cells can also cause β-cell apoptosis (Trivedi et al., 2016, Dudek et al., 2006). Furthermore, both T-cells stimulate B-cell production, activating islet-resident M1 macrophages and causing insulitis and β-cell destruction, leading to loss of insulin secretory action (Arif et al., 2004). Deletion of T-cells, *T-bet* or B-cells in mice, all led to T1D-resistance and abrogation of insulitis (Mora et al., 1999, Zhang et al., 2019, Noorchashm et al., 1997, Esensten et al., 2009).

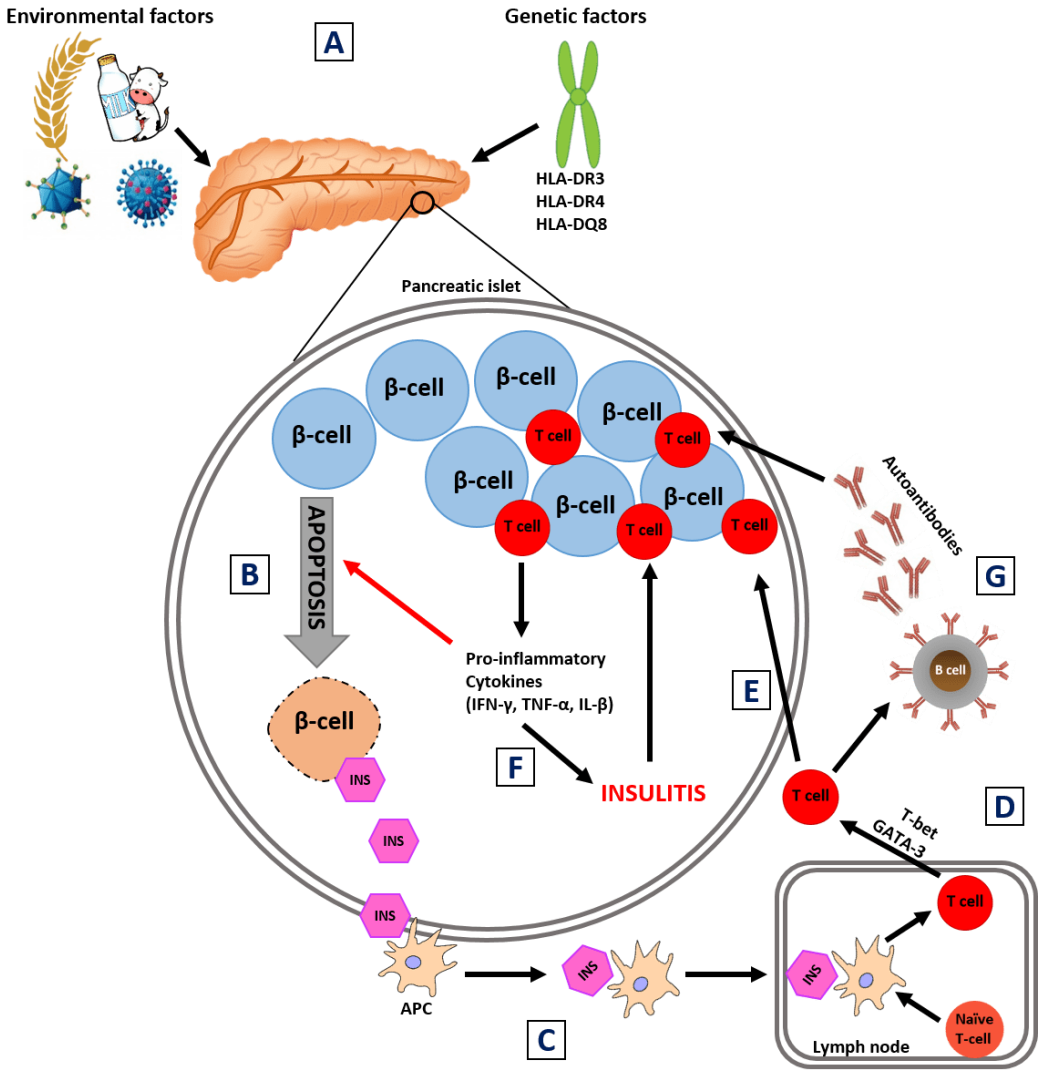

Figure 1: Schematic representation of the pathophysiology of autoimmune Type 1 diabetes (T1D). T1D can be caused by environmental factors such as gluten and cow's milk exposure during infancy and enteroviral infections, and genetic factors like HLA alleles (A). These factors can trigger β-cell apoptosis, leading to release of β-cell antigens (eg insulin) (B). Insulin induces APC, promoting activation of naïve T-cells in lymph nodes into mature T-cells (C). *T-bet* and *GATA3* promote differentiation of T-cells into effector T-cells (D), which migrate into the islets (E) and secrete pro-inflammatory cytokines, further aggravating apoptosis and insulitis (F). T-cells also induce mature B-cells to produce autoantibodies which exacerbate inflammation in the pancreas (G). HLA: Human leukocyte antigen, APC: Antigen presenting cells, *T-bet*: T box transcription factor, *GATA3*: GATA binding protein 3, TNF-α: Tumor necrosis factor- alpha, IFN-γ: Interferon- gamma, INS: Insulin. [Adapted from (Lazo-de-la-Vega-Monroy and Fernandez-Mejia, 2011)].

1.2 Type 2 diabetes (T2D)

T2D, formerly known as non-insulin dependent or adult-onset diabetes mellitus, accounts for over 90% of all diabetic cases (Bruno et al., 2005). Globally, there are around 463 million adults (20-79 years of age) living with diabetes, of which 75% of the cases occur in low and middle-income countries, with China and India as the epicenters for this growing health epidemic (International Diabetes Federation, 2019, Shaw et al., 2010). The number of individuals with diabetes is still rising and it is estimated that by 2045, there will be 700 million people living with diabetes worldwide (Williams et al., 2020). The prevalence of T2D also varies between ethnicities and race. According to the Center for Disease Control and Prevention (CDC) in the USA, Native Indian/Alaskan Natives have the highest prevalence of T2D (15.1%), followed by African (12.7%), Hispanic (12.1%) and Asian (8.0%) Americans with Caucasian-Americans having the lowest prevalence (7.4%). Pacific Nations also show high diabetes prevalence, with over 30% prevalence in American Samoa and 25% in the Polynesian and Micronesian islands (NCD Risk Factor Collaboration, 2016).

1.2.1 Diabetes in Australia

Australia has the 7th highest prevalence of diabetes mellitus in the world, with over 1.2 million diabetic adults above 20 years of age (5.6% of the population) (International Diabetes Federation, 2019). Indigenous Australians are 3 times more likely to develop T2D than non-indigenous Australians (Minges et al., 2011). Additionally, the annual health cost burden for T2D and its associated complications was estimated to be $14.6 billion in 2013 (Lee et al., 2013). The escalating diabetes prevalence and related economic costs highlight the imperative need to expand our knowledge about T2D aetiology, and to implement better healthcare policies to counteract the impact of this growing diabetes epidemic.

1.2.2 Aetiology of T2D

T2D is a heterogeneous multifactorial disorder, resulting from the pathogenic interaction of environmental and genetic risk factors.

1.2.2.1 Environmental risk factors for T2D

Obesity is identified as a primary risk factor for the development of T2D, since 90% of individuals with T2D are either obese or overweight (World Health Organization, 2017). Several environmental factors such as an unhealthy energy-dense diets and physical inactivity due to sedentary lifestyles, are associated with the development of obesity and increased risk of T2D (Bellou et al., 2018).

A strong association between T2D and consumption of soft drinks containing high fructose corn syrup and red meat has been reported by many studies (Nseir et al., 2010, Panagiotakos et al., 2005, Neuenschwander et al., 2019). Similarly, increased saturated fat intake have been linked to obesity and T2D (Thanopoulou et al., 2003, van Dam et al., 2002). In contrast, the Mediterranean diet which is rich in polyunsaturated fats and is a good source of macronutrients, was found to be inversely correlated to T2D (Naja et al., 2012, Beigrezaei et al., 2019, Salas-Salvadó et al., 2015). Therefore, changes towards a healthy dietary pattern (i.e. consumption of diets low in added sugars, high in fiber and low in saturated fat content) can have a beneficial effect in reducing T2D risk and weight loss.

Additionally, adoption of healthy eating associated with regular physical activity have been shown to reduce or delay the risk and incidence of T2D in individuals at risk (Hemmingsen et al., 2017). An hour of sedentary TV watching was found to increase T2D risk by 3.4% (Rockette-Wagner et al., 2015). Re-allocation of even 30 mins of sedentary time to light-intensity physical activity improved insulin sensitivity by 5%, while assigning that time for

moderate to vigorous intensity physical exercise caused a 15% change in homeostatic model assessment of insulin resistance (HOMA-IR) (Yates et al., 2015). Collectively, these studies allude to the impact of diet and physical activity on the risk of T2D, and how targeted interactions of these two factors can have a positive influence to reduce T2D susceptibility.

1.2.2.2 Genetic risk factors for T2D

Although T2D development is heavily influenced by lifestyle factors, genetic susceptibility also plays a role in the pathogenesis of the disease. Population studies have shown that offspring of one diabetic parent had a 3.5-fold higher risk, and offspring of both parents with T2D had a 6-fold higher risk of developing T2D, compared to offspring with no diabetic parents (Meigs et al., 2000). Offspring with maternal diabetic history were observed to have higher T2D risk and higher birth weight, compared to a paternal diabetic history (Meigs et al., 2000, Lauenborg et al., 2011). Another study of nearly 35,000 twin pairs from various countries in Europe and Australia, reported a lower T2D discordance rate of 5.1% among monozygotic twins compared to same-sex dizygotic twins (8%), with heritability estimated at 72% (Willemsen et al., 2015). While these studies show the heritability of T2D from parent to offspring, no dominant locus for T2D susceptibility has been identified. Therefore, T2D is recognized as a polygenic disorder associated with small gene effects of variants of multiple genetic loci, instead of a large single gene effect.

One of the earliest methods of studying the polygenic nature of T2D involved the analysis of candidate genes with known functions and association with T2D. These studies identified various single nucleotide polymorphisms (SNPs), including the peroxisome proliferator-activated receptor-γ (*PPARγ*) Pro12Ala polymorphism, which was associated with reduced T2D risk in Caucasians, but not in South Indian or Iranian population (Altshuler et al., 2000,

Radha et al., 2006, Mirzaei et al., 2009). Additionally, studies on Turkish and UK populations linked variants in ATP-binding cassette transporter sub family C member 8 (*ABCC8*) and potassium inwardly rectifying channel subfamily J member 11 (*KCNJ11*) to increased T2D risk (Gloyn et al., 2003, Gonen et al., 2012). Other studies have also reported polymorphisms that confer T2D risk in fatty acid binding protein (FABP) 2 and 6, hepatic nucleotide factor 1 (HNF1) homeobox, cyclin dependent kinase inhibitor 2B (CDKN2B) and solute carrier family 30 member 8 (SLC30A8) genes (Fisher et al., 2007, Nikitin et al., 2017, Daimon et al., 2003).

Another approach used to study the genetics of T2D includes linkage analysis, a technique that searches for genetic markers that are inherited together due to their close proximity to each other on the same chromosome. The use of this technique resulted in the discovery of various prospective variants associated with T2D risk on the loci of chromosomes 4, 10, 14 and 16 (Guan et al., 2008). However, this technique could only link few genes to T2D pathogenesis, such as calpain-10 (*CAPN10*), adiponectin and transcription factor 7-like 2 (*TCF7L2*) (Nam et al., 2018, Cropano et al., 2017).

The arrival of genome-wide association studies (GWAS) in the 2000s prompted a great breakthrough in the study of the genetic determinants of diabetes due to its capacity to rapidly scan the entire genome to find SNPs that commonly occur in individuals with T2D, without any prior hypothesis or knowledge of gene function. A recent meta-analysis of GWAS involving over 60,000 T2D cases and 0.5 million controls combined from 3 GWAS sets in Europe (DIAGRAM, GERA and UKB), identified 139 variants already known to be associated with T2D, of which 16 were linked to insulin secretion and 25 to insulin sensitivity (Xue et al., 2018). Additionally, this study also led to the discovery of another 39 novel variants that had not been associated with T2D. Overall, the most significant T2D susceptibility-associated locus reported was the previously known rs7903146 of the *TCF7L2* gene, which is a transcription factor

involved in the wingless-related integration site (Wnt) signaling pathway (Xue et al., 2018). GWAS was also performed in different populations such as the Northern Han Chinese, Moroccan and Tunisian and the sub-Saharan population, which identified even more novel variants associated with T2D risk such as the rs17106184 allele of the Fas-associated factor 1 (*FAF1*) gene and zinc finger RANBP2-type containing 3 (*ZRANB3*) gene, which were not reported in the European GWAS gene sets (Cauchi et al., 2012, Rao et al., 2016, Adeyemo et al., 2019). This highlighted the need to perform trans-ethnic GWAS across different ancestries to identify more alleles associated with T2D risk (Mahajan et al., 2014).

Furthermore, with the technological advancements in gene engineering and the lower costs of high throughput sequencing, many novel loci formerly unknown to be associated with T2D are being discovered through whole genome and exome sequencing. This brings further insights into the pathogenesis of T2D and potential for prospective novel therapies. The mechanisms by which these novel genes contribute to the pathophysiology of T2D can be further investigated through genetic manipulation of rodent models to generate knockout or transgenic mice for candidate genes.

Therefore, for better understanding of the pathophysiological alterations that occur in T2D and their association to common genomic variants, it is first necessary to understand the normal metabolic physiology involved in the maintenance of glucose homeostasis.

1.3 Pancreas architecture and β-cell biology

The pancreas is a complex organ located in the upper abdominal area below the stomach. Anatomically, it can be divided in 3 parts: the widest section is called the head which lies within the C-curve of the duodenum, the middle body extends laterally overlying the abdominal aorta, followed by the narrow tail extending towards the spleen (Longnecker, 2014) (Figure 2A). In mice, these three sections are known as the duodenal, gastric and splenic lobes, and are not as distinct due to their distribution around the proximal small intestine (Dolenšek et al., 2015).

The pancreas is a dual-functioning organ with both exocrine and endocrine features. The exocrine pancreas corresponds to 98% of the total pancreatic tissue, and is composed of grape-like clusters of exocrine cells called acini and duct cells (Takahashi, 1984). These acinar cells secrete digestive enzymes (trypsin, amylase and lipase) and electrolytes through the pancreatic duct into the duodenum, to aid digestion (Husain and Thrower, 2009). In contrast, the endocrine component populates only 2% of the entire pancreatic mass, and constitutes small clusters of endocrine cells called islets of Langerhans (Figure 2A) (Haist, 1971).

Although islet number differs between species (between 1-15 million in humans and 1000-5000 in mice), the average islet size is relatively similar among mammals (100-200 μm in diameter) (Saito et al., 1978, Bock et al., 2005, Kim et al., 2009a, Pfeifer et al., 2015). Human and rodent studies have both shown that pancreatic islet area and size increase with maturation, but then decline with aging, without change in total islet number (Kehm et al., 2018, Mizukami et al., 2014). This could be due to a decline in the proliferative and regenerative capacity of the islets with age (Kehm et al., 2018).

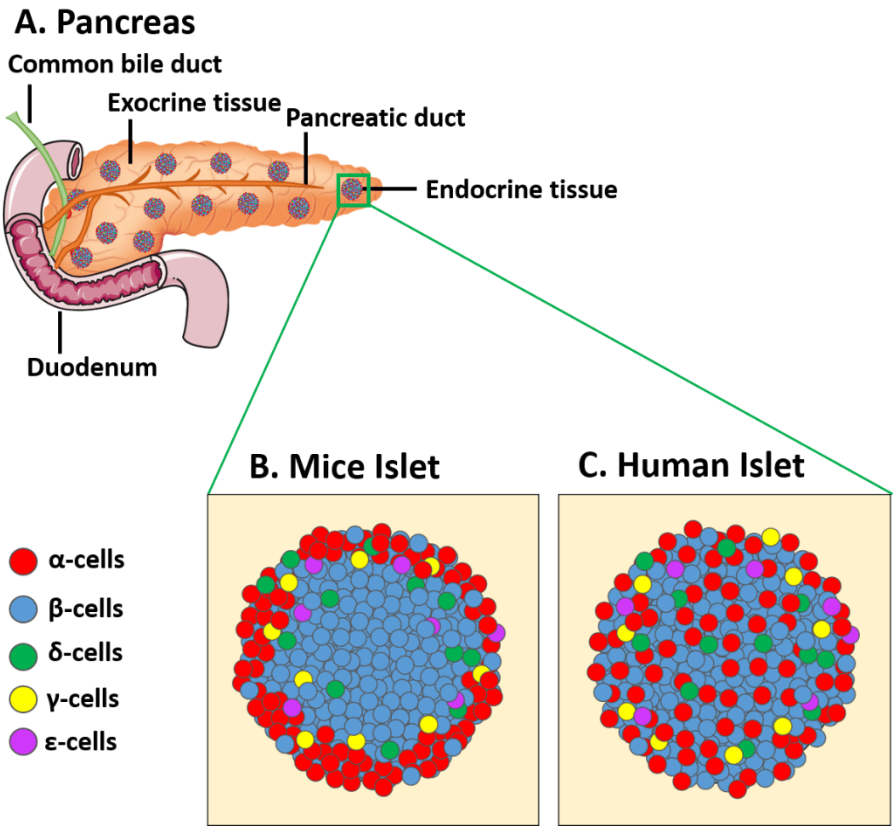

Figure 2: Anatomic representation of pancreas and its endocrine component. The pancreas is made up of mostly exocrine tissue embedded with small clusters of endocrine cells, called the islets of Langerhans (A). Islets are made up on five cell types: α-cells, β-cells, δ-cells, γ-cells and ε-cells. In mice islets, insulin-secreting β-cells are mainly found in the islet core, surrounded by a mantle of non- β-cells (B). In human islets, β-cells are usually distributed throughout the islet without an evident organization (C). [Adapted from (MacDonald and Rorsman, 2006)].

The endocrine portion of the pancreas is formed by the pancreatic islets, which are composed of five different cell types: insulin producing beta cells (β-cells), glucagon producing alpha cells (α-cells), somatostatin producing delta cells (δ-cells), pancreatic polypeptide (PP) producing gamma cells (γ-cells) and ghrelin producing epsilon cells (ε-cells).

The spatial distribution of these endocrine cells in the islets differ between rodents and humans. In rodents, the β-cells are located at the core of the islets and surrounded by a mantle of α-cells, δ-cells and γ-cells (Dybala and Hara, 2019, Brissova et al., 2005, Pfeifer et al., 2015) (Figure 2B). In human islets, β-cells are mostly equally distributed and interspersed between α-cells and δ-cells, while the γ-cells and ε-cells are mostly located on the periphery of the islets (Cabrera et al., 2006, Brissova et al., 2005) (Figure 2C). However, some studies have observed that human islets can also have other patterns of endocrine cell distribution, such as the rodent core-mantle β-cells distribution, as well as a clustered or dispersed configuration (Bosco et al., 2010, Dybala and Hara, 2019).

These different endocrine cell distribution patterns are designed to ensure cell to cell communication through extracellular spaces and gap junctions, (Cabrera et al., 2006). Furthermore, the pancreatic islets are highly vascularized, constituting around 8% of the total islet volume, thereby allowing modulation of the blood flow and cellular interactions between the endocrine cells (Henderson and Moss, 1985). Together, the intra-islet micro-capillary network and spatial arrangement of the endocrine cells influence and regulate the hormonal secretion of each other and maintain whole body glucose homeostasis.

1.3.1 Islet β-cell hormones

The β-cells are the most abundant endocrine cells of the islets, comprising 50-70% of total endocrine cells in humans and 60-80% in mice (Brissova et al., 2005, Cabrera et al., 2006) (Figure 2C). The most important role of the β-cell is to maintain glucose homeostasis by producing and releasing insulin into circulation, which stimulates uptake of circulating blood glucose into its target tissues, including skeletal muscles, adipose tissue and liver. The mechanisms involved in these processes will be discussed in detail in the following sections.

Amylin, also known as islet amyloid polypeptide (IAPP), is a 37 residue peptide protein that is co-secreted with insulin, in an insulin: amylin ratio of 100:1 by human β-cells (Cooper et al., 1987, Westermark et al., 1986). Amylin plays a role in preventing hyperglycaemia by inhibiting glucagon secretion, promoting satiety and slowing gastric emptying (Gedulin et al., 2006, Mack et al., 2007). Islet amyloid deposits of amylin were found to be present on the β-cells of over 95% of T2D patients and was associated with loss of β-cell mass in humans (Westermark et al., 1986, Bedrood et al., 2012). Although amylin is associated with T2D in humans, monkeys and cats, the same is not observed in mice and rats, since rodent amylin lacks the proline amino acid residue necessary for the formation of fibrils (de Koning et al., 1993, Yano et al., 1981, Betsholtz et al., 1989, Chiu et al., 2013). Therefore, transgenic mice specifically expressing the human form of amylin in the β-cells of obese diabetic mouse models are used to study the pathophysiology of amylin in human diabetes. These studies suggest that high fat (HF) diet-induced obesity is partly responsible for both amylin and insulin mal-processing, leading to amyloid deposits on β-cells (Hull et al., 2003).

1.3.2 Islet α-cell hormone

The α-cells make up 20-40% of the total cell number in humans and 10-20% in mice (Cabrera et al., 2006, Brissova et al., 2005). These cells secrete glucagon, a 29 amino acid peptide, derived from proglucagon *via* proteolytic cleavage by the enzyme prohormone convertase 2 (PC2) (Rouille et al., 1994, Furuta et al., 2001). Glucagon is normally secreted in response to hypoglycaemia. It maintains glucose homeostasis by stimulating glycogenolysis and gluconeogenesis in the liver, leading to increased blood glucose levels (Ikezawa et al., 2003, Shah et al., 2000).

1.3.3 Islet δ, γ and ε-cells and their hormones

Together, δ-cells and γ-cells make up less than 10% of endocrine cells in human islets and less than 5% in mice (Cabrera et al., 2006, Brissova et al., 2005). The δ-cells produce somatostatin which acts as a paracrine regulator of β-cells and α-cells, inhibiting the secretion of insulin and glucagon, respectively (Vergari et al., 2019, Briant et al., 2018). Pancreatic polypeptide (PP) is released by the γ-cells in response to food ingestion, particularly after ingestion of a protein-rich meal (Koska et al., 2004). Following meal consumption, PP is secreted to slow down digestion and prevent the post-prandial increase in circulating glucose levels, by inhibiting the release of pancreatic digestive enzymes and stimulating insulin secretion (Asakawa et al., 2003b, Liu et al., 2008, Rabiee et al., 2011). Finally, ε-cells comprise of less than 1% of total islet cells. It secretes ghrelin, the "hunger hormone", which regulates energy expenditure by promoting food intake and fat deposition (Cabrera et al., 2006, Asakawa et al., 2003a, Druce et al., 2005).

1.4 Insulin biogenesis

Insulin is considered one of the most important hormones of the body and is encoded by the *INS* gene, located on chromosome 11. The *INS* gene is almost exclusively expressed in the pancreatic β-cells, although it is also found in low levels in the brain, particularly in the hypothalamus (Hrytsenko et al., 2007). While most animals including humans have only one copy of the *INS* gene, rodents have two non-allelic insulin genes (*INS1* and *INS2*), which differ in the number of introns and chromosomal locations (Soares et al., 1985).

The *INS* gene is regulated by a complex network of key transcriptional factors, such as paired box (*Pax*) 4 and 6, pancreatic and duodenal homeobox-1 (*Pdx1*), neurogenic differentiation-1 (*NeuroD1*) and V-maf musculoaponeurotic fibrosarcoma oncogene homolog A (*MafA*). These transcription factors act upon the highly conserved 340 bp insulin promoter region, that lies immediately upstream of the transcription initiation start site (Wang et al., 2001, Kataoka et al., 2002, Sharma et al., 1999) (Figure 3A). Insulin biosynthesis is a complex event that comprises the formation of various intermediate molecules, in response to increased circulating blood glucose levels (Ozawa et al., 2014) (Figure 3).

Insulin mRNA translates into a 110 amino acid long single chain inactive precursor called preproinsulin, which is composed of a hydrophobic N-terminal signal peptide, followed by the insulin B chain, C-peptide and insulin A-chain (Dodson and Steiner, 1998) (Figure 3B). Although preproinsulin synthesis initiates in the cytosol, its signal peptide directs it across the rough endoplasmic reticulum (ER) membrane into the lumen, by cytosolic ribonucleoprotein signal recognition particles (SRP) (Okun and Shields, 1992). Upon entering the ER, a signal peptidase proteolytically cleaves the signal peptide and SRP from preproinsulin, which undergoes post-translational processing to yield proinsulin. The proinsulin then folds to align the carboxy-terminal A chain and the amino-terminal B chain, which are linked by the

connecting peptide (C-peptide), and forms three disulphide bonds (Huang and Arvan, 1995) (Figure 3C).

Properly folded proinsulin is cleaved in the ER by specific peptidases such as prohormone convertases (PCs) PC1/3 and PC2, which produces equimolar molecules of C-peptide and insulin (Ozawa et al., 2014) (Figure 3D). The active insulin and C-peptide molecules are then packaged together into dense clustered secretory granules by the Golgi complex and are subsequently stored in the cytoplasm. Inside the granules, the insulin molecule can also be stored in the form of insoluble hexamers, which are co-crystallized with two zinc ions in the center. While these zinc ions are necessary for crystallization of hexameric insulin, its absence does not affect insulin processing or secretion (Nicolson et al., 2009, Lemaire et al., 2009). Finally, upon stimulation for secretion, the contents of the secretory granules are released into circulation by exocytosis through the portal system.

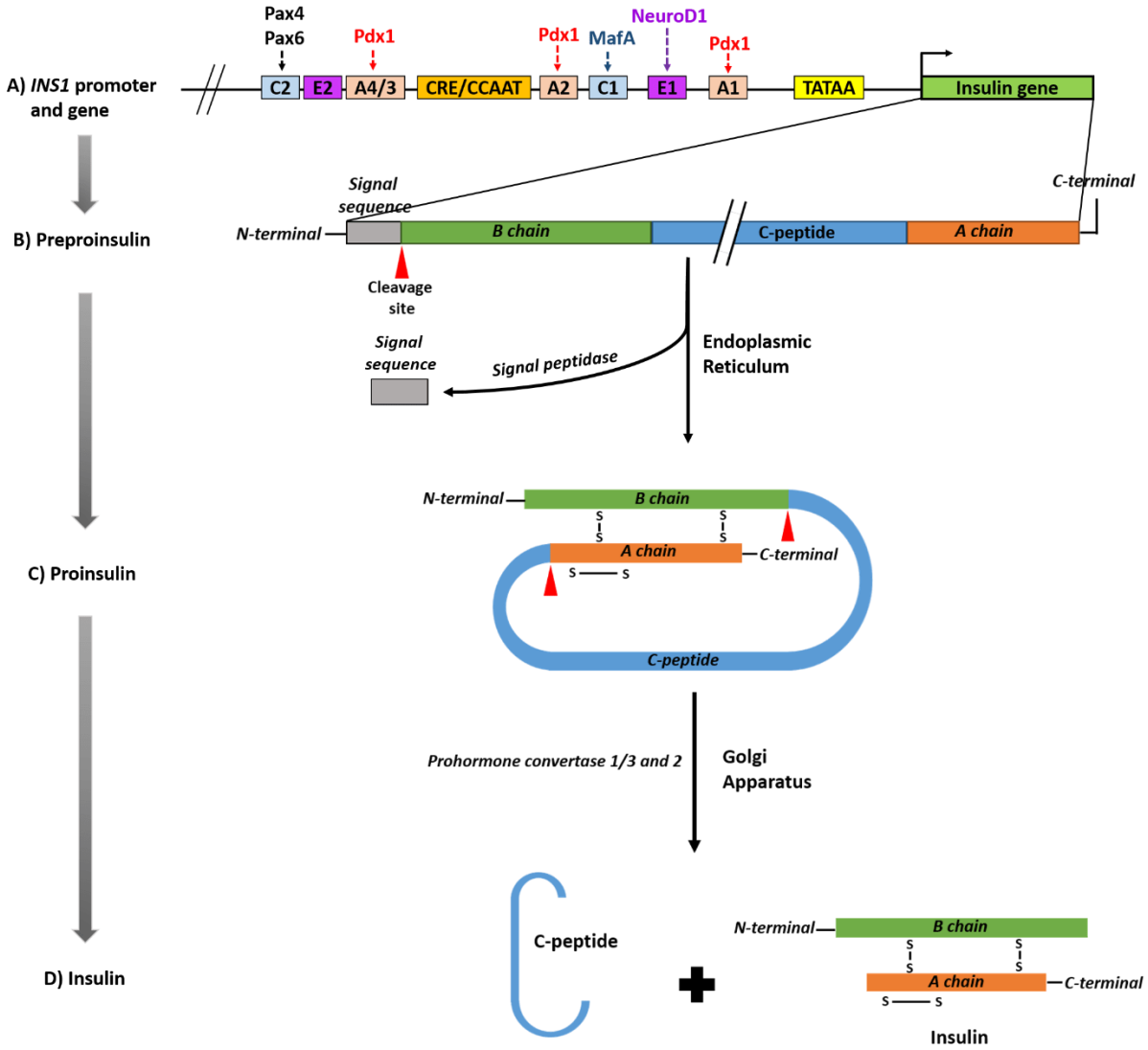

Figure 3: Schematic representation of insulin synthesis by rodent pancreatic β-cells. Proximal area of *INS1* promoter region with transcription factors and insulin gene (A). Insulin mRNA translates into a precursor molecule preproinsulin, made up of hydrophobic N-terminal signal sequence, B-chain, C-peptide chain and A-chain on the C-terminal. In the ER, signal peptidases cleaves the signal sequence to form proinsulin (B). Proinsulin folds to align the A-chain and the B-chain, forming three disulphide bonds (C). In the Golgi apparatus, prohormone convertases 1/3 and 2 cleaves proinsulin into insulin and C-peptide, which is then packaged into secretory vesicles and stored in the cytoplasm (D). A1-4, C1-2, E1: cis-regulatory elements, Pax: Paired box, Pdx: Pancreatic and duodenal homeobox, Neuro-D1: Neurogenic differentiation-1, MafA: V-maf musculoaponeurotic fibrosarcoma oncogene homolog A. [Adapted from (Melloul et al., 2002, Kaufman, 2011)].

1.5 Insulin Secretion

Islet β-cells continually monitor and respond to elevated blood glucose and nutrient levels by secreting insulin to maintain glucose homeostasis. Insulin secretion is a dynamic process modulated by a complex and multifactorial network of factors of metabolic, neuronal and hormonal origin. It is a biphasic process which involves the release of two distinct populations of insulin granules present in the cytoplasm of the β-cells- the readily releasable pool (RRP) and the reserve pool (RP) (Grodsky, 1972). These different pools of insulin granules are released in a pulsatile biphasic process (1st and 2nd phase), when glucose levels in circulation are elevated (>3 mM) (Curry et al., 1968, Porte and Pupo, 1969). The RRP constitutes 0.3 to 0.7% of the total reserve of insulin granules that are already primed to the plasma membrane. These granules are rapidly released during the 1st phase of insulin secretion, upon an increase of intracellular calcium concentration, lasting no longer than 5-10 mins. Once the RRP is depleted, the 2nd sustained and prolonged phase initiates where insulin granules from the RP are released (Noda et al., 1996). During this phase, the RRP is replenished with insulin granules from the RP, allowing the β-cells to synthesize, process and release more insulin (Noda et al., 1996). This phase is maintained until normoglycaemia is restored.

1.5.1 Glucose stimulated insulin secretion (GSIS)

Glucose is regarded as the primary stimuli for insulin secretion, while other nutrients such as free fatty acids (FFA) and amino acids (particularly arginine and leucine), incretin hormones (glucagon-like peptide-1 (GLP-1) and glucose-dependent insulinotropic polypeptide (GIP)), and neurotransmitters (acetylcholine) are considered as potentiators (Rorsman and Ashcroft, 2018, Nauck et al., 1986, Molina et al., 2014). However, glucose needs to be metabolized by the β-cell to generate triggering and amplifying signals to stimulate insulin secretion. It is

understood that the readily releasable pool of insulin is promptly released through the K_{ATP} dependent pathway, whereas the more sustainable insulin exocytosis observed during the second phase is obtained through synergetic interaction between the K_{ATP} dependent and K_{ATP} independent pathway.

1.5.1.1 Triggering pathway of insulin secretion

The K^+_{ATP} dependent pathway, also known as the classical pathway, is widely accepted as the main pathway for GSIS (Figure 4). After ingestion of a carbohydrate-containing meal, the elevation in circulating blood glucose levels leads to an increased influx of glucose into the β-cell through specific glucose transporters (GLUT1 in humans and GLUT2 in rodents) (McCulloch et al., 2011).

Glucose is then phosphorylated by glucokinase, the first enzyme in the glycolytic pathway, which produces glucose-6-phosphate. Glycolysis leads to the production of metabolic substrate pyruvate, which is oxidized through the Krebs cycle by the mitochondria, to generate energy in the form of adenosine triphosphate (ATP) (Rorsman and Trube, 1985, Ashcroft et al., 1984). The sequential increase in the cytoplasmic ATP:ADP ratio leads to the closure of the ATP-sensitive K^+ (K^+_{ATP}) channels, inhibiting the efflux of K^+ ions and consequently promoting the depolarization of the plasma membrane (Puljung et al., 2019). This process results in the opening of voltage-gated Ca^{2+} channels and extracellular Ca^{2+} influx, which triggers the release of RRP insulin granules (Klec et al., 2019, Ashcroft and Rorsman, 1989).

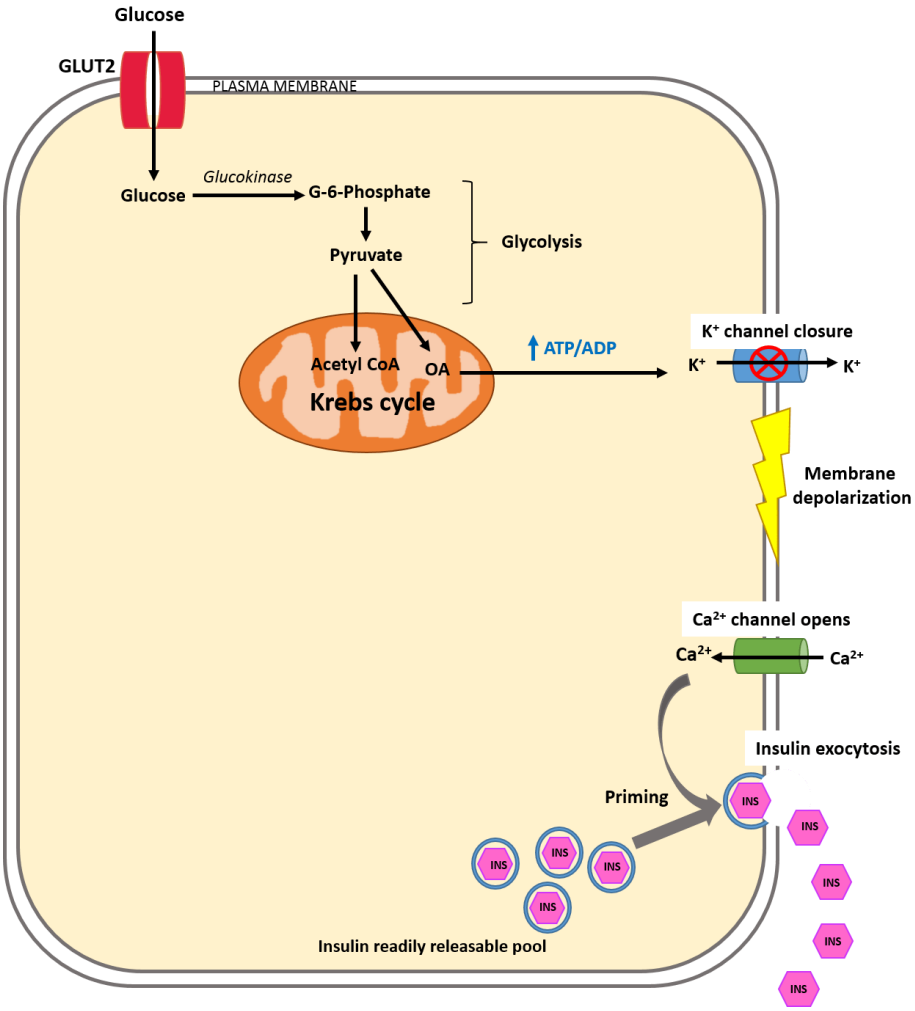

Figure 4: Schematic representation of the K^+_{ATP} channel-dependent triggering pathway leading to β-cell insulin secretion. Glucose enters the β-cell through GLUT2 and undergoes glycolysis to generate pyruvate, which is oxidized through the Krebs cycle to generate ATP. The subsequent increase in ATP: ADP ratio leads to closure of K^+_{ATP} channels and depolarization of the plasma membrane, which leads to the opening of Ca^{2+} channels and Ca^{2+} influx. The increase in intracellular Ca^{2+} promotes immediate exocytosis of the readily releasable insulin pool granules (1st phase insulin secretion). GLUT: glucose transporter, G-6-Phosphate: Glucose-6-phosphate, OA: oxaloacetate, INS: Insulin granules.

1.5.1.2 Amplifying pathway of insulin secretion

While the K^+_{ATP} dependent pathway triggers the initiation of insulin release by the β-cells (also known as 1st phase), it does not explain the prolonged and sustained insulin release that occurs around 15 minutes after the initial glucose stimulation. Therefore, additional metabolic signals which are independent of the K^+_{ATP} channels are required to maintain insulin secretion elicited by glucose. The presence of an amplifying pathway was further supported through studies performed in K^+_{ATP} channel knockout mice and by *in vitro* experiments conducted using isolated islets exposed to depolarizing concentrations of K^+ ions or the K^+_{ATP} channel opener diazoxide (Gembal et al., 1992, Komatsu et al., 1999, Shiota et al., 2002). These studies proposed an interplay of both pathways in insulin secretion, where the K^+_{ATP} dependent pathway initiates the 1st phase of insulin release, while the K^+_{ATP} independent pathway acts in synergy with the first pathway to amplify the insulin secretory response to Ca^{2+} ions.

However, the K^+_{ATP} independent pathway is complex and not yet fully understood. Based on the high levels of pyruvate carboxylase expression in the β-cell, an anaplerotic enzyme, several studies have proposed that metabolic coupling factors (MCFs) generated from anaplerosis (*i.e.* Malonyl-CoA, NADH/NAD+, succinate, glutamate, fatty acyl-CoAs) could be involved in amplification pathways (Liu et al., 2002, Fransson et al., 2006, Prentki et al., 2013, Brun et al., 1996, Ivarsson et al., 2005, Maechler and Wollheim, 1999). Prentki *et al* have also shown that increased accumulation of Krebs cycle intermediates results in elevated levels of mitochondrial citrate, which is subsequently transported to the cytosol, where it is converted into malonyl-CoA through the enzymatic action of citrate-lyase and acetyl-CoA carboxylase (Roduit et al., 2004).

Augmented levels of malonyl-CoA in the cytoplasm inhibits carnitine palmitoyl transferase 1 (CPT1), a mitochondrial enzyme responsible for the translocation of long chain acyl-coenzyme

A (LC-CoA) into the mitochondria for fatty acid oxidation (Herrero et al., 2005, Roduit et al., 2004). CPT1 inhibition leads to increased accumulation of cytosolic LC-CoA, which together with glycerol-3-phosphate (Gly3P) derived from glycolysis, are re-esterified into complex glycerolipids that could be indirectly or directly potentiating insulin secretion (El-Azzouny et al., 2014, Evliyaoğlu et al., 2018) (Figure 5).

Additionally, Prentki *et al* have also described the existence of a cycle in the β-cells where these glycerolipids are constantly formed and broken-down by lipase enzymes, therefore producing different molecules that can potentiate GSIS (Nolan et al., 2006b). Even though there are still ongoing studies investigating the functions and effects of these glycerolipids, emerging evidence of the impact of inhibition of the glycerolipid-FFA cycle on insulin secretion and its association with insulin-resistant obesity, proposes a more important role of this cycle in FFA-augmented GSIS (Prentki et al., 2020, Mugabo et al., 2017, Mugabo et al., 2016).

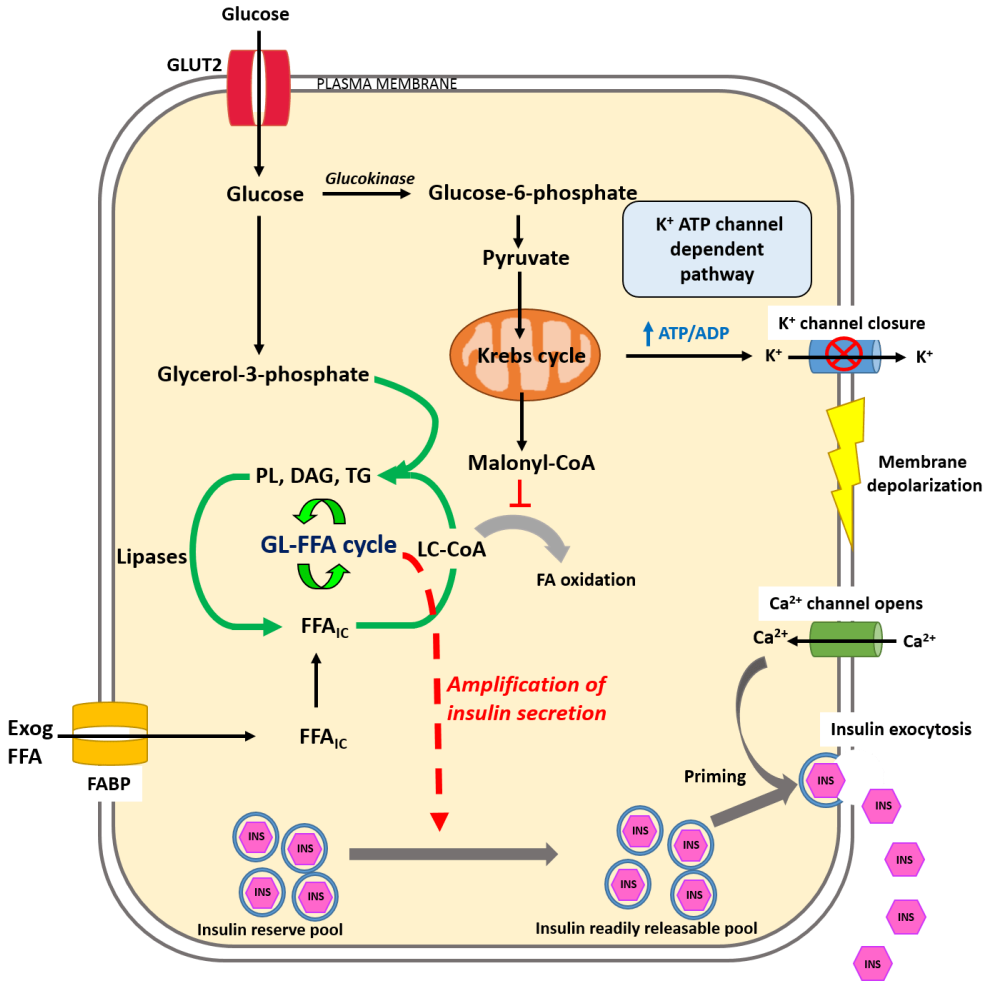

Figure 5: Glycerolipid-FFA cycling in fatty acid-augmented glucose stimulated insulin secretion in pancreatic β-cells. In the β-cells, glucose enters through GLUT2 and either undergoes glycolysis to generate pyruvate which enters the Krebs cycle to increase ATP:ADP ratio. This leads to closure of K^{+}_{ATP} channels and opening of Ca^{2+} channels and Ca^{2+} influx, leading to triggering pathway of insulin secretion. Malonyl-CoA inhibits CPT1, which redirects LC-CoA away from fatty acid oxidation, and towards esterification processes with glycerol-3-phosphate to form neutral lipids like PL, DAG and TG. These are broken down by lipases to generate signals which amplify GSIS. Exogenous FFA can also enter the β-cell and augment GSIS through the glycerolipid-FFA cycle. GLUT: Glucose transporter, PL: Phospholipid, DAG: Diacylglycerol, TG: Triacylglycerol, FFA_{IC}: Intracellular Free fatty acids, GL: Glycerolipid, LC-CoA: Long chain-Coenzyme A, FA: Fatty acids.

1.5.2 Incretin hormones and cAMP-mediated insulin secretion

The incretin effect is defined as an important physiological amplifier of insulin secretion following oral ingestion of glucose, and is responsible for up to 70% of the insulin response to the glucose load (Nauck et al., 1986). The two most important incretin hormones that play a major role in postprandial regulation of insulin secretion are GLP-1 and GIP (Drucker, 2013). GLP-1 is secreted by the enteroendocrine L-cells throughout the small and large intestine, whereas GIP is secreted by the endocrine K-cells of the intestinal epithelium of the duodenum and jejunum (Holst, 2019). Both hormones act through distinct G-protein receptors (GPR) which are highly expressed on β-cell surfaces, and lead to the formation of cyclic adenosine monophosphate (cAMP) (Dou et al., 2015).

Incretin-induced insulin secretion occurs through cAMP signaling, which is regulated by the action of two enzymes: adenylyl cyclase (AC) and cyclic nucleotide phosphodiesterase (PDE) (Figure 6). AC catalyzes the conversion of ATP to cAMP and increases insulin secretion, whereas PDE is responsible for its degradation (Dou et al., 2015, Tengholm and Gylfe, 2017). The importance of cAMP as a GSIS regulator was demonstrated in *in vitro* studies through its modulation using forskolin (an AC stimulator) and 3-isobutylmethylxanthine (IBMX) (a PDE inhibitor) (Komatsu et al., 2002).

The activity of cAMP is mediated through the stimulation of downstream pathways coupled to two enzymes, protein kinase A (PKA) and exchange protein directly activated by cAMP (Epac). PKA regulates the spatial local compartmentalization of cAMP signaling, promoting cAMP-mediated enhancement of Ca^{2+} signaling and subsequent amplification of GSIS (Kaihara et al., 2013, Light et al., 2002). On the other hand, Epac mediates the potentiating effects of cAMP on 1st phase of insulin exocytosis, by recruiting insulin granules to the plasma membrane

through activation of Ras-like guanosine triphosphatase Rap1 (Ozaki et al., 2000, Shibasaki et al., 2004, Takahashi et al., 2015).

cAMP alone is a poor inducer of insulin secretion, and requires glucose-stimulated elevation in Ca^{2+} concentrations to amplify insulin release (Hellman et al., 1974). Even sub-stimulatory glucose levels have been found to increase cAMP concentrations in β-cells, which oscillates in synchrony with Ca^{2+} in periods of 2-10 minutes to generate the pulsatile insulin secretion (Dyachok et al., 2008). Therefore, cAMP-mediated GSIS is another important pathway that can by-pass the K^{+}_{ATP} channel to amplify insulin secretion.

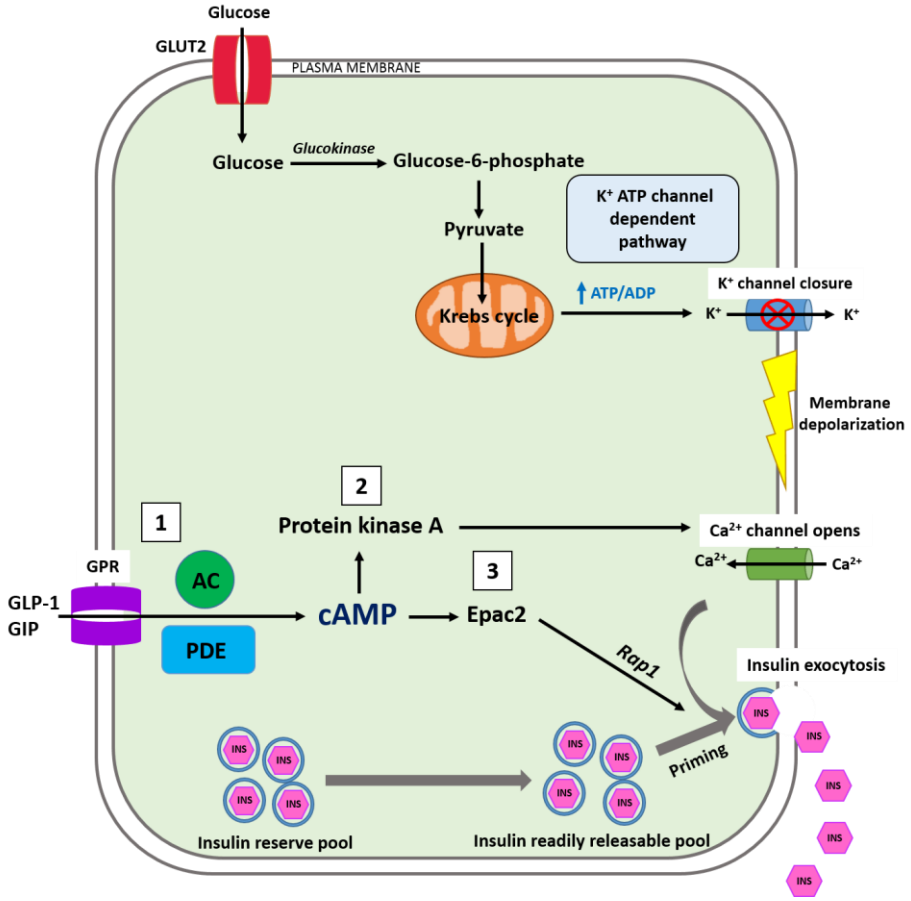

Figure 6: cAMP signaling and the incretin-mediated insulin secretion in pancreatic β-cells. 1) cAMP signaling is triggered by incretins GLP-1 and GIP, which increase cAMP concentrations in the β-cells. AC catalyzes the conversion of ATP to cAMP, while PDE causes cAMP degradation. 2) cAMP binds to protein kinase A and promotes Ca^{2+} signaling and subsequent amplification of GSIS. 3) Epac2 recruits insulin granules to the plasma membrane to potentiate insulin exocytosis. GLUT: Glucose transporter, cAMP: Cyclic adenosine monophosphate, AC: adenylyl cyclase, PDE: Phosphodiesterase, Epac: Exchange protein directly activated by cAMP, Rap1: Ras-related protein 1, GPR: G_{α}-protein coupled receptor, GLP-1: Glucagon-like peptide-1, GIP: Glucose-dependent insulinotropic polypeptide.

1.6 Insulin action on key peripheral target tissues

The primary metabolic effects of insulin are to induce glucose uptake in peripheral tissues such as skeletal muscle, heart and adipose tissues and to suppress hepatic glucose production *via* inducing phosphorylation of the intracellular domain of insulin receptor that initiates an intracellular signaling cascade (Figure 7). Overall insulin has anabolic effects on carbohydrate, protein and lipid metabolism.

Glucose uptake into and release from hepatocytes is primarily mediated by GLUT2 which is insulin independent (Thorens et al., 1990). During periods of starvation, hepatocytes undergo gluconeogenesis in the absence of insulin and convert stored glycogen into glucose *via* glycogenolysis, which rapidly effluxes through GLUT2. However in the post-prandial stage, insulin inhibits gluconeogenesis and glycogenolysis in the liver and promotes glycogen synthesis, such that the passage of glucose *via* GLUT2 is into hepatocytes (Wang et al., 2019). Insulin also promotes hepatic *de novo* lipogenesis from carbohydrate catabolism. Furthermore, the synthetized fatty acids are esterified into triacylglycerides (TG) and exported out of the liver as very low density lipoproteins (VLDL) (Olofsson et al., 2000).

Insulin has a similar effect on carbohydrate metabolism in the skeletal muscles. It increases glucose uptake into myocytes by translocating GLUT4 from intracellular vesicles to the plasma membrane and promotes glycogen synthesis and glycolysis (Vogt et al., 2000, Keildson et al., 2014). Glucose uptake by the skeletal muscles accounts for around 80% of whole body glucose clearance (Thiebaud et al., 1982). During fasting or states of high energy demand such as exercise, skeletal muscles serve as the main site for oxidation of fatty acids from adipose tissue and intramuscular triglyceride (IMTG), which serve as the primary fuel source (van Loon et al., 2003). However, in the postprandial state, muscle energy metabolism shifts to primarily glucose

oxidation, and consequently, fatty acids are instead stored as IMTG (Kelley and Mandarino, 2000).

The adipose tissue accounts for around 20% of whole body glucose clearance (Favaretto et al., 2014). Insulin promotes uptake and storage of fatty acids in adipocytes following activation of their hydrolysis of TG in chylomicrons and VLDL by lipoprotein lipase. Fatty acid transport into adipocytes is *via* fatty acid binding proteins (FABP) and fatty acid translocase CD36 (Vroegrijk et al., 2013). Glucose uptake and the glycolytic pathway provide glycerol-3-phosphate as the backbone for fatty acid esterification into TG, which is stored in the form of cytosolic lipid droplets (Puri et al., 2007, Nye et al., 2008). Conversely, insulin suppresses TG hydrolysis, thereby reducing FFA and glycerol efflux into circulation (Meijssen et al., 2001).

Therefore, disturbance in the balance of glucose homeostasis can lead to metabolic disorders such as metabolic syndrome (MetS) and T2D, underlining to the importance of understanding the mechanisms and effects of insulin signaling on peripheral tissues.

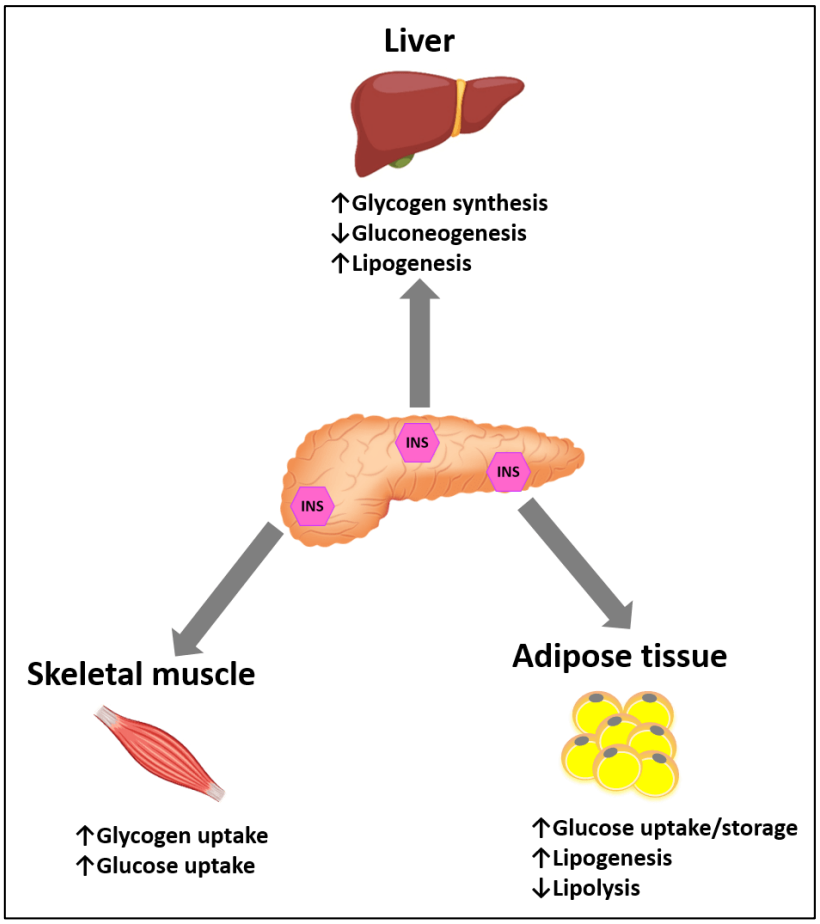

Figure 7: Insulin action on peripheral tissues. Insulin binds to its receptor on the hepatocytes, myocytes and adipocytes, sending a signaling cascade to promote glycogen synthesis and lipogenesis in the liver, glycogen and glucose uptake in the skeletal muscles, and glucose uptake/storage and lipogenesis in the adipose tissues.

1.7 Pathophysiology of T2D

T2D is a complex metabolic disorder characterized by elevated glucose levels in circulation, caused by a combination of genetic susceptibility and an unhealthy lifestyle. The main factors involved in the pathogenesis of T2D are insulin resistance (IR) in the peripheral tissues and liver and islet β-cell dysfunction, leading to impaired insulin secretion and/or action.

1.7.1 Insulin resistance

Insulin resistance is the metabolic condition where normal concentrations of insulin produced by the β-cells fails to elicit optimal physiological responses, resulting in impaired uptake of glucose by target tissues such as adipose tissue, skeletal muscle and reduced suppression of hepatic glucose production. The impaired insulin action is attributed to a number of mechanisms, including inability of insulin to bind to its receptor due to receptor down regulation, a compromised insulin receptor signaling pathway or a combination of these defects.

IR in the adipose tissue leads to decreased lipid storage and impaired inhibition of lipolysis, such that it is associated with increased glycerol and FFA in serum (Salgin et al., 2012, Mahendran et al., 2013). Hepatic IR is characterized by impaired suppression of hepatic gluconeogenesis, (Iozzo et al., 2003, Kotronen et al., 2008, Jornayvaz et al., 2011). Thus, IR can contribute to reduced glucose uptake by the adipose tissues and skeletal muscles and increased hepatic glucose production, contributing to hyperglycaemia if it cannot be compensated by increased insulin secretion (Li et al., 2000a). However, there is no consensus on which peripheral organ is the primary tissue developing IR. While some studies show IR in the skeletal muscles as the primary defect, others propose liver as the first tissue to develop IR (Petersen et al., 2007, Pearson et al., 2016b, Kraegen et al., 1991). Nonetheless, it was reported

that once one tissue becomes insulin resistant, the subsequent chronic increases in circulating glucose and FFA affects the other tissues in a knock-on effect (Pearson et al., 2016b).

Alternately, hyperinsulinaemia has been implicated by some as the cause for IR by downregulation of its receptors, leading to reduced glucose uptake and alterations in the insulin receptor tyrosine kinase domain (Catalano et al., 2014). The subsequent hyperglycaemia creates a greater demand for β-cell insulin secretion to compensate for the impaired insulin action. This forms a vicious cycle, further contributing to IR and eventually islet β-cell apoptosis (Rachdaoui et al., 2019). Nolan and Prentki have subsequently proposed that peripheral IR may be an adaptive response developed by the peripheral tissues to protect themselves against the detrimental effects of excessive fuel and increased demand for energy storage (Nolan and Prentki, 2019). The possible change in the interpretation of insulin resistance as a protective response, rather than a T2D causative factor, can provide new insights into the mechanisms involved in the pathogenesis of T2D, as well as novel therapeutic targets.

1.7.2 β-cell dysfunction

Numerous studies have established that β-cell dysfunction is the primary requisite determinant for the development of hyperglycaemia and subsequent onset of T2D (Lyssenko et al., 2005, Godsland et al., 2004, Fukushima et al., 2004, Weyer et al., 1999). Additionally, genetic studies on glycaemic traits have also corroborated with this view, as the majority of genes associated with T2D risk have been identified in genes affecting β-cell mass and function, instead of IR (Dupuis et al., 2010). This outlook is also supported by the findings that most obese individuals do not develop T2D, instead they maintain glucose homeostasis by promoting an adaptive increase in insulin secretion and β-cell mass in response to IR, also known as β-cell compensation (Succurro et al., 2008). Development of T2D will occur only in individuals that

are unable to sustain this compensatory response for a long period (Echouffo-Tcheugui et al., 2019).

This adaptive process has been segregated into five distinct stages based on changes in β-cell mass, phenotype and function (Weir and Bonner-Weir, 2004) (Figure 8). The first stage is characterized by increased insulin secretion by the β-cells to maintain glucose homeostasis, evoked by increased β-cell mass and function (Jetton et al., 2005). This stage is associated with increased expression of insulin and β-cell proliferation genes such as *PDX1* (Srinivasan et al., 2002, Ahlkvist et al., 2013, van Citters et al., 2002, Jetton et al., 2005). Additionally, the insulin secretory function of the β-cells are also enhanced by upregulation of GLUT2 and the K^{+}_{ATP} dependent and independent pathways of insulin secretion (Reimer and Ahrén, 2002, Liu et al., 2005).

The second stage is of stable β-cell adaptation where fasting blood glucose levels rise to 5-6.5 mmol/l, and β-cells are no longer compensating to maintain glucose homeostasis. This stage is characterized by the loss of 1^{st} phase of insulin secretion, whereas the 2^{nd} phase is still partially preserved (Kanat et al., 2011). There is an initial loss of β-cell mass and consequent reduction in GSIS. Altered gene and protein expression of key β-cell genes and transcription factors lead to β-cell dedifferentiation (Cinti et al., 2016).

The third stage is a short transient period of unstable early decompensation. Clinically, this stage is not very pronounced, but is observed when normoglycaemic patients suddenly present with fasting glucose level up to 16 mmol/l with or without any symptoms (Weir and Bonner-Weir, 2004). External factors such as changes in calorie intake, exercise and/or oral medications can prolong stage 2 for years, reverse stage 3 back to 2, or progress to stage 4 (Florez et al., 2012, Knowler et al., 2002).

The fourth stable decompensation stage occurs when the glucose rises to levels of frank diabetes: 16-20 mmol/l. This stage is characterized by severe β-cell dedifferentiation with a 50% loss of β-cell mass (Butler et al., 2003). For T2D patients, this stage may last a lifetime since there is enough insulin to not progress to ketoacidosis, which occurs in stage 5. A stress response of increased antioxidant and anti-apoptotic genes such as glutathione peroxidase, is also activated to protect the β-cells (Laybutt et al., 2002). Of note, this stage is relatively shorter for T1D and some rare forms of T2D, characterized by a quick transition to the severe decompensation stage 5 of profound β-cell failure and development of ketoacidosis (Duca et al., 2019, Sjoholm, 2019). The final stage results in complete reliance on exogenous insulin for survival.

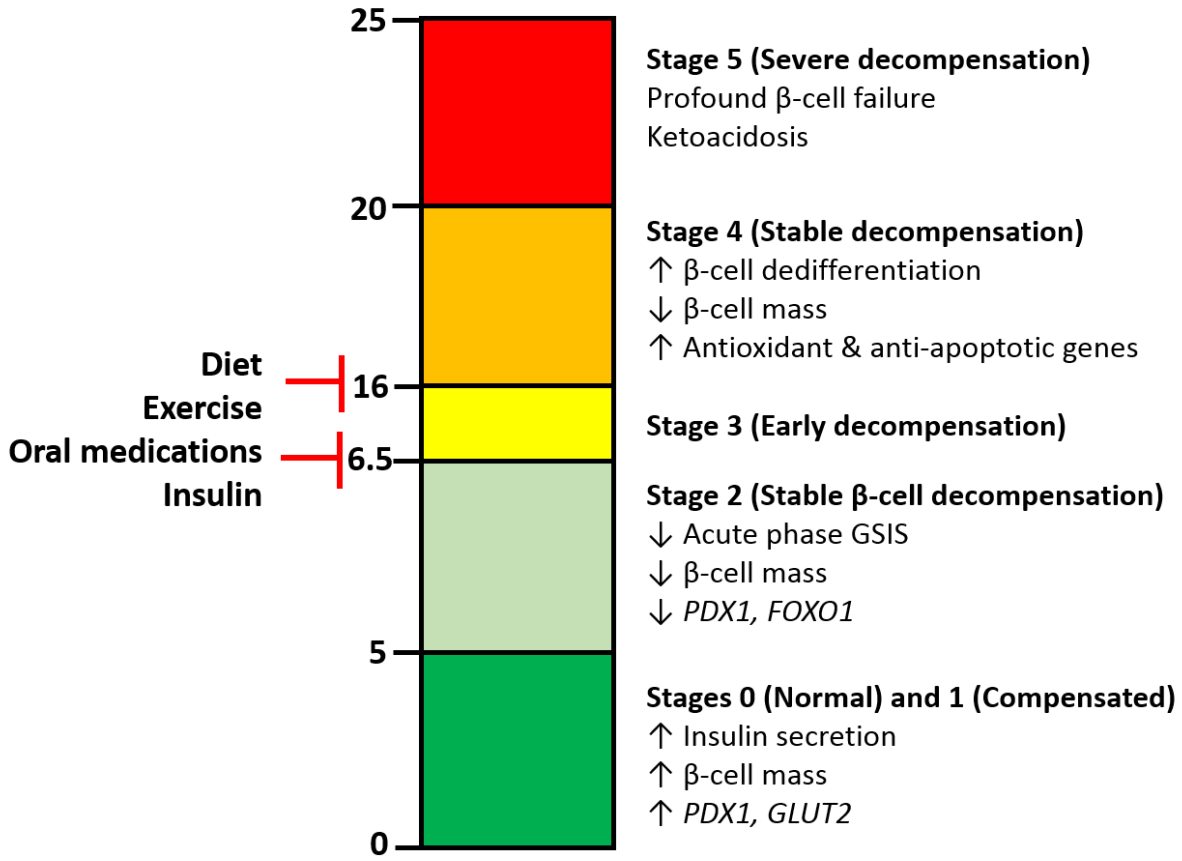

Figure 8: The five stages of β-cell dysfunction culminating in diabetes mellitus. In stage 1, β-cell compensation occurs, failure of which leads to stage 2. Factors such as diet, exercise, oral medications and insulin can affect progression to and from the 3rd stage. In the 4th stage, there is considerable loss of β-cell mass and identity. The 5th stage ends in β-cell failure and ketoacidosis. Numbers in the left are the fasting blood glucose levels in mmol/l. Figure adapted from (Weir and Bonner-Weir, 2004).

1.7.3 Mechanisms involved in β-cell dysfunction

β-cell failure occurs when the balance between proliferative and apoptotic signaling is lost and compensation fails due to cell exhaustion. There are several hypotheses proposed for the development of β-cell dysfunction and failure including metabolic stressors such as hyperglycaemia, hyperlipidaemia or both, as well as pathophysiological stress responses such as oxidative stress, ER stress, islet inflammation and amyloidosis.

1.7.3.1 Glucotoxicity

The term glucotoxicity was used for the first time by Unger and Grundy to describe the effects of chronic exposure of β-cells to supra-physiological glucose concentrations (Unger and Grundy, 1985). This leads to irreversible detrimental changes in β-cell function, particularly insulin synthesis and secretion, eventually promoting cell death (Solomon et al., 2012, Khaldi et al., 2004, Unger and Grundy, 1985).

Glucotoxicity is associated with progressive loss of β-cell identity known as dedifferentiation, due to reduced expression of genes and transcription factors associated with β-cell function such as *INS*, *PDX1* and *NeuroD1*, and ion channels (Henquin et al., 2015, Poitout et al., 1996, Olson et al., 1993, Hall et al., 2018, Laybutt et al., 2002). It is also accompanied by increased expression of genes that are not usually expressed in β-cells such as lactate dehydrogenase-A, uncoupling protein 2 (UCP2) and glucose-6-phosphatase, in addition to genes associated with stress, inflammation and apoptosis (Laybutt et al., 2002, Ebrahimi et al., 2020). Induction of apoptosis was also observed in cultured human and mice islets exposed to high glucose concentrations (Federici et al., 2001, McKenzie et al., 2010).

1.7.3.2 Lipotoxicity

Under physiological conditions, FFAs act as a major fuel source for skeletal muscles and liver, and acute exposure to high FFA concentrations can stimulate insulin secretion (Cen et al., 2016, Gravena et al., 2002). However, chronic exposure to high levels of FFA, also known as lipotoxicity, can be detrimental to β-cell function. This effect will depend not only on the duration and concentration of FA exposure, but also on the type of FA species and their chain length. Prolonged exposure of islet β-cells to saturated non-esterified fatty acids (NEFA) such as palmitate induces apoptosis, whereas unsaturated NEFA such as oleate protects the β-cells from lipotoxicity (Tuo et al., 2012, Maedler et al., 2003). Several studies have shown that prolonged culture of islets in lipotoxic conditions increases islet TG content, impairs insulin synthesis and GSIS, along with reduced glucose utilization and oxidation (Lupi et al., 2002, Patanè et al., 2000).

Lipotoxicity can also prevent the nuclear translocation of PDX1 and reduce MafA expression, thereby decreasing insulin transcription and inhibiting insulin promoter activity (Hagman et al., 2005). It can increase the expression of genes associated with fatty acid metabolism, oxidative stress and ER stress, leading to β-cell apoptosis, while down-regulating genes related to β-cell differentiation, glycolysis and pyruvate metabolism (Cnop et al., 2014, Hall et al., 2014, Laybutt et al., 2007, Lupi et al., 2002).

1.7.3.3 Glucolipotoxicity

The term "glucolipotoxicity" postulates that glucose and FFA alone cannot induce significant β-cell toxicity, as individually they can be detoxified by the β-cells. However, in combination at high concentrations for prolonged periods of time, they become synergistic in inducing deleterious cellular effects (Prentki et al., 2002, Roche et al., 1998). Chronic exposure of β-cells to both elevated glucose and FFA leads to the accumulation of LC-CoA and other lipid

metabolites that can impair GSIS and insulin signaling, and promote apoptosis (Véret et al., 2011, Yu et al., 2002, Qu et al., 1999, Briaud et al., 2001). Long-term exposure to glucolipotoxic conditions causes downregulation of key β-cell genes such as insulin and *NeuroD1* (Jacqueminet et al., 2000, Briaud et al., 2001, Kim et al., 2009b). Furthermore, glucolipotoxicity can also induce oxidative stress through mammalian target of rapamycin complex 1(mTORC1), by activating the jun N-terminal kinase (JNK) pathway. This results in reduced insulin gene expression by translocation of *PDX1* from the nucleus to the cytoplasm (Tang et al., 2018, Bachar et al., 2009).

1.7.3.4 Oxidative stress

Pancreatic β-cells are highly metabolically active due to their role as glucose sensors and corresponding insulin synthesis. However, this increased glycolytic flux leads to higher demand for glucose metabolism in the mitochondria, which is one of the major sites for the production of reactive oxygen species (ROS) (Cadenas and Davies, 2000). Since the β-cells display the lowest levels of anti-oxidant enzymes among metabolic tissues, they are highly vulnerable to oxidative stress (Miki et al., 2018, Lenzen et al., 1996).

ROS can bind to DNA to create structural variations that can alter gene transcription (Cadet et al., 2017). It can also interact with proteins to inactivate and/or degrade them, consequently disrupting associated signaling pathways (Thomas et al., 2009). Noticeably, in diabetic human islets, oxidative stress-related DNA damage and increased ROS formation results in impaired GSIS and reduced β-cell mass (Sakuraba et al., 2002, Del Guerra et al., 2005). Additionally, anti-oxidant islet treatment improves GSIS and glucose homeostasis, and reduces β-cell apoptosis (Lee et al., 2011).

Oxidative stress can also be induced by pro-inflammatory cytokines (Gurgul et al., 2004). Human and rodent islets exposed to glucotoxic or lipotoxic conditions, secretes pro-inflammatory cytokine IL-1β, which increases the activation of inducible nitrogen synthase (iNOS) and free radical nitric oxide (NO) (Böni-Schnetzler et al., 2008, Sakai et al., 2003, Arafat et al., 2007, Maedler et al., 2002). This disrupts the mitochondrial electron transfer chain and ATP synthesis (Michalska et al., 2010). Additionally, pro-inflammatory cytokines can also activate ER stress through reactive nitrogen species (RNS) synthesis, which depletes ER Ca^{2+} levels and triggers β-cell apoptosis through the JNK pathway (Wang et al., 2009, Tong et al., 2015).

1.7.3.5 Endoplasmic reticulum stress

The endoplasmic reticulum (ER) is responsible for the folding and processing of insulin from preproinsulin precursors in the β-cells. Under physiological conditions, molecular chaperones of the ER bind to newly formed proteins, to initiate proper folding and promote identification of misfolded proteins for degradation (Ghiasi et al., 2019). Therefore, ER homeostasis is regulated by the chaperones and degradation pathways, where a unique equilibrium between the cellular protein demand and the ER protein folding capacity is maintained.

In β-cells, fluctuations in glucose levels can trigger up to a 20-fold increase in demand for insulin biosynthesis and secretion (Westerlund and Bergsten, 2001). This heavy requirement of proinsulin synthesis in the ER can cause an unfolded protein response (UPR) or ER stress response (Scheuner et al., 2005). The UPR is an intracellular signaling pathway that senses ER stress by the action of three ER stress sensors: protein kinase RNA-like ER kinase (PERK), activating transcription factor-6 (ATF6) and inositol-requiring ER to nucleus signal kinase-1-alpha (IRE1α). PERK prevents entry of nascent protein into the ER, thus redirecting resources

to proper folding of existing proteins in the ER (Gao et al., 2012, Sowers et al., 2018, Gupta et al., 2010). ATF6 increases chaperone genes expression to improve protein folding capacity (Li et al., 2000b, Martindale et al., 2006). IRE1α induces cytoplasmic translocation of misfolded/unfolded proteins for proteasome degradation (Han et al., 2013, Uemura et al., 2009, Calfon et al., 2002). If all these responses fail to compensate for the ER stress, PERK and IRE1α can switch from adaptive mechanisms to self-destruction, therefore initiating programmed cell death (Li et al., 2019, Demay et al., 2014).

Even in a healthy state, β-cells have higher UPR activity than other cells due to the fluctuating demands for insulin with changing glucose levels, leading to misfolding in 20% of proinsulin (Iwawaki et al., 2004, Wang et al., 2011). In T2D, the increased demand for constant β-cell compensation in response to IR leads to higher amounts of misfolded or unfolded proinsulin, activating UPR and resulting in apoptosis. Chronic β-cell exposure to glucotoxicity led to increased expression of ER stress markers and activation of IRE1α signaling, promoting apoptosis (Marchetti et al., 2007, Lipson et al., 2006, Lipson et al., 2008). Lipotoxicity causes ER stress in β-cells through various mechanisms, such as inhibition of ER-to-Golgi trafficking of proteins, leading to protein accumulation and depletion of Ca^{2+} levels in the ER. This consequently leads to impaired ER-signaling and induction of apoptosis (Cunha et al., 2008, Cnop et al., 2007, Preston et al., 2009, Karaskov et al., 2006, Oyadomari et al., 2002).

In T2D, both oxidative stress and ER stress are interconnected, creating a vicious cycle of cell damage leading to β-cell apoptosis (Wang and Sevier, 2016). Proper folding of proinsulin in the ER accounts for 25% of the total cellular ROS production and protein misfolding during ER stress leads to further increase in ROS formation, thus promoting oxidative stress (Haynes et al., 2004, Inaba et al., 2010, Tu and Weissman, 2004). Other factors such as pro-inflammatory cytokines, amylin accumulation and hypoxia are also associated with the induction of ER stress-

mediated apoptosis in β-cells, but will not be further discussed in this thesis (Demine et al., 2020, Huang et al., 2007, Zheng et al., 2012).

1.7.3.6 Inflammation

Inflammation is associated with both glucotoxicity and lipotoxicity in the pathogenesis of T2D. Increased expression of the pro-inflammatory cytokine IL-1β was reported in the β-cells of T2D patients, while *in vitro* experiments on isolated non-diabetic human islets exposed to high glucose concentrations led to elevated IL-1β production and release, causing β-cell dysfunction (Maedler et al., 2002, Böni-Schnetzler et al., 2008). Hyperglycaemia activates the NOD-, LRR- and pyrin domain-containing-3 (NLRP3) inflammasome, which further stimulates IL-1β maturation and secretion, subsequently stimulating the production of other pro-inflammatory cytokines such as TNF-α, monocyte chemoattractant protein 1 (MCP-1) and IL-6 (Minn et al., 2005, Filhoulaud et al., 2019, Maedler et al., 2002). These pro-inflammatory cytokines promote β-cell dedifferentiation through the downregulation of transcription factor forkhead box protein O1 (FOXO1) in both human and mice islets (Nordmann et al., 2017). Likewise, FFA can also induce the expression of IL-1β in islets (Böni-Schnetzler et al., 2009). It can up-regulate the expression of pro-inflammatory genes, either directly *via* binding and activation of toll-like receptors (TLR), or indirectly through phosphorylation of the serine residues of insulin receptor substrate 1 (IRS-1) through the JNK pathway (Shi et al., 2006, Hage Hassan et al., 2016).

Furthermore, increased production and release of cytokines IL-6, IL-8 and macrophage inflammatory protein-1α (MIP-1α) in response to chronic hyperglycaemia, have been associated with promotion of increased migration of monocytes and neutrophils to islets (Ehses et al., 2007). Moreover, immuno-histochemical studies conducted on islets from T2D patients, HF-fed C57BL/6 mice and other rodent models of diabetes such as the GK rat and *db/db* mice,

observed an increase in macrophage numbers, which shifted from an anti-inflammatory M2 to a pro-inflammatory M1-phenotype (Ehses et al., 2007, Cucak et al., 2014). The increased inflammatory response contributes to the development of fibrosis in islets, leading to reduced β-cell mass and function (Homo-Delarche et al., 2006).

1.8 Mouse models of diabetes

The laboratory mouse (*Mus musculus)* plays a central role in the study of biochemical and pathophysiological features of human diseases and its complications. It is evolutionarily more closely related to humans than any other model organisms besides primates, while also being cheap and convenient to maintain in research institutions due to its small size. Despite their biological similarity, mice have two insulin genes (*Ins 1* and *Ins2*), unlike humans with only one insulin gene. Murine *Ins1* is expressed predominantly in the pancreatic β-cells, whereas *Ins2* is expressed in both the β-cells and thymus (Wentworth et al., 1986). The structure of the islets including localization of β-cells also varies between mice and humans, as previously discussed in section 1.3. Furthermore, human islets were observed to be resistant to toxins and cytotoxic agents that were detrimental to mice islets (Tyrberg et al., 2001, Eizirik et al., 1994), and the human β-cell transcriptome was found to be dissimilar to mice and rat β-cell transcriptome (Benner et al., 2014). However, mice are still increasingly used for islet experiments in diabetes studies, since human islets can only be obtained post-mortem, which are difficult to acquire. Therefore, many islets studies continue to be performed on mice islets and findings are later validated in humans.

Publication of the mouse genome sequence, together with advances in precise genetic manipulating techniques like CRISPR/Cas9, has further propelled the use of mice models to study the mechanistic functions of candidate genes in the pathophysiology of diabetes

(Waterston et al., 2002). Numerous mouse models were generated to study T2D, ranging from monogenic obese mice that develop diabetes such as Lep $^{ob/ob}$ mice with leptin deficiency and the Lepr $^{db/db}$ mice with leptin receptor deficiency (Skowronski et al., 2017, Do et al., 2016); as well as polygenic diabetes in the C57BL/6J diet-induced obesity (DIO) mice and New Zealand Obese (NZO) mice (Evans et al., 2014, Schwenk et al., 2015).

1.8.1 Non-obese diabetic (NOD) mouse

The non-obese diabetic (NOD) mouse is the most widely used model for the study of autoimmune T1D (Pearson et al., 2016a). The development of the NOD mice colony initiated with the identification of a female mouse in the inbred cataract Shionogi mouse (CTS) colony, that exhibited polyuria, glycosuria and weight loss, and died of ketoacidosis without producing any offspring (Makino et al., 1980). The NOD mouse colony was established many years later, through selective breeding of mice positive for urine glucose. At the 20th generation, the presence of intra- and peri-islet lymphocyte infiltration was described for the first time in the pancreas of these mice, with an incidence of around 80% in females and 20% in males by 30 weeks of age (Makino et al., 1980). With successful colony establishment, this NOD colony (also known as NOD/Shi) was subsequently distributed to other countries for research purposes, including South Korea, USA and Australia. The colony in USA was first established in the University of California at Los Angeles (UCLA), which was further expanded by Prof Linda Wicker, creating the NOD/MrkTac colony from TACONIC Biosciences. These mice had a diabetes incidence of 60% in females at 12 weeks of age and 40% in males at 24 weeks of age.

Another widely used NOD sub-strain outside Japan is the NOD/ShiLtJ (formerly NOD/LtJ) mice from Jackson Laboratories in USA, which has a diabetes incidence of 90% in females and 54% in males by 30 weeks of age. The differences in diabetes occurrence between the NOD

colonies distributed around the world led to the recognition that environmental factors such as diet, animal husbandry and gut microbiota play a role on the incidence of diabetes development. Further mechanistic explanation was provided by Simecek *et al*, reporting that continuous inbreeding over 10 generations of NOD mice leads to genetic divergence, therefore promoting significant differences in the diabetic phenotype among the sub-strains, compared to the original NOD/Shi colony (Simecek et al., 2015).

Similar to human T1D, autoimmune diabetes in the NOD mice was associated with insulitis and autoantibodies directed against pancreatic islet antigens (Carrero et al., 2013). Chronological development of islet autoimmunity in NOD mice and its transcriptional signature was further reported by Carrero *et al* and was divided into three phases (Carrero et al., 2013). The initial alteration described was the presence of infiltrating myeloid cells, even in developing islets at 4 weeks of age, and Type I interferon (IFN) signature from 4-6 weeks of age. This was followed by T-cell activation between 8-12 weeks of age, which was also marked by leukocyte islet infiltration and unsynchronized spreading of insulitis in the pancreas. At the last stage of the disease, a distinct NF-κB signature was observed along with β-cell destruction and loss of β-cell mass and circulating insulin levels (Carrero et al., 2013).

Further studies also revealed that development of T1D in the NOD mice is regulated by multiple genetic polymorphisms, with the strongest genetic determinant found in major histocompatibility complex (MHC) regions. The MHC class II molecules DQ8 and DQ2 in humans, and murine homologue molecule I-Ag^7 on the $H2^{g7}$ (insulin dependent diabetes loci 1: Idd1) MHC haplotype, located on chromosome 17 of the NOD mice, were strongly associated with T1D susceptibility (Ikegami et al., 1995, Concannon et al., 2005). A substitution of proline-aspartic acid (amino acid positions 56 and 57) by histidine-serine in the I-Ag^7 β chain led to binding of the peptides to a negatively charged carboxy terminal, therefore altering the

β-cell peptides presented to CD4+ T-cells, and subsequently triggering the autoimmune attack (Reich et al., 1994, Bhatnagar et al., 2001). These results highlight the role of the $H2^{g7}$ haplotype on the Idd1 locus of NOD mice in the development of autoimmunity, and also suggests potential areas for therapeutic intervention.

1.8.2 Congenic NOD sub-strain: O-NOD^{k} mice

The NOD.BR-$H2^{k}$ mice (abbreviated as the original **O-NOD^{k}**) is a congenic sub-strain of the NOD mice, in which the potent T1D-susceptibility locus, Idd1-$H2^{g7}$ locus of the MHC Class II, has been replaced by the T1D-resistant Idd1-$H2^{k}$ locus. Therefore, the O-NOD^{k} mouse is protected from developing autoimmune diabetes.

This sub-strain was developed in 1993 by Podolin and colleagues, by outcrossing NOD/MrkTac mice from Taconic Farm (Germantown, NY) to the B10.BR/SgSnJ (abbreviated as B10.Br) mice strain from the Jackson Laboratories (Bar Harbor, ME) (Podolin et al., 1993) (Figure 9). The progeny was repeatedly backcrossed to the NOD/MrkTac strain, and future breeders for this congenic strain were selected based on their heterozygosity at the MHC, after detection of class I and II MHC products. After backcrossing the progeny 5 times to the NOD/MrkTac mice, N6 male and female $H2^{k}$ MHC heterozygotes were inter-crossed, and $H2^{k}$ MHC homozygotes progeny were inbred (brother-sister mating) in order to fix the $H2^{k}$ MHC haplotype of the B10.Br strain on the NOD background (Figure 9). Histological examination of pancreatic sections of these mice revealed the presence of peri-vascular and peri-ductal lymphocytic infiltration that developed spontaneously by 7-10 months of age, however, without the development of insulitis or autoimmune T1D (Podolin et al., 1993).

A colony of this NOD^{k} sub-strain developed by Podolin *et al* was maintained by Prof Linda Wicker at Merck Laboratories. Later, breeding pairs were passed on to Prof Chris Goodnow at Stanford, USA in 1995 and maintained by brother-sister mating, before the colony was re-established at the Hugh Ennor Building (HEB) at the Australian National University (ANU) in Canberra, Australia. This NOD^{k} sub-strain was used for various immunological studies for over 10 generations and introduced into the Nolan laboratory 10 years ago, henceforth abbreviated as the original **O-NOD^{k}** mice colony.

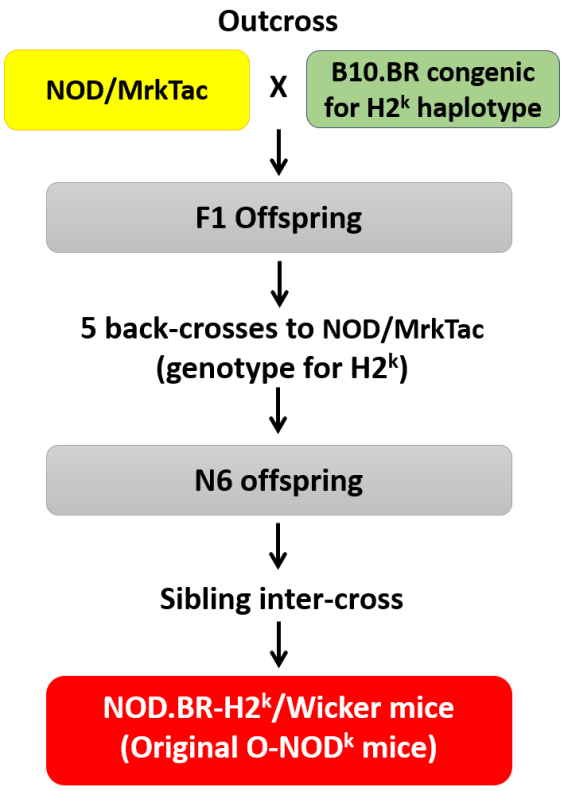

Figure 9: Creation of the T1D-resistant O-NOD^{k} mice colony. NOD/MrkTac mice were outcrossed with B10.BR mice which are congenic for the H2^{k} haplotype. Offspring that were heterozygous for the H2^{k} haplotype were backcrossed five times to the NOD/MrkTac mice. In the N6 offspring, the potent T1D-susceptibility locus, Idd1-H2^{g7} locus of the MHC Class II of the NOD/MrkTac mice had been replaced by the T1D-resistant Idd1-H2^{k} locus of the B10.Br mice. The offspring were then intercrossed (brother-sister mating) to generate the NOD.BR-H2^{k}/Wicker mice which were T1D-resistant. This colony was re-established at the Australian National University (ANU) in Canberra and nicknamed as the original or O-NOD^{k} mice colony.

1.8.3 Transgenic mice for β-cell dysfunction: NOD^{k}.insHEL mice

A previous study conducted in the Nolan laboratory using the O-NOD^{k} mice showed that overexpression of the hen egg lysozyme (HEL) protein under the insulin promoter in these mice leads to the development of non-immune mediated diabetes, therefore indicating the presence of β-cell fragility (Dooley et al., 2016). This study gave rise to the hypothesis that environmental factors such as nutrient stress could also be inducing a similar dysfunction in the β-cells. Subsequent results obtained from the Nolan group (data unpublished) showed that male O-NOD^{k} mice (not expressing HEL) subjected to 16 weeks of HF diet, develop obesity, glucose intolerance, hyperinsulinemia and T2D.

A comparative longitudinal HF-feeding study between the O-NOD^{k} mice and C57BL/10 mice carrying the same H2^{k} haplotype (B10^{k}) have also suggested that the hyper-responsiveness of O-NOD^{k} β-cells to nutrient excess, may be rendering them vulnerable to β-cell injury, while the low responsiveness of the B10^{k} β-cells may have a protective function against loss of β-cell mass (data unpublished). These observations further supported the premise that non-immune islet susceptibility factors may be contributing to the pathogenesis of both T1D and T2D. However, during the course of this study, refreshment of the O-NOD^{k} mice colony was conducted which led to interesting observations.

1.8.4 Refreshment of the O-NOD^{k} mice colony: RF-NOD^{k} mice

Mice colony refreshment was performed by outcrossing the O-NOD^{k} mice with NOD/ShiLtJ mice, sourced from the Animal Resource Centre in Perth, Australia (Figure 10). The progeny of these breeder mice was genotyped at each step to ensure that they carried the H2^{k} haplotype, and were backcrossed twice to the NOD/ShiLtJ mice. N2 male and female offspring carrying the H2^{k} haplotype were then inter-crossed (brother-sister mating) two times to generate the new

refreshed mice colony, henceforth referred to as RF-NOD^{k} mice. Subsequent phenotypic characterization of these RF-NOD^{k} mice was conducted to confirm the presence of the diabetic phenotype. Remarkably, it was observed that the new colony of RF-NOD^{k} mice had lower weight gain than the O-NOD^{k} mice, and were unexpectedly resistant to the development of diet-induced T2D. Therefore, through this process, our laboratory obtained two different NOD^{k} sub-strains: the O-NOD^{k} mice (diabetes-prone) and the RF-NOD^{k} mice (diabetes-resistant).

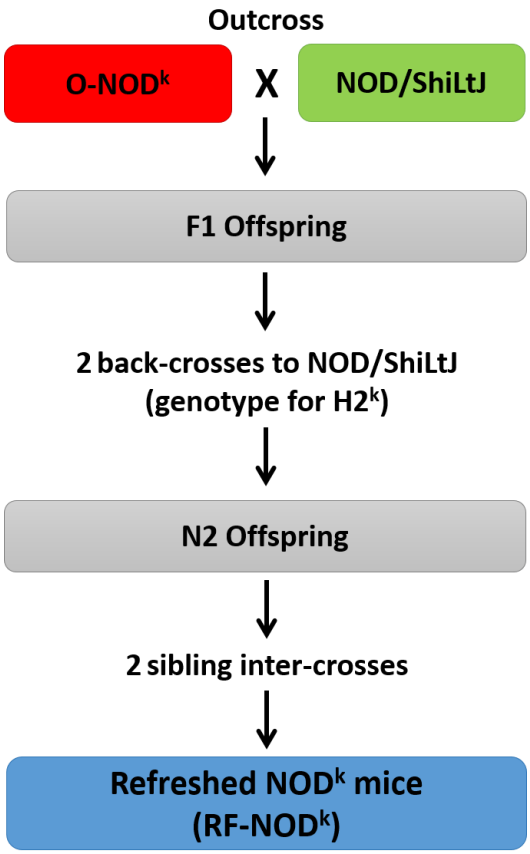

Figure 10: Creation of the HF-diet induced T2D-resistant RF-NOD^k mice colony. O-NOD^k mice were outcrossed with NOD/ShiLtJ mice from the Animal Resource Centre in Perth, Australia. Offspring that were heterozygous for the H2^k haplotype were backcrossed two time to the NOD/ShiLtJ mice. The N2 offspring were inter-crossed (brother-sister mating) to create the refreshed or RF-NOD^k mice colony.

1.9 Rationale and aims of the study

Since both O-NOD^k and RF-NOD^k mice were maintained in the same facility and under identical environmental conditions (*i.e.* temperature, air quality, HF diet composition and housing) during the entire study period, the diabetic phenotype disparities observed between the two sub-strains of mice are possibly genetic in origin.

Therefore, we hypothesized that O-NOD^k mice have a very strong diabetes susceptibility factor within its genome, which is not present in the RF-NOD^k mice. This genetic factor could be increasing the vulnerability of β-cells to nutrient-induced injury and failure.

The **overall aim** of this thesis was to determine the factors causing diabetes susceptibility in the O-NOD^k mice when stressed by HF diet.

The two specific aims of the study were:

1. To characterize in detail the metabolic phenotype of the diabetes prone O-NOD^k mice compared to the diabetes resistant RF-NOD^k mice.

   A long-term study of 24 weeks was designed for phenotypic characterization of both mice sub-strains when challenged by HF-feeding. Determination of *in vivo* β-cell function, blood chemistry and histological analysis of the pancreas was also conducted in O-NOD^k and RF-NOD^k mice, after prolonged HF-feeding. Furthermore, *in vitro* β-cell function tests were performed on isolated islets in order to ascertain differences in GSIS, in the presence of fatty acids and IBMX, which could be associated with the diabetes phenotype in the O-NOD^k mice.

2. To determine the genetic cause of diabetes susceptibility in the O-NOD^{k} mice that is absent in the RF-NOD^{k} mice.

   Selective cross-breeding of the two mice sub-strains was performed to establish the inheritance of the genetic factor causing the diabetes phenotype in O-NOD^{k} mice. Additionally, whole genome sequencing and islet RNA sequencing was conducted in the O-NOD^{k} and RF-NOD^{k} mice, to define the role of potential candidate genes in the development of diabetes in the HF-fed O-NOD^{k} mice.

Chapter 2
Materials and Methods

This chapter describes the research design of the study including animal sources and housing, experimental set up and procedures, reagents and kits used for data collection and statistical analysis.

2.1 Materials

Table 2: List of reagents used in this study

Reagent	Cat #	Manufacturer	Location
Absolute ethanol	214	Univar, Ajax Fine Chem	NSW, Australia
Anti-insulin antibody	ML1013-K	Millipore-Linco	Billerica, USA
Bovine serum albumin (RIA grade)	A7888	Sigma Aldrich, Merck	Darmstadt, Germany
Bovine serum albumin (BSA) Heat shock fraction V, pH7	A7906	Sigma Aldrich, Merck	Darmstadt, Germany
Bovine serum albumin (BSA) Fatty acid free	A6003	Sigma Aldrich, Merck	Darmstadt, Germany
Calcium Chloride ($CaCl_2$)	C7902	Sigma Aldrich, Merck	Darmstadt, Germany
3,3'-Diaminobenzidine (DAB)	D4293	Sigma Aldrich, Merck	Darmstadt, Germany
DNase I (Grade II from bovine pancreas)	10104159001	Roche	IN, USA
Ethylenediaminotetracetic acid (EDTA)	E9884	Sigma Aldrich, Merck	Darmstadt, Germany
5% Fetal bovine serum (FBS)	10082-147	Gibco, Life Technologies Corp	NY, USA
Glucose	G8270	Sigma Aldrich, Merck	Darmstadt, Germany
Glutamine	G3126	Sigma Aldrich, Merck	Darmstadt, Germany

Glycerol	G7793	Sigma Aldrich, Merck	Darmstadt, Germany
Free glycerol reagent	F6428	Sigma Aldrich, Merck	Darmstadt, Germany
Goat anti-guinea pig immunoglobulin G	GAGP.2.0-50mL	Monash Institute	VIC, Australia
Guinea pig anti-rat insulin serum	ML1013K	Abacus, Millipore	MA, USA
Guinea pig serum	NGPS.5mL	Monash Institute	VIC, Australia
Hanks Balanced Salt Solution (HBSS)	14065-056	Gibco, Invitrogen	NY, USA
Harris Haematoxylin solution	HHX2.5L	POCD, Artarmon	NSW, Australia
4-*(2-hydroxyethyl)-1*-piperazineethanesulfonic acid (HEPES)	H4034	Sigma Aldrich, Merck	Darmstadt, Germany
Histopaque 1077	10771	Sigma Aldrich, Merck	Darmstadt, Germany
Histopaque 1119	11191	Sigma Aldrich, Merck	Darmstadt, Germany
Hydrogen peroxide (H_2O_2)	23620.292	VWR Chemicals	France
^{125}I- labelled insulin	MP9011	Abacus, Millipore	MA, USA
Purified human insulin	I-9278	Sigma Aldrich, Merck	Darmstadt, Germany
Ketamine	Ilium Ketamine	Troy laboratories	NSW, Australia
Liberase	05-401-020-001	Roche	IN, USA
Magnesium Chloride ($MgCl_2$)	M9272	Sigma Aldrich, Merck	Darmstadt, Germany
Magnesium Sulphate ($MgSO_4.7H_2O$)	230391	Sigma Aldrich, Merck	Darmstadt, Germany
Medite	41-4012-00	Pertex	Germany

2-mercaptoethanol	M6250	Sigma Aldrich, Merck	Darmstadt, Germany
Milli-Q water	G8270	Sigma Aldrich, Merck	Darmstadt, Germany
10% neutral buffered formalin	ANBFB	Biostain	VIC, Australia
Penicillin/streptomycin	15140-122	Invitrogen	NY, USA
Phosphate buffer solution (PBS)	09-8912-100	Astral Scientific	NSW, Australia
Polyethylene glycol (PEG)	89510	Sigma Aldrich, Merck	Darmstadt, Germany
Polygonal Guinea–pig anti-insulin	A0564	Dako	Glostrup, Denmark
Polygonal rabbit anti- guinea pig horseradish peroxidase	P0141	Dako	Glostrup, Denmark
Potassium Chloride (KCl)	P5405	Sigma Aldrich, Merck	Darmstadt, Germany
Potassium Hydroxide (KOH)	P5958	Sigma Aldrich, Merck	Darmstadt, Germany
RNaseZap	AM9780	Thermofisher Scientific	MA, USA
Roswell Park Memorial Institute (RPMI) medium	11879-020	Thermofisher Scientific	MA, USA
Sodium bicarbonate ($NaHCO_3$)	S3817	Sigma Aldrich, Merck	Darmstadt, Germany
Sodium Chloride (NaCl)	S5886	Sigma Aldrich, Merck	Darmstadt, Germany
Sodium dodecyl sulfate (SDS)	L6026	Sigma Aldrich, Merck	Darmstadt, Germany
Sodium oleate	S1120	Nu-Chek-Prep	MN, USA
Sodium palmitate	S1109	Nu-Chek-Prep	MN, USA
Sodium phosphate (NaH_2PO_4)	S5011	Sigma Aldrich, Merck	Darmstadt, Germany

Sodium pyruvate	P2256	Sigma Aldrich, Merck	Darmstadt, Germany
Thimerosal	T5125	Sigma Aldrich, Merck	Darmstadt, Germany
TG reagent	T2449	Sigma Aldrich, Merck	Darmstadt, Germany
Tris	AM9856	Thermofisher Scientific	MA, USA
Xylazine	Ilium Xylazine	Troy laboratories	NSW, Australia
Xylene	534056	Sigma Aldrich, Merck	Darmstadt, Germany

2.2 Mice breeding and maintenance

NOD.BR-H2^k/ Wicker.ANU mice, abbreviated as the original NOD^k or O-NODk mice for this project, were obtained from Prof. Christopher Goodnow's laboratory at the John Curtin School of Medical Research (JCSMR) at the Australian National University (ANU). The refreshed-NOD^k mice (RF-NOD^k mice) were created by crossing female O-NOD^k mice with male NOD.Shi/LtJ mice (as previously described in Chapter 1).

All mice were housed at The Canberra Hospital (TCH) and Hugh Ennor building (HEB) at ANU, where they were bred and maintained under specific pathogen-free conditions in an artificial 12-hour light/dark cycle. Mice were kept in individually ventilated cages (IVCs) with a maximum of 5 mice per cage, in a temperature controlled room of 21-24^{o}C with 40-60% humidity. Cages were provided with standard laboratory normal chow (NC) diet (59.8% carbohydrate, 20.0% protein and 5.4% fat by weight; energy content 12MJ/g) supplied by Gordon's Specialty Stockfeed (NSW, Australia) and autoclaved tap water.

O-NOD^{k} and RF-NOD^{k} mice were placed on continuous mating to produce litters, which were weaned at 3 weeks of age on a NC diet. According to the experimental design of each study, male O-NOD^{k} and RF-NOD^{k} mice were randomly distributed (at 4 to 8 weeks of age), into two diet groups- NC diet (5.4% fat), or a HF diet (41% carbohydrate, 22.6% protein, 23% fat by weight; energy content 20MJ/kg; SF03-020) supplied by Specialty Feeds (Glen Forrest, Western Australia), until the end of the study period. The HF diet used in this study is an atherogenic diet with a lower fat content and 0.19% cholesterol than commonly used in rodent studies (40-60%) (Speakman, 2019). However, this diet is physiologically similar to human diet, and is associated with the development of T2D and NAFLD as previously described (Liang et al., 2018, Farrell et al., 2014).

All animal procedures were approved by the ANU Animal Ethics Committee under the protocols A2014/14 and A2017/26. All animals received care in compliance with the guidelines prescribed by this committee and the National Health and Medical Research Council, Australian Code for the Care and Use of Animals for Scientific Purposes (NHMRC, 2013).

2.3 Phenotypic characterization of the mice models

2.3.1 Mice physiological studies

2.3.1.1 Fortnightly body weight and blood glucose monitoring

Body weight was recorded every fortnight using an electronic balance (Fx-200i, A&D Company Ltd, South Korea), between 9-10AM. At the same time, non-fasting blood glucose levels were also assessed in conscious mice. Blood glucose was measured using a glucometer (StatStrip Xpress™, Nova Biomedical, Flintshire, UK), through analysis of 5 µL of blood

collected from a small incision made in the lateral tail vein of restrained mouse, according to manufacturer's recommendations.

2.3.1.2 Glucose tolerance testing

Mice were subjected to an intraperitoneal glucose tolerance test (ipGTT) for identification of glucose intolerance. O-NOD^{k} and RF-NOD^{k} mice were fasted for 4 (8AM -12PM) or 6 hours (8AM -2PM), according to experimental design. Body weights were measured to calculate the glucose injection dose (1 g glucose/kg body weight) of 12.5% glucose solution. Fasting blood was collected from a small incision at the lateral tail vein into microtubes containing 10 µL of 0.5M EDTA for plasma separation.

Blood glucose (5 µL) was determined at time 0, and 5, 15, 30, 60, 90 and 120 minutes post glucose injection. Additional blood collection (60 µL) at 15 and 90 minutes was also performed for measurement of plasma insulin. At the end of the experiment, all mice were returned to their specific cages. The plasma samples collected were stored in a -80^{o}C freezer for insulin radioimmunoassay measurements. The respective area under the curve (AUC) for glucose (time 0-120 minutes) was calculated using the trapezoid method.

2.3.2 Euthanasia and tissue harvesting

2.3.2.1 Anaesthesia and cardiac blood sampling

At the end of the experimental period, a final non-fasting tail blood collection was withdrawn from conscious mice into EDTA-rinsed microtubes containing 10 µL of 0.5M EDTA solution. After centrifugation (6000 rpm, 15 minutes, 4^{o}C), plasma samples obtained were transferred to

a new set of tubes and stored in a -80^{o}C freezer for further blood chemistry analysis. Mice were subsequently anaesthetized with a mixed solution of ketamine (20 mg/mL) and xylazine (100 mg/mL), prepared in saline solution (ratio 1:1:8, v:v:v, respectively), administered intra-peritoneally (10 µL per gram body weight). After loss of pedal sensitivity, cardiac blood sample was collected through cardiac puncture and was immediately transferred into a 4 mL BD Vacutainer (Cat#366164, BD UK, Plymouth, UK), and kept on ice until later centrifugation (6000 rpm, 15 minutes, 4^{o}C). Plasma collected from these samples were then stored in a -80^{o}C freezer for further analysis.

2.3.2.2 Tissue collection

Following cervical dislocation of the mice, the abdominal cavity was cut through and opened widely. The pancreas was carefully dissected from the small and large intestines, and from its attachments to the duodenum and spleen. All visible fat and lymph nodes were removed under a dissecting microscope (Stemi 1000, Carl Zeiss, Germany). Other tissues including liver, gastrocnemius muscle (right leg) and adipose tissue (subcutaneous, epididymal and brown adipose tissue) were also dissected. All tissues were weighed on an electronic scale (FX-200i, A&D company Ltd, South Korea).

Whole pancreas and a small portion of the liver were fixed in 10% neutral buffered formalin solution for 18hours, washed in 70% ethanol and later transported to the ACT Pathology department at TCH for paraffin embedding. The remaining parts of the liver (bigger lobe) were cut into small sections and snap-frozen in 7 mL screw cap tubes. Epididymal and subcutaneous fat pads obtained from the right side of the mouse, brown adipose tissue (BAT) dissected from the dorsal adipose tissue, behind the neck of the mouse, and gastrocnemius muscle from the right leg of the mouse were also snap-frozen in 7 mL screw cap tubes and stored in a -80^{o}C freezer for future analyses.

2.3.3 Plasma chemistry analysis

2.3.3.1 Quantification of plasma insulin by radioimmunoassay (RIA)

Quantification of tail plasma insulin levels was determined by radioimmunoassay (RIA). This protocol involves the incubation of a fixed concentration of radio-labelled tracer antigen (^{125}I-labelled insulin) with a known amount of anti-insulin antibody, so that there is limited antigen binding sites on the antibody. Therefore, when plasma sample containing unknown amounts of unlabeled insulin is added, it generates a competition between labelled and unlabeled insulin for binding sites of the antibody. Thus, an increased concentration of unlabeled antigen decreases the ratio of antibody-bound tracer to free tracer and *vice versa.* Once the free tracer is separated from this system by centrifugation, the remaining fraction containing antibody-bound tracer can be quantified and used for indirect determination of insulin concentration in test samples.

Briefly, a standard curve was generated using purified human insulin diluted in bovine serum albumin (BSA)-sodium phosphate buffer (see Appendix for preparation) at concentrations of 0, 0.0625, 0.125, 0.25, 0.5, 1, 2, 4, 8 and 16 ng/mL. 50 µL of standards and plasma samples previously diluted in BSA-sodium phosphate buffer, were distributed into polypropylene tubes (Cat# Z376795, Sigma Aldrich, Merck, Darmstadt, Germany) in duplicates. Addition of 50 µL of ^{125}I insulin tracer (re-suspended in 35 mL of BSA-Sodium Phosphate buffer) at <0.143 µCi/mL and 50 µL of diluted guinea pig anti-rat insulin serum to these tubes was followed by overnight incubation at 4^{o}C. Four duplicate tubes containing 50 µL of tracer alone were prepared without the addition of guinea pig anti-rat insulin serum to determine the total count and non-specific binding, respectively, required for data analysis.

On the next day, 500 µL of secondary antibody mixture consisting of 335 µL of polyethylene glycol (PEG)- sodium phosphate buffer (see Appendix for preparation), 85 µL BSA-sodium

phosphate buffer, 40 µL of (1:5 diluted in PEG-sodium phosphate buffer) goat anti-guinea pig immunoglobulin G and 40 µL of (0.057 mg/mL diluted in PEG-sodium phosphate buffer) guinea pig serum were added to all tubes (except total count tubes) and incubated for 2 hours at 4^{o}C. All tubes, except total count tubes, were centrifuged at 2500 rpm for 15 minutes at 4^{o}C, and then inverted to discard the supernatant to remove any unbound tracer, thus separating the antibody-bound tracer from the free tracer. The quantity of unlabeled antigen (plasma insulin) was determined indirectly by measuring the radioactivity of the retained pellets by counting it at 1 minute/tube using the γ-counter (2480 Automatic gamma counter, WIZARD^{2}®, Perkin Elmer, MA, USA).

2.3.3.2 Quantification of plasma proinsulin

The proinsulin ELISA kit, (Cat# 8-PINMS-E01, Alpco, NH, USA) was used to measure plasma proinsulin levels from non-fasting tail blood collected at time of harvesting, according to manufacturer's instructions. This kit is based on a sandwich type immunoassay. The intra-assay percentage coefficient of variation (CV%) varied from 4-6.9% and the inter-assay CV% was between 6-9.7%, with respective acceptable range as per the provided Certificate of analysis.

In brief, lyophilized high and low controls and standards were reconstituted in deionized water according to the Certificate of Analysis provided by the kit, to create a standard curve at concentrations of 0, 4, 15, 100 and 300 pM proinsulin. 10 µL of standards, controls and mouse plasma samples were added to the antibody-coated 96 well plate followed by addition of 100 µL of a peroxidase conjugated anti-proinsulin antibody. The plate was then incubated for 2 hours at room temperature with constant shaking at 720 rpm on a micro-plate shaker. After washing the plate (6x) with wash buffer provided by the kit, the plate was incubated at room temperature for 30 minutes with shaking at 720 rpm with 100 µL of 3,3',5,5'-

Tetramethylbenzidine (TMB) substrate. 100 µL of stop solution was then added to stop the reaction between the TMB and peroxidase, giving it a colorimetric end point.

The absorbance of the plate was measured at both 450 nm and 620 nm using the Spectrophotometer (Multitaskin Ascent, 354 Thermo Labsystems, Finland). Absorbance values at 620 nm was subtracted from the absorbance values obtained at 450 nm to remove background absorbance. After correction for blanks, a standard curve was plotted with the average measurements of each standard sample against its known concentration. An XY graph was created based on the resulting values and the equation generated was used to determine the proinsulin concentration of the unknown samples.

2.3.3.3 Quantification of plasma C-peptide

Quantitative determination of tail plasma C-peptide levels obtained at harvesting was performed with a sandwich type immunoassay, using a commercial ELISA kit (Cat #80-CPTMS-E01, Alpco, NH, USA) according to manufacturer's instructions. The intra-assay CV% varied from 2.87-4.5% and the inter-assay CV% was between 6.6-8.7%, with respective acceptable results range described in the Certificate of analysis provided by the manufacturer.

In brief, lyophilized standards provided by the kit were reconstituted in deionized Milli-Q water according to the Certificate of Analysis provided by the kit, to generate a standard curve containing 0, 60, 250, 750, 1500 and 3000 pM of C-peptide. Lyophilized low and high controls were also provided by the manufacturer. 10 µL of standards, controls and plasma samples were distributed in duplicates wells of a 96-well microplate provided by the kit. 100 µL of peroxidase conjugated anti-C-peptide antibody previously prepared, was added in each well. The plate was then incubated at room temperature for 2 hours with constant shaking at 720 rpm on a micro-plate reader (Multitaskin Ascent, 354 Thermo Labsystems, Finland). After washing the plate

(3x) with wash buffer provided by the kit, the bound conjugate was detected by its reaction with 100 µL of TMB substrate. After 10 minutes of incubation at room temperature with constant shaking at 720 rpm, a colorimetric pigment developed. This reaction was then stopped by addition of 100 µL of stop solution, giving it a colorimetric end point.

The absorbance was then measured at 450 nm using the Spectrophotometer (Multitaskin Ascent, 354 Thermo Labsystems, Finland). After background subtraction, a standard curve was plotted for average 450 nm measurements of each standard against its known concentration to generate an XY graph. The equation obtained based on this graph was then used for determination of the C-peptide concentration of each unknown sample.

2.3.3.4 Quantification of plasma Triacylglyceride (TG)

Plasma TG levels were measured from non-fasting plasma collected from tail blood at the time of harvesting using a Triglyceride Determination kit (Cat# 432-40201, Wako, Osaka, Japan) according to manufacturer's instructions. This TG colorimetric kit measures the glycerol released from enzymatic hydrolysis of TG into FFA and glycerol by lipoprotein lipase. A standard curve containing 0, 1.5, 3, 6, 9, 12, 15 and 18 µg/µL of glycerol was produced. 10 µL of samples, standards and blank were distributed in duplicates in a 96-well microplate (IWAKI, Cat# 3860-96, Osaka, Japan). 150 µL of freshly prepared Working Reagent A was added to per well and the microplate was incubated at 37^{o}C for 10 minutes. The plate was allowed to cool at room temperature for 5 minutes and its absorbance was read at 600 nm using the FLUOstar optima spectrophotometer (Serial # 413-2046, BMG Labtech, NC, USA). The absorbance values of the blanks at 600 nm was subtracted from each well and a standard curve was plotted using the measurements of the standards at 600 nm against their known concentrations. The concentration of TG for each unknown sample was determined based on this standard curve.

2.3.3.5 Quantification of plasma non-esterified fatty acids (NEFA)

Circulating plasma NEFA levels were measured using the Wako NEFA C kit (Cat# 279-75401, Wako Chemicals, Osaka, Japan) as per manufacturer's instructions, in non-fasting tail blood plasma collected at the time of harvest. During NEFA measurement, acyl-CoA synthase converts circulating NEFA into acetyl-CoA, AMP and pyrophosphoric acid in the presence of coenzyme A and ATP. Addition of acyl-CoA oxidase then oxidizes the acetyl-CoA produced, and generates hydrogen peroxide. This allows oxidative condensation of *3-methy-N-ethyl-N* (β-hydroxyethyl)-aniline with 4-aminoantipyrine into a purple colored colorimetric end-product, which is measured at 540 nm.

In brief, 1 mmol/L of the standard solution provided by the kit was used to create standard concentrations of 0, 0.125, 0.25, 0.5, 1, 2 and 3 mmol/L. 2.5 µL of the standards and plasma samples were pipetted in duplicates into a 96-well plates (Cat#167008, Nunc, Thermo Fischer Scientific, Roskilde, Denmark). 50 µL of Reagent A (prepared by combining 1 bottle of color A with 10 mL of solvent A) was added to each well and incubated at 37^{o}C for 10 minutes. Afterwards, 100 µL of Reagent B (prepared by mixing 1 bottle of color B with 20 mL of solvent B) was added to each well and incubated at 37^{o}C for further 10 minutes. The plate was then allowed to cool for 5 minutes at room temperature.

Absorbance was read at 540 nm using the FluoStar Optima Spectrophotometer (Serial #413-2046, BMG Labtech, NC, USA). Absorbance at 540 nm was corrected by subtracting the absorbance values obtained in the blank wells. A standard curve was plotted using the measurements of the standards against their known concentrations, and NEFA concentration of the unknown samples were determined according to this standard curve.

2.3.4 Quantification of hepatic triacylglyceride (TG) content

Hepatic TG content was determined by measurement of the glycerol released from TG hydrolysis, promoted by lipoprotein lipase action.

Briefly, 500 µL of 0.5 M KOH prepared in ethanol (see appendix for preparation) was added to 40-50 mg of liver tissue and homogenized for 10 seconds in a 2 mL microtube (Cat# 34127-3317, Edwards Instruments Co, USA) using a tissue homogenizer (Tissue Tearor, Model 985370, 5000 to 32,000 rpm speed, BioSpec products Inc., OK, USA). This was followed by incubation in a 70^{o}C water bath (Ratek shaking water bath, VIC, Australia) for 20 minutes, followed by cooling at room temperature (20-25^{o}C) for 10 minutes. 1 mL of 0.15 M $MgSO_4$ solution (see Appendix for preparation) was added to each sample to solubilize the lipids. A blank sample containing 500 µL of 0.5 M KOH and 1 mL of 0.15 M $MgSO_4$ was also prepared.

All samples were briefly vortexed (Ratek Vortex mixer, VIC, Australia) and centrifuged at 4750 rpm (Rotor# SX4750, Allegra®X- 15R centrifuge, Beckman Coulter, CA, USA) for 5 minutes at 4^{o}C. The supernatant was then transferred into a new set of 2 mL microtubes (Cat# 34127-3317, Edwards Instruments Co, USA). A Triglyceride Determination kit (Cat# TR0100, Sigma Aldrich, Merck, Darmstadt, Germany) was used to measure TG according to manufacturer's instructions. A standard curve of 0, 0.052, 0.104, 0.156, 0.208 and 0.26 g/L of glycerol was generated. 10 µL of samples, standards and blank were distributed in duplicates in a 96-well microplate (IWAKI, Cat# 3860-96, Osaka, Japan). 160 µL of freshly prepared free glycerol Reagent A) was added per well and incubated at room temperature for 15 minutes. 40 µL of TG Reagent B was then added per well, and followed by another incubation at room temperature for another 15 minutes. The microplate was then measured for its absorbance at 540 nm using the FLUOstar optima spectrophotometer (BMG Labtech microplate reader, VIC, Australia).

A standard curve was constructed using the absorbance values obtained against the known values of the glycerol standards. Absorbance values corresponding to the blanks were subtracted from all samples and an XY scatter graph was created to determine trendline and trendline regression. Glycerol values were calculated based on the linear regression equation generated. Glycerol values were normalized to their corresponding liver tissue weights to obtain total glycerol mg/g tissue, which was then converted to total triacylglycerides by multiplying by the factor value of 9.62, which is the ratio between triolein (MW= 885) and glycerol (MW= 92) molecular weights.

2.3.5 Histological analysis of the pancreas

2.3.5.1 Haematoxylin and eosin (H&E) staining and scoring

Paraffin embedded pancreas were sectioned into 4 µm thick sections and stained with haematoxylin & eosin (H&E) by the ACT Pathology department at TCH, according to their standard laboratory protocol. H&E stained slides were then scanned using an Axio Scan.Z1 slide scanner (Carl Zeiss) at 20x magnification or analyzed under microscope. Histological analysis of blinded sections was also performed by an experienced pathologist Prof Jane Dahlstrom using predetermined rating scales. One section each was scored for islet morphology, presence of exocrine pancreas and islet inflammation, pancreatic fat deposition and islet endocrine cell apoptosis were evaluated as detailed in the scoring sheet (Appendix-Table 1).

2.3.5.2 Insulin Immunohistochemistry (IHC)

Pancreatic paraffin blocks were cut into 3 non-consecutive sections of 4 µm thickness at distance of 100 µm apart, by ACT Pathology department at TCH. The slides were de-

paraffinised through two washes in xylene solvent and rehydrated in graded ethanol solutions (100, 90 and 70%). The slides were then washed in cold water and immersed in PBS to prevent drying of the slides. In order to reduce background or unspecific staining, slides were blocked in 5% fetal bovine serum/PBS solution for 15 minutes. The slides were then incubated for 1 hour with a primary antibody: (polygonal guinea-pig anti-insulin) (diluted 1:100 in 5% FBS/PBS solution) in a humidified incubation chamber at room temperature.

Unbound primary antibody was removed by washing twice in PBS. Endogenous peroxidase was blocked by 20 minutes incubation with 3% H_2O_2-PBS. Following another wash (2x) in PBS, the slides were stained with a secondary antibody (polygonal rabbit anti-guinea pig horseradish peroxidase) (diluted 1:40 in 5% FBS/PBS solution) for 45 minutes in a humidified incubation chamber at room temperature. Unbound secondary antibody was washed out with PBS (2 minutes, 2x) and slides were stained with 450 μL of DAB (see Appendix for preparation) for exactly 2 minutes for colour development. The horseradish peroxidase in the secondary antibody binds with DAB as a substrate and oxidizes it, producing a brown color. Excess DAB was washed off with PBS (2 minutes, 2x) and tap water (1 minute).

The slides were counterstained with Harris Haemotoxylin solution for 2 minutes and rinsed under running water. They were then immersed in 1% sodium bicarbonate solution for 15 seconds and again washed under tap water. Finally, the slides were dehydrated in graded ethanol solutions (70, 90 and 100%), and incubated in xylene solvent through two washes (2 minutes each). The slides were then cover-slipped using a small amount of Medite.

2.3.5.3 Measurement of β-cell mass

Insulin immune-stained sections were scanned using Axio Scan.Z1 at 20x magnification. Digital images obtained were converted to jpeg format and analyzed on the ImageJ 1.48v

software (Wayne Rasband, National Institute of Health, USA). Any remaining fat tissue and lymph node present in the scanned image was removed using the erase tool. Images were subsequently converted to RGB stack and threshold values adjusted accordingly for identification of exocrine tissue area (0-247) or insulin-stained area (0-165). The scale was calibrated for 0.9133 pixels/μm^2. Total islet area and corresponding β-cell area was individually demarcated and analyzed for each pancreatic section using the drawing and ROI manager tool. The % of β-cell area/ pancreas and β-cell mass were determined in all the 3 levels according to the following equations:

% β-cell area per pancreas = (Total islet area/ total pancreas area) x 100

β-cell mass= (Fractional β-cell area) x (pancreas weight (mg)

2.3.5.4 Islet size distribution

Based on their size, all islets in a single level of the pancreas section were distributed into the following groups: small islets (<499, 500- 2999 and 3000- 8999 μm^2); medium islets (9000- 14,999 and 15,000- 20,999 μm^2) and large islets (21,000- 49,999 and > 50,000 μm^2).

2.3.6 Islet β-cell function assessment *in vitro*

2.3.6.1 Pancreatic islet isolation

Pancreatic islets were isolated by enzymatic digestion of the pancreas followed by density gradient purification. Following euthanization by cervical dislocation, the abdominal cavity of the mouse was widely opened. The common bile duct was located and the ampulla of Vater was clamped to prevent leakage of enzymatic solution into the gut lumen. Excess fat was removed from around the hepato-pancreatic duct with forceps.

A 2 mL enzymatic solution containing HBSS, HEPES, liberase enzyme and DNAse I (refer to Appendix for preparation) was injected into the proximal end of the common bile duct towards the duodenum, using a 30G ½ needle (0.3 x 13 mm, Cat# 304000, BD precision glide™ needle, NJ, USA) and 3 mL syringe (Cat# 302113, BD Biosciences, NJ, USA). The injection of the enzymatic solution promoted subsequent distention of the pancreas, which was then carefully dissected and placed in a Nunclon delta tube (Cat# Z688657, Sigma Aldrich, Merck, Darmstadt, Germany) and kept on ice until digestion.

Digestion was performed in a 37ºC water bath over 16 minutes incubation. Subsequently, the tubes were shaken vigorously by hand for 30 seconds to facilitate digestion. Digestion was stopped by addition of cold HBSS solution (preparation in Appendix) containing 1% BSA-fraction V. The digested tissue was then transferred to a 50 mL centrifuge tube and its volume completed up to 30 mL with HBSS-1% BSA solution, and centrifuged at 1,400 rpm for 3 minutes at 11ºC. The supernatant was decanted into a waste container, pellet was resuspended in 15 mL of HBSS-1% BSA solution, and then filtered through a double layer of gauze (Cat# CGS10NS, BSN Medical, VIC, Australia) into a new 50 mL tube to remove any undigested tissue. The tissue suspension was centrifuged again at 1,400 rpm for 3 minutes at 11ºC and supernatant was discarded.

In order to prepare the Histopaque density gradient for islet purification, pellet was homogenized in 5 mL of Histopaque 1119 by gentle vortexing. The tube was then tilted at a 45º angle and 3 mL of Histopaque 1077, followed by 3 mL of HBSS-1% BSA solution was slowly stratified along the walls of the tube. The gradient was then centrifuged at 2,100 rpm for 20 minutes at 11ºC without braking. Islets contained in the interface were aspirated using a glass Pasteur pipette (Cat# 63A53, Chase Scientific Glass Inc, NY, USA), previously rinsed in 5% BSA-KRBH solution and eluted into a new 50 mL tube. Recovered islets were washed twice in 30 mL HBSS-1% BSA solution. Pelleted islets were finally resuspended in 10 mL of HBSS-

1% BSA solution and transferred into a new sterile petri dish (Cat# 351029, Falcon Corning, NY, USA). Using a 10 µL micropipette, islets were hand-picked under a stereomicroscope (Stemi 1000 microscope, Carl Zeiss, Germany) and transferred into a new dish with 10 mL of HBSS-1% BSA solution.

2.3.6.2 Static insulin secretion

Freshly isolated islets were transferred into a new petri dish containing 10 mL of RPMI-1640 medium complete (see Appendix for media preparation) supplemented by 11 mM glucose and incubated overnight at 37^{o}C with 5% CO_2. On the next day, batches of 8 uniformly sized islets were distributed inside filters placed in 24-well microplates (Cat# 3820-024, Iwaki, Japan) and incubated for 2 hours at 37^{o}C with 5% CO_2, in the presence of 1 mL/well RPMI complete supplemented by 3 mM glucose to reduce their metabolism. Islets were then washed in a KRBH washing buffer (see Appendix for preparation). Thereafter, the islets were pre-incubated in 1 mL/well of KRBH solution containing 3 mM glucose and 0.5% BSA (Cat# A7888) for 40 minutes at 37^{o}C with 5% CO_2.

Following pre-incubation, the islets were washed in KRBH wash buffer and incubated in 1.2 mL/well of KRBH solution supplemented with 3 mM glucose and 1 mL/well of KRBH solution with 16 mM glucose, both in the presence and absence of a 0.25 mM fatty acid (palmitate: oleate, 1:1, v:v) mix for 45 mins at 37^{o}C with 5% CO_2 (refer to Appendix for preparation).

After 5 minutes of incubation, 200 µL of incubation solution from wells with 3 mM glucose was collected in 1.5 mL microtubes for measurement of background insulin secretion. After 45 minutes, plates were immediately placed on ice to stop insulin secretion. Incubation solution from all wells were transferred to 1.5 mL microtubes and stored at -20^{o}C for further quantification of secreted insulin. Islets from respective filters were washed in KRBH solution

and transferred to 7 mL vials (Cat# 58.536, Sarstedt, Germany) containing 1 mL of 75% ethanol acidified with 1.5% hydrochloric acid and stored in a -20ºC freezer. Islet intracellular content was released by sonication (10 times) using an ultrasonic homogenizer at power output 20 and pulser 40 (Omni Ruptor 250, Omni International Inc., GA, USA), which was later quantified using an insulin ultrasensitive kit (Cat# 62IN2PEH, Cisbio Bioassays, Codolet, France).

A similar procedure was carried out for measurements of insulin secretion in response to IBMX. Therefore, after new batches of isolated islets were cultured in an incubation solution of KRBH solution supplemented by 3 mM or 16 mM glucose, both in the presence or absence of 0.1 M IBMX.

2.3.6.3 Islet protein content

Following islet isolation and overnight recovery, batches of 60 islets of homogenous sizes were hand-picked under a stereomicroscope and transferred into a 1.5 mL tube. Islets were washed twice in 1 mL of sterile cold PBS with centrifugation at 1400 rpm for 3 minutes at 4ºC. After removal of supernatant, 50 µL of protein lysis buffer (see Appendix for preparation) was added to the pellet. Samples were sonicated (10 times) using an ultrasonic homogenizer at power output 20 and pulser 40 (Omni Ruptor 250, Omni International Inc., GA, USA). Islet protein content was measured using a commercial protein assay kit (Cat # 23227, Pierce BCA protein assay kit, Thermoscientific, MA, USA) as per manufacturer's instructions.

Briefly, a 10 mg/mL standard stock solution was made using BSA fraction V in protein lysis buffer. This solution was serially diluted in the same buffer to generate a standard curve of concentrations 0, 0.0625, 0.125, 0.25, 0.5, 1 and 2 mg/mL BSA. 10 µL of standards and samples were added to a 96 well plate in duplicates, followed by addition of 200 µL of working reagent (reagent A + reagent B). The plate was incubated at 37ºC for 30 minutes. Plate was then cooled

to room temperature for 5 minutes and any bubbles formed in the wells were removed prior to absorbance reading at 540 nm using a plate reader (Multitaskin Ascent 354, Thermo Labsystems, Finland). Background absorbance value was subtracted from all wells and a standard curve was generated to determine the protein concentration of the samples.

2.3.6.4 Homogeneous time resolved fluorescence (HTRF) insulin assay

Secreted insulin and islet intracellular content obtained in the static GSIS experiments were measured using the insulin ultrasensitive kit (Cat# 62IN2PEH, Cisbio Bioassays, Codolet, France) as per manufacturer's instructions. The limit of detection (LoD) for the kit was 0.005 ng/mL and CV% ranged from 0.2% to 3.4% for the standard curve.

The principle of this kit is based on homogeneous time resolved fluorescence (HTRF) technology, whereby insulin is detected in a sandwich type assay made of a donor monoclonal antibody Europium Cryptate and an acceptor antibody (XL665). These two antibodies bind to insulin and excitation of Europium Cryptate with a light source generates Fluorescence Resonance Energy Transfer (FRET) towards XL665, which causes its fluorescence that can be later measured by a spectrophotometer at 665 nm wavelength. Therefore, the sample can be measured by analyzing the signal intensity, which is directly proportional to the number of insulin-antibody complexes formed in the samples.

In brief, anti-insulin-Europium Cryptate antibody and anti-insulin-XL665 antibody were both reconstituted in 2.5 mL of deionized Milli-Q water and mixed to generate a 20x stock solution. Insulin standard provided by the kit was also reconstituted in Milli Q water as per instructions on the vial to obtain a 500 ng/mL stock solution. The 20x stock solution of the antibodies were further diluted 20x in detection buffer provided by the kit to obtain working antibody solution. To create standards at concentrations 8, 3.2, 1.28, 0.51, 0.20, 0.08 and 0.03 ng/mL, serial

dilutions of the stock 500 ng/mL insulin standard was prepared in GSIS pre-incubation solution. Samples were also diluted in GSIS pre-incubation solution to normalize insulin signals for all groups.

10 µL of standards and diluted samples were distributed in triplicates into wells of a white flat-bottomed 384-well plate (Cat# M3561, Sigma Aldrich, Merck, Darmstadt, Germany), followed by addition of 5 µL each of working antibody solutions of Europium Cryptate and XL665. The plate was then sealed with a MicroAmp optical adhesion film (Cat# 4311971, Applied Biosystems, CA, USA) and incubated overnight (16 hours) at room temperature. After this period, the plate sealer was carefully removed and the FRET signal produced was read using the Infinite M1000Pro spectrophotometer (Serial #1307001801, Tecan, Mannedorf, Switzerland) in two different excitation:emission settings (317:665 nm and 317:620 nm). The ratio of both signal readings (respectively) were then applied to the standard curve equation to obtain insulin values for each sample.

2.4 Genetic characterization of the mice models

2.4.1 Whole genome sequencing

2.4.1.1 DNA extraction and quality assessment

Liver samples obtained from a previous study conducted in our laboratory using HF-fed O-NOD^{k} and RF-NOD^{k} mice (12 and 16 weeks of age, respectively) were used for DNA extraction (n=2/ group). DNA extraction was carried out by the Genomics Research team at the Australian Phenomics Facility and the Biomolecular Resource Facility (BRF) at ANU using the Qiagen QIAsymphony DSP DNA Mini Kit (Cat #937236, Qiagen, Venlo, Netherlands) and automated

QIAsymphony instrument (Cat # 9001297, Qiagen, Venlo, Netherlands), as per manufacturer's instructions. The quality and quantity of the purified genomic DNA was determined by the ratio of its absorbance at 260 nm and 280 nm using a spectrophotometer (Nanodrop One, Thermo Fischer Scientific, MA, USA).

2.4.1.2 Bioinformatics analysis of whole genome sequencing

DNA samples obtained from the 4 mice were send to Macrogen Inc. in South Korea for whole genome sequencing, which created libraries using the TruSeq DNA PCR-free kit (Cat# 20015962, Illumina, CA, USA) and performed sequencing using the Illumina™ HiSeq X Ten sequencing platform (Illumina, CA, USA) using 150 bp paired-end reads. Sequenced data was demultiplexed and converted to FASTQ files using the Illumina bcl2fastq software. The raw data were subsequently send to the BRF at ANU for bioinformatics analysis, which was performed by Dr. Vicky Cho from the ANU Genome Informatics group and Dr. Matt Field from James Cook University.

2.4.1.2.1 Alignment and Quality control

Quality of raw sequencing reads of whole genome sequence were checked with FastQC and were analyzed using a variant detection bioinformatics pipeline previously described elsewhere (Andrews et al., 2012). The output reads were aligned to a reference C57BL/6J mouse genome using the Burrows-Wheeler Aligner (BWA) (Li and Durbin, 2009), generating sorted BAM alignment files of using SAMtools (Li et al., 2009).

PCR duplications and sequence reads of low quality were identified and removed using the Picard (MarkDuplicates) software (Broad Institute, MA, USA) (Ebbert et al., 2016). The genome analysis tool kit (GATK) (version 4.0.5.2, Broad Institute, MA, USA) pipeline was

used for variant calling for each sample individually at first, and then jointly to increase genotyping accuracy, to detect single nucleotide variants (SNVs) as well as small insertions and deletions (indels) (McKenna et al., 2010). Large structural variants were called using Manta (Illumina, CA, USA, available under open source GPLv3 license) (Chen et al., 2016).

2.4.1.2.2 Mouse line specific variants and Loss of Heterozygosity regions

To identify variants specific to mouse lines, the 2 O-NOD^{k} samples were considered as the "diseased/ tumour" samples and were compared to the 2 RF-NOD^{k} samples which were considered as the "normal" samples. SNVs and small indels were called using MuTect2 (Benjamin et al., 2019) and structural variants using Manta (Chen et al., 2016). Loss of heterozygosity (LOH) variants were called using GATK tools (version 4.0.5.2, Broad Institute, MA, USA).

2.4.1.2.3 Annotation and Filtering

All variants were annotated with gene information and filtered with dbSNP, which is the largest public domain database for SNPs (Sherry et al., 2001). Sorts Intolerant from Tolerant (SIFT) (Ng and Henikoff, 2001) was used to predict the likelihood of an amino acid substitution in the protein being damaging to protein function. SIFT score generates a score that ranges from 0-1 with values between 0.0 and 0.05 representing variants that are considered deleterious, whereas values between 0.05 and 1.0 predicts variants that are benign (i.e. well tolerated) and therefore do not result in a deleterious phenotype. SIFT scores obtained for SNVs detected in this study were used to estimate its potential damage (Ng and Henikoff, 2003). Of note, SIFT scores cannot be used to predict damaging phenotypes for indels or structural variants. Finally, SNVs were analyzed based on their homozygosity/heterozygosity. Final selection of possible SNPs

involved in T2D predisposition in the O-NOD^{k} mice was based on their gene expression in islet β-cells and their described gene function in the β-cell.

2.4.2 RNA sequencing

2.4.2.1 Islet RNA isolation

After enzymatic digestion of the pancreas and islet separation via Histopaque gradient, hand-picked islets from NC and HF-fed O-NOD^{k} and RF-NOD^{k} mice were transferred into 1.5 mL microtubes, and washed twice in 1 mL of sterile cold PBS by centrifugation at 1400 rpm for 5 minutes at 4^{o}C. Supernatant was removed and 350 µL of RLT lysis buffer (provided in the RNeasy mini kit, Cat #74106, Qiagen, Venlo, Netherlands) supplemented with 1% mercaptoethanol, was added to the islets. Samples were homogenized by up and down pipetting and were then stored in a -80^{o}C freezer until future RNA extraction.

Prior to RNA extraction, all equipment and work space were wiped with RNaseZap to remove RNase contamination. RNA samples lysates were pipetted directly onto a QIAshredder spin column (Cat #79656, Qiagen, Venlo, Netherlands) placed inside a 2 mL collection tube and centrifuged for 2 minutes at maximum speed (13,400 rpm). The spin column was discarded and 350 µL of 70% ethanol was added to the homogenized lysates in the collection tube. After homogenization, the samples were transferred into an RNeasy mini spin column (RNeasy Mini Kit, Cat #74106, Qiagen, Venlo, Netherlands) loaded on a 2 mL collection tube and centrifuged for 15 seconds at 13,400 rpm. The flow-through in the collection tube was discarded and 350 µL of RW1 buffer (provided by the kit) was added to the spin column, which was centrifuged for 15 seconds at 13,400 rpm. The flow-through in the collection tube was discarded again.

In order to allow on column DNA digestion during the RNA purification protocol, 80 µL of incubation mix (1:8 dilution of DNAse I in buffer RDD from the RNase-Free DNase sets, Cat

#79254, Qiagen, Venlo, Netherlands) was added directly onto the RNeasy column silica gel membrane, followed by incubation at room temperature for 15 minutes. A subsequent wash was performed by addition of 350 µL of buffer RW1 and centrifugation for 15 seconds at 13,400 rpm. The RNeasy spin column was then transferred onto a new 2 mL collection tube and washed twice with 500 µL of buffer RPE (provided by the kit) followed by centrifugation for 15 seconds at 13,400 rpm. The RNeasy spin column was then transferred onto a new 2 mL collection tube and centrifuged for 2 minutes at 13,400 rpm with open lids to remove any RPE residues.

RNA samples were eluted from the spin column through addition of 20 µL of RNase-free water directly onto the silica-gel membrane of the spin column, and centrifuged for 1 minute at 13,400 rpm. The RNA obtained was stored in a -80^{o}C freezer for further analysis.

2.4.2.2 RNA quantification

The eluted RNA was assessed for concentration and integrity/quality via the analysis of RNA integrity number (RIN) using the Agilent 2100 Bioanalyzer (Cat #G2938B, Agilent, Waldbronn, Germany) and the Agilent RNA 6000 Nano kit (Cat #5067-1511m Agilent, Waldbronn, Germany). RNA samples were denatured in a gradient thermal cycler (PC 960G, Corbett Research, Mortlake, Australia) at 70^{o}C for 2 minutes, and kept on ice until RIN analysis.

Briefly, 550 µL of RNA gel matrix was pipetted into a spin filter (provided by the kit) and centrifuged at 4000 rpm for 10 minutes at room temperature. 65 µL of the filtered gel was aliquoted into a 0.5 mL RNase-free micro-centrifuge tube. RNA 6000 Nano dye concentrate was equilibrated to room temperature for 30 minutes and vortexed for 10 seconds. 1 µL of the Nano dye was added to the 65 µL pre-prepared gel, followed by vortexing and centrifugation at 12,000 rpm for 10 minutes at room temperature.

An Agilent RNA 6000 Nano chip, which contains 16 interconnected micro-channels, was placed on the chip priming station to separate the RNA fragments by electrophoresis according to their size. 9 µL of the gel-dye mix was added to all micro-channels of the Nano chip. 5 µL of RNA marker and 1 µL of Nano ladder was added to their respective micro-channels. 1 µL of the denatured RNA samples were added to the sample wells. The chip was vortexed for 1 minute at 2400 rpm and then run on the Agilent 2100 Bioanalyzer instrument. Only samples displaying RIN values greater than 8.0 were used for RNA Sequencing (RNA-seq).

2.4.2.3 RNA sequencing (RNA-seq)

RNA-seq was performed by Dr Maxim Nekrasov at the Australian Cancer Research Foundation (ACRF) BRF at JCSMR, ANU. The libraries were prepared using the Illumina TruSeq Stranded mRNA library kit (Cat# 20020594, Illumina, CA, USA) as per manufacturer's instructions. The libraries were sequenced using the Illumina NextSeq 500 system using a high output flow cell at 150 bp paired-end reads, which can generate up to 800 million paired reads per sample on high output.

2.4.2.4 Bioinformatics analysis of RNA sequencing

2.4.2.4.1 Reading alignment and Quality control assessment

Bioinformatics analysis for the RNA-seq data was performed by Dr. Zhi-Ping Feng and Mr Cameron Jack at the ANU Bioinformatics Consultancy (ABC). Sequence quality was checked on the raw reads with FASTQC. The libraries were then mapped against the reference C57BL/6J mouse genome (GRCm38.95) using Hisat2 (Kim et al., 2019), sorted and summarized with samtools (v1.8) (Li et al., 2009) and then quantified based on Ensembl genome annotation, considering SNPs and annotation of transcripts

(http://ftp.ensembl.org/pub/release-95/gtf/mus_musculus/mus_musculus.GRCm38.95.gtf.gz). Reference assembly of the transcriptome was conducted using StringTie (Pertea et al., 2016), transcript counts were generated using ballgown and the FPKM (Fragment Per Kilo-base Per Million) count matrix was converted to raw count matrix based on Monocle2 (Qiu et al., 2017). The quality of raw count matrix was evaluated with some diagnostic figures, such as principal component analysis (PCA), multidimensional scaling (MDS), density or box plots and heat map to observe the intra- and inter-group variability. The PCA plot is similar to MDS that show a 2-dimensional projection of distances between samples to reflect the total variation of the data set and depicts clustering among samples of each group, allowing identification of outliers. The outliers and the noise level were determined**.**

Although highly variable samples increase noise in the sequencing data, removing them from the analysis altogether would reduce the power of the study. Therefore, a more appropriate approach would be to reduce the weight of the observations from these samples. This can be achieved by considering how heterogeneous these samples are at both sample and observational levels (Liu et al., 2015). A log-linear variance model can be fitted at the sample level to include common sample-specific or group-specific parameters shared between genes. At the observational level, "voom" can be used to obtain weights from the mean-variance relationship of the log-counts-per-million (Law et al., 2014). Finally, both sample and observational level weights can be combined to achieve a differential expression analysis with more power and less false discoveries (Liu et al., 2015). Therefore sample weights were calculated using this methodology from the open source "limma package" (Law et al., 2016). All the quality checks and diagnostic analyses were performed in R using the camera R package.

2.4.2.4.2 De-noise and normalization

Lowly expressed genes were filtered out to reduce the noise of RNA-seq or to reduce the severity of correction for false discovery rates (FDR) and to improve the power of detection (Risso et al., 2011). The filtered gene count matrix of 16058 genes and 16 samples was transformed to normal distribution using voom (Law et al., 2014) with sample quality adjustment and normalized with trimmed mean of M values (TMM) method to prevent skewing by highly expressed genes (Robinson and Oshlack, 2010). This allows correct ranking of gene expression levels, inter- and intra-sample group comparisons, and increases the robustness of detection of differential expressed genes (DEGs). The voom transformed object was then fitted to a linear model with moderated t-statistic with empirical Bayes method. The p-values were calculated according to the Benjamin-Hockberg (BH) FDR method to adjust for multiple hypothesis testing. All these analysis were provided in the limma package, interactive views were generated with Glimma (Law et al., 2016, Su et al., 2017) and the gene expression were visualized in Interactive Genomics Viewer (IGV) (Robinson et al., 2020).

2.4.2.4.3 Identification of differentially expressed genes (DEGs)

DEGs were defined by pair-wise comparison between two groups using the limma-voom tool (Ritchie et al., 2015). This tool tested the null hypothesis stating that a specific gene is equally expressed in both groups of mice. Therefore, if a significant difference in gene expression is detected, the hypothesis is rejected and the specific gene is deemed as a DEG. Subsequently, a comprehensive list of genes with corresponding significant p-values, adjusted p-values (a.k.a. q-values) using the BH methods to control for FDR and log fold change (log FC) for each gene is generated for further analysis (Law et al., 2014). Genes with an adjusted p-value ($q<0.05$) were considered as differentially expressed genes. Pair-wise comparisons were conducted

between the O-NOD^{k} and RF-NOD^{k} mice groups, which were fed on chow and HF diet. Following this analysis, heat maps were generated using ClustVis in order to visualize clustering of multi-variate data (Metsalu and Vilo, 2015). Pathway analysis was conducted on gene sets using the Molecular signatures database (MSigDB) Hallmark gene sets (Liberzon et al., 2015).

2.5 Statistical analysis

Statistical analysis in this thesis was performed using GraphPad PRISM software version 9 (San Diego, CA, USA). Results obtained were expressed as means ± standard error of the mean (SEM). Unpaired Student's t-test was performed for comparison of the means between 2 groups. Two-way analysis of variance (ANOVA) was used for multiple comparisons, followed by Bonferroni post hoc testing. Differences between groups were considered significant when p values were < 0.05. Chi-square analysis was performed during the histological analysis of the pancreas to determine the significance of the number of affected mice to the unaffected mice. Statistical package of the social sciences (SPSS) was used for curve analysis during the longitudinal experiments to measure body weight and non-fasting blood glucose, as well as the glucose excursion during ipGTT. Analysis for the GSIS experiments in Chapter 4 was conducted on repeated measures using three-way ANOVA with Tukey post-hoc testing.

Power calculations were performed to determine how much study power was anticipated to be achieved with the mice numbers used for each study. For the long term study described in Chapter 3, twelve mice per group provides 90% power to detect an increase in blood glucose levels from 7 mM to 20 mM with α=5%. Twelve mice per group provides 90% power to detect 56% increase of insulin secretion with α-5% in the *in vitro* GSIS study in Chapter 4.

Chapter 3

Results

Long-term phenotypic characterization of O-NOD^{k} and RF-NOD^{k} mice

3.1 Introduction

An individual's metabolic tissue responses to over-nutrition determine whether an unfavourable metabolic phenotype will install or not. Consumption of diets rich in saturated fat causes insulin resistance in muscle, liver and adipose tissue, which leads to enhanced β-cell secretory response (β-cell compensation) in order to maintain normoglycaemia. However, several studies showed that T2D only develops in individuals unable to sustain β-cell compensation for longer periods, therefore, highlighting the importance of β-cell dysfunction in diabetes progression and development (Sakuraba et al., 2002, Butler et al., 2003).

β-cell function can be assessed *in vivo* by glucose tolerance tests, which are extensively used as a clinical tool to predict increased risk and provide diagnosis for T2D (Beer et al., 1990, Jaruratanasirikul et al., 2016). Furthermore, impaired insulin biosynthesis and/or abnormal insulin processing are also associated with β-cell dysfunction, with T2D individuals displaying elevated levels of proinsulin in circulation (Kim et al., 2000, Pfützner and Forst, 2011, Nakamura et al., 2020). Studies conducted in mice also showed that abnormally elevated blood glucose levels result in augmented proinsulin biosynthesis and its premature release, prior to proper post-translational modifications (Alarcón et al., 1995). Finally, failure of β-cells to dynamically adapt to increased insulin demand during excess fuel surfeit is linked to reduced β-cell mass and increased apoptosis (Sakuraba et al., 2002, Butler et al., 2003).

This chapter, therefore, investigates the pathophysiological mechanisms involved in T2D development in two mice sub-strains, the T2D-prone O-NOD^{k} and the T2D-resistant RF-NOD^{k} mice. We aimed to examine the long-term effects of HF feeding on: *i)* diabetes incidence, *ii)* pancreatic islet β-cell function *in vivo* and β-cell mass, *iii)* pancreatic, including islet, inflammation and fat deposition, *iv)* adipose tissue distribution and, *v)* hepatic fat deposition.

3.2 Experimental design

Age-matched male O-NOD^{k} and RF-NOD^{k} mice were weaned at 3 weeks of age onto a standard rodent normal chow (NC) diet. At 4 weeks of age, experimental mice were randomly allocated to either NC or HF diet for 20 weeks (n=12 mice/ group, distributed into 3 different cohorts), which is detailed in Figure 11. As described in Chapter 2, fortnightly body weight and non-fasting tail blood glucose levels were monitored until the end of the study. At 13 and 23 weeks of age, mice were subjected to intraperitoneal glucose tolerance tests (ipGTT, 1g glucose/kg body weight) after 4 hours of fasting. At the end of the study period or after blood glucose readings of ≥20 mM (18 to 24 weeks of age), tail blood was collected for blood chemistry analysis and insulin-sensitive tissues were dissected and weighed, and hepatic TG content was quantified. Finally, the pancreas was excised and processed for histological analysis (detailed description of protocol in Chapter 2).

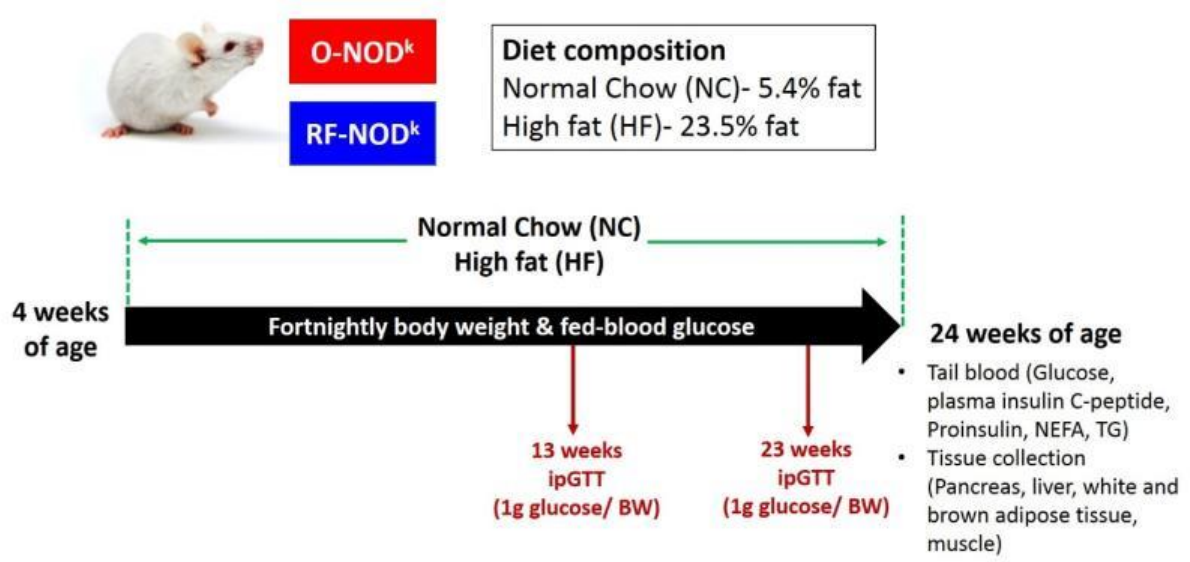

Figure 11: Experimental design of the long-term study for phenotypic characterization of O-NOD^k and RF-NOD^k mice. Male O-NOD^k and RF-NOD^k mice placed on either NC or HF diet at 4 weeks of age for 20 weeks. Body weight and non-fasting blood glucose were monitored fortnightly. Mice were subjected to ipGTT (1g/kg body weight) at 13 and 23 weeks of age after 4 hours of fasting. At euthanasia, when mice were 24 weeks of age or after two consecutive blood glucose readings above 20 mM, non-fasting tail blood and various tissues were collected for further analysis. NC: Normal chow, HF: High fat, ipGTT: Intraperitoneal glucose tolerance test, NEFA: Non-esterified fatty acids, TG: Triacylglyceride.

3.3 Results

3.3.1 Fortnightly body weight

At 4 weeks of age, both O-NOD^{k} and RF-NOD^{k} mice had similar body weights, but on both NC and HF diets the O-NOD^{k} mice had higher body weight growth curves compared to their respective NC and HF diet-fed RF-NOD^{k} mice (Figure 12A).

HF-feeding was associated with increased body weight gain in both mice sub-strains. At 8 weeks of age, both O-NOD^{k} and RF-NOD^{k} mice displayed significant increases in absolute body weight compared to their chow-fed controls (34.5 ± 0.5 *vs* 29.4 ± 0.5 g, O-NOD^{k} mice HF *vs* NC, respectively, $p<0.0001$) (29.9 ± 0.9 *vs* 26.1 ± 0.4 g, RF-NOD^{k} mice HF *vs* NC, respectively, $p<0.01$) (Figure 12A). The O-NOD^{k} mice were significantly heavier on a HF diet compared to the RF-NOD^{k} mice from 8 weeks of age onwards (34.5 ± 0.5 *vs* 29.9 ± 0.9 g, respectively, $p<0.001$) with maximum weight observed at 20 weeks of age (49.2 ± 0.7 *vs* 41.9 ± 1.0 g, HF-fed O-NOD^{k} *vs* RF-NOD^{k} mice, respectively, $p<0.001$) (Figure 12A).

Similar observations were made when body weight gain was analyzed (Figure 12B). The decline in the body weight gain of the HF-fed O-NOD^{k} mice observed from 20 weeks of age onwards resulted from the ethical culling of the heavier mice that had developed extreme hyperglycaemia at 18 weeks of age.

Together, these results show differential weight gain between O-NOD^{k} and RF-NOD^{k} mice, with O-NOD^{k} mice being more predisposed to weight gain than RF-NOD^{k} mice, irrespective of the diet.

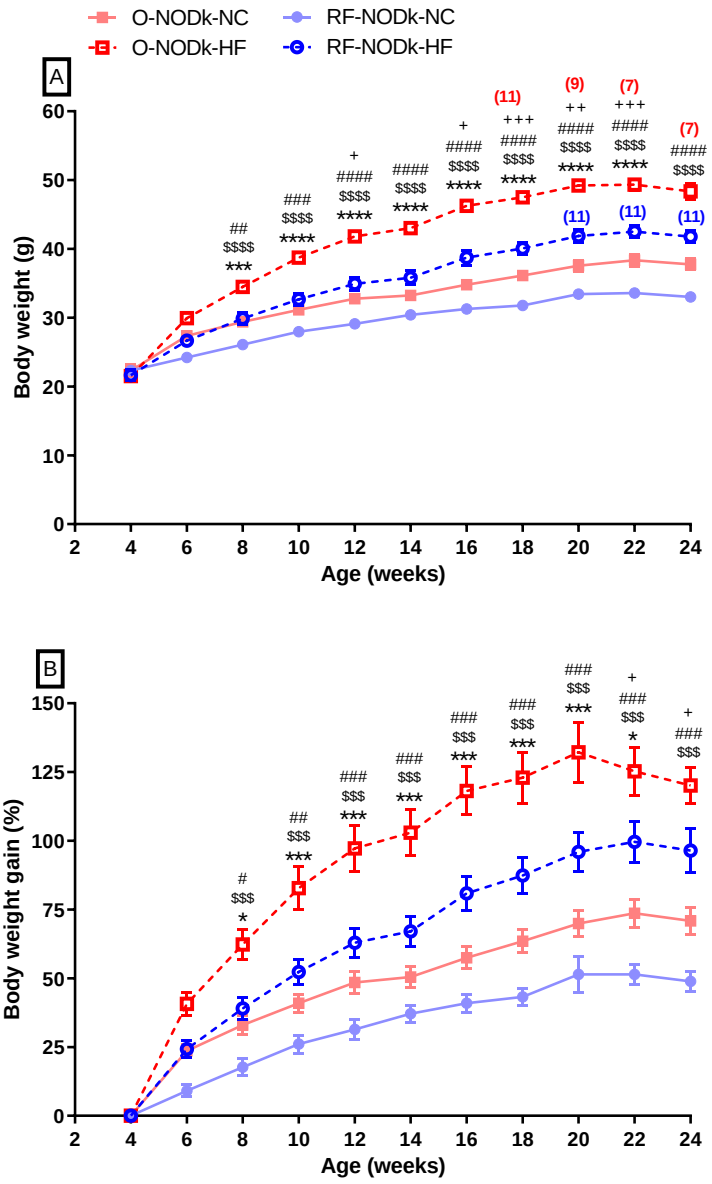

Figure 12: Time-course responses of body weight and weight gain in the O-NOD^{k} and RF-NOD^{k} mice submitted to dietary intervention. Fortnightly assessment of body weight (A) and weight gain (B) in male O-NOD^{k} and RF-NOD^{k} mice placed on either NC or HF diet from 4 to 24 weeks of age. Data are means ± SEM for 12 mice per group until 16 weeks of age. Numbers in brackets depict the number of surviving HF-fed O-NOD^{k} mice during the experimental period. Two-way ANOVA with Bonferroni post-hoc test; $^{+}$p<0.05, $^{++}$p<0.01, $^{+++}$p<0.001, NC-fed O-NOD^{k} *vs* NC-fed RF-NOD^{k}; $^{\$\$\$}$p<0.001, $^{\$\$\$\$}$p<0.0001, O-NOD^{k}-NC vs HF; $^{\#}$p<0.05, $^{\#\#}$p<0.01, $^{\#\#\#}$p<0.001, $^{\#\#\#\#}$p<0.0001, RF-NOD^{k} NC *vs* HF; *p<0.05, ***p<0.001, ****p<0.0001, HF-fed O-NOD^{k} *vs* HF-fed RF-NOD^{k}.

3.3.2 Non-fasting blood glucose time-course and survival curve

Non-fasting (9-10 AM) tail blood glucose levels were measured fortnightly from weaning until the end of the study (24 weeks of age).

On a NC diet, both O-NOD^{k} and RF-NOD^{k} mice maintained normoglycaemia throughout the study (Figure 13A). Long-term HF-feeding increased blood glucose levels (BGL) of only 2 RF-NOD^{k} mice. The first mouse gradually developed increased blood glucose levels after 10 weeks of HF-feeding, and had to be ethically culled at 20 weeks of age due to the development of overt diabetes (BGL= 26.4 mM). The second mouse remained until the end of the study, since it developed hyperglycaemia only at 20 weeks of age (BGL=15.5 mM), but did not reach the cut off level of 20 mM in the following weeks.

On the other hand, HF-fed O-NOD^{k} mice displayed progressive elevation in blood glucose levels, clearly evident at 16 weeks of age compared to NC-fed O-NOD^{k} mice (13.2 ± 1.4 mM *vs* 6.6 ± 0.2, respectively, $p<0.001$) and to its HF-fed RF-NOD^{k} mice counterpart (13.2 ± 1.4 *vs* 7.9 ± 0.9 mM, respectively, $p<0.001$). The incidence of overt diabetes, leading to ethical culling of mice before the end of the study, was also higher in these mice (5 out of 12 mice) compared to HF-fed RF-NOD^{k} mice (1 out of 12 mice) (chi-squared, $p<0.01$). Therefore, while HF-fed RF-NOD^{k} mice only had a 16.6% incidence of hyperglycaemia, 75% of HF-fed O-NOD^{k} mice developed hyperglycaemia (defined as 9AM non-fasting BGL ≥12 mM) by 24 weeks of age (log rank (Mantel-Cox) test, $p=0.042$) (Figure 13B).

Taken together, these results show that O-NOD^{k} mice develop progressive hyperglycaemia when subjected to HF-feeding, while RF-NOD^{k} mice mostly maintain normoglycaemia.

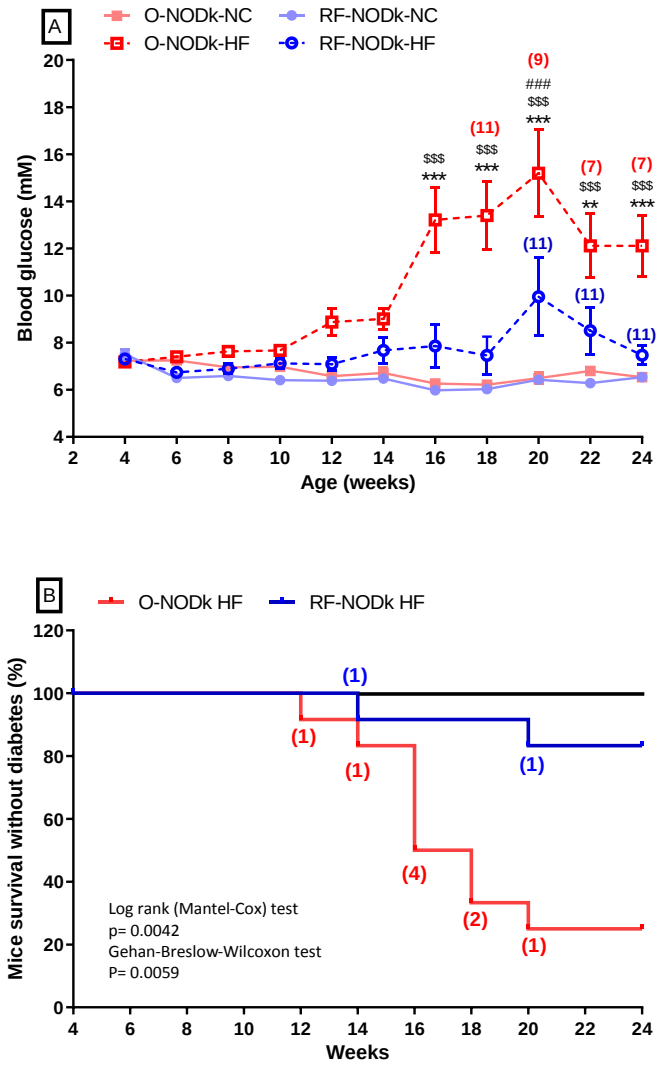

Figure 13: Fortnightly non-fasting blood glucose and survival curve of O-NOD^{k} and RF-NOD^{k} mice submitted to diet intervention. 9AM non-fasting blood glucose levels obtained from mice subjected to NC or HF diet from 4 until 24 weeks of age (A). Numbers in brackets in Figure 13A depict the number of surviving HF-fed O-NOD^{k} and RF-NOD^{k} mice during the experimental period. Survival curve showing the % of mice without diabetes (< 12 mM) at the end of the study (B). Numbers in brackets in Figure 13B depict the number of HF-fed mice that develop diabetes (≥ 12 mM) during the experimental period. Data are means ± SEM for 12 mice per group until 16 weeks of age. Statistical significance in blood glucose time-course was evaluated by Two-way ANOVA with Bonferroni post hoc test; $^{\$\$\$}$p<0.001, O-NOD^{k} NC *vs* HF; $^{\#\#\#}$p<0.001, RF-NOD^{k} NC *vs* HF; **p<0.01, ***p<0.001, HF-fed O-NOD^{k} *vs* HF-fed RF-NOD^{k}. Survival curve was analyzed by log rank (Mantel-Cox) test and Gehan-Breslow-Wilcoxon test.

3.3.3 Glucose tolerance tests (GTT)

Both O-NOD^{k} and RF-NOD^{k} mice were submitted to ipGTT at 13 and 23 weeks of age, in order to determine possible differences in blood glucose regulation and insulin secretion under NC and HF diet-stressed conditions.

At 13 weeks of age, both sub-strains of mice fed on a NC diet had similar levels of fasting blood glucose and plasma insulin at time 0' min. On the other hand, HF-fed mice had higher fasting blood glucose, compared to their NC-fed control mice (8.0 ± 0.4 *vs* 5.8 ± 0.2 mM, HF-fed O-NOD^{k} *vs* NC-fed O-NOD^{k} mice) (7.5 ± 0.3 *vs* 5.6 ± 0.2 mM, HF-fed RF-NOD^{k} *vs* NC-fed RF-NOD^{k}) (Figure 14A). HF-feeding also increased insulinaemia in both sub-strains. Remarkably, HF-fed O-NOD^{k} mice had three times higher insulin levels that their RF-NOD^{k} mice counterparts (4.5 ± 2.0 *vs* 1.5 ± 0.4 ng/mL, respectively, $p<0.001$) (Figure 14B). The ratio between fasting insulin and glucose levels at time 0' min was significantly higher in the HF-fed O-NOD^{k} compared to NC-fed O-NOD^{k} mice (0.51 ± 0.18 *vs* 0.12 ± 0.02 ng/µmol, respectively, $p<0.01$). The HF-fed O-NOD^{k} mice also had a higher fasting insulin and glucose ratio compared to their HF-fed RF-NOD^{k} counterparts (0.51 ± 0.18 *vs* 0.19 ± 0.05 ng/µmol, respectively, $p<0.05$).

During the ipGTT conducted at this age, both NC-fed mice groups exhibited similar and excellent glucose tolerance (Figure 14A), despite no significant elevations in plasma insulin levels (Figure 14B). HF-feeding led to increased glucose excursions consistent with HF-diet induced glucose intolerance in both sub-strains of mice, however O-NOD^{k} mice exhibited more severe glucose intolerance ($p<0.001$). Similar observations were also made when the respective areas under the curves (AUC) were calculated (1552 ± 98 *vs* 1171 ± 107, HF-fed O-NOD^{k} *vs* HF-fed RF-NOD^{k} mice, respectively, $p<0.01$) (Figure 14C). Interestingly, a post-glucose load rise in insulinaemia was not observed in either of the HF-fed mice sub-strains (Figure 14B).

Nonetheless, $AUC_{insulin}$ (0-90 mins) was higher in HF-fed mice compared to NC controls ($p<0.0001$), which was attributed to higher baseline insulin levels (Figure 14D). However, when the change in insulin levels were calculated for the 1st 15 mins (Δ0-15 min), an apparent lack of glucose-stimulated insulin secretion was observed in all groups of mice (Figure 14F).

Finally, the HOMA-IR, which can be an indicator of insulin resistance, was found to be increased in the HF-fed mice of both sub-strains compared to the NC-fed mice (45.5 ± 23.7 *vs* 4.7 ± 1.1, HF-fed O-NOD^{k} *vs* NC-fed O-NOD^{k} mice, respectively, $p<0.01$) (12.9 ± 4.4 *vs* 3.6 ± 1.2, HF-fed RF-NOD^{k} *vs* NC-fed RF-NOD^{k} mice, respectively, $p<0.05$) (Figure 14E). This suggests that HF-feeding may have caused insulin resistance in these mice. However, since there was no significant sub-strain differences between the O-NOD^{k} and RF-NOD^{k} mice on either NC or HF diet, it is unlikely to be associated with the diabetes phenotype observed in the O-NOD^{k} mouse model.

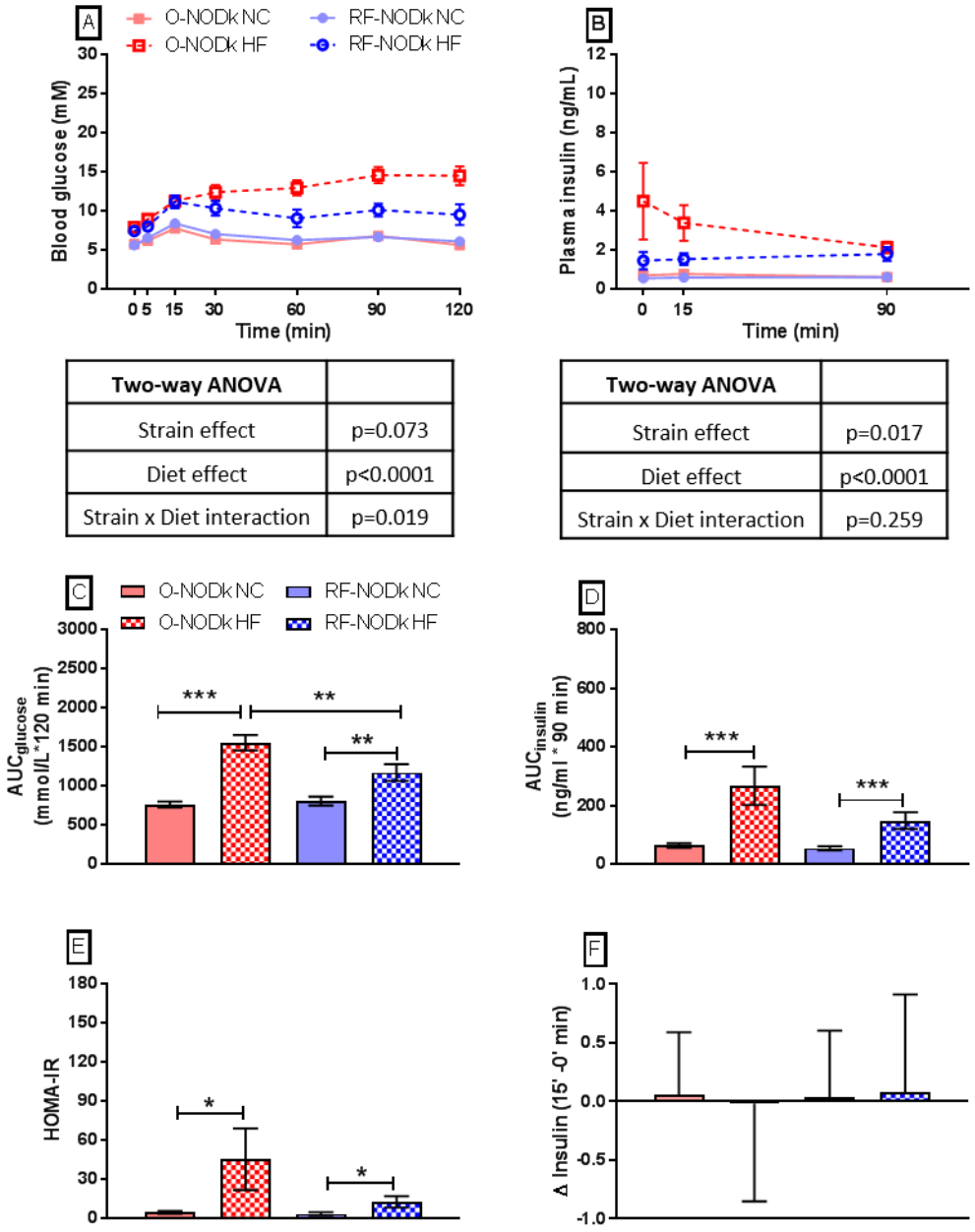

Two-way ANOVA	
Strain effect	p=0.073
Diet effect	p<0.0001
Strain x Diet interaction	p=0.019

Two-way ANOVA	
Strain effect	p=0.017
Diet effect	p<0.0001
Strain x Diet interaction	p=0.259

Figure 14: Intraperitoneal glucose tolerance test (ipGTT) performed in O-NOD^{k} and RF-NOD^{k} mice at 13 weeks of age. Blood glucose (A) and plasma insulin excursion (B), along with corresponding area under the curve (C and D, respectively), HOMA-IR (E) and change in insulin levels from 0 to 15 min (F) and were assessed during the ipGTT. Data are means ± SEM for 12 mice per group. Statistical significance was analyzed by SPSS and Two-way ANOVA followed by Bonferroni post-hoc test for glucose and insulin excursion and One-way ANOVA for AUC; *p<0.05, **p<0.01, ***p<0.001.

At 23 weeks of age, surviving mice from each group were subjected to another ipGTT. HF-feeding resulted in increased fasting glucose in both sub-strains of mice compared to their respective NC-fed control groups (Figure 15A). The increase in glycaemia however was significantly greater in HF-fed O-NOD^{k} mice compared to HF-fed RF-NOD^{k} mice (11.3 ± 1.4 *vs* 7.8 ± 0.9 mM, respectively, $p<0.05$) (Figure 15A). The HF-fed O-NOD^{k} and RF-NOD^{k} mice were hyperinsulinaemic compared to the respective NC-fed mice. HF-fed O-NOD^{k} mice had higher fasting insulin levels compared to HF-fed RF-NOD^{k} mice (8.1 ± 2.0 *vs* 3.8 ± 0.8 ng/mL, respectively, $p<0.001$) (Figure 15B).

Even at this age, all NC-fed mice maintained excellent glucose tolerance. On the other hand, long-term HF-feeding led to the development of severely impaired glucose tolerance in both mice groups, worse in the O-NOD^{k} mice sub strain (ANOVA, strain effect $p<0.01$; diet effect $p<0.0001$) (Figure 15A). As a result, $AUC_{glucose}$ was significantly higher in the HF-fed O-NOD^{k} mice compared to HF-fed RF-NOD^{k} mice (2294 ± 248 *vs* 1517 ± 236, respectively, $p<0.01$) (Figure 15C). At this age, HF-fed O-NOD^{k} mice were also unable to induce an increase in plasma insulin concentration in response to the intraperitoneal glucose load during the test (Figure 15B). Although $AUC_{insulin}$ was higher in HF-fed mice of both groups ($p<0.0001$), there was no significant sub-strain difference ($p=0.369$) (Figure 15D). Interestingly, during the 1st 15 mins of the GTT, only the HF-fed O-NOD^{k} mice displayed reduced insulin levels in response to the glucose load compared to the rest of the groups ($p<0.01$) (Figure 15F).

Finally, the HOMA-IR index was similar to the observations made at 13 weeks of age, where both HF-fed mice displayed higher HOMA-IR compared to the NC-fed mice (Figure 15E). However, HF-fed O-NOD^{k} mice had a significantly higher HOMA-IR index compared to the HF-fed RF-NOD^{k} mice (116.9 ± 44.3 *vs* 36.1 ± 10.8, respectively, $p<0.01$). This suggests that at 23 weeks of age, the HF-fed O-NOD^{k} mice may have a higher degree of insulin resistance compared to the HF-fed RF-NOD^{k} mice.

Accumulative evidence suggests that when subjected to HF-feeding, O-NOD^{k} mice develop impaired glucose tolerance at 13 weeks of age, which further aggravates by 23 weeks of age. Despite having higher fasting plasma insulin levels, these mice are unable to secrete more insulin in response to the ip glucose load during the GTT, suggesting β-cell dysfunction.

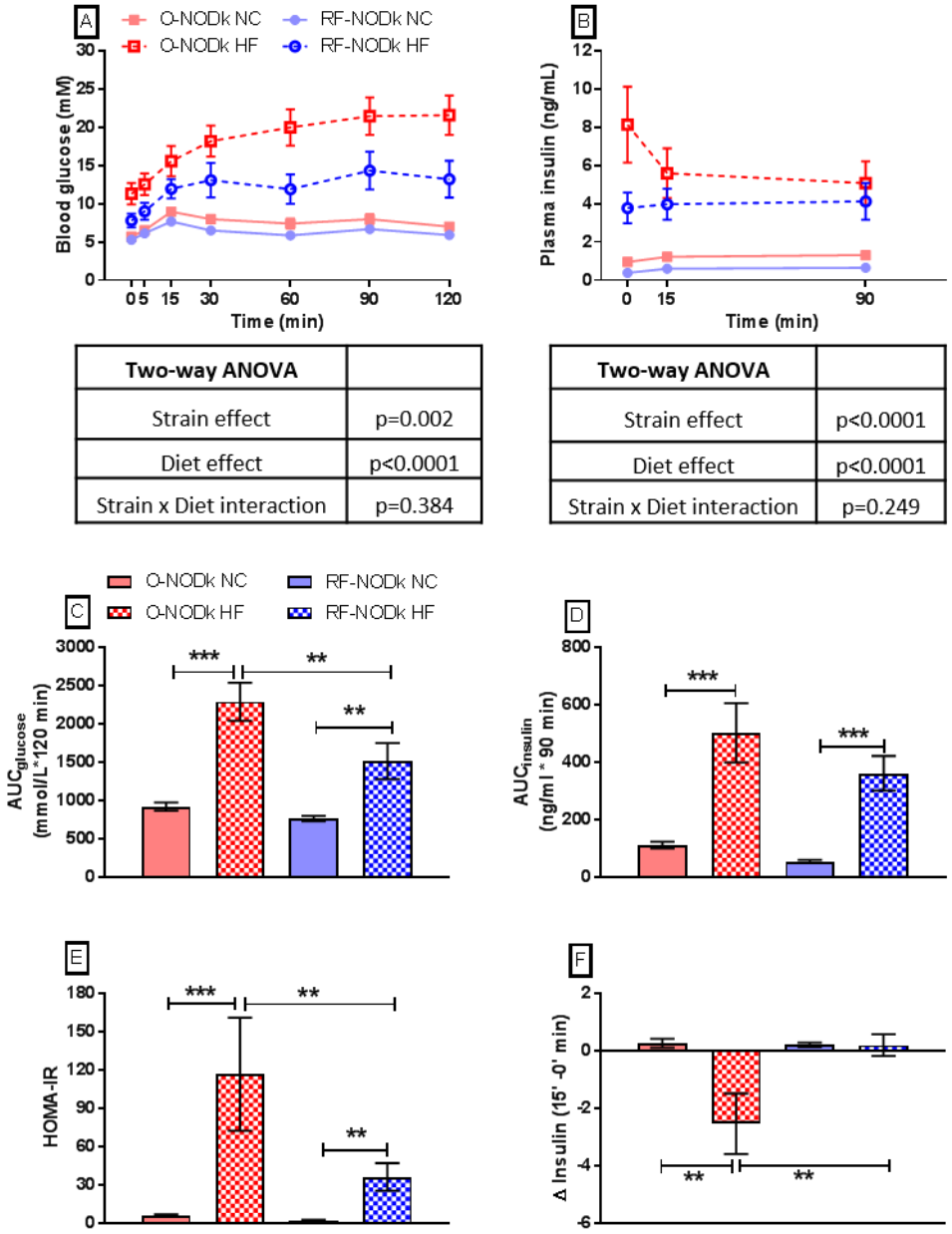

Two-way ANOVA	
Strain effect	p=0.002
Diet effect	p<0.0001
Strain x Diet interaction	p=0.384

Two-way ANOVA	
Strain effect	p<0.0001
Diet effect	p<0.0001
Strain x Diet interaction	p=0.249

Figure 15: Intraperitoneal glucose tolerance test (ipGTT) performed in surviving O-NOD^{k} and RF-NOD^{k} mice at 23 weeks of age. Blood glucose (A) and plasma insulin excursion (B), along with corresponding area under the curve (C and D, respectively), HOMA-IR (E) and change in insulin levels from 0 to 15 min (F) and were assessed during the ipGTT. Data are means ± SEM for 7-12 mice per group. Statistical significance was analyzed by SPSS and Two-way ANOVA followed by Bonferroni post-hoc test for glucose and insulin excursion and One-way ANOVA for AUC; *p<0.05, **p<0.01, ***p<0.001.

3.3.4 Blood chemistry profiles at end point

3.3.4.1 Blood glucose and plasma insulin ratios

At the end of the study (18-24 weeks of age), non-fasting blood glucose and plasma insulin levels were measured from tail blood of O-NOD^{k} and RF-NOD^{k} mice. Subsequently, the ratio between non-fasting circulating insulin and glucose levels were assessed as an indirect determinant for the presence of insulin resistance in these mice.

NC-fed mice from both sub-strains remained normoglycaemic at the end of the study. On the other hand, non-fasting blood glucose levels were significantly increased in the HF-fed O-NOD^{k} mice compared to the NC-fed O-NOD^{k} mice (16.8 ± 1.9 *vs* 6.3 ± 0.2 mM, respectively, $p<0.001$) as well as the HF-fed RF-NOD^{k} mice, which remained mostly normoglycaemic (16.8 ± 1.9 *vs* 9.1 ± 1.6 mM, respectively, $p<0.001$) (Figure 16A).

Compared to NC-fed control mice, plasma insulin levels in response to HF-feeding were increased in both sub-strains of mice (3.5 ± 0.8 *vs* 32.6 ± 5.4 ng/mL, NC-fed *vs* HF-fed O-NOD^{k} mice, $p<0.001$; 1.8 ± 0.2 *vs* 17.9 ± 5.7 ng/mL, NC-fed *vs* HF-fed RF-NOD^{k} mice, $p<0.05$) (Figure 16B). Insulinaemia was also significantly higher in the HF-fed O-NOD^{k} mice compared to HF-fed RF-NOD^{k} mice (32.6 ± 5.4 *vs* 17.9 ± 5.7 ng/mL, $p<0.05$).

The ratio between non-fasting plasma insulin and blood glucose levels was increased with HF-feeding in both mice sub-strains (Figure 16C). Interestingly, although there was no difference between the two HF-fed mice groups, among the NC-fed mice, there was a subtle increase in the ratio in the O-NOD^{k} mice compared to the NC-fed RF-NOD^{k} mice (0.52 ± 0.11 *vs* 0.27 ± 0.03 ng/µmol, respectively, $p<0.05$). This highlights the presence of insulin hypersecretion and insulin resistance in the O-NOD^{k} mice, which may even be present under NC-fed condition, compared to the RF-NOD^{k} mice.

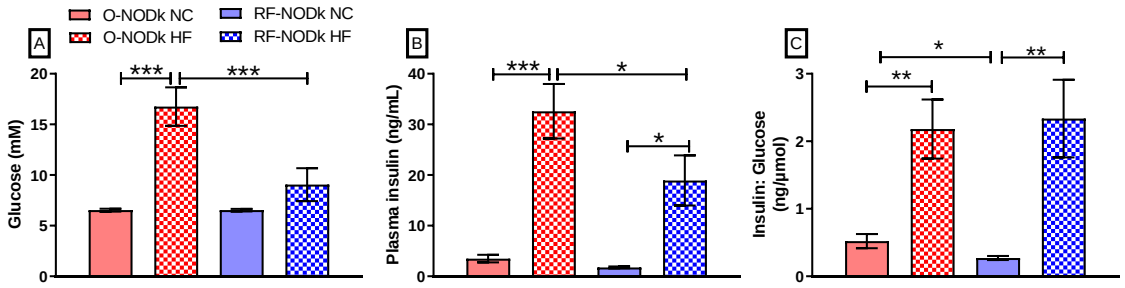

Figure 16: Non-fasting blood glucose and plasma insulin and their insulin: glucose ratio of O-NOD^{k} and RF-NOD^{k} mice at the end of the diet intervention study. 9AM non-fasting blood glucose (A), plasma insulin (B) and the ratio between insulin and glucose (C) was analyzed from tail blood collected from O-NOD^{k} and RF-NOD^{k} mice at the end of the study (18-24 weeks of age). Data are means ± SEM for 10-12 mice per group. Two-way ANOVA with Bonferroni post-hoc test; $^{*}p<0.05$, $^{**}p<0.01$, $^{***}p<0.001$.

3.3.4.2 Plasma insulin and its derivatives

In order to maintain normoglycaemia in conditions of excessive nutrients, pancreatic β-cells are required to increase insulin production while maintaining coordination of insulin gene transcriptional and post-translational modifications, to generate functional insulin hormone. Therefore, at the end of the study (18-24 weeks of age), the non-fasting circulating levels of insulin and c-peptide, as well as proinsulin from which both are derived, were quantified in tail plasma samples obtained from non-fasted O-NOD^{k} and RF-NOD^{k} mice (Figure 17).

As previously described, insulinaemia was significantly increased with HF-feeding in both sub-strains of mice, which was more evident in the HF-fed O-NOD^{k} mice compared to HF-fed RF-NOD^{k} mice (Figure 17A). No differences in proinsulin levels were observed between NC-fed O-NOD^{k} and RF-NOD^{k} mice (Figure 17B). However, long-term HF-feeding led to increased plasma proinsulin levels, more evident in HF-fed O-NOD^{k} mice compared to the HF-fed RF-NOD^{k} mice (3.7 ± 0.6 *vs* 1.6 ± 0.6 ng/mL, respectively, $p<0.01$). Circulating c-peptide levels were also similar within the NC-fed mice of both sub-strains and increased with HF-feeding (Figure 17C). However, similar to the findings with plasma proinsulin and insulin levels, c-peptide levels were higher in HF-fed O-NOD^{k} mice compared to HF-fed RF-NOD^{k} mice (17.4 ± 3.1 *vs* 9.9 ± 3.4 ng/mL, respectively, $p<0.05$).

The ratio between proinsulin and insulin did not differ among any of the mice groups (Figure 17D) indicating normal insulin processing. The ratio between proinsulin and c-peptide was similar between the two mice sub-strains on NC diet (Figure 17E). Although HF-feeding did not alter proinsulin: c-peptide ratio in any sub-strain, a significant difference was noted in HF-fed O-NOD^{k} mice when compared to the HF-fed RF-NOD^{k} mice. Finally, the ratio between insulin and c-peptide was observed to be equally elevated (2x) in both sub-strains of mice

subjected to long-term HF-feeding in comparison to their respective NC-fed controls (Figure 17F), suggesting possible insulin clearance defects in both sub-strains.

Collectively, these results clearly demonstrate that by the end of the study, both O-NOD^{k} and RF-NOD^{k} mice developed hyperinsulinaemia in response to nutrient stress caused by HF-feeding, which was more evident in the O-NOD^{k} sub-strain. The increased circulating insulin levels observed in these mice was accompanied by higher proinsulin and c-peptide levels in circulation and no differences in proinsulin: insulin ratio between the groups, therefore suggesting normal insulin processing. HF-fed mice of both sub-strains also displayed higher insulin: c-peptide ratio, suggestive of similar delayed insulin clearance.

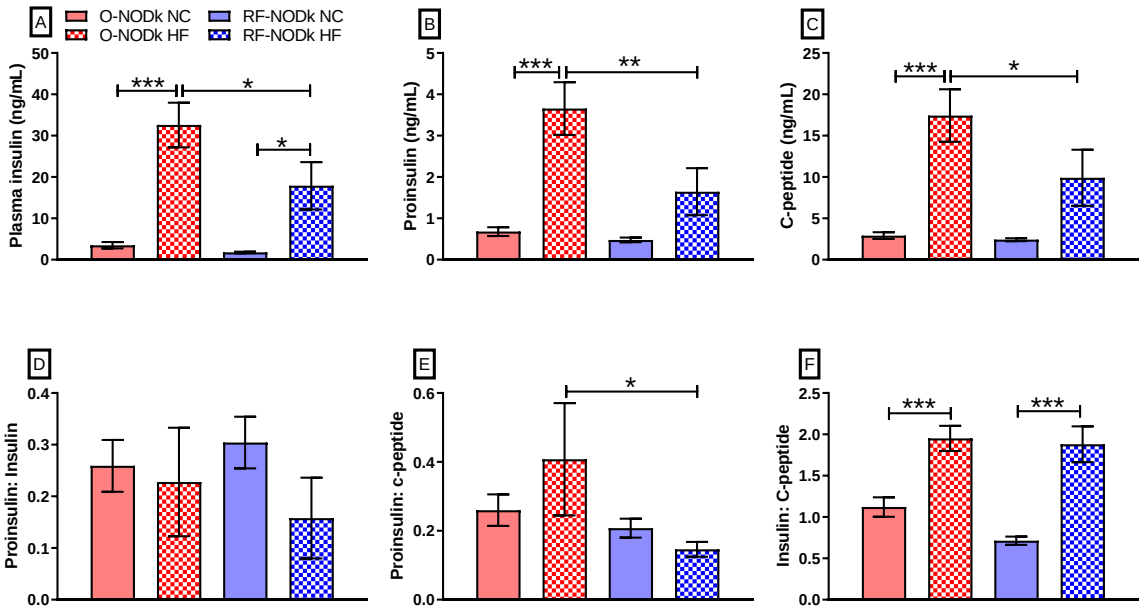

Figure 17: Analysis of insulin processing in O-NOD^{k} and RF-NOD^{k} mice submitted to prolonged dietary intervention. Non-fasting tail blood plasma was used to measure insulin (A), proinsulin (B), and C-peptide (C) of NC and HF-fed O-NOD^{k} and RF-NOD^{k} mice at the time of harvest (18 to 24 weeks of age). The ratios between proinsulin and insulin (D), proinsulin and c-peptide (E) and insulin and c-peptide (F) were also assessed. Data are means ± SEM for 10-12 mice per group. Two-way ANOVA with Bonferroni post-hoc test; *p<0.05, **p<0.01, ***p<0.001.

3.3.4.3 Plasma NEFA and TG

Obesity and insulin resistance lead to augmented NEFA in the circulation due to the inability of insulin to suppress adipose tissue lipolysis (Almandoz et al., 2013, Meijssen et al., 2001). Additionally, insulin resistance also leads to over-production of TG-rich hepatic VLDLs and promotes delayed VLDL clearance, therefore causing hyperlipidaemia and increased risk of cardiovascular diseases in T2D patients (Adiels et al., 2008). Hence, based on the previous observations of increased body weight gain and diabetes in the HF-fed O-NOD^{k} mice, non-fasting plasma NEFA and TG levels were assessed in both mice groups at the end of the study (18-24 weeks of age).

Both sub-strains of mice had low levels of circulating NEFA with NC diet intake (~ 0.7 mmol/L) (Figure 18A). However, 20 weeks of HF-feeding promoted equal elevations in NEFA levels in the O-NOD^{k} and RF-NOD^{k} mice, compared to their respective NC-fed controls (~42%, $p<0.001$ *vs* respective controls).

Likewise, plasma TG levels were also similar between the NC-fed O-NOD^{k} and RF-NOD^{k} mice (3.8 ± 0.4 *vs* 4.7 ± 0.4 mmol/l, respectively, $p>0.05$) (Figure 18B). However, HF-feeding increased plasma TG levels in the O-NOD^{k} mice by 41% and by 51% in the RF-NOD^{k} mice. Similar to NEFA, at the end of the study, both HF-fed O-NOD^{k} and RF-NOD^{k} mice displayed comparable levels of plasma TG (6.5 ± 0.6 *vs* 7.1 ± 0.6 mmol/l, respectively, $p>0.05$).

Together, these results show that HF-feeding caused a significant but similar increase in circulating NEFA and TG levels in both O-NOD^{k} and RF-NOD^{k} mice compared to the NC-fed counterparts.

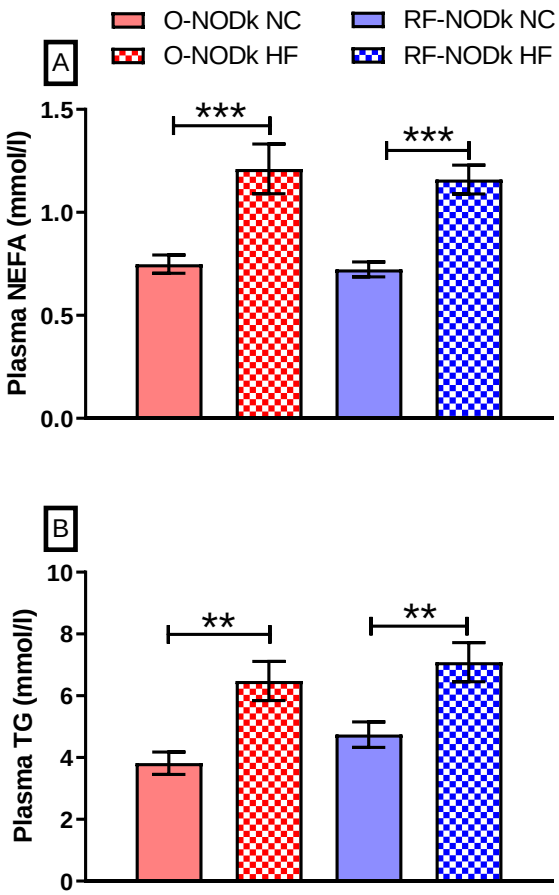

Figure 18: Plasma NEFA and TG levels in O-NOD^{k} and RF-NOD^{k} mice at the end of the intervention period. Non-fasting tail blood plasma was used to measure non-esterified fatty acids (NEFA) (A) and triglycerides (TG) (B) of NC and HF-fed O-NOD^{k} and RF-NOD^{k} mice at the end of the study (18 to 24 weeks of age). Data are means ± SEM for n=9-12 mice per group. Two-way ANOVA with Bonferroni post-hoc test; $^{**}p<0.01$, $^{***}p<0.001$.

3.3.5 Adipose tissue expansion

HF-feeding is strongly associated with diet-induced obesity, insulin resistance and T2D (Black et al., 2013). Additionally, lack of adipose tissue expansion to safely accommodate excess nutrients in subcutaneous tissue has been implicated in the pathogenesis of non-alcoholic fatty liver disease (NAFLD), non-alcoholic steatohepatitis (NASH) and T2D (Jun et al., 2008, Scherer, 2019). Therefore, after 20 weeks of dietary intervention, fat pad depots were assessed in the O-NOD^{k} and RF-NOD^{k} mice. WAT tissue weights (subcutaneous and epididymal) and brown adipose tissue (BAT) are presented as absolute tissue weights (in grams) and as % of body weight in Figure 19.

Subcutaneous fat depots were increased in the O-NOD^{k} mice compared to the RF-NOD^{k} mice, even on a NC diet (0.358 ± 0.027 *vs* 0.224 ± 0.015 g, respectively, $p<0.05$) (Figure 19A). Prolonged HF-feeding (~20 weeks) led to approximately two times increase in the absolute weight of subcutaneous fat in both sub-strains of mice. HF-fed O-NOD^{k} mice displayed higher subcutaneous tissue weight compared to HF-fed RF-NOD^{k} mice (1.037 ± 0.028 *vs* 0.890 ± 0.064 g, respectively, $p<0.05$). When the tissue weights were normalized to the mice body weight, greater subcutaneous fat depots were still evident in NC-fed O-NOD^{k} compared to NC-fed RF-NOD^{k} mice, but the difference between HF-fed O-NOD^{k} and HF-fed RF-NOD^{k} mice was no longer evident (Figure 19B).

Epididymal WAT weights of NC-fed O-NOD^{k} mice were higher than the NC-fed RF-NOD^{k} mice (0.577 ± 0.038 *vs* 0.305 ± 0.021 g, respectively, $p<0.01$) (Figure 19C). The HF diet intervention led to a 67% increase in the epididymal fat of O-NOD^{k} mice, whereas in the RF-NOD^{k} mice, it was significantly higher with 245% increase in tissue weight. However, when both HF-fed mice sub-strains were compared to each other, their absolute epididymal adipose tissue weights at the end of the study were similar. When the epididymal tissue weights were

normalized to the mice body weight, greater epididymal depots were still evident in NC-fed O-NOD^{k} compared to NC-fed RF-NOD^{k} mice. Furthermore, the greater epididymal tissue expansion in response to HF-feeding in the HF-fed RF-NOD^{k} compared to HF-fed O-NOD^{k} was evident (2.5 ± 0.1 *vs* 2.0 ± 0.1, respectively, $p<0.01$) (Figure 19D).

Finally, BAT weight was higher in NC-fed O-NOD^{k} compared to NC-fed RF-NOD^{k} mice (0.120 ± 0.005 *vs* 0.086 ± 0.004 g, respectively, $p<0.01$) (Figure 19E). Both mice sub-strains challenged by long-term HF-feeding developed increased BAT depots, with higher BAT weight observed in the O-NOD^{k} mice compared to RF-NOD^{k} mice (0.196 ± 0.006 *vs* 0.170 ± 0.012 g, respectively, $p<0.05$). However, this difference in BAT was not observed when the absolute tissue weights were normalized to % of body weight (Figure 19F).

Collectively, these adipose tissue data shows that the O-NOD^{k} sub-strain of mice has higher fat deposition on NC diet compared to the RF-NOD^{k} mice. Both sub-strains have marked accumulation in size of the three fat depots with HF feeding, but expansion within the epididymal depot is greater in the RF-NOD^{k} sub-strain.

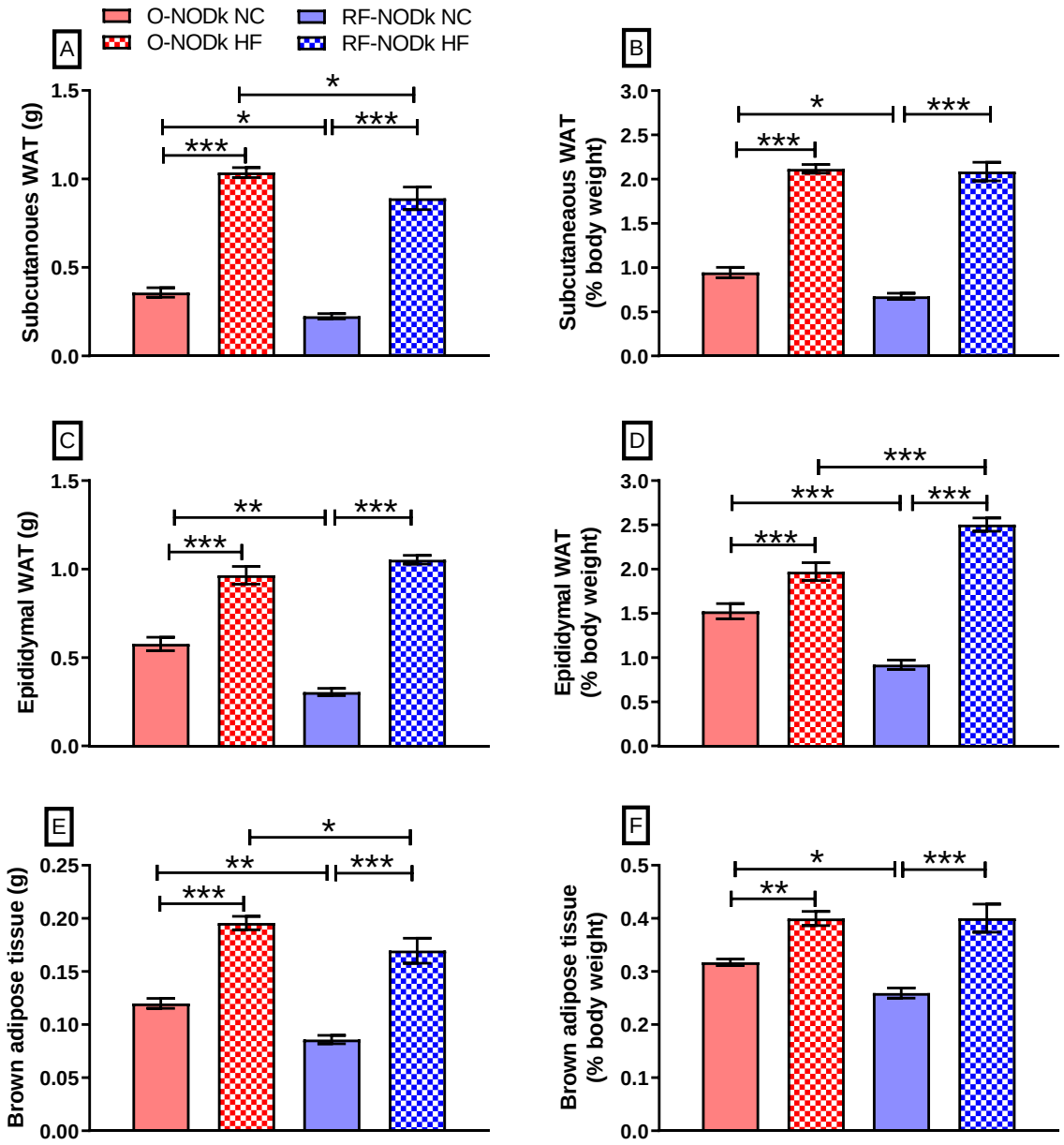

Figure 19: White and brown adipose tissue weights (WAT and BAT) in O-NOD^{k} and RF-NOD^{k} mice at the end of the study. Subcutaneous and epididymal WAT and BAT are presented as absolute weights (A, C, E) and as % of body weight (B, D, F) in O-NOD^{k} and RF-NOD^{k} mice at 18-24 weeks of age. Data are means ± SEM for n=12 mice per group. Two-way ANOVA with Bonferroni post-hoc test; *p<0.05, **p<0.01, ***p<0.001.

3.3.6 Ectopic lipid deposition in liver

Lack of safe storage of nutrient excess in subcutaneous adipose tissue can lead to ectopic fat deposition into visceral adipose tissue depots as well as into non-adipose tissues, such as the liver, muscle and pancreas (Goossens, 2017). Therefore, at the end of the dietary intervention, liver tissues from O-NOD^{k} and RF-NOD^{k} mice were excised and used for lipid storage assessment.

Both sub-strains of NC-fed mice had similar liver weights and in both, HF-feeding led to a liver weight increase (Figure 20A). However, liver weight was significantly higher in the HF-fed O-NOD^{k} compared to HF-fed RF-NOD^{k} mice (3.4 ± 0.1 *vs* 2.2 ± 0.1 g, respectively, $p<0.001$). On normalization of absolute liver tissue weights to their corresponding body weights, only HF-fed O-NOD^{k} mice displayed significant hepatomegaly (Figure 20B).

Hepatic TG levels were similarly low in both NC-fed mice sub-strains (Figure 20C). However, long-term HF diet intervention led to a significant increase in hepatic TG accumulation in both mice sub-strains. Notably, HF-fed O-NOD^{k} mice displayed higher hepatic TG content per gram of liver tissue than HF-fed RF-NOD^{k} mice (158.6 ± 14.5 *vs* 106.0 ± 16.2 mg/g, respectively, $p<0.01$) (Figure 20C).

Together, these results show that although HF-feeding leads to increased liver weights due to hepatic TG accumulation in both mice sub-strains, only the O-NOD^{k} mice develop hepatomegaly, which was concomitant with increased hepatic TG content.

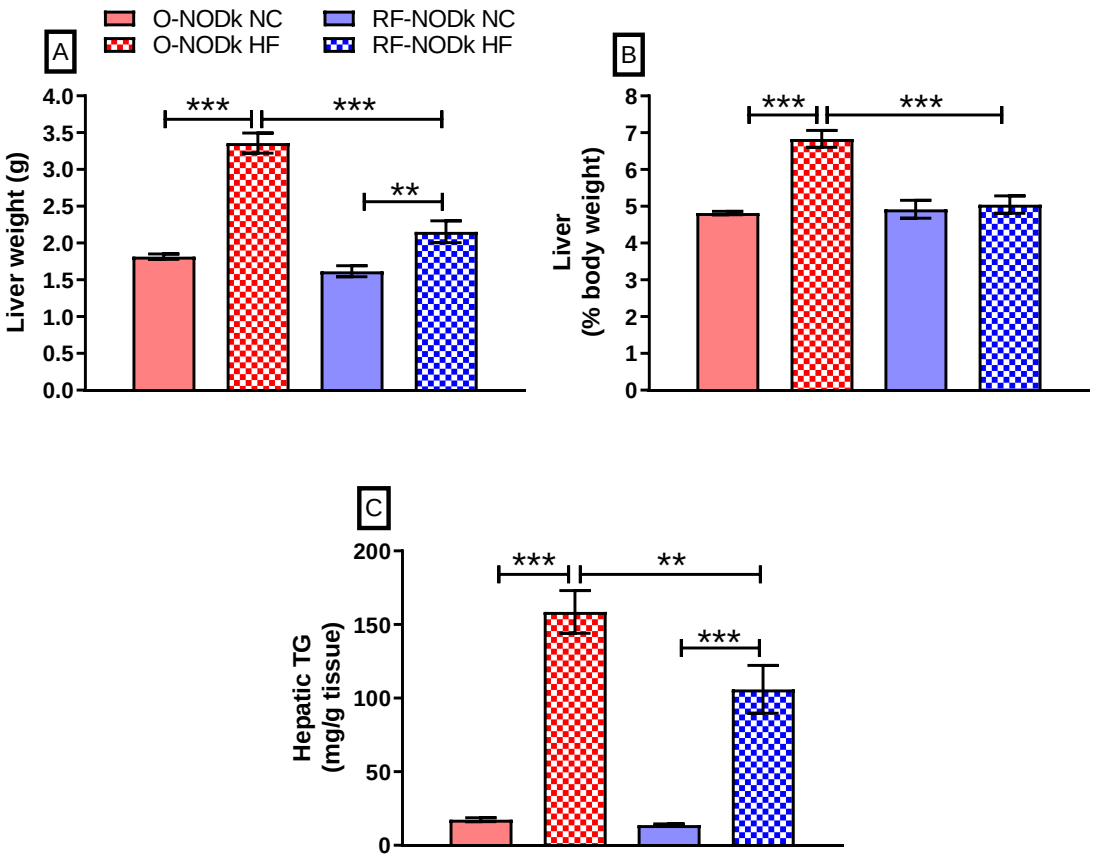

Figure 20: Effect of prolonged HF-feeding on liver weight and hepatic fat accumulation in O-NOD^{k} and RF-NOD^{k} mice. Liver tissue presented as absolute weight (A), normalized by % of body weight (B) and corresponding hepatic triacylglyceride (TG) accumulation (C) in O-NOD^{k} and RF-NOD^{k} mice at the end of the study at 18-24 weeks of age. Data are means ± SEM for n=12 mice per group. Two-way ANOVA with Bonferroni post-hoc test; **p<0.01, ***p<0.001.

3.3.7 Gastrocnemius muscle mass

Reductions in muscle mass (sarcopenia) have been associated with obesity, impaired insulin sensitivity and T2D (Srikanthan et al., 2010, Atlantis et al., 2009, Lee et al., 2017, Srikanthan and Karlamangla, 2011). Hence, muscle mass was assessed in gastrocnemius muscle of O-NOD^{k} and RF-NOD^{k} mice at the end of the study (18-24 weeks of age). The right gastrocnemius muscle weights of all mice groups are presented as absolute tissue weights (Figure 21).

There was no difference in gastrocnemius muscle in terms of absolute weight among both O-NOD^{k} and RF-NOD^{k} mice sub-strains, on either NC or HF diet (Figure 21A). However, when normalized to body weight, 23 and 18% reduction in muscle weight was observed in both HF-fed O-NOD^{k} and RF-NOD^{k} mice compared to their NC-fed controls, respectively (Figure 21B). Muscle weight was also lower in the HF-fed O-NOD^{k} mice than the RF-NOD^{k} mice counterparts. This was in line with current literature showing reduction in muscle mass with increased obesity.

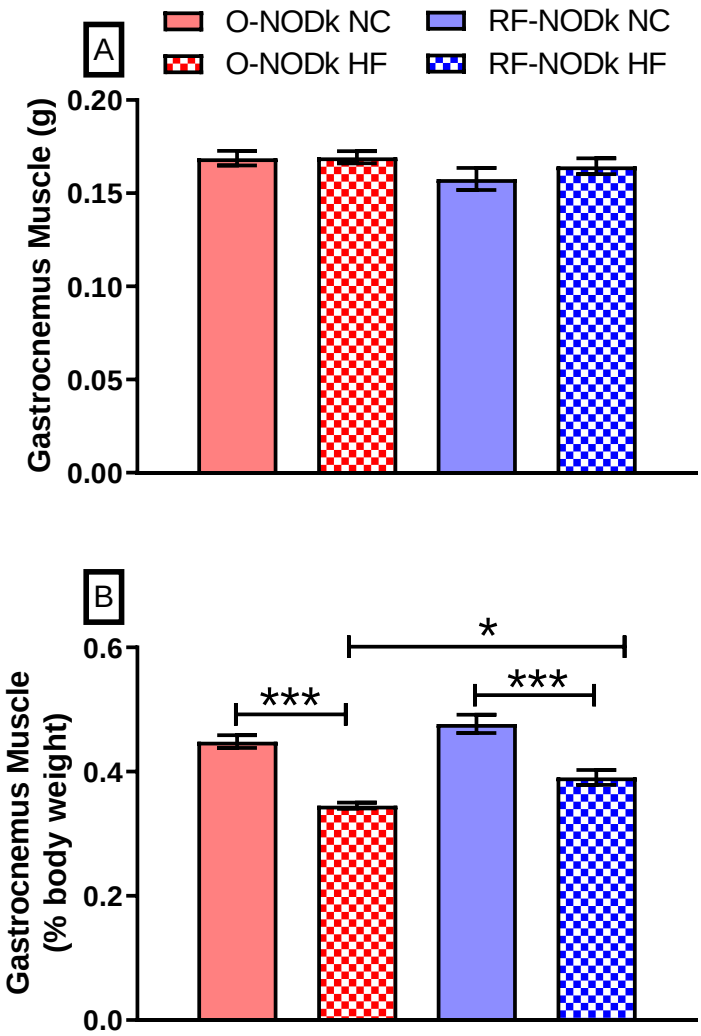

Figure 21: Gastrocnemius muscle mass in O-NOD^{k} and RF-NOD^{k} mice at the end of the study. Gastrocnemius muscle weight presented as absolute weight (A) and normalized by % of body weight (B) in O-NOD^{k} and RF-NOD^{k} mice at the end of the study at 18-24 weeks of age. Data are means ± SEM for n=12 mice per group. Two-way ANOVA with Bonferroni post-hoc test; *p<0.05, **p<0.01, ***p<0.001.

3.3.8 Pancreatic tissue weight and histological analysis

Obesity can promote alterations in the endocrine pancreas, including increased number of pancreatic islets and islet hypertrophy (enlargement) and augmented β-cell mass (Bock et al., 2003, Roat et al., 2014). Additionally, prolonged exposure to a nutrient excess environment can also lead to ectopic fat deposition in the pancreas, if the adipose storage capacity is exceeded. The appearance of fat depots in pancreas has been associated with β-cell dysfunction, although it is not necessarily the cause. Similarly, infiltration of macrophages in the islets can cause inflammation, consequently leading to β-cell dysfunction (Böni-Schnetzler et al., 2008, Maedler et al., 2002). Hence, pancreatic histological analysis and comparative islet morphometry could provide critical information regarding development of T2D in HF-fed O-NOD^{k} mice and protection in RF-NOD^{k} mice.

3.3.8.1 Pancreas tissue weight

Pancreas tissue was dissected from both O-NOD^{k} and RF-NOD^{k} mice at the end of the study (18-24 weeks of age) and weighed. The absolute pancreas tissue weight was similar among all mice groups and no diet or sub-strain effect on the pancreas weight was observed (Figure 22A). However, when normalized to body weight, a 30% reduction in pancreas weight was observed in both HF-fed mice compared to their chow controls (Figure 22B).

3.3.8.2 Pancreas islet morphology

Blinded microscopic analysis of H&E stained pancreatic sections revealed that both O-NOD^{k} and RF-NOD^{k} mice fed on a NC diet have regular round and oval-shaped islet morphology, whereas both mice groups subjected to prolonged HF-feeding presented more enlarged and complex shaped islets (Figure 23).

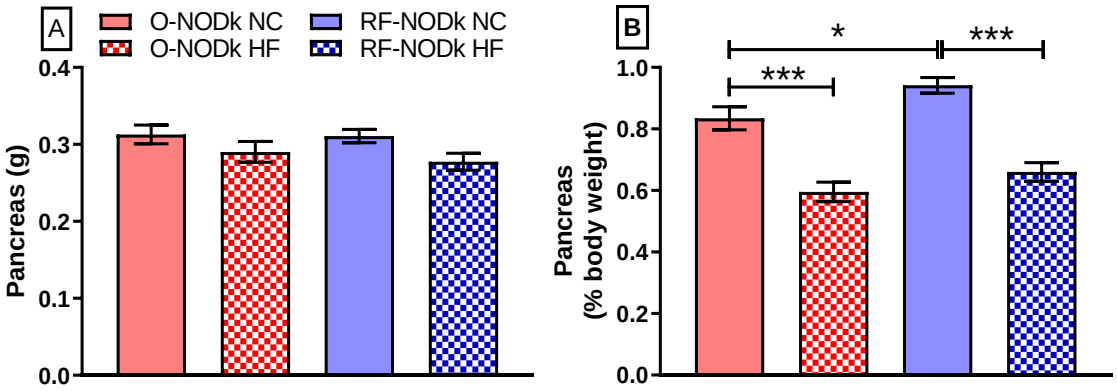

Figure 22: Pancreatic tissue weights of NC and HF-fed O-NOD^{k} and RF-NOD^{k} mice at end point. Pancreas weight presented as absolute weight (A) and normalized by % of body weight (B) in O-NOD^{k} and RF-NOD^{k} mice at the end of the study at 18-24 weeks of age. There was no differences in absolute pancreas weight between O-NOD^{k} and RF-NOD^{k} mice on both NC and HF diet, but a 30% reduction was observed when tissue weight was normalized to body weight. Data are means ± SEM for n=12 mice per group. Two-way ANOVA with Bonferroni post-hoc test; *p<0.05, ***p<0.001.

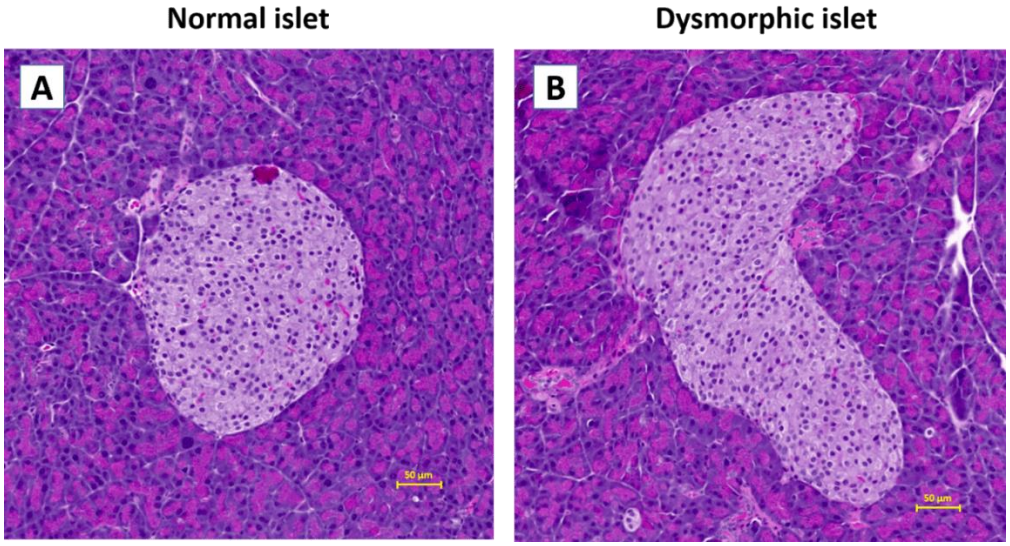

Figure 23: Representative images of H&E stained pancreatic sections depicting enlarged complex shaped islet morphology of O-NOD^{k} and RF-NOD^{k} mice. Normal islets were represented by regular round and oval-shaped morphology in NC-fed mice (A), while larger complex shaped islets (B) were observed in HF-fed mice of both sub-strains of mice. Scale bar is 50µm, 20x magnification.

3.3.8.3 Fat accumulation in the pancreas

During tissue fixation in formalin for preparation of H&E slides, the lipids from adipocytes present in the pancreas section are dissolved, leaving the area occupied by these fat cells empty. This allows indirect evaluation of fat accumulation within the pancreatic sections by determination of these "empty" fat cells. Pancreatic fat deposition was evaluated in one single section of the entire pancreas that was H&E stained and scanned using slide scanner, as per the protocol detailed in Chapter 2.3.5.1. Since the entire pancreas was scanned, all areas of the pancreas including the head, tail and body were included in the analysis.

Representative images of the fat deposits in O-NOD^{k} and RF-NOD^{k} mice are shown in Figure 24 and scored according to a pre-determined criteria for the number of fat deposits (see Appendix Table 1). In general, both groups of mice fed on a NC diet displayed infrequent fat deposits within the pancreas (Table 3). On the other hand, HF-feeding led to a higher percentage of mice with greater number of pancreatic fat deposits compared to NC-fed mice (chi-square, $p<0.001$). This HF diet effect was particularly evident in the O-NOD^{k} mice, which had 8 out of 12 mice that presented with moderate amount of fat deposits, while HF-fed RF-NOD^{k} mice only had 2 mice with similar amount of fat accumulation (chi-square, $p<0.05$). A Pearson's correlation coefficient test was performed on the glucose levels of the mice and the severity of the pancreas fat accumulation, which showed a positive correlation between the two parameters ($r=0.6096$, $p<0.0001$).

Together, these results show that HF-feeding was associated with increased fat infiltration in the pancreas. However, O-NOD^{k} mice developed a greater degree of pancreatic fat accumulation compared to the RF-NOD^{k} mice which was directly related to glucose concentrations, suggesting that pancreas fat is associated with the diabetes phenotype of these mice. However, conclusions about causality are not possible.

Table 3: Summary of H&E-stained pancreas sections scored for the presence of fat deposits in pancreatic sections of NC or HF-fed O-NOD^{k} and RF-NOD^{k} mice (18-24 weeks of age)

Mice groups	Degree of pancreatic fat deposition				Total mice
	Infrequent	Mild	Moderate	Severe	
O-NOD^{k}- NC	8	4	0	0	12
O-NOD^{k}-HF	1	3	8	0	12
RF-NOD^{k}-NC	11	1	0	0	12
RF-NOD^{k}-HF	6	4	2	0	12

Results are presented as number of mice in each group with respective degrees of fat deposits from one pancreatic section.

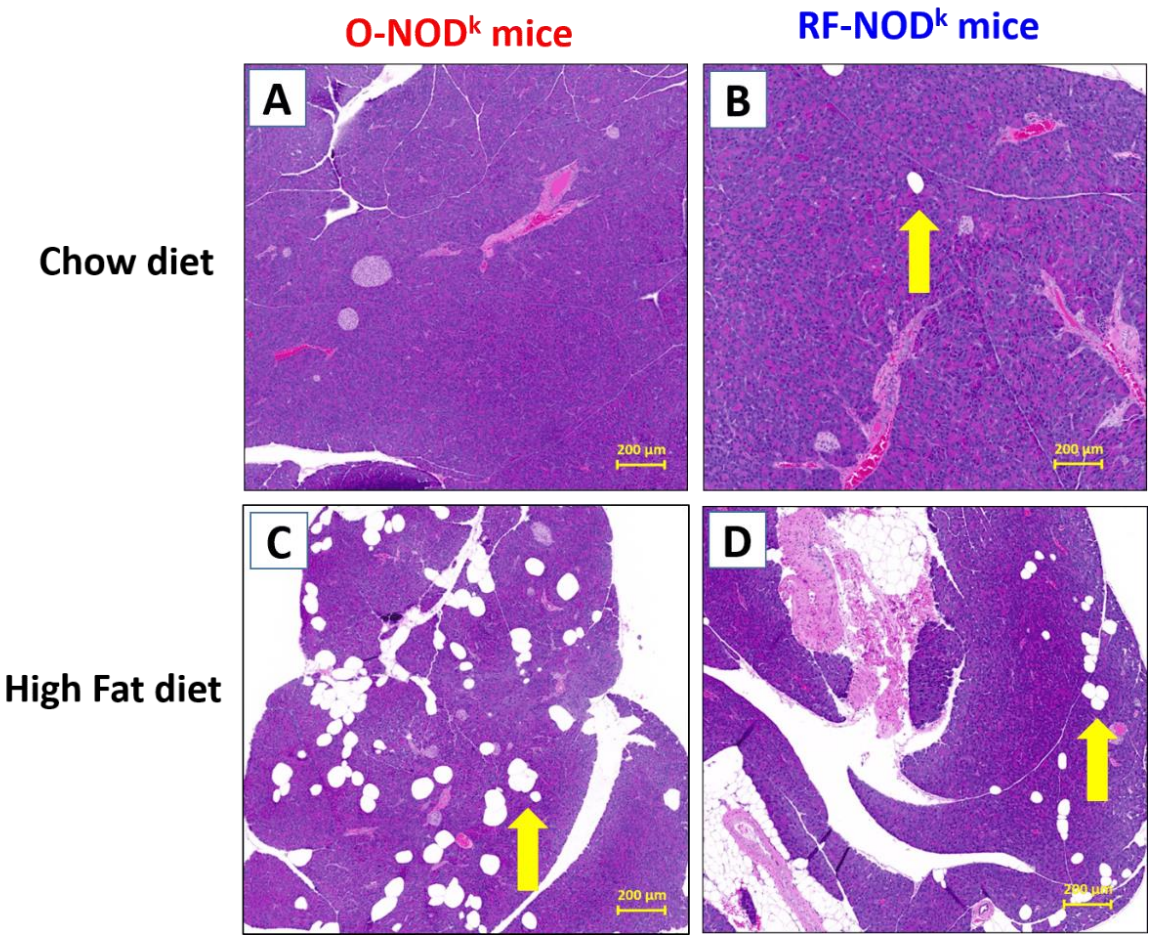

Figure 24: Representative images of H&E-stained pancreas sections illustrating fat deposits in O-NOD^k and RF-NOD^k mice at the end of study. Most NC-fed mice (A-B) showed minimal fat deposits (infrequent fat infiltration), whereas HF-feeding led to increased fat deposition in both mice groups, with noticeable higher number in the O-NOD^k mice (moderate fat infiltration) compared to the RF-NOD^k mice (mild fat infiltration) (C-D). Scale bar is 200µm, 20x magnification. Yellow arrows point towards areas of fat deposition.

3.3.8.4 Pancreatic inflammation

Although the NOD^{k} mice have the MHC H2^{k} locus of the B10 mice which protects them from autoimmune diabetes, the presence of insulitis was evaluated in all pancreatic sections to eliminate the possibility of an immune attack being responsible for β-cell death and diabetes development in the O-NOD^{k} mice.

Histological examination showed no evidence of islet insulitis among any of the mice groups studied. However, a small percentage of mice presented chronic peri-ductal (<10%) and peri-islet (<5%) inflammation, which was detected at low levels in both O-NOD^{k} and RF-NOD^{k} mice (Figure 25 and Table 4).

Among the NC-fed mice group, only 3 out of 12 O-NOD^{k} mice and 6 out of 12 RF-NOD^{k} mice, presented with mild peri-ductal inflammation. Contrastingly, HF-feeding caused an increase in chronic peri-ductal inflammation in both sub-strains of mice (11 out of 12 mice for each sub-strain, chi-square, $p<0.001$). HF-fed O-NOD^{k} mice group had a higher number of mice that presented with moderate peri-ductal inflammation, affecting a greater percentage of ducts, compared to RF-NOD^{k} mice. Out of the 11 HF-fed O-NOD^{k} mice with chronic peri-ductal inflammation, 7 mice had inflammation affecting less than 10% of its ducts, 3 mice had 10-50% of ducts with inflammation, and only 1 mouse had more than 50% of its ducts affected by chronic inflammation (Table 4). On the other hand, among the 11 affected HF-fed RF-NOD^{k} mice, most of them had less than 10% of the ducts affected by chronic inflammation. The one HF-fed RF-NOD^{k} mouse that developed a high degree of duct inflammation (>50%) was the mouse that also developed overt diabetes. Nonetheless, no sub-strain effect was observed in the degree of chronic peri-ductal inflammation between O-NOD^{k} and RF-NOD^{k} mice (chi-square, not significant).

Peri-islet inflammation was absent in all NC-fed mice, and was observed in only 3 HF-fed mice of each sub-strain, affecting less than 5% of the total number of islets present in the section (Table 4).

Collectively, these results show the absence of invasive insulitis in both O-NOD^{k} and RF-NOD^{k} mice. Chronic peri-ductal inflammation, mostly of mild degree, was observed in both sub-strains of mice, which increased with HF-feeding, but did not differ between the mice sub-strains. Chronic peri-islet inflammation was seen in a small number of mice in both sub-strains, with <5% off islets being affected when present.

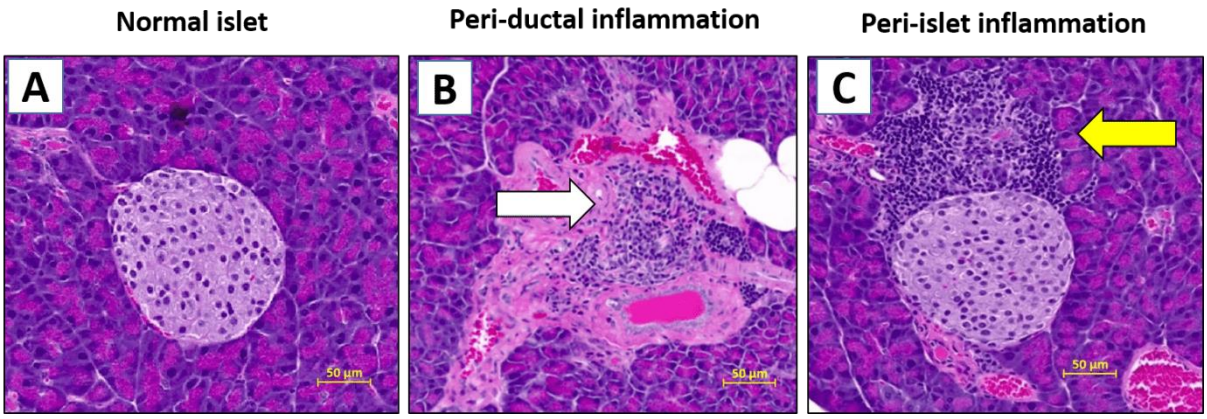

Figure 25: Representative images of H&E stained pancreas sections showing chronic peri-ductal and peri-islet inflammation in O-NOD^{k} and RF-NOD^{k} mice. Normal islet with no inflammation (A), peri-ductal (B) and peri-islet (C) chronic inflammation in the pancreas. Scale bar is 50µm, 20x magnification. White arrows point towards the region of peri-ductal inflammation, while yellow arrows point towards the region of peri-islet inflammation.

Table 4: Summary of H&E-stained pancreas sections scored for degree of chronic peri-ductal and peri-islet inflammation in NC and HF-fed O-NOD^{k} and RF-NOD^{k} mice (18-24 weeks of age)

Mice groups	Incidence of peri-ductal inflammation				Incidence of peri-islet inflammation	
	Number of affected mice	% of ducts affected			Number of affected mice	% of islets affected (average of 3 mice)
		< 10%	10-50%	>50%		
O-NOD^{k} NC	3/12	3	0	0	0	-
O-NOD^{k} HF	11/12	7	3	1	3	3.5%
RF-NOD^{k} NC	6/12	6	0	0	0	-
RF-NOD^{k} HF	11/12	9	1	1	3	5%

Results are presented as number of mice in each group with respective degrees of chronic inflammation from one pancreatic section. The incidence of peri-islet inflammation over the total number of islets was obtained for each of the 3 mice affected.

3.3.8.5 Islet cell apoptosis

The H&E stained pancreas sections were also preliminarily screened for the presence of apoptosis in the islet cells, which was identified by the presence of cells with a dense nucleus with fragmented chromatin and dark eosinophilic cytoplasm (Figure 26).

On the NC diet, O-NOD^{k} mice displayed no islet cell apoptosis, whereas only 1 RF-NOD^{k} mouse presented with evidence of apoptosis in 2.5% of the total islets on its pancreas section (Table 5). On the other hand, when stressed by prolonged HF-feeding, more mice developed islet cell apoptosis in both sub-strains (chi-square, $p<0.001$). This was further exacerbated in the O-NOD^{k} mice, where 10 out of 12 mice showed evidence of apoptosis in approximately 5% of the total number of islets, compared to only 3 out of 12 HF-fed RF-NOD^{k} mice with apoptosis present in an average of 6% of the total islets (chi-square, $p<0.01$).

Interestingly, all mice displaying apoptotic pancreatic islet cells are the ones that developed hyperglycaemia after prolonged HF diet exposure. This may suggest an increase in islet apoptosis with the development of T2D. However, in order to confirm the presence of apoptosis specifically in the β-cells, further quantification through dual immunohistochemistry for insulin (β-cell marker) and activated caspase-3 (apoptosis marker) is required.

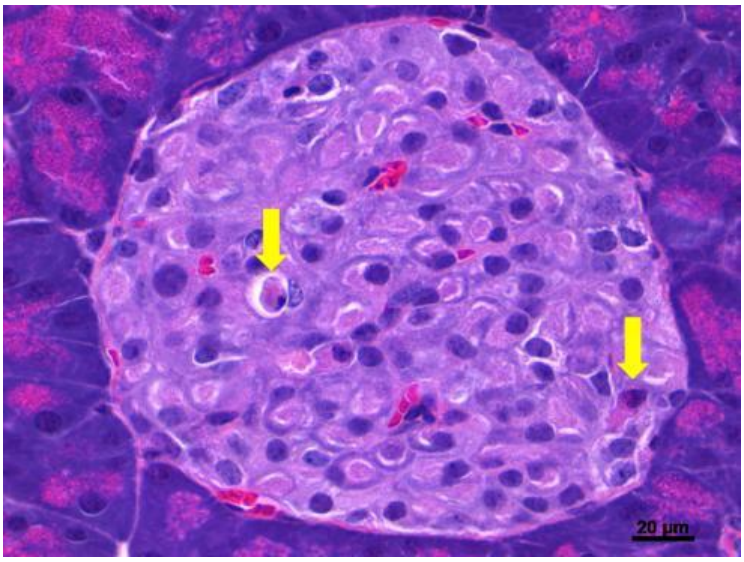

Figure 26: Representative image of H&E stained pancreas sections showing islet cell apoptosis in HF-fed O-NOD^{k} mice. Scale bar is 20µm, 20x magnification. Yellow arrows point towards cells with dense nucleus and dark pink eosinophilic cytoplasm.

Table 5: Summary of H&E-stained pancreas sections scored for the presence of islet cell apoptosis in chow and HF-fed O-NOD^{k} and RF-NOD^{k} mice (18-24 weeks of age)

Mice groups	Incidence of apoptosis	
	Number of mice affected	% of total islets with apoptosis in affected mice
O-NOD^{k} NC	0/12	-
O-NOD^{k} HF	10/12	5.1 %
RF-NOD^{k} NC	1/12	2.5%
RF-NOD^{k} HF	3/12	6.2%

Results are presented as number of mice in each group with evidence of islet cell apoptosis from one pancreatic section, and the % of total islets with evidence of apoptosis in the affected mice (n=12 mice per group).

3.3.9 Assessment of insulin immuno-stained areas in pancreatic sections

Pancreatic sections from NC-fed and HF-fed O-NOD^k and RF-NOD^k mice were immuno-stained for insulin and used for determination of islet morphometry, β-cell area and β-cell mass. Due to the development of severe hyperglycaemia in some HF-fed mice, the results were also stratified according to their non-fasting blood glucose levels at the time of harvesting.

3.3.9.1 Islet number and size

The number and size of islets were blindly assessed from a single level of insulin immune-stained pancreas sections for all mice groups (Figure 27). Both O-NOD^k and RF-NOD^k mice fed on a NC or HF diet displayed similar islet numbers per pancreas section, regardless of their diet (Figure 28A). However, when the total islet numbers were expressed per mm^2 of pancreas, a significant increase in islet number was observed in both HF-fed O-NOD^k and HF-fed RF-NOD^k mice compared to their NC controls (87.6 ± 4.8 *vs* 71.4 ± 4.9, HF-fed *vs* NC-fed O-NOD^k mice, respectively, $p<0.05$) (99.1 ± 5.6 *vs* 77.0 ± 4.9, HF-fed *vs* NC-fed RF-NOD^k mice, respectively, $p<0.05$) (Figure 28B). Nonetheless, there was no sub-strain difference in islet numbers expressed per pancreas section or per mm^2 of pancreas.

These islets were then distributed according to their average size into different groups (Figure 29). Islets smaller than 9000 μm^2 can be identified as "small" islets, islets sized between 9000 and 21,000 μm^2 considered as "medium", and islets larger than 21,000 μm^2 as "large" islets. Small islets constituted around 75% in number of the total islets in both O-NOD^k and RF-NOD^k mice irrespective of diet, compared to the medium and large islets. The highest islet frequency distribution was observed within the 500-2999 μm^2 group for both mice sub-strains. Among the small islet groups, there was no significant alteration in size distribution between the NC controls. Among the HF-fed mice groups, O-NOD^k mice had a lower number of very small

islets (<499 μm^2) compared to HF-diet RF-NOD^k mice (14 ± 2 *vs* 25 ± 3 islets per pancreas, respectively, $p<0.01$) (Figure 29).

In the medium sized islet groups, NC-fed O-NOD^k mice had a significantly reduced number of islets in the 15,000-20,999 um^2 range compared to NC-fed RF-NOD^k mice ($p<0.05$). On the other hand, HF-feeding in the O-NOD^k mice led to more islets in the 9000-14,999 um^2 size range compared to its NC control ($p<0.05$). Nonetheless, there were no sub-strain differences in medium-sized islet distribution between the HF-fed O-NOD^k and HF-fed RF-NOD^k mice. Finally, the NC-fed O-NOD^k and RF-NOD^k mice had similar distribution of large islets. A diet effect was observed in which HF-fed O-NOD^k mice displayed higher frequency of bigger islets compared to NC-fed O-NOD^k mice ($p<0.05$). However, no significant difference in islet size and numbers were observed between the HF-fed O-NOD^k and HF-fed RF-NOD^k mice (Figure 29).

Together, these results show that although HF-feeding led to an increase in overall islet number per mm^2 of pancreas in both O-NOD^k and RF-NOD^k mice, its effect on islet size was more evident in O-NOD^k mice with a shift evident from small islets to large islets. The only clear difference between sub-strains was a lower number of the smallest islets in HF-fed O-NOD^k compared to HF-fed RF-NOD^k mice (Figure 29).

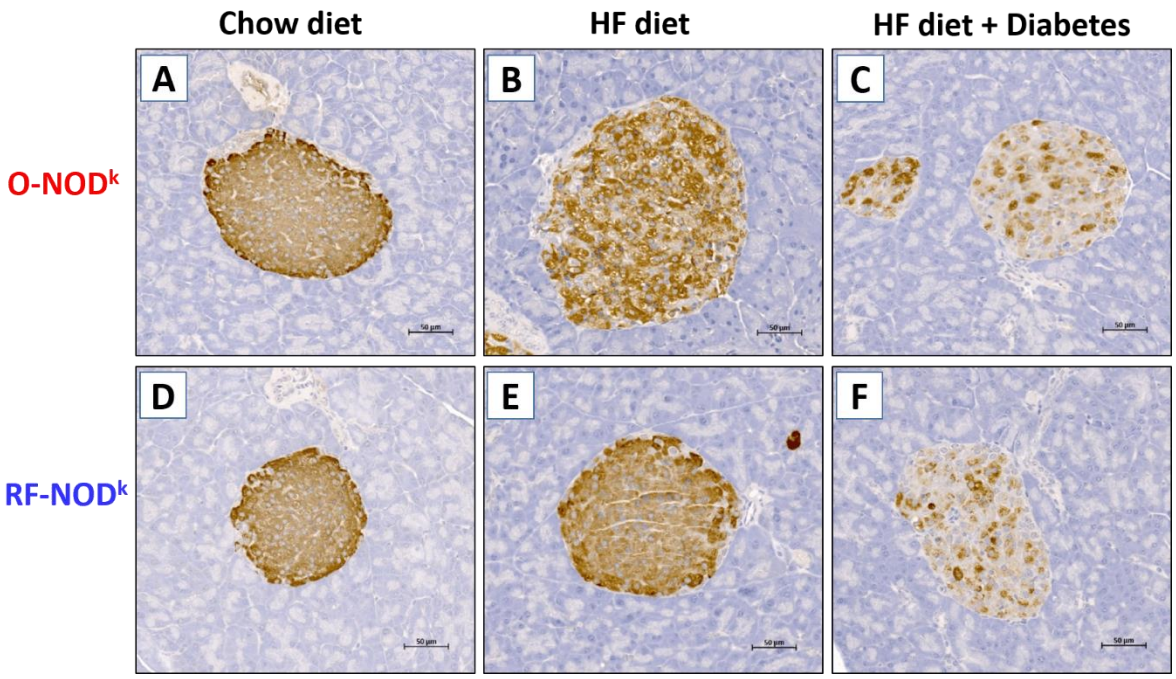

Figure 27: Representative images of islets immuno-stained for insulin in pancreatic sections of NC and HF-fed O-NOD^k and RF-NOD^k mice at the end of the long term study (18 to 24 weeks of age). Islets of mice on NC diet (A and D) and HF diet (B and E) were stained for insulin (brown). Box C represents the islets of HF-fed O-NOD^k mice that developed hyperglycaemia (> 12 mM non-fasting blood glucose levels), displaying less intense insulin staining than the rest of the groups. Similarly, in box F, the islet of the single HF-fed RF-NOD^k mouse that developed T2D shows a similar reduction in islet insulin staining as the diabetic O-NOD^k mice in box C. Scale bar is 50µm, 20x magnification.

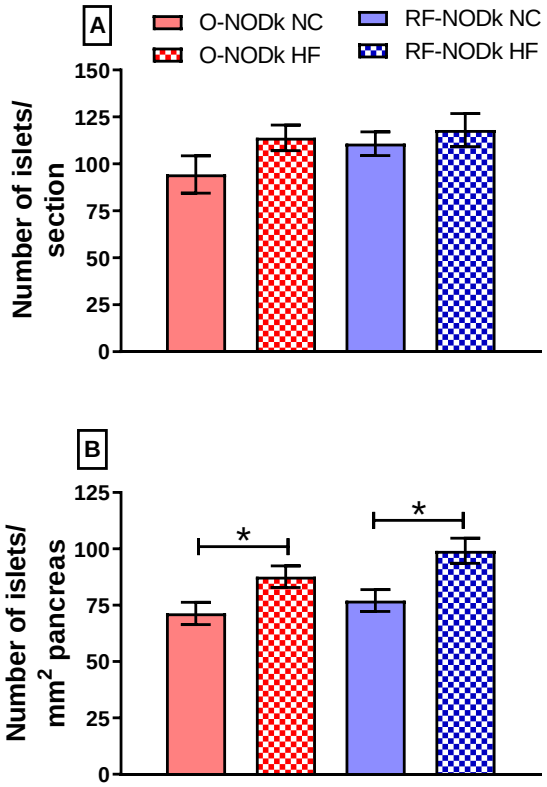

Figure 28: Total number of islets present in insulin IHC-stained pancreatic sections of NC and HF-fed O-NOD^{k} and RF-NOD^{k} mice at the end of the long term study (18 to 24 weeks of age). No significant difference in average islet number per pancreas section was observed among any of the groups (A). However, when islet numbers were normalized by pancreatic section area (mm^2), HF-fed mice of both sub-strains showed significantly higher number of islets compared to chow controls (B). Data are means ± SEM for n=8 mice per group from an average of 3 pancreatic sections. Two-way ANOVA with Bonferroni post-hoc test. *$p<0.05$.

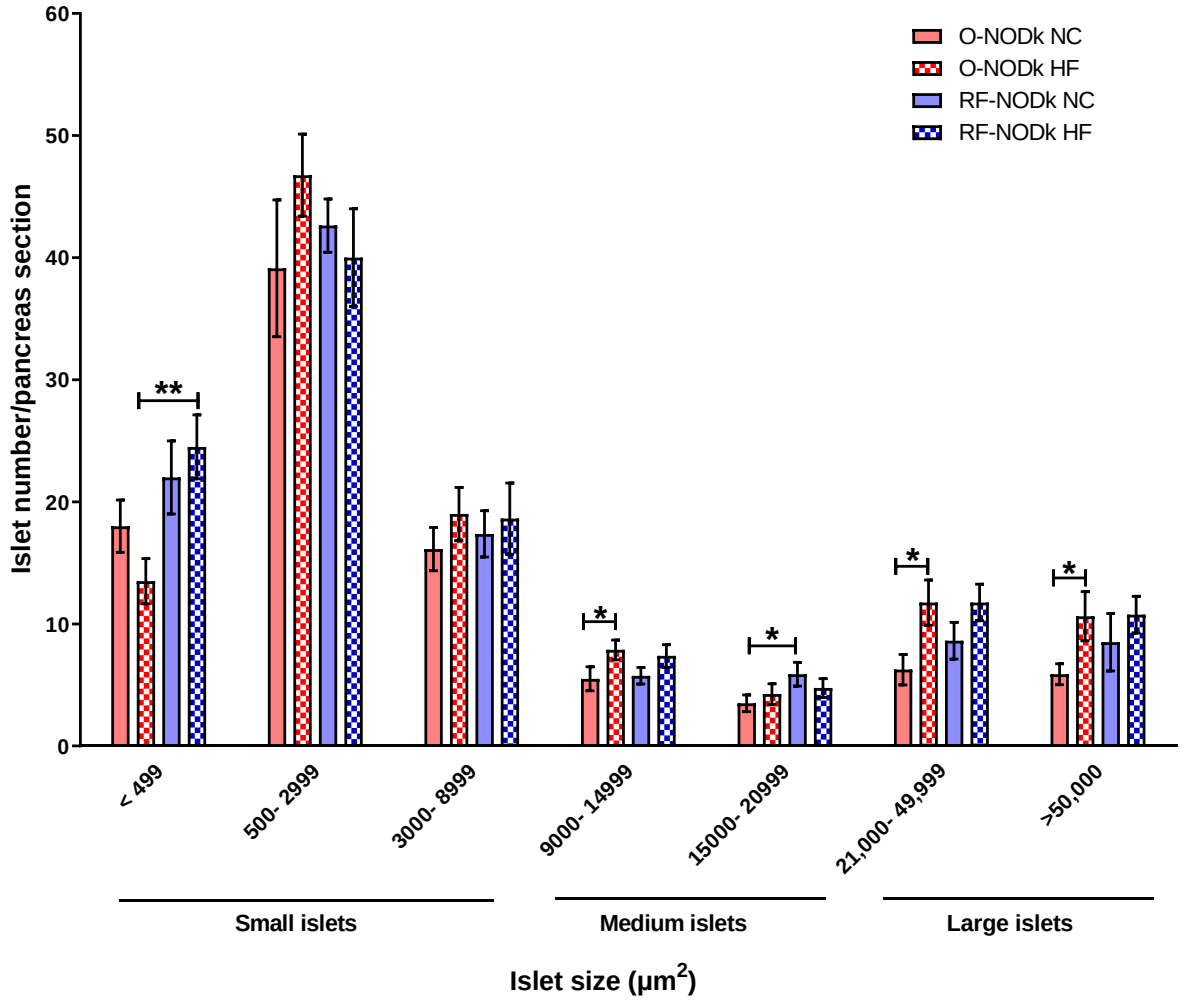

Figure 29: Relative frequency distribution of the size of islets in pancreatic sections of NC and HF-fed O-NOD^{k} and RF-NOD^{k} mice at the end of the long-term study (18 to 24 weeks of age). Islets with sizes below 9,000 um^2 were designated as small islets, 9,000- 20,999 um^2 as medium-sized islets and above 21,000 um^2 as large islets. There was no significant difference in islet size distribution between the two sub-strains fed on a HF diet. Data are means ± SEM for n=8 mice per group from an average of 3 pancreatic sections. Two-way ANOVA with Bonferroni post-hoc test. $^{*}p<0.05$, $^{**}p<0.01$.

3.3.9.2 Islet β-cell area

β-cell area was expressed per islet as well as per the total area of the pancreas (Figure 30A and C). The results were also further stratified according to the fed-state blood glucose levels (Figure 30B and D).

The % of β-cell area per islet area was similar between both mice groups fed on a NC diet (Figure 30A). In response to prolonged HF-feeding, only O-NOD^{k} mice had significantly lower β-cell area compared to its NC control (74.5 ± 1.1 *vs* 60.2 ± 4.1%, respectively, $p<0.05$). However, when the islet β-cell area was stratified based on the mice blood glucose levels, it was observed that hyperglycaemic HF-fed O-NOD^{k} mice (BGL ≥ 12 mM) had a significant reduction compared to the rest of the HF-fed O-NOD^{k} mice group (56.0 ± 3.7 *vs* 72.9 ± 6.5 %, respectively, $p<0.05$) (Figure 30B). A similar decrease was also observed in the single diabetic HF-fed RF-NOD^{k} mouse compared to the rest of the normoglycaemic HF-fed RF-NOD^{k} mice group (49.5 ± 0 *vs* 65.4 ± 4.5 %, respectively).

The % β-cell area occupied in the total area of the pancreas section (Figure 30C), was similar among the mice groups, except the HF-fed RF-NOD^{k} mice which showed a significant increase compared to its NC control (0.9 ± 0.1 *vs* 0.6 ± 0.1 %, respectively, $p<0.05$). Upon stratification based on blood glucose levels, HF-fed mice of both groups with glucose levels below 12 mM, displayed greater β-cell area than the NC-fed mice (1.2 ± 0.2 *vs* 0.7 ± 0.1 %, HF-fed *vs* NC-fed O-NOD^{k} mice, respectively, $p<0.01$) (0.9 ± 0.1 *vs* 0.6 ± 0.1 %, HF-fed *vs* NC-fed RF-NOD^{k} mice, respectively, $p<0.01$) (Figure 30D). However, % β-cell area per pancreas was significantly reduced in the hyperglycaemic HF-fed mice of both O-NOD^{k} and RF-NOD^{k} mice, compared to the rest of the sub-strains respective HF-fed group.

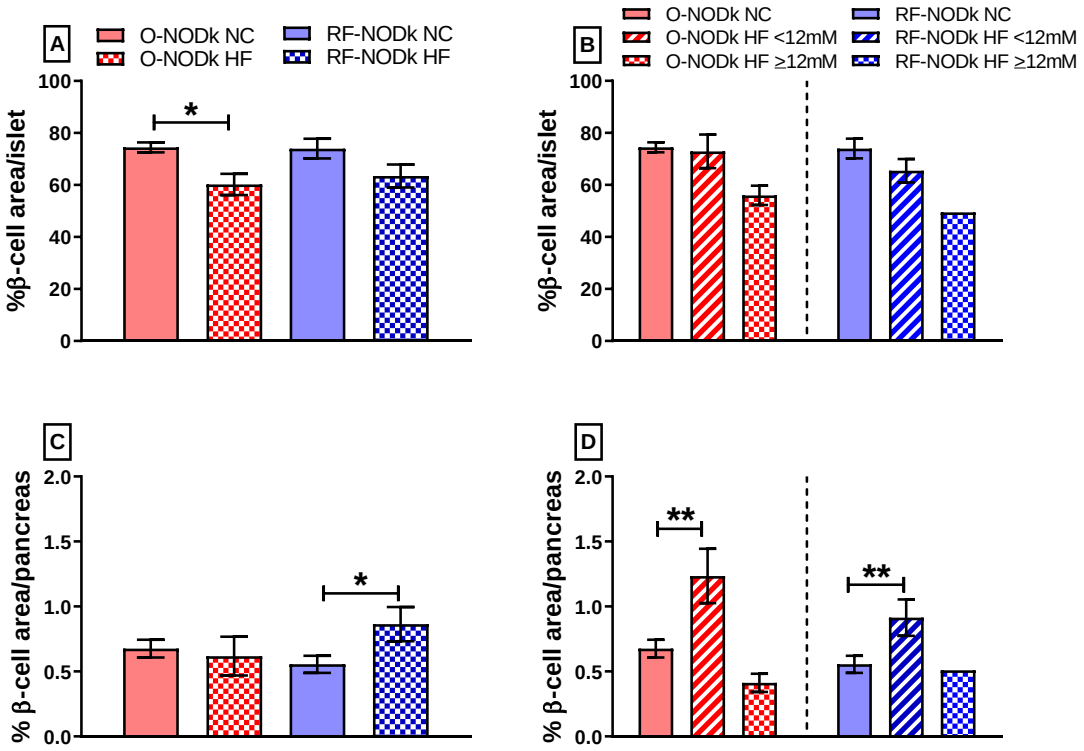

Figure 30: β-cell area of NC and HF-fed O-NOD^{k} and RF-NOD^{k} mice at the end of the long term study (18 to 24 weeks of age). The % β-cell area per islet area (A) and per pancreas section (C). Results obtained for HF-fed O-NOD^{k} mice group were also stratified according to blood glucose levels (≥ or < 12 mM at fed state) (B and D). HF-fed mice with elevated blood glucose levels presented a reduction in the % β-cell area per islet and per pancreas section compared to HF-fed mice without elevated glucose. Data are means ± SEM for n=8 mice per group from an average of 3 pancreatic sections. HF O-NOD^{k} mice with glucose <12 mM (n=2 mice) and ≥12 mM (n=6 mice), HF RF-NOD^{k} mice with glucose (< 12mM (n=7 mice) and ≥12 mM (n=1 mouse). Two-way ANOVA with Bonferroni post-hoc test. $^{*}p<0.05$, $^{**}p<0.01$.

3.3.9.3 β-cell mass

Initial islet β-cell mass assessment of the NC-fed mice revealed that O-NOD^{k} mice had increased pancreatic β-cell mass compared to NC-fed RF-NOD^{k} mice (2.3 ± 0.3 *vs* 1.7 ± 0.1, respectively, $p<0.05$, n=8 mice/ group) (Figure 31A). On the contrary, while the HF diet intervention did not cause significant changes in the O-NOD^{k} mice, it led to increased β-cell mass in the RF-NOD^{k} mice compared to its NC-fed RF-NOD^{k} mice (2.6 ± 0.5 *vs* 1.7 ± 0.1 mg, respectively, $p<0.05$). Despite this, no significant differences were observed in the β-cell mass of HF-fed O-NOD^{k} and HF-fed RF-NOD^{k} mice.

However, when the β-cell mass of the HF-fed mice groups were stratified based on their glycaemic levels, discernible differences were observed between the groups (Figure 31B). In the HF-fed O-NOD^{k} mice with elevated blood glucose levels (≥ 12 mM), there was a noticeable decrease in β-cell mass compared to the non-diabetic mice (1.2 ± 0.3 *vs* 3.8 ± 1.0 mg, respectively, $p<0.001$), which was also reduced when compared to control NC-fed O-NOD^{k} mice (1.2 ± 0.3 *vs* 2.2 ± 0.3 mg, respectively, $p<0.01$). Similarly, the single diabetic HF-fed RF-NOD^{k} mouse also displayed approximately a 50% reduction in its β-cell mass compared to the rest of its normoglycaemic group.

The difference in islet β-cell mass after stratification based on blood glucose levels suggests the presence of β-cell compensation in mice with increased β-cell mass and blood glucose < 12 mM, whereas mice with overt diabetes (BGL ≥ 12 mM) have β-cell decompensation in association with loss of β-cell mass. Loss of β-cell mass with hyperglycaemia was evident in both sub-strains of mice, but occurred with much greater frequency in the more diabetes-prone O-NOD^{k} mice (6 of 8 HF-fed O-NOD^{k} mice compared to 1 of 8 HF-fed RF-NOD^{k} mice) (chi-square, $p<0.05$).

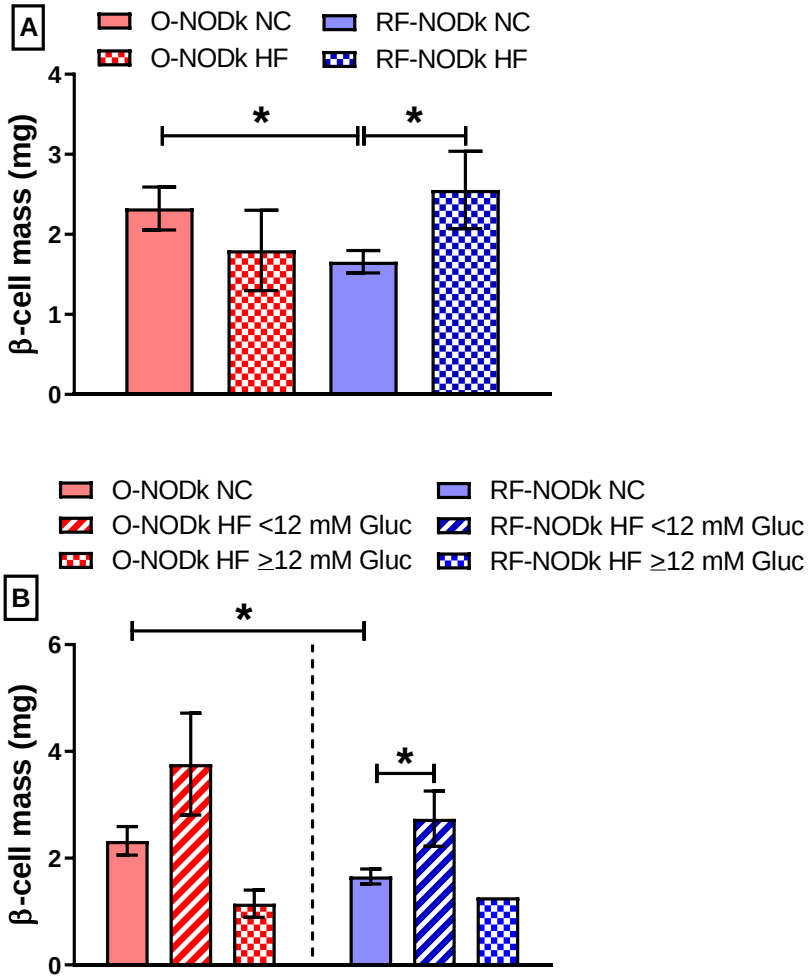

Figure 31: β-cell mass in NC and HF-fed O-NOD^{k} and RF-NOD^{k} mice at the end of the long-term study (18 to 24 weeks of age). Results are shown as β-cell mass per mice group (A) or stratified based on non-fasting blood glucose levels (≥ or < 12 mM) (B). HF-fed mice with elevated blood glucose levels presented a significant reduction in β-cell mass. Data are means ± SEM for n=8 mice per group from an average of 3 pancreatic sections. HF O-NOD^{k} mice with glucose <12 mM (n=2 mice) and ≥12 mM (n=6 mice), HF RF-NOD^{k} mice with glucose (< 12mM (n=7 mice) and ≥12 mM (n=1 mouse). Two-way ANOVA with Bonferroni post-hoc test. $^{*}p<0.05$.

3.4 Discussion

Although the O-NOD^k and RF-NOD^k mice both have similar genetic backgrounds, originating from the same NOD mouse strain, albeit with divergent ancestries, their phenotypes were observed to be variable with regards to diabetes penetrance. Prolonged exposure to HF-feeding revealed that O-NOD^k mice is more predisposed to weight gain than the RF-NOD^k mice. Since all O-NOD^k mice develop obesity when fed on a HF diet and show no evidence of resistance to diet-induced obesity (DiO), this makes them a great model for HF diet studies. Increased energy intake and/or reduced expenditure could be possible factors contributing to weight gain in the O-NOD^k mice. Additionally, several studies have found that rodents overconsume HF diet due to its higher palatability (Licholai et al., 2018, van de Giessen et al., 2012). Hence, possible differences in palatability sensing between the O-NOD^k and RF-NOD^k mice could also be playing a role in diet consumption. Therefore, proper measurements of energy expenditure, physical activity and food intake, using specialized metabolic cages that causes minimum levels of stress to the mice, are required to address these points (Kalliokoski et al., 2013).

In this study, we also observed that when O-NOD^k mice were stressed by HF diet, they develop obesity-related T2D. These findings suggest that O-NOD^k mice may carry inherent genetic variants that increase the predisposition of pancreatic β-cells to failure in conditions of nutrient-related stress. The development of hyperglycaemia in the 2 HF-fed RF-NOD^k mice expands the possibility that RF-NOD^k mice may also be susceptible to the development of diabetes, albeit at a slower frequency, possibly after 24 weeks of age. However, it is also likely that these 2 RF-NOD^k mice may have retained parts of the genetic material that manifests diabetes susceptibility in the O-NOD^k mice. During the colony refreshment of the O-NOD^k mice (Figure 10), the progeny was only back-crossed two times to the NOD/ShiLtJ mice (as described in Chapter 1), which means that the RF-NOD^k mice still carry 12.5% of genetic material from O-

NOD^{k} mice. Therefore, these 2 RF-NOD^{k} mice may provide essential information for future genetic analysis.

Hyperglycaemic and euglycaemic-hyperinsulinaemic clamps are the gold standard for studying β-cell function and peripheral insulin sensitivity, but it is expensive and requires highly specialized techniques (Uwaifo et al., 2002, Shah et al., 2016). However, due to its simplicity and low costs, GTT are routinely conducted as a first screening test to predict the development of T2D. At 13 weeks of age, ipGTT revealed the development of impaired glucose tolerance (IGT) in the HF-fed O-NOD^{k} mice in the presence of elevated fasting insulin levels. Additionally, it was also observed that the glucose load was unable to trigger a rise in insulin levels, suggesting the presence of β-cell dysfunction in these mice. In human studies, a stepwise decline in 1st phase insulin secretion has been described in obese youth transitioning from normal glucose tolerance to IGT and T2D, while defects in 2nd phase insulin secretion was specifically observed with T2D (Weiss et al., 2005). Although the RF-NOD^{k} mice were also non-responsive independent of diet, it was more evident in the HF-fed O-NOD^{k} mice. Therefore, HF-fed O-NOD^{k} mice may already have defects in their 1st phase insulin secretion response. However, in order to confirm reduced insulin secretion in these mice *in vivo,* hyperglycaemic clamp studies will be required. Nonetheless, β-cell function and insulin release can be determined *in vitro* in isolated islets through GSIS tests, which were performed in the mice and are described in Chapter 4.

In this study, a subtle increase in plasma insulin levels were observed in the O-NOD^{k} mice compared to the RF-NOD^{k} mice, even on a NC diet, which was further exacerbated with HF-feeding in both O-NOD^{k} and RF-NOD^{k} mice at both fed and fasting states. This phenotype was stronger in the O-NOD^{k} mice compared to RF-NOD^{k} mice, highlighting the possibility of inherent insulin hypersecretion in the O-NOD^{k} mice and increased β-cell responsiveness to excessive nutrients. Prolonged exposure to HF diet resulted in marked hyperinsulinaemia in O-

NOD^{k} mice compared to RF-NOD^{k} mice. However, plasma insulin levels in this study were measured by radioimmunoassay (RIA), using anti-insulin primary antibody that has 40% cross-reactivity with proinsulin. Unfortunately, this type of measurement can over-estimate insulin levels (Stickle et al., 1999, Hanley et al., 2002). Therefore, separate assays specifically for proinsulin and c-peptide were used to assess insulin derivatives.

Our results showed that circulating proinsulin and c-peptide levels were increased in response to HF-feeding, principally in the O-NOD^{k} mice, therefore reflecting possible augmented β-cell function in these mice in comparison to RF-NOD^{k} mice. The ratio between insulin and c-peptide was elevated in both O-NOD^{k} and RF-NOD^{k} mice with HF-feeding. This may imply a possible defect in hepatic insulin clearance in these mice, resulting in increased insulin in circulation. Reduced hepatic insulin clearance has been associated with reduced insulin sensitivity and decline in β-cell function (Galderisi et al., 2019). However, since both O-NOD^{k} and RF-NOD^{k} mice displayed similar reduction in insulin clearance, this defect seems to be a secondary event and not the main cause promoting T2D development. Further experiments specifically designed to measure insulin clearance by the liver are required.

Acute elevation of circulating NEFA levels in normoglycaemic subjects and non-diabetic subjects predisposed to T2D have been associated with reduced insulin clearance and development of hyperinsulinaemia, whereas prolonged exposure was linked to impaired insulin secretion due to lipotoxic effects on the β-cell (Balent et al., 2002, Kashyap et al., 2003). Similarly, high plasma TG levels are characteristic of diabetes dyslipidaemia and an abnormal lipid profile, and can highlight high risk of cardiovascular diseases in T2D patients (Hermans and Valensi, 2018). In this study, HF-feeding induced similar increases in circulating NEFA and TG levels in both O-NOD^{k} and RF-NOD^{k} mice, evidencing the presence of dyslipidaemia and dysregulated adipose tissue lipolysis, developed as a consequence of adipose insulin resistance (Kim et al., 2017, Howe et al., 2011).

The adipose tissue profile of the O-NOD^{k} and RF-NOD^{k} mice showed that long-term HF-feeding led to a similar increase in subcutaneous fat depots in proportion to the body weights of both mice sub-strains. However, HF diet-induced increase in the epididymal fat tissue per % of mice body weight was almost 3 times higher in the HF-fed RF-NOD^{k} mice compared to the O-NOD^{k} mice. Despite the increased weight gain, HF-fed O-NOD^{k} mice did not substantially increase their epididymal fat pads as the RF-NOD^{k} mice. Although epididymal fat is technically visceral fat, it may not behave the same as intraabdominal visceral fat. The latter is more susceptible to the development of crown-like structures around dead cells, in comparison to subcutaneous fat (Murano et al., 2008). Epididymal morphometric analysis is required to determine whether the adipocytes of the HF-fed O-NOD^{k} mice are atrophied and if they are surrounded by obesity-associated inflammatory cells, which could suggest WAT dysfunction. This could explain the lesser expansion of this fat depot in HF-fed O-NOD^{k} mice in comparison with HF-fed RF-NOD^{k} mice (Weisberg et al., 2003). On the contrary, BAT expansion could be reflective of increased activity, thus resulting in increased energy dissipation and protection against diet-induced obesity and T2D (Wang et al., 2015, Hamann et al., 1996). In this study, BAT weights were equally increased with HF-feeding in both O-NOD^{k} and RF-NOD^{k} mice. Therefore, BAT is unlikely to play a primary role in the development of diabetes in the O-NOD^{k} mice.

Excessive nutrient intake in obesity has been associated with reduced adipocyte insulin sensitivity, leading to the inability of adipocytes to store more NEFA, causing lipid spill-over to other non-adipose tissues (Almandoz et al., 2013). Since the HF-fed O-NOD^{k} mice had higher body weight than the RF-NOD^{k} mice, but a disproportionately lower increase in epididymal fat depots, this suggests that excess fat in these mice may instead be directed ectopically towards other peripheral tissues such as liver and muscles. While no difference in gastrocnemius muscle weight was observed among any of the mice groups, interestingly, O-

NOD^{k} mice developed significant hepatomegaly after long-term HF diet consumption. This increase was concomitant with a greater increase in hepatic TG content in HF-fed O-NOD^{k} mice, indicative of liver steatosis. The steatotic phenotype of the O-NOD^{k} mice could be due to increased uptake of saturated fats from the HF diet or resulting from reduced FFA uptake by the adipose tissue due to adipose tissue dysfunction. It could also be associated with anomalies in the liver such as increased *de novo* lipogenesis and/or impaired FFA clearance, since hepatic *de novo* lipogenesis is exacerbated by hyperglycaemia and insulin resistance in NAFLD (Smith et al., 2020, Crescenzo et al., 2013). Since hepatic TG accumulation is inversely correlated to hepatic insulin sensitivity and insulin clearance, it could potentially be contributing to the metabolic phenotype observed in the HF-fed O-NOD^{k} mice (Kotronen et al., 2007, Fabbrini et al., 2009, Najjar and Perdomo, 2019).

Although an increase in pancreas size has been described with obesity in subjects, careful interpretation of these results needs to be exercised since these observations were derived from human studies using imaging techniques such as computed tomography (CT) scans (Saisho et al., 2007). Furthermore, pancreas tissue weights resulting from human autopsy reports are also not precise due to the difficulty in separation of the tissue from its surrounding tissues and duodenal walls (Yagihashi, 2017). Thus, it can be argued that the pancreas tissue weights observed in our study cannot be directly compared to clinical reports. Interestingly, in our study, prolonged HF-feeding did not lead to major alterations in pancreas weight in both sub-strains, which was similar to observations made on C57BL/6J mice subjected to a similar length of HF diet intervention (He et al., 2020).

Increasing incidences of pancreatic steatosis have been described in humans and in rodent models of T2D, defined as non-alcoholic fatty pancreas disease (NAFPD) (Lee et al., 2009, Sepe et al., 2011, Mathur et al., 2007). However, there is still disparity in current literature about the link between pancreatic fat and T2D. While some studies report no relation between

the two (Yamazaki et al., 2016, Saisho et al., 2007), others have found a positive association between pancreatic steatosis and T2D (Lim et al., 2014, Bi et al., 2019). In rodents, increased pancreatic fat accumulation was associated with HF diet-induced obesity and T2D (Quiclet et al., 2019). In this study, higher incidence of fat deposition was observed in the pancreas of most obese mice. Notably, a diet-strain interaction was observed with higher number of fat deposits observed in HF-fed O-NOD^{k} mice compared to RF-NOD^{k} mice. There was a positive correlation between glycaemic levels and severity of pancreatic fat accumulation, suggesting a possible association between T2D and pancreatic steatosis in these mice. Therefore, prolonged HF-feeding and ectopic fat accumulation in the pancreas, could be associated with β-cell dysfunction and potentially the diabetes phenotype of the O-NOD^{k} mice. Causality between the two, however, is not possible from this study.

Although the NOD mice develop spontaneous insulitis on a NC diet (Alonso et al., 2015), no evidence of acute insulitis was observed in any of the mice groups studied herein, regardless of their diet or sub-strain background. This is consistent with the protective effects of the MHC H2^{k} haplotype in the NOD^{k} mice. Instead, chronic inflammation in the peri-ductal region was observed in both O-NOD^{k} and RF-NOD^{k} mice fed on NC or HF diet, in varying degrees. While mice fed on a NC diet displayed minimal peri-ductal inflammation, HF-feeding was associated with greater severity of inflammation in O-NOD^{k} mice, although the number of ducts affected were mostly less than 10% of total ducts. However, since the chronic inflammation was only present in the peri-ductal and peri-islet region of the pancreas, and did not infiltrate the islets, it is unlikely to be a causal factor for the development of T2D in the O-NOD^{k} mice.

Several morphometric studies conducted in rodent models of obesity-induced T2D have reported an association between obesity and large islets displaying abnormal morphology (Janssen et al., 2001, Roat et al., 2014). In our study, visual inspection of H&E stained pancreas

sections provided qualitative evidence of the presence of large complex-shaped islets in the HF-fed mice, while insulin immune-stained pancreas sections allowed quantitative measurement of islet number and size.

A significant difference in total islet number was not expected since islet neogenesis occurs mostly during fetal development (Levetan, 2010, Bock et al., 2003, Kehm et al., 2018). Interestingly, in this study, when the total islet numbers were normalized to the area of the pancreas section, an increase in islet number was observed in both HF-fed mice, suggesting a potential role of HF-feeding with islet neogenesis. The size distribution of the islets showed that small islets made up approximately 75% of the total islet numbers. Deng *et al* reported an association between smaller islets and T2D, while a disproportionate loss of large islets was observed in T2D patients (Deng et al., 2004, Kilimnik et al., 2011). Contrarily, in this study, the number of small islets was similar between the diabetic and normoglycaemic mice. Additionally, while HF-feeding did not affect the islet size of the RF-NOD^{k} mice, implying no islet expansion, there was an increase in the number of large islets in the O-NOD^{k} mice in response to HF diet. Expansion in islet size is well-documented in rodent models fed on a HF-diet (Gupta et al., 2017, Roat et al., 2014). Further experiments are required to test for the expression of proliferation marker Ki67, in order to determine an association between islet size and the diabetes phenotype in the HF-fed O-NOD^{k} mice. However, since no major differences in the frequency of large islets was observed with HF-feeding between O-NOD^{k} and RF-NOD^{k} mice, this is unlikely to influence the metabolic phenotype observed among the two mice sub-strains.

Butler *et al* have reported almost 50% increase in β-cell mass in obese subjects compared to lean controls, while other studies have also positively correlated β-cell mass to body mass index (BMI) (Butler et al., 2003, Yoon et al., 2003). Similar increases in β-cell mass was observed in

mice models with obesity (Hull et al., 2005, Sone and Kagawa, 2005, Wang and Brubaker, 2002). Furthermore, during the pathogenesis of T2D, the β-cell compensation phase is normally associated with higher β-cell mass due to increase in β-cell neogenesis, which is followed by progressive loss of β-cell mass with T2D (Butler et al., 2003, Yoneda et al., 2013). In accordance with current literature, HF-feeding was associated with increased β-cell mass in both O-NOD^{k} and RF-NOD^{k} mice with normoglycaemia. This suggests that these mice may possibly be undergoing β-cell compensation in response to increased insulin resistance and HF diet-induced obesity. Likewise, a decline in β-cell mass was observed in HF-fed O-NOD^{k} mice with glucose levels over 12 mM and the single diabetic HF-fed RF-NOD^{k} mouse, indicative of the onset of β-cell decompensation and loss of β-cells in these mice.

β-cell apoptosis has been associated with decreased β-cell mass in T2D (Butler et al., 2003, Sakuraba et al., 2002). A three-fold increase in apoptotic cell death was reported in obese diabetic patients compared to lean controls, while other studies have also shown the effect of hyperglycaemia and lipotoxicity on apoptotic β-cell death (Federici et al., 2001, Shimabukuro et al., 1998, Butler et al., 2003). Although there was no evidence of islet apoptosis in the control NC-fed mice, our preliminary results from H&E-stained pancreatic sections showed the presence of a small percentage of apoptotic cells in the islets of diabetic HF-fed O-NOD^{k} and RF-NOD^{k} mice. While this suggests a possible association between islet apoptosis and development of hyperglycaemia, a more refined technique to confirm the existence of β-cell apoptosis in these islets, such as dual immunohistochemistry for insulin and activated caspase-3, are required.

In summary, when challenged by prolonged HF-feeding, O-NOD^{k} mice present a varied phenotype of obesity, diabetes and hyperinsulinemia. At 13 weeks of age, these mice develop IGT which is accompanied by loss of 1st phase insulin secretion and inability to induce an appropriate insulin response to glucose. After 18 weeks of HF-feeding, they also develop

hepatic steatosis-induced hepatomegaly and have a higher degree of pancreatic fat accumulation. HF-fed O-NOD^{k} mice with non-fasting blood glucose below 12 mM are still in the compensation phase with enlarged islets and increased β-cell mass. On the other hand, mice that had developed overt diabetes have significantly reduced β-cell mass, possibly due to apoptosis, without any evidence of classic insulitis. Therefore, further *in vitro* β-cell function tests are required to determine whether any other alterations in the insulin secretory function of the β-cells could be playing a role in the development of the diabetes phenotype of the O-NOD^{k} mice.

Chapter 4

Results

In vitro assessment of β-cell function in

O-NOD^{k} and RF-NOD^{k} mice

4.1 Introduction

Insulin resistance and β-cell dysfunction are the hallmark characteristics of T2D, leading to persistent hyperglycaemia. Therefore, regulation of the insulin secretory function of pancreatic β-cells is vital for maintaining glucose homeostasis. Although glucose is known as the main insulin secretion stimulator, GSIS by the β-cells is also modulated by other factors such as fatty acids, amino acids, neuronal stimulus and hormones (Rorsman and Ashcroft, 2018). In particular, fatty acids are known to play a role in amplification pathways of insulin secretion, which is an important process observed during compensatory insulin secretion, established in response to obesity-associated insulin resistance. Previous studies have shown that fatty acids can induce a marked increase in insulin secretion, particularly in high glucose concentrations (Gravena et al., 2002, Nolan et al., 2006a).

In the previous chapter, long-term HF-feeding led to the development of impaired glucose tolerance and hyperinsulinaemia in the O-NOD^{k} mice, followed by the development of T2D. The *in vivo* studies showed that at 13 weeks of age, HF-fed O-NOD^{k} mice were glucose intolerant in association with marked fasting hyperinsulinaemia and a complete lack of insulin secretion in response to a glucose load during ipGTT, suggestive of islet β-cell dysfunction. On the other hand, HF-fed RF-NOD^{k} mice were much less glucose intolerant, with lesser abnormalities in insulinaemia. Therefore, these results suggest the islet β-cells of O-NOD^{k} mice in response to chronic HF-feeding, over-secrete insulin in the basal state and develop impaired nutrient-induced insulin secretion. Worsening glycaemic control in HF-fed O-NOD^{k} mice is then associated with β-cell apoptosis, loss of β-cell mass and the development of a severe T2D phenotype. Thus, in this chapter, pancreatic islets from both groups of mice (O-NOD^{k} and RF-NOD^{k}) submitted to 4 weeks of diet intervention were isolated for *in vitro* GSIS experiments. The duration of the diet exposure (4 weeks) selected for these experiments was based on

previous observations showing that mice from both groups were still normoglycaemic during this period, therefore allowing evaluation of islet β-cell function prior to the onset of significant hyperglycaemia and its well-known islet glucotoxic effects.

The GSIS experiments, as well as assessing glucose as the only secretagogue, also investigated the effects of acute exposure of pancreatic islets to a mix of fatty acids (palmitate and oleate), which are the most common physiological dietary fatty acids. Additionally, we also evaluated the effects of the glucose-dependent insulin secretagogue IBMX, which increases intracellular cAMP levels and potentiates GSIS in a dose-dependent manner (Komatsu et al., 2002). Finally, in order to account for the varied islet sizes with different insulin secretory capacity in the endocrine pancreas, normalization parameters such as total islet protein content and total insulin content (TIC) were used as reliable correction factors for insulin secretion during the GSIS experiments (Henquin, 2019).

Therefore, the aim of this chapter was to *(i)* evaluate whether these two sub-strains of NOD^k mice display differential insulin secretory responses to nutrient stimulus and *(ii*) whether these responses would be influencing their phenotype.

4.2 Experimental design

Age-matched male O-NOD^k and RF-NOD^k mice were randomly distributed into NC or HF diet groups for feeding from 4-8 weeks of age (Figure 32). Body weight and non-fasting blood glucose levels were monitored fortnightly until the end of the study. Prior to euthanasia, tail blood was collected for plasma insulin analysis. Islet isolation was performed following enzymatic digestion of the mouse pancreas, as described in Chapter 2. Following overnight incubation, batches of 8 size-matched islets were submitted to static insulin secretion in the

presence of low (3 mM) and high (16 mM) glucose, either in the absence or presence of 0.25 mM fatty acids (palmitate: oleate mix, 1:1), or 0.1 mM IBMX (detailed in Chapter 2). Secreted insulin and respective islet insulin contents were measured at the end of the incubation period. Islet protein content was also quantified from islets collected prior to GSIS. This study was performed in 8 week old mice fed on HF diet for 4 weeks, since islet β-cells at this age should not be affected by apoptosis yet. If GSIS was performed at a later age, the islets would have been depleted of insulin due to the high insulin secretion demand and too fragile to be isolated for *in vitro* studies.

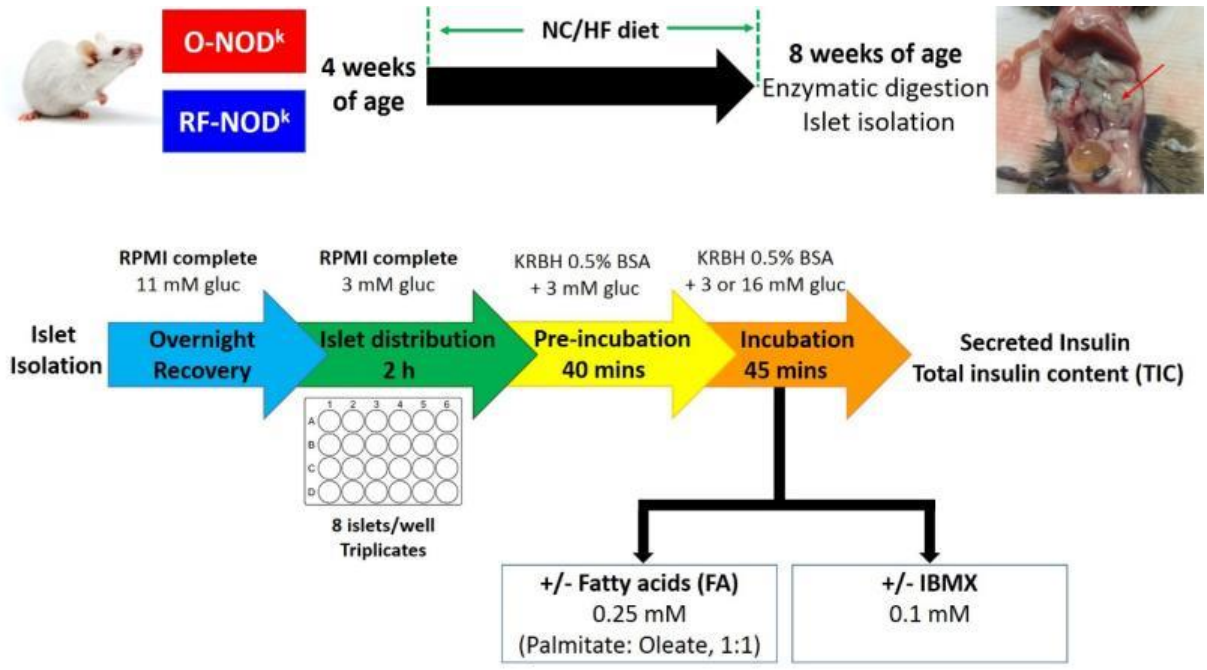

Figure 32: Experimental design of the *in vitro* study to assess β-cell function in the islets of male O-NOD^k and RF-NOD^k mice undergoing diet intervention from 4 to 8 weeks of age. Mice were placed on NC or HF diet from 4 to 8 weeks of age and pancreatic islets were isolated at the end of the study period for *in vitro* static insulin secretion.

4.3 Results

4.3.1 Body weight, non-fasting glucose and plasma insulin

At 8 weeks of age, O-NOD^{k} and RF-NOD^{k} mice on a NC diet showed no difference in body weight (Figure 33A). However, on a HF diet, O-NOD^{k} mice were heavier when compared to its NC control (30.9 ± 0.7 *vs* 27.2 ± 0.4 g, HF-fed O-NOD^{k} *vs* NC-fed O-NOD^{k}, respectively, $p<0.001$) and its HF-fed RF-NOD^{k} mice counterpart (30.9 ± 0.7 *vs* 26.5 ± 0.3 g, HF-fed O-NOD^{k} *vs* HF-fed RF-NOD^{k} mice, respectively, $p<0.001$).

All groups of mice were normoglycaemic when fed on a NC diet, but when stressed by HF-feeding, both mice sub-strains developed fed-state mild hyperglycaemia compared to their NC-fed controls (O-NOD^{k}, 7.6 ± 0.1 *vs* 6.4 ± 0.2 mM, HF *vs* NC, $p<0.001$; RF-NOD^{k}, 7.3 ± 0.2 *vs* 6.3 ± 0.1 mM, HF *vs* NC, $p<0.001$) (Figure 33B). Nonetheless, neither of the HF-fed mice sub-strains had developed diabetes by 8 weeks of age.

Fed-state plasma insulin levels were similar between the NC-fed control O-NOD^{k} and RF-NOD^{k} mice (Figure 33C). However, after 4 weeks of HF-feeding, the plasma insulin levels in the O-NOD^{k} mice were elevated compared to the RF-NOD^{k} mice (5.4 ± 1.1 *vs* 2.7 ± 0.3 ng/mL, respectively, $p<0.01$).

Taken together, these results show that after 4 weeks of HF-feeding, O-NOD^{k} mice were heavier and more hyperinsulinaemic than the RF-NOD^{k} mice. Both sub-strains, however, had developed a similar degree of fed-state mild hyperglycaemia. Thus at this age, we were able to perform *in vitro* assessment of β-cell function in islets that were not yet stressed by more than mild hyperglycaemia.

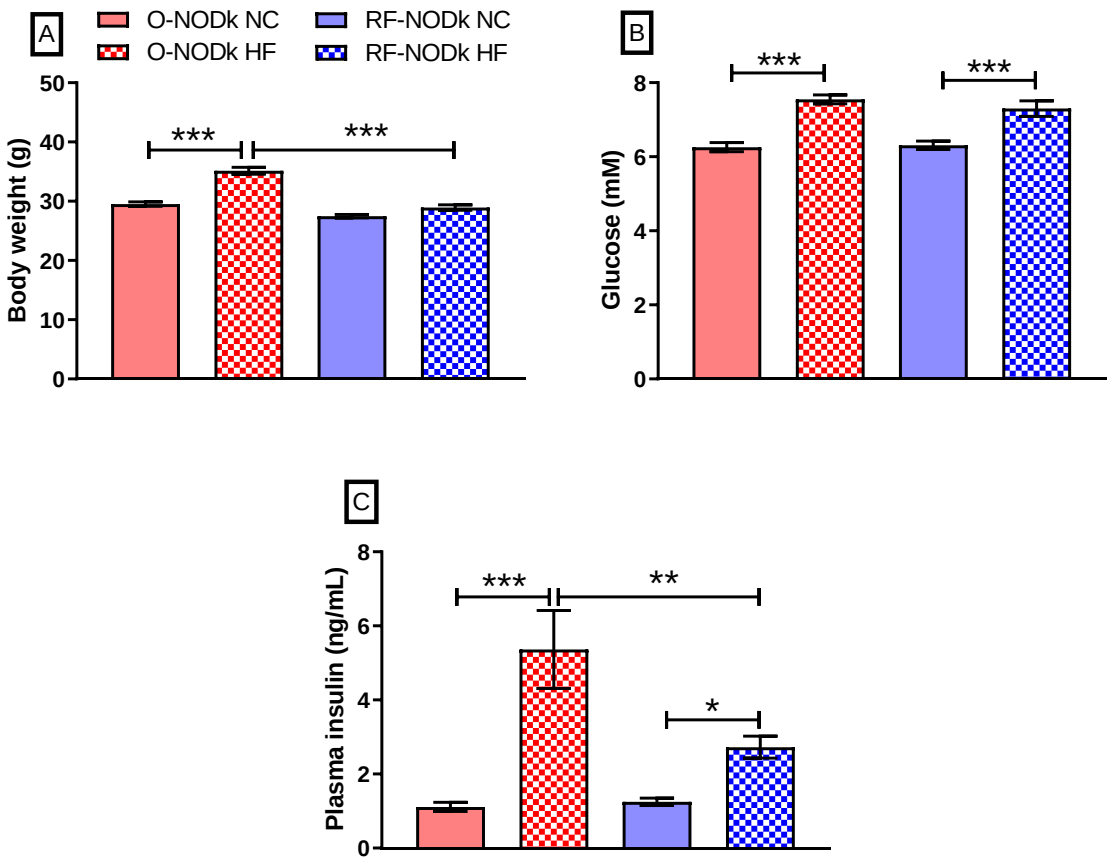

Figure 33: O-NOD^{k} and RF-NOD^{k} mice responses to 4 weeks of HF diet intervention. Male O-NOD^{k} and RF-NOD^{k} mice were fed on NC or HF diet from 4 to 8 weeks of age. At the end of the dietary period, HF-fed O-NOD^{k} mice were heavier than RF-NOD^{k} mice counterparts and NC-fed controls (A). Both groups of HF-fed mice developed mild elevation in fed-state blood glucose (B), which was accompanied by development of significant hyperinsulinaemia in the O-NOD^{k} mice (C). Data are means ± SEM for 12 mice per group. Two-way ANOVA with Bonferroni post-hoc test, *p<0.05, **p<0.01, ***p<0.001.

4.3.2 Total islet protein content

The presence of pancreatic islet heterogeneity in terms of size, cellular composition and architecture demonstrates the importance of normalization of GSIS during functional islet studies, since small islets secrete relatively more insulin due to higher proportion of β-cells (Dybala and Hara, 2019, Farhat et al., 2013). Hence, in order to correct for any possible effect of variable islet size on insulin secretion, normalization parameters like total islet protein content are used. In this study, no differences in islet protein content were observed between the O-NOD^{k} and RF-NOD^{k} mice, on either NC (0.326 ± 0.03 *vs* 0.393 ± 0.06 µg/islet, respectively, $p>0.05$) or HF diet (0.389 ± 0.06 *vs* 0.352 ± 0.03 µg/islet, respectively, $p>0.05$) (Figure 34A). However, it is to be noted that islet protein content is not β-cell specific and will include protein from other endocrine cell types in the islet.

4.3.3 Total islet insulin content (TIC)

Another parameter frequently used for normalization of insulin secretion is total islet insulin content (TIC), which provides information about whole islet insulin content, irrespective of β-cell function or defects in insulin secretion. Therefore, after static insulin secretion, all islets from different mice groups and conditions were recovered and sonicated in acid ethanol and insulin measurement for determination of TIC. As shown in Figure 34B, no difference in TIC was observed between the O-NOD^{k} and RF-NOD^{k} mice, on both NC (40.902 ± 1.15 *vs* 40.956 ± 2.21 ng/islet, respectively, $p>0.05$) or HF diet (42.738 ± 1.61 *vs* 40.259 ± 1.55 ng/islet, respectively, $p>0.05$). Finally, TIC normalized by total islet protein content to standardize for any differences in islet size, was similar across all groups ($p>0.05$) (Figure 34C). Together, these results suggest that 4 weeks of HF-feeding does not induce any significant alterations in islet protein or insulin content.

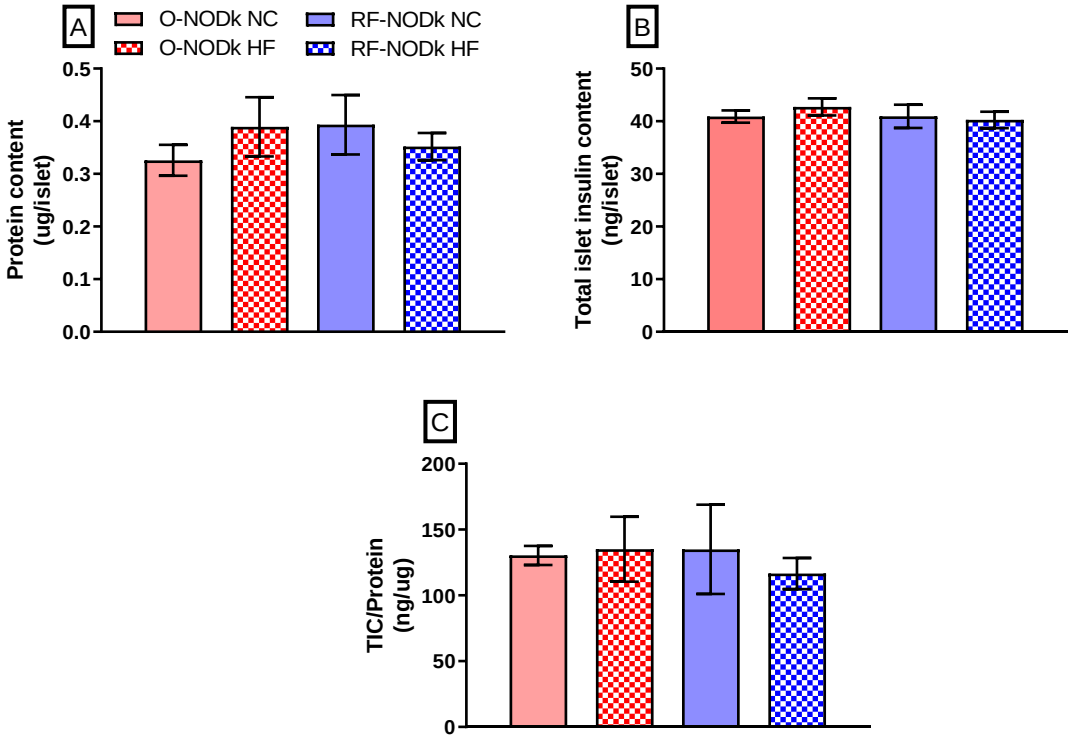

Figure 34: Islet protein and total islet insulin contents in O-NOD^{k} and RF-NOD^{k} mice following 4 weeks of dietary intervention. Groups of 60 islets of equal sizes were used for protein quantification (A). Islets used for static insulin secretion (8 islets/well) were sonicated in acid ethanol for total insulin content (TIC) assessment (B). TIC was also normalized by islet protein content (C). No significant difference in islet protein content or TIC was observed between any mice groups. Data are means ± SEM for 8-10 mice/group. Two-way ANOVA, non-significant.

4.3.4 GSIS in the presence and absence of fatty acids

Static islet insulin secretion assays were used to evaluate the β-cell function of the two sub-strains of mice fed on NC and HF diet for 4 weeks, in response to low and high glucose concentrations, in the presence or absence of fatty acids. As expected, incubation of islets in 16 mM compared to 3 mM glucose robustly stimulated insulin secretion from 2.4-2.9 fold depending on mice sub-strain and diet, but on average 2.7 fold ($p<0.0001$) (Figure 35). Insulin secretion in the presence of a mix of fatty acids (1:1 palmitate and oleate) increased insulin secretion from 1.3-1.6 fold depending on sub-strain and diet, but on average by 1.4 fold at 3 mM glucose ($p<0.0001$) and from 1.2-1.3 fold, but on average 1.3 fold at 16 mM glucose ($p<0.0001$) (Figure 35).

In the absence of fatty acids, expressed per islet, insulin secretion at 3 mM glucose was not different between groups, irrespective of sub-strain or diet. Insulin secretion in the presence of 16 mM glucose, however, was increased in islets of both HF-fed NOD^{k} mice strains compared to their islets of their respective NC-fed counterparts (Figure 35A). Of note is a higher insulin secretion in response to 16 mM glucose in islets of HF-fed O-NOD^{k} mice compared to islets of HF-fed RF-NOD^{k} mice (Figure 35A).

In the presence of fatty acids, expressed per islet, insulin secretion at 3 mM glucose was again not different between groups, irrespective of sub-strain or diet. Similar to in the absence of fatty acids, insulin secretion at 16 mM glucose in the presence of fatty acids was increased in islets of HF-fed O-NOD^{k} and HF-fed RF-NOD^{k} mice compared to their NC-fed counterparts (Figure 35B). A sub-strain difference was again seen, with higher secretion in HF-fed O-NOD^{k} mice compared to HF-fed RF-NOD^{k} mice when islets were incubated in 16 mM glucose and fatty acids (Figure 35B)

The pattern of results was similar, whether secretion was expressed per islet (Figure 35A&B), as a percentage of TIC (Figure 35C&D), or per islet protein (Figure 35E&F). However, the finding of a sub-strain difference was less apparent when the results were expressed per TIC or per protein.

Collectively, these results suggest that, when subjected to HF-feeding, O-NOD^{k} mice display increased β-cell responsiveness to both high glucose alone and high glucose in combination with fatty acids.

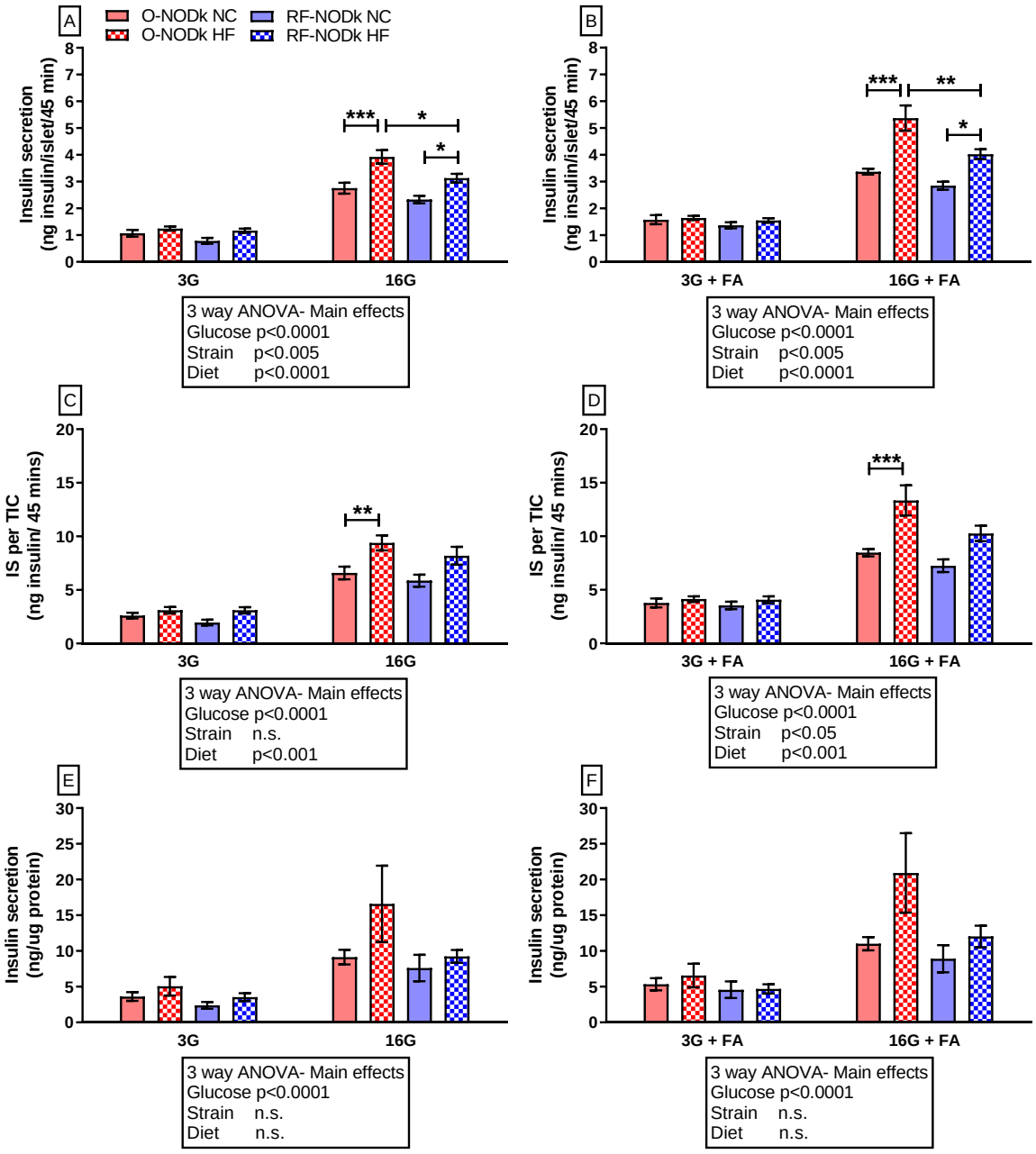

Figure 35: Glucose stimulated insulin secretion (GSIS) in the presence or absence of fatty acids, in O-NOD^{k} and RF-NOD^{k} mice after 4 weeks of HF-feeding. GSIS was assessed in isolated islets of both mice sub-strains, which were incubated with low and high glucose levels in the presence or absence of fatty acids (palmitate:oleate 1:1 mix). Insulin secretion (IS) is expressed as ng insulin/islet/45 min (A&B), IS normalized to percentage of total insulin content (TIC) /45 min (C&D) and IS normalized to islet protein/45 min (E&F). Data are means ± SEM for 7-11 mice/group. Repeated measures three-way ANOVA with Tukey post-hoc testing; *p<0.05, **p<0.01, ***p<0.001.

4.3.5 Effect of secretagogue IBMX on GSIS

Static GSIS was also examined in the presence of IBMX (0.1 mM), a phosphodiesterase inhibitor that elevates intracellular cAMP levels in the β-cells (Zhang and Tzanakakis, 2017). As expected, IBMX in the secretion incubation media led to an increase in insulin secretion from 1.6-1.7 fold depending on sub-strain and diet, but on average by 1.7 fold at 3 mM glucose ($p<0.0001$) and by 1.4 fold irrespective of sub-strain and diet at 16 mM glucose ($p<0.0001$) (Figure 36).

In the absence of IBMX, expressed per islet, insulin secretion at low glucose was again not different between groups, irrespective of sub-strain or diet (Figure 36A). Insulin secretion in the presence of 16 mM glucose, but in the absence of IBMX, was increased in both HF-fed NOD^k mice strains compared to their respective NC-fed counterparts (Figure 36A). Insulin secretion in response to 16 mM glucose in the absence of IBMX in HF-fed O-NOD^k mice compared to HF-fed RF-NOD^k mice was again found to be higher, consistent with a sub-strain difference (Figure 36A). These results are consistent with those of Figure 35A in which glucose was the only secretagogue.

In the presence of IBMX, expressed per islet, insulin secretion at 3 mM glucose was not different between groups, irrespective of sub-strain or diet. Insulin secretion at 16 mM glucose in the presence of IBMX was increased in islets of HF-fed O-NOD^k and HF-fed RF-NOD^k mice compared to their NC-fed counterparts (Figure 36B). A sub-strain difference of islet insulin secretion in response to 16 mM glucose plus IBMX was observed, with higher secretion in HF-fed O-NOD^k mice compared to HF-fed RF-NOD^k mice (Figure 36B).

The pattern of results was similar, whether secretion was expressed per islet (Figure 36A&B), as a percentage of TIC (Figure 36C&D), or per islet protein (Figure 36E&F). While the secretion at 16 mM glucose in the absence and presence of IBMX was statistically higher in

HF-fed O-NOD^{k} mice compared to HF-fed RF-NOD^{k} mice when secretion was expressed according to islets (Figure 36A&B) and TIC (Figure 36c&D), the difference was only significantly different in the presence of IBMX when the results were expressed per islet protein (Figure 6E&F).

Together, these results suggest that through PDE inhibition, IBMX has a significantly greater effect in elevating insulin secretion in the HF-fed O-NOD^{k} mice compared to the RF-NOD^{k} mice.

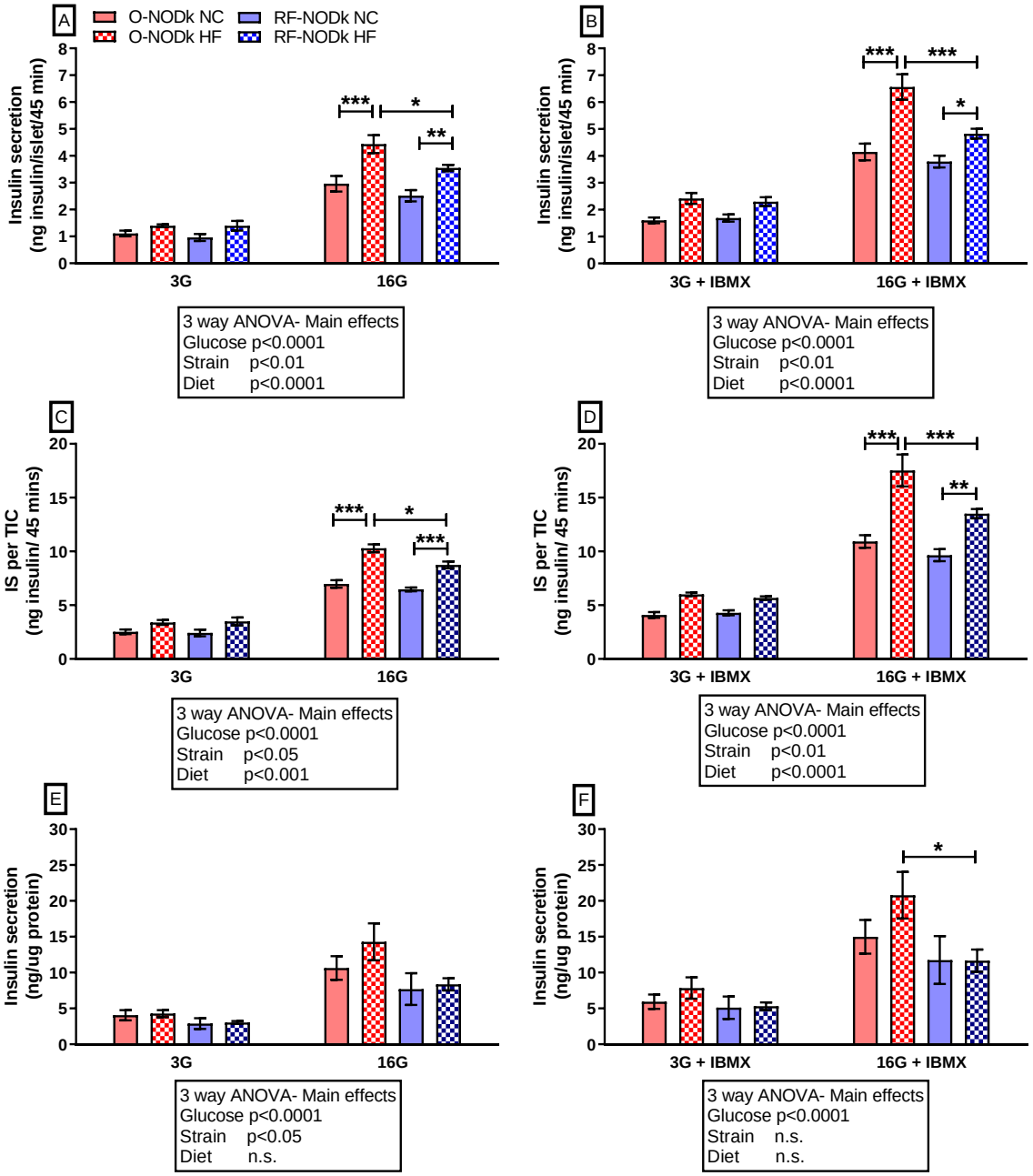

Figure 36: Glucose stimulated insulin secretion (GSIS) in the presence or absence of IBMX in O-NOD^{k} and RF-NOD^{k} mice. GSIS was assessed in isolated islets of O-NOD^{k} and RF-NOD^{k} mice and incubated at basal and high glucose in the presence or absence of 0.1 mM IBMX. Insulin secretion (IS) is expressed as ng insulin/islet/45 min (A&B), IS normalized to percentage of total insulin content (TIC) /45 min (C&D) and IS normalized to islet protein/45 min (E&F). Data are means ± SEM for 9 mice/group. Repeated measures three-way ANOVA with Tukey post-hoc testing; *p<0.05, **p<0.01, ***p<0.001.

4.4 Discussion

Several studies have suggested that insulin hyper-secretory responses to nutrient stimulus can cause β-cell metabolic acceleration and cellular stress, which in turn leads to dysfunction and cell death (Rumala et al., 2020, Corkey, 2012, Cen et al., 2016). The results presented in this chapter evaluated the *in vitro* secretory responses of islet β-cells from O-NOD^{k} and RF-NOD^{k} mice, and revealed that HF-fed O-NOD^{k} mice have an increased insulin responsiveness to glucose when compared to RF-NOD^{k} mice, which may be making them more vulnerable to cellular stress and consequently more predisposed to T2D development.

At 8 weeks of age, O-NOD^{k} mice were heavier and more hyperinsulinaemic after 4 weeks of HF-feeding compared to RF-NOD^{k} counterparts. Similarly, their blood glucose levels were mildly elevated (~ 17% higher) in response to HF feeding, but none of them developed a more than mild degree of hyperglycaemia prior to the experiments. No alterations in either islet protein or TIC were observed between the groups, thereby excluding islet degranulation as a possible factor promoting the development of hyperglycaemia in the HF-fed mice.

Static incubation of isolated islets in the presence of low glucose levels showed no difference in basal insulin secretion rates between O-NOD^{k} and RF-NOD^{k} mice on either diet. In accordance with GSIS studies reported in current literature (Weksler-Zangen et al., 2008, Rebelato et al., 2018), high glucose concentrations stimulated insulin secretion in both groups of mice. Interestingly, a more significant glucose potentiation in insulin secretion was observed in islets from O-NOD^{k} mice, and principally in those submitted to HF-feeding. The difference in the insulin response of the two mice sub-strains to glucose stimulation is not unexpected. Various studies performed using diet induced obese C57BL/6 mice sub-strains have reported within-strain variability in GSIS (Hull et al., 2017, Attané et al., 2016). The most interesting fact in our results is that the *in vitro* islet insulin response to glucose does not fully translate to

the *in vivo* insulin responses observed during the ipGTT in Chapter 3, where HF-fed O-NOD^{k} mice, although hyperinsulinaemic prior to glucose stimulation, did not increase their insulin secretion in response to the glucose load. Therefore, it is possible that compared to the controlled *in vitro* conditions of this experiment, islets within a whole body environment may respond differently to glucose stimulation due to various interactions between other tissues and circulating metabolites and other substances that could be inhibiting nutrient-stimulated insulin secretion *in vivo*. Some possible ways to alter the culture medium conditions of the *in vitro* GSIS experiments to mimic *in vivo* conditions could be to culture the islets in serum from a donor mouse, or high FFA/glucose to mimic a glucolipotoxic environment, instead of resting the islets overnight in a culture medium with 11 mM glucose. However, this would require different serum mediums for each mice group since the *in vivo* conditions of chow-fed mice would be different from the HF-fed mice.

In this same GSIS experiment, the effect of fatty acids on insulin secretion was also studied, since one of the ways fatty acids can potentiate GSIS is by depending on Ca^{2+} oscillations to stimulate insulin exocytosis (Gerst et al., 2019). Additionally, long chain fatty acids also activate free fatty acid receptor 1 (FFAR1, also known as GPR40) on the β-cells, which enhances Ca^{2+} release from the ER through activation of inositol 1,4,5-triphosphate (IP3) receptors, stromal interaction molecule 1 (STIM1) and Ca^{2+} channel Orai1 (Usui et al., 2019). Thus GPR40 activation leads to potentiation of GSIS in response to fatty acids, whereas deletion of GPR40 impairs *in vivo* GSIS (Alquier et al., 2009, Kebede et al., 2008).

At both basal (3 mM) and elevated (16 mM) glucose, fatty acids augmented insulin secretion by respectively 40% and 30%. Once again, this augmentation in GSIS was most notably significant in the HF-fed O-NOD^{k} mice. Comparable observations were made by Gravena *et al* when acute stimulation of islets from human and rats with fatty acids led to a glucose dose-

dependent insulin response, with low response at 3 mM glucose and highest insulin secretion at 16 mM (Gravena et al., 2002). These findings also parallel observations made in the C57BL/6NJ and C57BL/6NN mice sub-strains, in which it has been speculated that the findings relate to genetic differences arising from mutations in genes such as *Rptor*, a key regulator of mTORC1 signaling (Attané et al., 2016). Hence the difference in islet β-cell function between the O-NOD^{k} and RF-NOD^{k} mice, which is more pronounced in HF diet induced obese conditions, could be attributed to genetic mutations in genes associated with insulin responsiveness such as glucose signaling, mitochondrial function, NADPH/NADP^{+} ratio and/or membrane polarization.

Currently, there is no consensus about the best way to present GSIS results. Furthermore, a study also showed no correlation of GSIS to normalization parameters, and suggested that GSIS performed on a small number of similar sized islets does not require normalization, and that raw GSIS was sufficient for interpretation (Slepchenko et al., 2019). Therefore, since raw insulin secretion prior to normalization and after normalization by TIC, presented similar results for the HF-fed O-NOD^{k} mice with the same trend corrected for protein, it appears that these mice are more predisposed to increased β-cell responsiveness to a nutrient stimulus compared to RF-NOD^{k} mice.

Additionally, the difference in insulin responses of the two mice sub-strains when stimulated by IBMX was investigated. Although Ca^{2+} is the key activating signal for insulin exocytosis, cAMP has a key K_{ATP} channel-independent amplifying role for insulin secretion in the β-cells (Tengholm, 2012). Since IBMX can increase intracellular cAMP levels, it is a known pharmacological glucose-dependent insulin secretagogue (Zhang and Tzanakakis, 2017). At basal glucose conditions, incubation with IBMX led to increased insulin secretion of about 70%. This augmentation by IBMX was of the order of 40% when islets were stimulated by

higher glucose concentrations. Although there was an increase in GSIS with HF-feeding in both mice sub-strains, it was significantly higher in the O-NOD^{k} mice compared to RF-NOD^{k} mice. This inter-sub-strain difference in insulin response was stronger compared to stimulation of islets with fatty acids, and was observed when GSIS was normalized by islet number, TIC and islet protein content. This shows that the β-cells of HF-fed O-NOD^{k} mice were significantly more insulin responsive to non-fuel stimulus such as IBMX, in the presence of high glucose.

Amplification of insulin secretion by incretin hormones such as GLP-1 also occurs through a similar pathway, by increasing cAMP levels in β-cells (Drucker, 2013, Drucker et al., 1987). GLP-1 secretion increases post-meal and accounts for almost 70% of the insulin response to glucose load (Drucker, 2013). The islets of HF-fed O-NOD^{k} mice are significantly more insulin responsive to IBMX-induced increased cAMP levels at high glucose concentrations. Thus, it can be speculated that in a whole body setting, post-prandial GLP-1-induced increase in cAMP in β-cells with high blood glucose levels could lead to the hyperinsulinaemia observed in HF-fed O-NOD^{k} mice. Nonetheless, further studies are required to investigate the effect of GLP-1 stimulation on insulin secretion of both mice strains, and to measure GLP-1 release in response to a glucose bolus and mixed meals to confirm this premise.

There are several possible reasons for the improved performance of the islets during the *in vitro* GSIS experiments compared to the *in vivo* ipGTT experiments. Firstly, the age difference of the mice and the differential period of HF feeding in each experiment could be playing a role in the improved performance in the *in vitro* experiments, as the mice were young and the islets less stressed by the HF diet due to the shorter period of exposure. At this age (8 weeks), the islets were not affected by hyperglycaemia or apoptosis. On the other hand, 13 week old mice were chosen for ipGTT since the mice were not yet diabetic at that age.

Another reason for higher insulin secretion from the islets could be due to the protocol used, where isolated islets were rested overnight in culture medium containing 11 mM of glucose, before GSIS experiments began. This could have allowed the islets to better recover after isolation, and therefore having a better performance (Alarcon et al., 2016). Unfortunately, the overnight recovery was essential to GSIS experiments as trial experiments performed at the same day of the islet isolation and after only 2 hours of recovery period did not result in successful insulin secretion. Unfortunately, the conditions used in our study did not fully mimic the *in vivo* conditions, which could also be affecting the results, as many factors present in the mouse circulation were absent during the overnight incubation. Alternatively, overnight recovery of the isolated islets in medium with heat-inactivated serum from a donor mouse submitted to similar dietary environment or overnight culture in medium containing high FFA and high glucose concentrations to mimic a glucolipotoxic environment, would perhaps be more appropriate for GSIS evaluation.

In summary, *in vitro* assessment of insulin secretion using isolated islets indicate that the insulin secretion responsiveness of HF-fed O-NOD^{k} mice is greater compared to RF-NOD^{k} mice, when stimulated by nutrient excess such as high glucose and fatty acids, as well as IBMX. This suggests that O-NOD^{k} mice could be more vulnerable to nutrient-induced β-cell stress and thereby increased T2D risk, through mechanisms related to increased β-cell work. Hyperinsulinaemia in these mice could also be inducing obesity and consequently peripheral insulin resistance as a protective mechanism, further aggravating the syndrome, and creating a vicious cycle resulting in T2D. Therefore, the higher insulin secretion responsiveness of the O-NOD^{k} mice compared to RF-NOD^{k} mice could be attributed to genetic differences with functional consequences associated with β-cell function. The genetic factors that could be influencing the metabolic phenotype observed in the mice sub-strains will be further investigated in the following chapters.

Chapter 5

Results

Inheritance of the diabetes phenotype:

Crossbreeding experiments

5.1 Introduction

Rodent models have been routinely used in the identification and characterization of novel genes and signaling pathways involved in the development of human diseases through selective breeding strategies. Also known as artificial selection, this process allows selection of naturally occurring polymorphisms or traits of interest at each generation, to produce distinct mouse lines that are homozygous for desired traits. This traditional form of genetic manipulation has been crucial for diabetes research. Several rodent models of T2D, presenting pathophysiological alterations similar to those observed in human disease, have been generated over the years (Goto et al., 1988, Attie et al., 2017, Nagao et al., 2012).

Selective breeding can also adopt a phenotype-driven forward genetics approach, to determine changes in allele frequency, which segregate at the loci and affect the phenotype of interest (Swallow and Garland, 2005). In a forward genetics study, mutagenic agents are normally used to generate random mutations in the mice, which are subsequently screened for specific disease phenotype. In this study, the diabetes phenotype observed in the O-NOD^{k} mice, is hypothesized to result from a genetic mutation. Based on this, a selective breeding study was designed where O-NOD^{k} and RF-NOD^{k} mice were cross-bred to create different mouse lines. The aim of this study was to determine the allelic frequency of the diabetes phenotype in the O-NOD^{k} mice, and identify possible segregation, according to Mendelian laws of inheritance.

Genetic heterogeneity in the same population is known to cause a spectrum of disease severity, based on the pattern of inheritance of the affected gene (McClellan and King, 2010). Hence, according to Mendelian laws of segregation, the F1 offspring generated from crossing O-NOD^{k} and RF-NOD^{k} mice, would inherit one copy of allele from each parent (van Dijk and Ellis, 2016). Punnett squares were also used for each test cross as a valuable tool to predict the genotype of the offspring, and to determine the expected Mendelian ratio according to parental

alleles. Correlation between the expected genotype ratios with the observed incidence of diabetes phenotype, helped us to ascertain whether the diabetic phenotype in the O-NOD^{k} mice is caused by a homozygous or heterozygous allele, and whether it is a dominant or recessive trait.

5.2 Experimental design

5.2.1 Cross-breeding to generate F1 mice

Six breeding cages were set up to generate F1 offspring, with 3 cages containing male O-NOD^{k} mice cross-bred with female RF-NOD^{k} mice, and another 3 cages with female O-NOD^{k} mice with male RF-NOD^{k} mice.

The F1 progeny obtained were weaned at 3 weeks of age on a NC diet. At 4 weeks of age, 38 male F1 mice were selected as experimental mice and placed on either NC diet (n=8) or HF diet (n=30), with fortnightly body weight and non-fasting blood glucose levels measurements until the end of the study at 24 weeks of age (Figure 37). At the end of the study, non-fasting tail blood was collected for blood glucose and plasma insulin analysis. Female F1 mice were maintained on a NC diet as breeders for the next generation.

The ratio of F1 male mice that develop T2D and mice that remain normoglycaemic, when subjected to long-term HF-feeding, was used to determine whether the diabetes susceptibility factor in the O-NOD^{k} mice was homozygous/ heterozygous and dominant/ recessive, based on predictive Punnett squares.

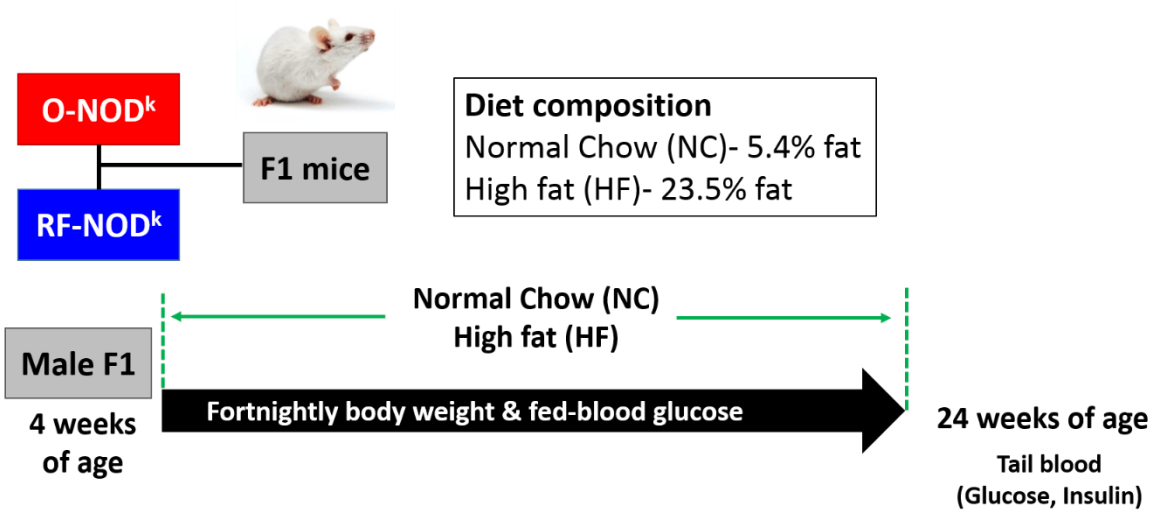

Figure 37: Experimental design of selective breeding to generate F1 mice by cross-breeding O-NOD^k and RF-NOD^k mice. O-NOD^k and RF-NOD^k breeding pairs were set up to generate F1 mice. A cohort of male F1 mice were placed on either NC or HF diet from 4 to 24 weeks of age. Fortnightly body weight and non-fasting blood glucose levels were measured at 9AM. At the end of the study, mice were euthanized and tail blood was collected for measurement of plasma insulin.

5.2.2 Back-crossing to generate F2, O-N1F1 and RF-N1F1 mice

In parallel to the phenotypic characterization of the F1 male mice, 3 additional breeding strategies were initiated when mice were sexually mature, to supplement the results observed in the F1 mice (Figure 38).

i. Male and Female F1 mice were inter-crossed to generate F2 progeny

ii. Female F1 mice was back-crossed to male O-NOD^{k} mice to generate O-N1F1 progeny

iii. Female F1 mice was back-crossed to male RF-NOD^{k} mice to generate RF-N1F1 progeny

The offspring generated from each breeding method was maintained as a separate mice line. At 3 weeks of age, F2, O-N1F1 and RF-N1F1 progenies were weaned on a NC diet. At 6 weeks of age, male F2 (n=28), O-N1F1 (n=33) and RF-N1F1 (n=30) mice were placed on HF diet until 24 weeks of age. As described in the previous section, phenotypic characterization including body weight and non-fasting blood glucose were performed fortnightly, with plasma insulin assessment at the end of the study. Mice that presented with two consecutive non-fasting blood glucose readings above 20 mM were considered to be too sick to continue with the study and were ethically culled.

Mice displaying non-fasting blood glucose levels $\geq$ 12 mM at the time of harvesting were considered to be diabetic. The ratio of male F2, O-N1F1 and RF-N1F1 mice displaying T2D phenotype at 24 weeks of age, was used to determine the mode of inheritance of the genetic factor causing diabetes susceptibility in the O-NOD^{k} mice, based on predictive Punnett squares.

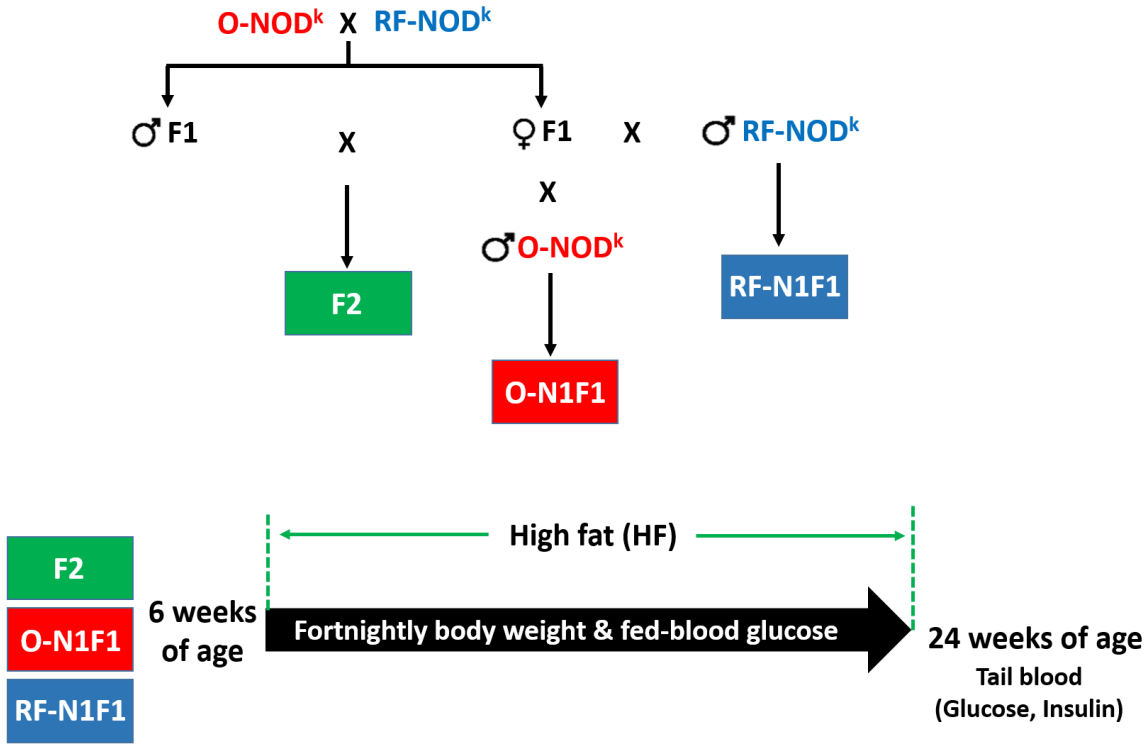

Figure 38: Breeding strategy used for the creation of F2, O-N1F1 and RF-N1F1 mice lines. Firstly, O-NOD^k and RF-NOD^k mice were crossed to generate F1 progeny. Male and female F1 mice were then inter-crossed to generate F2 mice (green box). Female F1 mice were back-crossed with male O-NOD^k mice to create O-N1F1 mice (red box); and finally, female F1 mice were back-crossed with male RF-NOD^k mice to produce RF-N1F1 mice (blue box). All offspring generated were weaned on a NC diet. At 6 weeks of age, male F2 (28), O-N1F1 (33) and RF-N1F1 (30) mice were subjected to a HF diet intervention program, with fortnightly body weight and non-fasting blood glucose monitoring. At the end of the study (24 weeks of age), tail blood was collected for measurement of plasma insulin.

5.3 Results

5.3.1 Phenotypic characterization of male F1 mice

At 4 weeks of age, all F1 mice displayed similar body weight (Figure 39A). However, with continuous nutrient excess provided by the HF diet, F1 mice started to exhibit progressive increase in body weight, compared to their NC-fed controls, significantly noticeable from 10 weeks of age (34.0 ± 0.5 *vs* 29.4 ± 0.5 g, respectively, $p<0.001$) (Figure 41A).

Despite this increased weight gain, most HF-fed F1 mice maintained normoglycaemia until the end of the study, similar to values observed in the NC-fed control mice (Figure 39B). At 16 weeks of age, 2 out of 30 mice developed hyperglycaemia with non-fasting blood glucose levels above 12 mM. This promoted a significant elevation in the average blood glucose levels of the HF-fed group compared to NC-fed controls (7.8 ± 0.5 *vs* 6.1 ± 0.2 mM, F1 HF-fed *vs* NC-fed mice, respectively, $p<0.05$). Interestingly, their blood glucose levels reduced over time, and by 24 weeks of age, did not differ from their NC-fed counterparts. Therefore, at the end of the study, 0 out of 30 HF-fed F1 mice displayed blood glucose levels above 12 mM.

At 24 weeks of age, long-term HF-feeding was observed to have caused 10 times higher plasma insulin levels in the F1 mice than the NC-fed mice (30.2 ± 5.9 *vs* 3.4 ± 1.0 ng/mL, F1 HF-fed *vs* NC-fed mice, respectively, $p<0.001$) (Figure 39C). The ratio between insulin and glucose was also significantly increased in the HF-fed F1 mice, compared to the NC-fed controls (Figure 39D). This HF diet-induced hyperinsulinaemia in the F1 mice without the development of hyperglycaemia suggests the development of insulin hypersecretion and/or delayed insulin clearance and insulin resistance.

Taken together, these longitudinal observations show that although the F1 mice (which are genetically 50% O-NOD^{k} mice and 50% RF-NOD^{k} mice) gained more body weight on a HF

diet, they did not display a T2D phenotype similar to the O-NOD^{k} mice. However, their insulin secretion profile is comparable to the HF-fed O-NOD^{k} mice (in Chapter 3). This suggests that, when subjected to prolonged HF diet intervention, the phenotype of the F1 mice is intermediate to the HF-fed O-NOD^{k} and RF-NOD^{k} mice.

Comparison of predicted and observed genotype and phenotype ratio

Based on Mendelian laws, if the allele causing T2D in the O-NOD^{k} mice is homozygous and the RF-NOD^{k} mice also carries a homozygous allele, all the F1 progeny would have the same phenotype (Figure 40A). However, if the RF-NOD^{k} mice has a heterozygous allele, then only 50% of the F1 mice would be diabetic, while the other half would be normoglycaemic (Figure 40B). On the other hand, if the diabetes susceptibility allele in the O-NOD^{k} mice is heterozygous, then the F1 mice generated by crossing O-NOD^{k} and RF-NOD^{k} mice would be 50% diabetic and 50% non-diabetic (Figure 40C).

Additionally, the selective breeding results would also permit us to predict if development of T2D in the O-NOD^{k} mice is caused by a dominant or recessive allele. Therefore, if all F1 mice placed on a HF diet develop T2D, then the allele would be classified as dominant (Figure 40D), whereas if all of them were normoglycaemic, then O-NOD^{k} mice carries a recessive allele (Figure 40E). Therefore, since overall 0/30 F1 male progeny developed diabetes, it implies that the diabetes susceptibility factor in the O-NOD^{k} mice is caused by a homozygous and recessive allele.

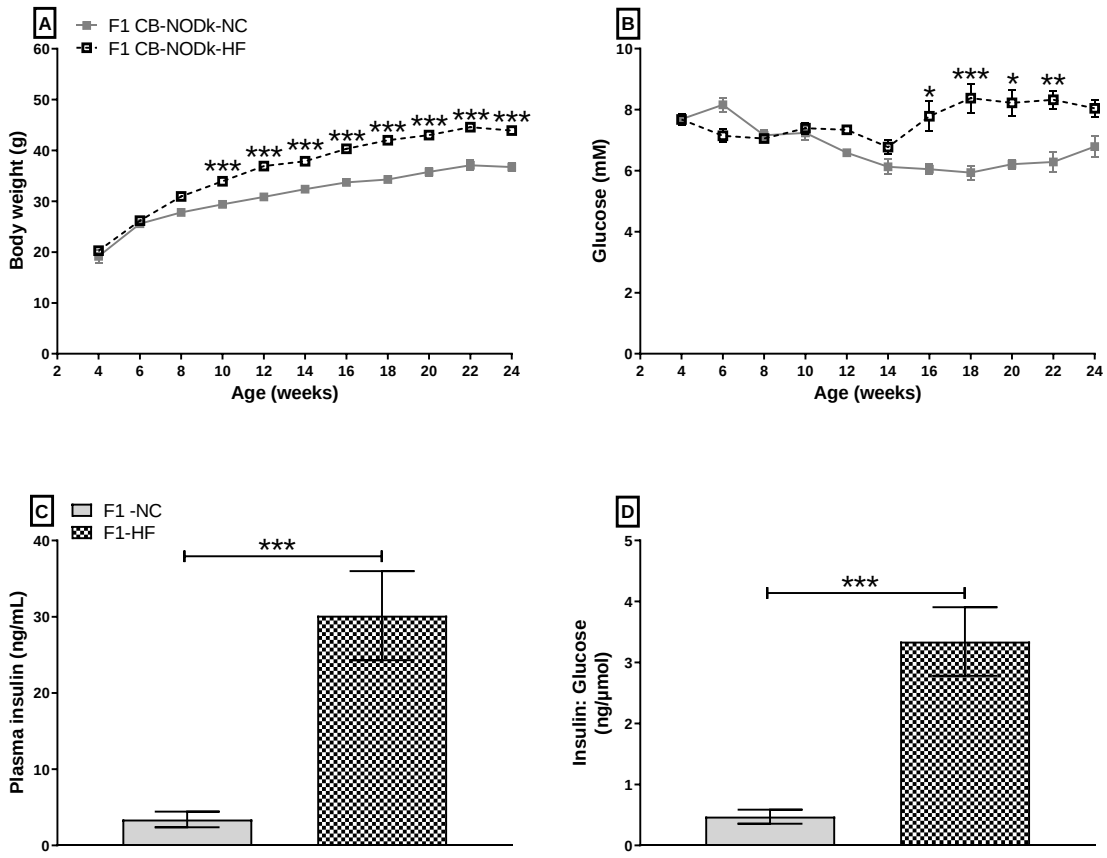

Figure 39: Time-course responses and end point blood chemistry of F1 offspring to dietary intervention. Fortnightly body weight (A) and non-fasting blood glucose levels (B) were measured in male F1 mice placed on either NC or HF diet from 4 to 24 weeks of age. Plasma insulin (C) levels were measured at the end of the study, and the ratio between insulin and glucose (D) at end point was assessed. Data are means ± SEM for NC (n=8) and HF (n=30) mice per group. Two-way ANOVA with Bonferroni post-hoc test, and Students T-test; *p<0.05, **p<0.01, ***p<0.001, F1 NC *vs* HF.

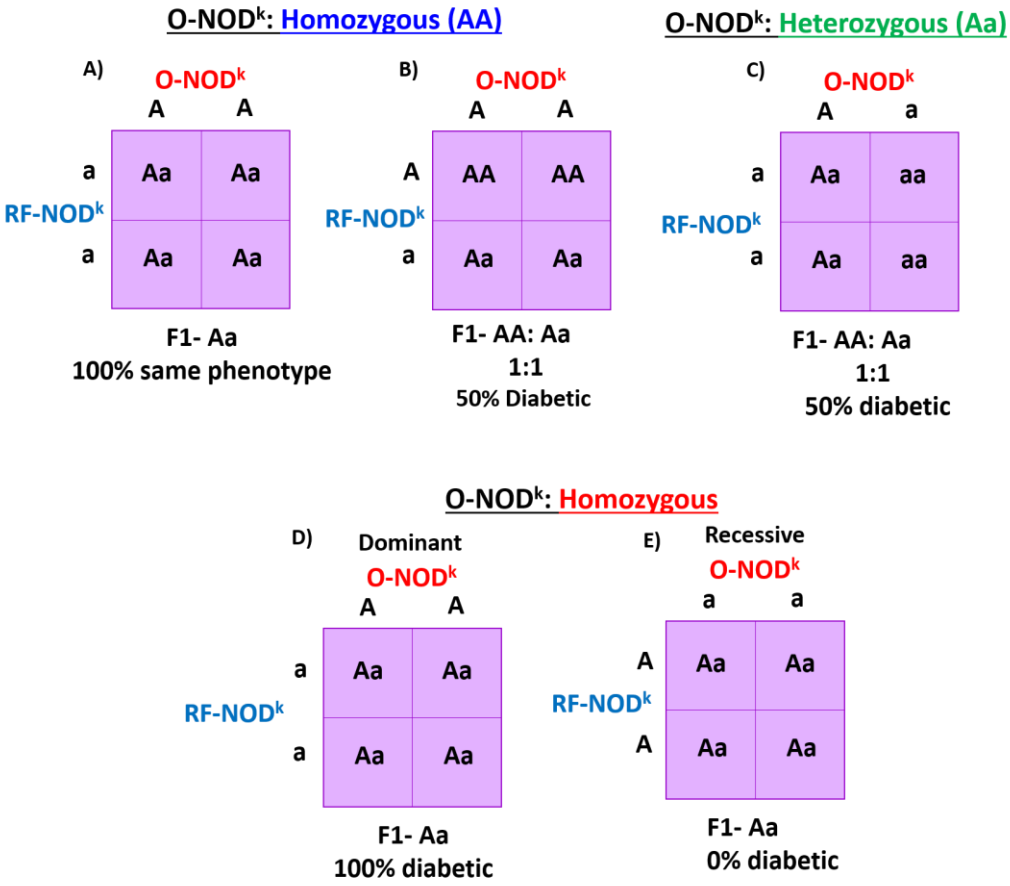

Figure 40: Punnett squares showing genotype prediction of F1 progeny generated by crossing O-NOD^k and RF-NOD^k mice. Based on Mendelian laws of segregation, the phenotype of the F1 progeny informs the likely Mendelian inheritance pattern. If the phenotype of the F1 progeny is the same for all mice (100% diabetic or 0% diabetic), the O-NOD^k must be homozygous for the diabetes-linked allele (A, D, E). If the F1 progeny are 100% diabetic, this will be due to the presence of a homozygous dominant diabetes-linked allele in the O-NOD^k mice (D). If the F1 progeny are 0% diabetic, this will be due to the presence of a homozygous recessive diabetes-linked allele in the O-NOD^k mice (E). If the phenotype of the F1 progeny are 50% diabetic, this will be due to either the O-NOD^k mice being homozygous for a recessive diabetes-linked allele and the RF-NOD^k mice being heterozygous for this allele, or the O-NOD^k being heterozygous for a dominant diabetes-linked allele (C).

5.3.2 Phenotypic characterization of male F2, O-N1F1 and RF-N1F1 mice

When challenged by a HF diet, F2, O-N1F1 and RF-N1F1 mice displayed similar progressive growth curves for body weight gain (Figure 41A). Non-fasting blood glucose levels begin to increase in the HF-fed O-N1F1 mice at 12 weeks of age, compared to the F2 mice (8.8 ± 0.5 *vs* 7.0 ± 0.2 mM, respectively, $p<0.05$) and RF-N1F1 mice (8.8 ± 0.5 *vs* 7.0 ± 0.1 mM, respectively, $p<0.05$) (Figure 41B). At this same age, 1 O-N1F1 mouse developed frank diabetes (two consecutive BGL readings >20 mM). With the progression of time, 4 more mice within this group had to be euthanized for the same reasons, before the end of the study.

The survival curve in Figure 41C shows the % of surviving mice without diabetes (non-fasting BGL < 12 mM), and the different time points when mice began to develop diabetes. The T2D diabetes phenotype in the O-N1F1 mice begin to appear from as early as 12 weeks of age, whereas the two RF-N1F1 mice developed diabetes towards the end of the study. Overall, F2 mice had a survival rate of 82% mice without the T2D phenotype, whereas the % survival of non-diabetic mice was 45% and 93% in the O-N1F1 and RF-N1F1 mice, respectively. Finally, all groups of mice were severely hyperinsulinaemic, but the O-N1F1 mice had the highest concentration (44.0 ± 6.3 ng/mL) compared to RF-N1F1 mice (23.5 ± 4.7 ng/mL) and F2 mice (26.5 ± 5.1 ng/mL) ($p<0.05$) (Figure 41D).

Collectively, these results show that despite similar body weight gain, a higher proportion (around 55%) of O-N1F1 mice develop diabetes (BGL ≥ 12 mM), accompanied by hyperinsulinaemia, which is a similar phenotype as the HF-fed O-NOD^{k} mice (in Chapter 3). On the other hand, most of the HF-fed RF-N1F1 mice maintain normoglycaemia with normal insulin secretion. HF-fed F2 mice had a higher proportion of hyperglycaemic mice than the RF-N1F1 mice (18% *vs* 7%, respectively), although their insulin levels were comparable to RF-N1F1 mice.

Comparison of predicted and observed genotype and phenotype ratio

By the end of the study, 5 out of 28 F2 mice and 18 out of 33 O-N1F1 mice had developed T2D. On the other hand, only 2 out of 30 RF-N1F1 mice developed diabetes. Based on Mendelian laws of segregation and the finding that 0% of the F1 mice developed diabetes which was suggestive of homozygous recessive inheritance of the diabetes genetic factor, predictive Punnett squares were created to determine the genotype and diabetes phenotype of the F2, O-N1F1 and RF-N1F1 mice.

It was expected that the F2 progeny would have a genotype ratio of AA: Aa: aa (1: 2: 1). Therefore, 25% of the F2 mice would be expected to have a genotype of "aa" and develop T2D when challenged by long-term HF-feeding. Fortnightly blood glucose measurements showed that 18% (5 out of 28 mice) of HF-fed F2 mice developed diabetes.

Similarly, a cross between F1 and O-NOD^{k} mice would generate an O-N1F1 progeny with an expected genotype ratio of Aa: aa (ratio 1:1), which would result in 50% of the O-N1F1 mice having an "aa" genotype and a diabetes phenotype. Long-term phenotyping of these mice resulted in the presence of T2D in 18 out of 33 O-N1F1 mice, further corresponding to 55% diabetes incidence.

Finally, back-crossing F1 mice with RF-NOD^{k} mice would result in an RF-N1F1 progeny with a genotype AA: Aa (ratio 1: 1), and consequently zero diabetes incidence, since none of the mice would be expected to have an "aa" genotype. Interestingly, 2 out of 30 RF-N1F1 mice, corresponding to 6% of the total number, unexpectedly developed diabetes when subjected to a prolonged HF diet program.

Together, these data reinforce the results obtained in the F1 mice study, where it was established that the diabetes phenotype in the O-NOD^{k} mice is caused by a homozygous and recessive allele.

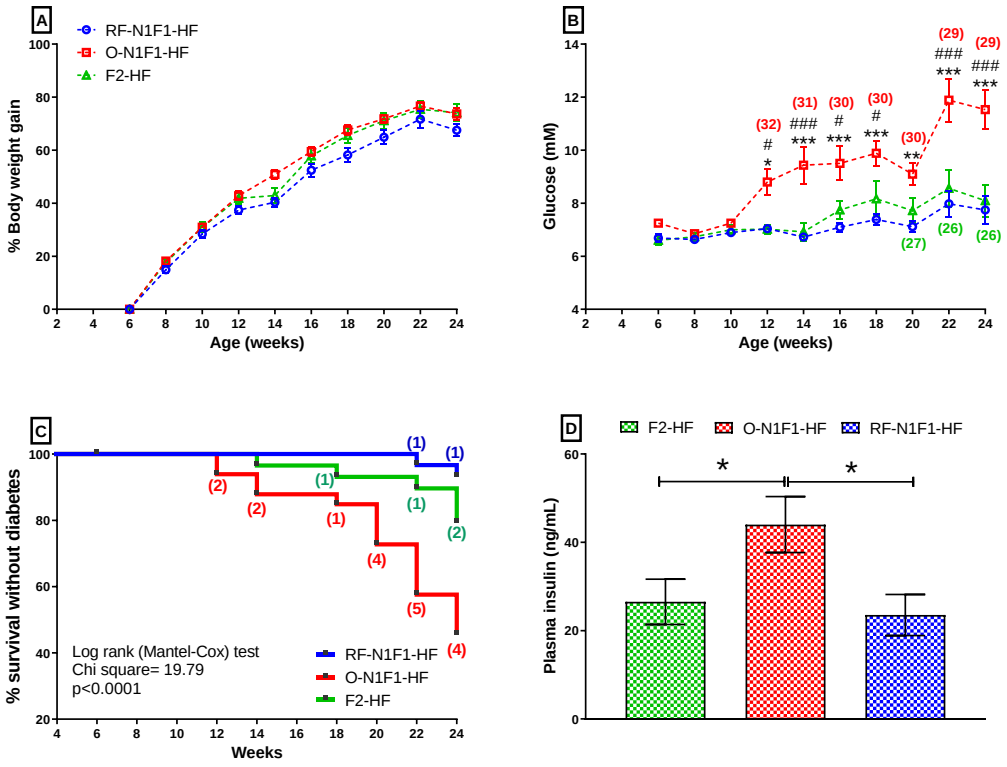

Figure 41: Longitudinal monitoring of body weight gain, non-fasting blood glucose levels, survival curve and end point plasma insulin levels in F2, O-N1F1 and RF-N1F1 mice challenged by HF diet. Fortnightly body weight gain (A), non-fasting blood glucose levels (B) and survival curve of mice without diabetes (C) were measured in male F2, O-N1F1 and RF-N1F1 mice placed on HF diet from 6 to 24 weeks of age. Mice that presented 2 consecutive BGL readings above 20 mM were ethically culled. The numbers in brackets in (B) denote the number of surviving mice at each time point, whereas numbers in brackets in the survival curve (C) are the number of mice that developed diabetes (blood glucose levels ≥ 12 mM) at different time points during the study. Plasma insulin levels were also measured at the time of harvest (D). Data are means ± SEM for 28 (F2), 33 (O-N1F1) and 30 (RF-N1F1) mice per group. Two-way ANOVA with Bonferroni post-hoc test; $^{\#}p<0.05$, $^{\#\#\#}p<0.001$, HF-fed F2 *vs* O-N1F1;*p<0.05, **p<0.01, ***p<0.001, HF-fed O-N1F1 *vs* RF-N1F1.

5.4 Discussion

In this study, a test cross was performed between O-NOD^k and RF-NOD^k mice to generate F1 progeny, which were then placed under nutrient stress conditions (HF diet) for 20 weeks. The ratio of F1 mice that developed diabetes was correlated to the predicted genotype ratio. However, none of the F1 male mice developed diabetes, therefore, suggesting that the diabetes susceptibility factor/ trait in the O-NOD^k mice is caused by a homozygous and recessive allele.

Phenotypic characterization of the F1 mice during the long-term diet intervention showed that these mice had an intermediate phenotype, with a normoglycaemic profile similar to HF-fed RF-NOD^k mice, but similar hyperinsulinaemia as HF-fed O-NOD^k mice. Since the F1 mice are expected to possess one allele each from its O-NOD^k and RF-NOD^k parents, it further shows that the diabetes phenotype is associated with homozygous alleles, whereas the heterozygosity in the F1 mice allele (Aa) could be playing a protective role by maintaining normoglycaemia. The generation of F2, O-N1F1 and RF-N1F1 mice lines, and further phenotypic characterization to determine the ratio of mice that developed diabetes when challenged by HF diet, supported the observations made in the F1 mice. It was established that the segregation of the diabetes susceptibility factor in the O-NOD^k mice followed Mendelian patterns of inheritance. Furthermore, it was observed to be a homozygous recessive trait.

Traditionally, human genetics has been classified as either rare monogenic traits or polygenic complex traits (Schork et al., 2009). Diseases such as T2D demonstrate complex traits, since its phenotype does not follow simple Mendelian inheritance laws. Instead, it arises from multiple traits affected by an interplay between genetic and environmental factors. Other disorders, such as cystic fibrosis for example, results from mutations in a single gene, the cystic fibrosis transmembrane conductance regulator (CFTR) (Dechecchi et al., 2018). However, recent studies have shown that despite the perceived different allelic architectures of diseases

with complex and rare traits, these two groups are not as dichotomous as previously believed, but instead are inter-connected (Blair et al., 2013). Furthermore, it has been reported that even complex diseases have a unique Mendelian disease allelic architecture that allows identification of illness based on its associated Mendelian loci (Blair et al., 2013). Therefore, the identification of particular traits involved in T2D development may be possible through associated Mendelian loci, if Mendelian patterns of inheritance are followed.

Results obtained from selective breeding of the two different sub-strains of NOD^{k} mice suggests that the diabetes trait in the O-NOD^{k} mice is segregated as a simple Mendelian homozygous recessive trait. This pattern of inheritance is very similar to cystic fibrosis, which is a Mendelian monogenic disorder with an autosomal recessive pattern, caused by inheritance of two copies of the mutated CFTR gene (Dechecchi et al., 2018). Furthermore, even though diabetes is considered a complex trait, rare familial monogenic forms such as maturity onset diabetes of the young (MODY) also exist, which has an autosomal dominant inheritance (Barrio et al., 2002). Therefore, it is possible that a homozygous recessive inheritance is causing increased diabetes susceptibility in the O-NOD^{k} mice, which is noticeable when these mice are challenged by a HF diet for prolonged time periods.

Interestingly, when F1 mice were back-crossed to RF-NOD^{k} mice and the male RF-N1F1 progeny were subjected to long-term HF-feeding, 2 RF-N1F1 mice developed diabetes. This was unexpected since the Punnett square predicted that none of the RF-N1F1 offspring would have a genotype that could lead to a diabetes phenotype. The development of diabetes in these 2 mice was similar to the development of hyperglycaemia in the 2 HF-fed RF-NOD^{k} mice in the long-term phenotyping study in Chapter 3. This further strengthens the hypothesis that since only 2 back-crosses were performed during generation of the RF-NOD^{k} mice colony (detailed in Chapter 1), the RF-NOD^{k} mice still have 12.5% genetic similarity to the O-NOD^{k} mice. Hence, some of the RF-NOD^{k} mice may have inherited the diabetes susceptibility factor of the

O-NOD^{k} mice within that 12.5%, which could be causing these unexpected development of diabetes in the mice. Therefore, analysis of the genotype of these mice will further strengthen the validity of candidate genes discovered through further genetic studies in the following chapters.

Chapter 6

Results

Genetic variants associated with diabetes susceptibility in O-NOD^{k} mice

6.1 Introduction

T2D is caused by a combination of environmental and genetic factors, as observed in monozygotic twin studies and the family history of T2D patients (Meigs et al., 2000, Willemsen et al., 2015). Rodent studies have also shown the strong effect of the genetic background of different mice strains on the insulin secretory response of the β-cells (Mitok et al., 2018). Heritable β-cell phenotypes, characterized by altered insulin secretory responses to different nutrient stimulus and differing T2D risk, have specific genetic architectures (Keller et al., 2019). Since many islet function genes are conserved between mice and humans, genome analysis of mouse models with diabetes can identify candidate genes that could be associated with the pathogenesis of diabetes in humans as well (Keller et al., 2018).

Genome wide association studies (GWAS) have identified over 143 genetic loci associated with T2D and glycaemic traits (Xue et al., 2018). However, GWAS has certain limitations as it does not account for environmental interactions, and either excludes or poorly covers variants with a minor allele frequency below 5% (Anderson et al., 2008). In contrast, next generation sequencing (NGS) techniques which have enabled whole genome sequencing (WGS), allows the identification of *de novo* variants from different population sets and structural variants that are overlooked with GWAS. Furthermore, the development of NGS and its increased affordability and availability has led to a surge in the use of WGS to rapidly sequence DNA, to determine genetic variants in both laboratory and clinical studies (Foley et al., 2015). Hence WGS has become an increasingly popular genome analysis method to identify novel gene variants.

Various bioinformatics pipelines are used to analyze WGS data. The Genome Analysis Toolkit (GATK) from the Broad Institute is considered the gold standard for identification of genetic variants from sequencing platforms. It provides various tools to map the sample sequence to a

reference genome, perform quality control and high confidence variant calling for SNPs and small structural variants (insertions and deletions) (Van der Auwera et al., 2013). GATK also allows exclusion of variants commonly found in healthy mice genomes, and variants that lead to amino acid substitution, therefore enabling selection of only predictive disease-causing variants. Amino acid substitution(s) can also affect protein function and lead to a range of phenotypes, classified as benign to deleterious, which is determined by a SIFT score (Ng and Henikoff, 2003). Thus, the use of GATK allows the discovery of gene sequence differences including SNPs, indels and structural variants. By using GATK to identify these gene sequence changes in T2D mouse models, one can discover novel gene variants in diabetic mice, which could be linked to T2D in humans also.

Phenotyping characterization studies in the previous chapters have established a clear T2D phenotype in the O-NOD^{k} mice, when challenged by long-term HF-feeding, which was not present in the RF-NOD^{k} mice. Since both groups were subjected to similar environmental conditions, it was hypothesized that a genetic variant in the O-NOD^{k} mice could be contributing to increased T2D susceptibility compared to RF-NOD^{k} mice.

The aim of this study was to examine the genome of phenotyped diabetes-prone HF-fed O-NOD^{k} and diabetes-resistant RF-NOD^{k} mice, to uncover genetic variants in O-NOD^{k} mice compared to RF-NOD^{k} mice, which may underlie the development of T2D in the O-NOD^{k} mice. This approach may lead to the discovery of novel genes that have not been associated with diabetes previously, as well as provide insights into the pathogenesis of T2D that could inform the development of novel therapies.

6.2 Experimental design

DNA was extracted from HF-fed O-NOD^{k} and RF-NOD^{k} mice (n=2/group) and sent to Macrogen Inc. for WGS (as described in Chapter 2). Bioinformatics analysis was performed on the genomic sequences of the samples, using the C57BL/6J mouse genome as a reference. SNVs and structural variants (insertions and deletions) were called using the GATK pipeline. Variants were called using Manta, and annotated with dbSNP. A multi-step filtering criteria was further applied to select SNVs that were non-synonymous (led to change in amino acid sequence), novel (not usually present in the mouse genome) and were predicted to result in a deleterious phenotype (based on their SIFT score) (Figure 42).

This strategy was used to generate a list of rare and deleterious variants that were predicted to be involved in pathogenic conditions. This was further shortlisted to select only homozygous SNVs, based on the results of the Selective breeding study in Chapter 5. A list of candidate genes was obtained and the expression and function of these genes were assessed to determine their potential role in the development of T2D. A list of homozygous insertions and deletions was also generated for further pathway analysis using ENRICHR software.

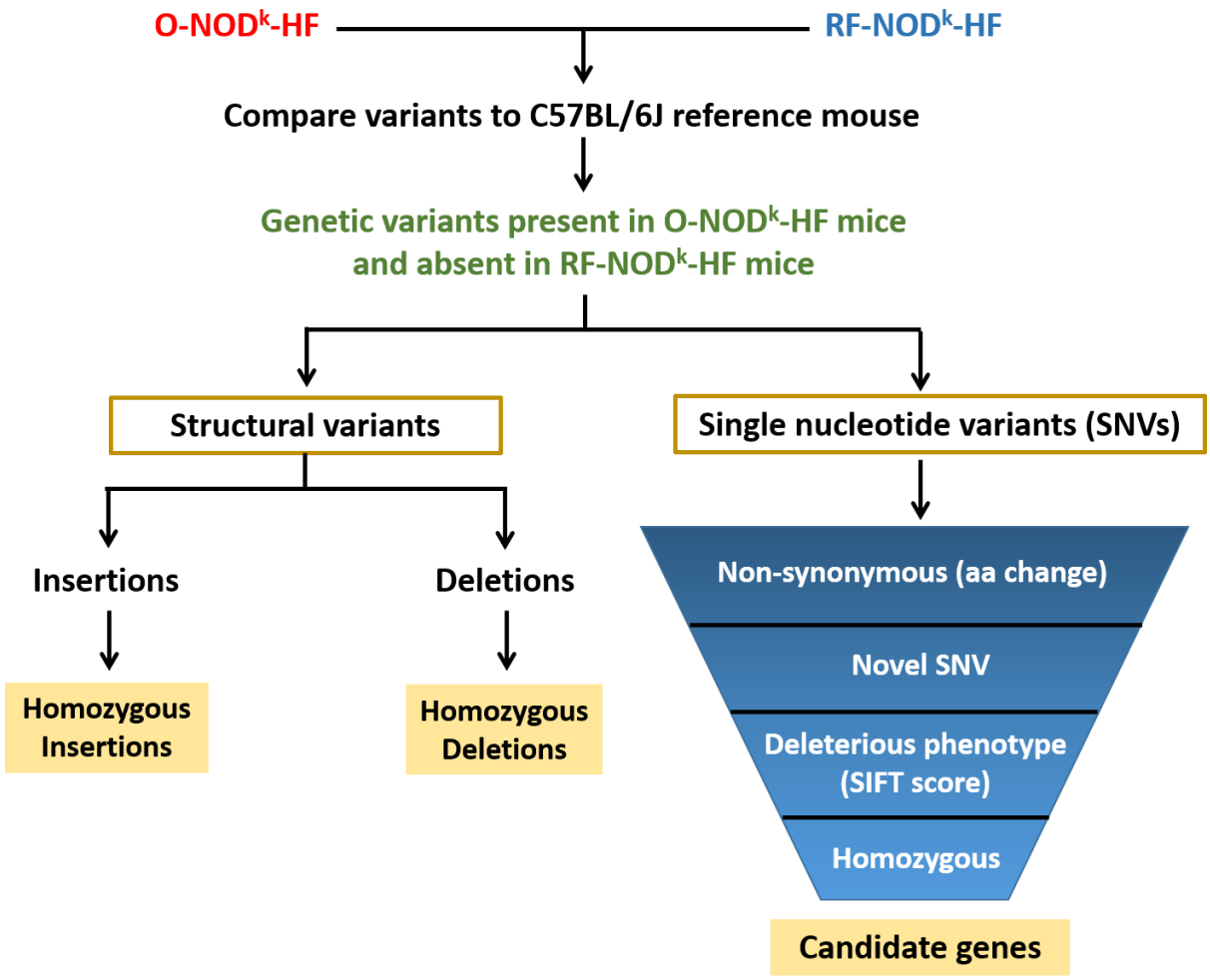

Figure 42: Workflow and filter strategy for identification of structural variants and SNVs that could be predisposing O-NOD^k mice to diabetes. DNA samples from hyperglycaemic HF-fed O-NOD^k and normoglycaemic RF-NOD^k mice (n=2/group) were sequenced and the libraries obtained were aligned to a reference C57BL/6J genome. Structural variants and single nucleotide variant (SNV) present only in the O-NOD^k mice were called with GATK, and annotated with dbSNP. A multi-step filtering was performed to generate SNVs that were non-synonymous, novel and were predicted to cause a deleterious phenotype based on their SIFT score. Final candidate gene selection was based on homozygosity.

6.3 Results

WGS was conducted on liver DNA samples of O-NOD^{k} and RF-NOD^{k} mice, submitted to HF-feeding for 8 and 12 weeks, respectively. As observed in Table 6, body weights and glycaemic levels of HF-fed O-NOD^{k} mice were higher than HF-fed RF-NOD^{k} mice at the time of DNA extraction. These mice were selected for WGS as being diabetes-prone (O-NOD^{k}) and diabetes-resistant (RF-NOD^{k}) mice.

6.3.1 Sequence alignment and Variant calling

WGS generated DNA libraries for each of the 4 mice, using the Illumina HiSeq XTen sequencing platform. The whole genome sequence was aligned to a reference C57BL/6J mouse genome, which after quality control and variant calling using GATK and Manta, generated a list of genetic variants present only in the O-NOD^{k} mice, but not in the RF-NOD^{k} mice. Of these, 6660 annotated variants were identified, including SNVs and 3950 structural variants (1405 insertions and 2545 deletions). Between the two HF-fed O-NOD^{k} mice, an 80% overlap of SNPs in their whole genome sequence was observed, whereas 72% overlap of SNPs was obtained between the two HF-fed RF-NOD^{k} mice."

6.3.2 Annotation and Filtering for SNVs

Initially, a total number of 1,048,575 SNVs were obtained, which were annotated with dbSNP to acquire their gene names and predicted genotype based on SIFT scores (Table 7). This led to identification of 286,978 variants, from which 31,475 variants present only in the genome of the O-NOD^{k} mice that were selected for further analysis. Following gene annotation, the 2710 SNVs obtained underwent a multi-step filtering system. Firstly, only SNVs that were non-

synonymous (i.e. led to a change in amino acid sequence) were selected to obtain 133 SNVs. Secondly, 117 SNVs that were novel/rare and not commonly observed in the mouse genome were chosen. Thirdly, 38 SNVs were selected that were predicted to have a damaging phenotype based on their SIFT score (0 to 0.05).

The final selection criteria applied was based on the results obtained in the Selective breeding study, which established that the diabetes susceptibility factor in the HF-fed O-NOD^{k} mice is likely to be caused by a homozygous recessive allele. Therefore, only homozygous SNVs were selected, which resulted in a list of 6 candidate genes that could be associated with the diabetes phenotype in the O-NOD^{k} mice, namely ATPase type 13A3 (*Atp13a3*), G protein-coupled receptor 125 (*Gpr125*), potassium voltage-gated channel, subfamily H (eag-related), member 7 (*Kcnh7*), myosin heavy polypeptide 4, skeletal muscle (*Myh4*), nuclear receptor co-repressor 1 (*Ncor1*) and olfactory receptor 954 (*Olfr954*) (Table 8).

The *Atp13a3* gene was selected based on a SNP present on mouse chromosome 16, which led to an amino acid change from tryptophan (W) to cysteine (C). The gene ontology (GO) terms associate this gene with a protein with ATPase activity that transports cations across membranes. The *Gpr125* gene codes for a member of the large family of adhesion G-protein coupled receptors that have roles in cell surface transmembrane receptor signaling. A non-synonymous amino acid change was found in the *Kcnh7* gene on chromosome 2, which is associated with potassium ion transmembrane transport and regulation of membrane potential. Chromosome 11 was found to have two different SNPs. The first SNP was present on the *Myh4* gene which codes for myosin heavy chain 4 which is integral to skeletal muscle contraction, while the second SNP was on the *Ncor1* gene. The GO terms associated with the *Ncor1* gene reveal its role in regulation of gene transcription and various pathways such as phosphatidylinositol-3-kinase signaling, cholesterol homeostasis, lipid transport and glycolysis, and its role as an immunometabolic regulator (Geiger et al., 2020). Finally, an amino acid

substitution was identified in the *Olfr954* gene which is associated with olfactory receptor activity and sensory perception of smell.

Notably, the SIFT score for *Ncor1* gene was not available, and the SIFT score for *Olfr954* gene was deleterious, but with low confidence. Therefore, it is possible that these SNPs may not lead to a damaging phenotype, and could be a tolerated SNP, hence requires cautious interpretation.

Table 6: Sample body weight and non-fasting blood glucose data of HF-fed male O-NOD^{k} and RF-NOD^{k} mice selected for whole genome sequencing.

#	Strain	Diet	Age	Body weight (g)	Non-fasting blood glucose (mM)
1	O-NOD^{k}	HF	12 weeks	43.3	12
2	O-NOD^{k}	HF	12 weeks	44.1	19
3	RF-NOD^{k}	HF	16 weeks	39.6	7
4	RF-NOD^{k}	HF	16 weeks	37.4	7

Table 7: List of candidate genes with single nucleotide variants (SNVs) present in the genome of only HF-fed O-NOD^{k} mice, predicted to have a deleterious phenotype

Criteria	All variants
Total passed variants	1,048,575
Annotated with dbSNP	286,978
Variants in O-NOD^{k} only	6660
Single nucleotide variants (SNVs)	2710
Non-synonymous SNVs	133
Non-synonymous + Novel SNVs	117
Non-synonymous + Novel + Damaging SNVs	38
Non-synonymous + Novel + Damaging + Homozygous SNVs	6

Table 8: List of candidate genes with SNPs present in the genome of HF-fed O-NOD^{k} mice that could be associated with the diabetes phenotype.

Gene	Description	Chrm	Co-ordinate	Ref base	Var base	Amino acid change	SIFT category	SIFT score	Associated GO terms
Atp13a3	ATPase type 13A3	16	30362642	C	A	W->C	Deleterious	0	ATPase activity; integral to membrane; metal ion binding; cation transport; ATP binding
Gpr125	G-protein-coupled receptor 125	5	49960675	C	T	R->Q	Deleterious	0	Transmembrane, neuropeptide, cell surface and G-protein coupled receptor signaling activity; external side of plasma membrane
Kcnh7	Potassium voltage-gated channel, subfamily H member 7	2	62736032	A	G	S->P	Deleterious	0.01	Potassium ion transmembrane transport; signal transduction; integral to plasma membrane; regulation of transcription and membrane potential; circadian rhythm
Myh4	Myosin heavy chain 4	11	67252228	C	A	A->D	Deleterious	0.01	Calmodulin and nucleotide binding; myofibril; actin binding; focal adhesion
Ncor1	Nuclear receptor co-repressor 1	11	62321179	C	T	A->T	N/A	N/A	A-β regulatory T cell differentiation; negative regulation of PI-3K signaling; positive regulation of histone deacetylation; cholesterol homeostasis; regulation of lipid transport and glycolysis
Olfr954	Olfactory receptor 954	9	39462157	G	A	S->N	Deleterious low confidence	0.03	Integral to membrane; olfactory receptor activity; sensory perception of smell

Chrm: Chromosome; Ref: Reference, Var: Variant.

6.3.3 Structural variants

Structural variants (i.e. insertions and deletions) were obtained when called through GATK and Manta. In total, 3950 structural variants were identified, of which 1405 were insertions and 2545 were deletions. Based on the results obtained in Chapter 5 that predicts predisposition to T2D in this mouse model is caused by a homozygous allele, a new filter was applied to select only homozygous insertions and deletions. This new filter generated a list of 621 insertions and 651 deletions. Of those, the great majority of insertions were observed to occur in chromosomes 4 and 5 (Figure 43A), whereas deletions were more frequently observed in chromosome 9 (Figure 43B). Notably, chromosomes 20, 21 and 22 did not display any insertions or deletions.

To gain mechanistic insights into any cumulative functions of the genes list manifesting these insertions and deletions, further analysis using the web-based Enrichr tool was performed for pathway enrichment identification. The top 10 pathways that were identified to be enriched with genes containing insertions, included pathways associated with insulin secretion, as well as pancreatic exocrine secretion, oxytocin signaling, glutamatergic synapses, cardiac adrenergic signaling, cardiomyopathies, axon guidance, gap junctions and purine metabolism (Table 9). Pathway enrichment analysis of the genes containing deletions were associated with neuronal/brain pathways including the nicotine addiction, endocannabinoid signaling, glutamatergic excitatory synapses, axon guidance and depression (Table 10).

While certain of the enrichment pathways may be implicated in β-cell function, it is still possible that a particular insertion or deletion not identified through the pathway enrichment analysis, could be associated with the diabetes phenotype in the HF-fed O-NOD^{k} mice. Manual curation of the 621 insertions and 651 deletions could assist in identification of candidate structural variants for further analysis.

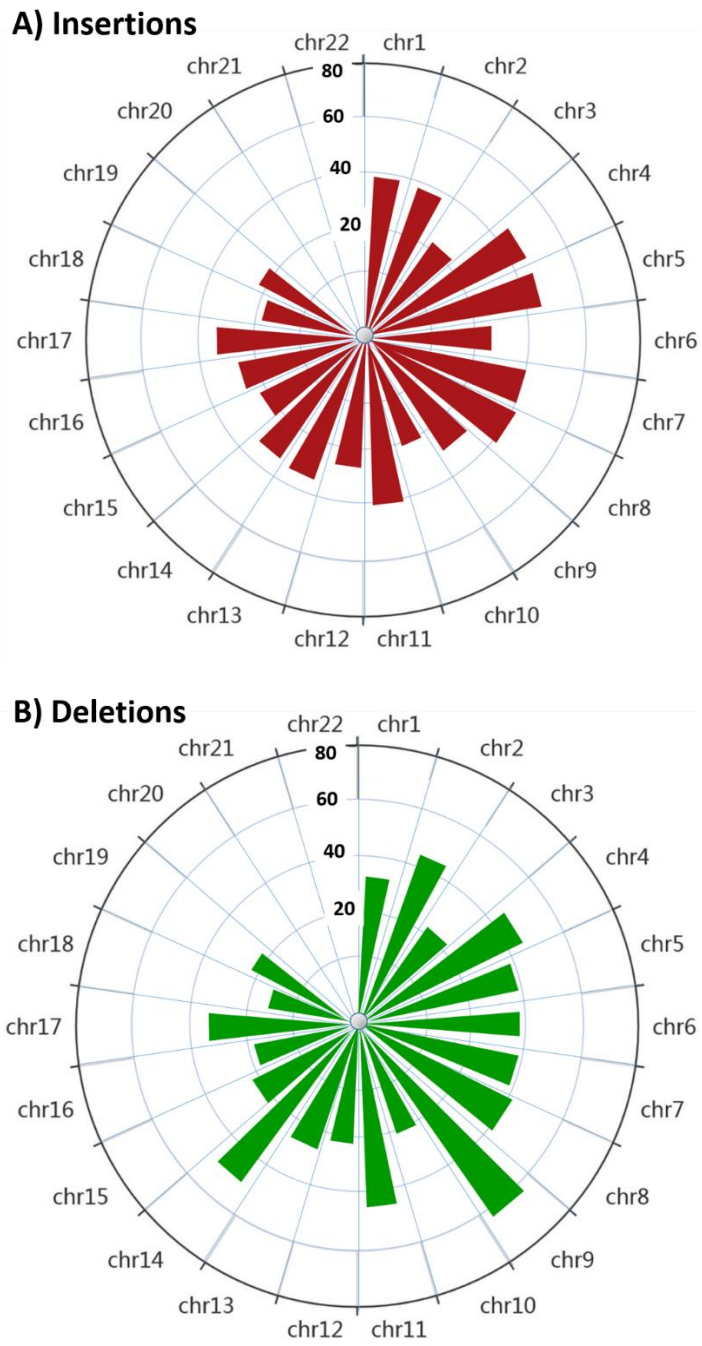

Figure 43: Chromosomal distribution of filtered homozygous insertions (red) and deletions (green) present in the genome of the HF-fed O-NOD^{k} mice. The triangles represent the number of homozygous structural variants in each chromosome of the O-NOD^{k} mice. Chromosome 4 and 5 has the highest number of insertions (46 and 45, respectively), while chromosome 9 has the most deletions (61).

Table 9: Enriched pathway analysis of filtered homozygous insertions present in the genome of the HF-fed O-NOD^{k} mice.

#	Pathway term	Adjusted p-value	Genes
1	Oxytocin signaling pathway	0.004	*Camk2b; Ryr2; Cacna2d3; Cacna2d2; Prkca; Adcy1; Ppp3cc; Gnaq; CD38; Ppp1r12b; Plcb1; CACNG3; MAP2K5; KCNJ3*
2	Arrhythmogenic right ventricular cardiomyopathy	0.006	*Ryr2; Tcf7l2; Sgcd; Itgb4; Itga2; Cacna2d3; Cacna2d2; Cacng3; Slc8a1*
3	Glutamatergic synapse	0.007	*Grin3a; Ppp3cc; Gnaq; Grm8; Cacna1a; Prkca; Grik1; Dlgap1; Adcy1; Plcb1; Shank2; Kcnj3*
4	Adrenergic signaling in cardiomyocytes	0.012	*Camk2b; Ryr2; Ppp2r5e; Gnaq; Cacna2d3; Cacna2d2; Prkca; Adcy1; Ppp2r3a; Plcb1; Cacng3; Slc8a1*
5	Pancreatic exocrine secretion	0.013	*Ryr2; Pla2g12a; Gnaq; Kcnma1; Sctr; CD38; Prkca; Adcy1; Plcb1; Cftr*
6	Dilated cardiomyopathy (DCM)	0.013	*Ryr2; Sgcd; Itgb4; Itga2; Cacna2d3; Cacna2d2; Adcy1; Cacng3; Slc8a1*
7	Gap junction	0.015	*Gnaq; Lpar1; Prkca; Grb2; Htr2a; Adcy1; Plcb1; Prkg1; Map2k5*
8	Purine metabolism	0.016	*Gucy2c; Pde11a; Pde4d; Pde2a; Pde3b; Pde3a; Pde6b; Hprt; Adcy1; Ak7; Gucy2f*
9	Axon guidance	0.017	*Sema5a; Epha5; Camk2b; Epha6; Arhgef12; Prkca; Sema4f; Unc5d; Rgma; Ppp3cc; Slit3; Ephb2; Epha3*
10	Insulin secretion	0.028	*Camk2b; Ryr2; Gnaq; Kcnma1; Prkca; Kcnn2; Adcy1; Plcb1*

Homozygous insertions present in the genome of the O-NOD^{k} mice were chosen to generate a list of 621 insertions. Pathway analysis was conducted on the genes with these insertions using web-based Enrichr tool to generate a list of top 10 enriched pathways with adjusted p-value <0.05.

Table 10: Enriched pathway analysis of filtered homozygous deletions present in the genome of the HF-fed O-NOD^{k} mice.

#	Pathway term	Adjusted p-value	Genes
1	Nicotine addiction	0.000001	*Gabrb3; Gsbrr3; Gabra2; Gabrb2; Gabra1; Gabrb1; Grin3a; Gabra6; Cacna1a; Gria3; Gabrg2*
2	Retrograde endocannabinoid signaling	0.0008	*Gabrb3; Gabra2; Gabrb2; Gabra1; Gabrb1; Gabra6; Cacna1a; Cacna1d; Gabrg2; Adcy5; Gabrr3; Ndufs6; Plcb1; Gria3; Kcnj3*
3	Axon guidance	0.0013	*Epha5; Ntng1; Trpc5; Epha6; Arhgef12; Dcc; Ptpn11; Unc5d; Efna5; Robo1; Ablimi; Plcg2; Pak7; Slit1; Slit3; Ephb1*
4	Glutamatergic synapse	0.0363	*Grin3a; Pla2g4e; Slc1a1; Cacna1a; Cacna1d; Slc1a6; Plcb1; Gria3; Adcy5; Kcnj3*
5	Long-term depression	0.0404	*Gucy1a2; Pla2g4e; Cacna1a; Plcb1; Prkg1; Crhr1; Gria3*

Pathways analysis was conducted on the 651 homozygous deletions identified in the O-NOD^{k} mice genome using Enrichr software, to generate a list of enriched pathways. Significant cut-off criteria adjusted $p < 0.05$.

6.4 Discussion

The whole genome sequence of diabetes-prone O-NOD^k and diabetes-resistant RF-NOD^k mice were mapped to a reference C57BL/6J mouse genome, to determine genetic variants present in the O-NOD^k mice that could be associated with its diabetes phenotype. Annotation and multi-step filtering of the variants generated a list of 6 candidate genes with SNPs leading to a substitution in amino acid, predicted to result in a deleterious phenotype. The 6 candidate genes were *Atp13a3, Gpr125, Kcnh7, Myh4, Ncor1* and *Olfr954*.

ATPase is a large superfamily of enzymes that couple ATP hydrolysis with transmembrane cation transport by creating an ion gradient. P-type ATPase is the largest member of the ATPase family, with a distinct simple architecture of only one catalytic subunit, transporting various ions and phospholipids across the lipid bilayer membrane (Kühlbrandt, 2004, Palmgren and Nissen, 2011). Its 5 subtypes are based on the type of ions they transport, such as the gastric H^+/K^+ ion transport pump (Vagin et al., 2002). ATP13A3 is a P-type 5B ATPase, which is a more recent, and hence least characterized class, with unknown substrate specificity, but is assumed to be a probable cation transporter as well (Sørensen et al., 2010, Axelsen and Palmgren, 1998). These ATPases are found on both internal membrane systems and plasma membranes (Sørensen et al., 2010).

Atp13a3 has been linked to aging and tumour suppression due to its increased expression in senescent parenchymal kidney cells (Habtemichael and Kovacs, 2002). It has also been proposed as a biomarker for difluoromethylornithine-based therapies in pancreatic cancer, due to its role in polyamine transport (Madan et al., 2016). While there is not much research conducted on *Atp13a3*, most studies have shown a strong association with pulmonary arterial hypertension (PAH). Gene knockdown in mice and in human pulmonary arterial endothelial cells led to the development of PAH, disruption of polyamine homeostasis and apoptosis (Gräf

et al., 2018, Legchenko et al., 2020, Liu et al., 2019). Although *Atp13a3* is expressed in all tissues, including the pancreas, currently there is no literature associating this gene with diabetes or any glycaemic traits (Schultheis et al., 2004). However, its role as a transmembrane cation transporter with unknown substrate specificity suggests that it could possibly play a role in the regulation of insulin secretion in the β-cells, similar to the ATP-sensitive K^+ channel and the voltage-dependent Ca^{2+} channel, which are also P-type ATPase channels.

The second candidate gene obtained from this study was *Gpr125*, which is also known as adhesion G protein-coupled receptor A3 (*Adgra3*). It is a member of the G protein coupled receptor (GPCR) family of integral membrane proteins. GPCRs are embedded in the plasma membrane and interact with specialized G-proteins to bind nucleosides GTP and GDP (Rosenbaum et al., 2009). In the presence of extracellular signal molecules, GPCRs trigger the activation of associated G-proteins and other membrane proteins (Rosenbaum et al., 2009).

There are 5 main subtypes of GPCRs based on their structure, and *Gpr125* is a member of the adhesion GPCR subtype (Fredriksson et al., 2003). *Gpr125* is an orphan receptor which is not yet fully characterized, but is known to be a cell surface receptor involved in transmembrane signaling receptor activity. Initially, *Gpr125* was studied for its role in Wnt/planar cell polarity (PCP) signaling, suggesting a possible role in controlling islet β-cell proliferation (Li et al., 2013). *Gpr125* was further associated with cancer, presenting a tumour suppressing function in colorectal cancer, but had oncogenic abilities in myeloid sarcoma (Wu et al., 2018, Fu et al., 2013). It has also been linked to autosomal recessive retinitis pigmentosa (Fahim et al., 1993). Although there is not much literature associating *Gpr125* and T2D, one RNA-seq study observed that HbA_1c levels in patients with T2D were associated with reduced *Gpr125* gene expression in blood at 2 years follow up (Slieker et al., 2018). Therefore, the role of *Gpr125* in cell surface receptor signaling pathways and its association with HbA_1c could suggest a possible link to the diabetes phenotype observed in the O-NOD^k mice.

Kcnh7, the third candidate gene with a predicted deleterious SNP is also known as Eag-related protein 3 (ERG-3). It is part of the ether-a-go-go (EAG) superfamily of voltage gated K^+ channels which can modulate the excitability of neurons. There are 3 sub-types based on their sequence and functions: Eag (Kv10) with 2 members, Erg (Kv11) with 3 members and Elk (Kv12) with 3 members (Kazmierczak et al., 2013). Most of these are expressed and associated with the nervous system. ERG-1 (Kv11.1) has been well characterized due to its role in regulation of the action potential repolarization in the heart (Lees-Miller et al., 2003). ERG-2 (Kv11.2, *Kcnh6*) has been associated with regulation of insulin secretion and glucose homeostasis. *Kcnh6* knockout led to increased intracellular calcium ions and hyperinsulinaemia in the short-term, and loss of β-cell mass and ER stress in the long-term (Yang et al., 2018). ERG-3 (*Kcnh7*) channels are expressed mainly in the brain, particularly in the cerebral cortex and olfactory bulb. Due to its role as a voltage-gated channel, mutations in this gene have been associated with seizures and auditory brain stem neurons (Hardman and Forsythe, 2009, Xiao et al., 2018). A potential role in the development of bipolar spectrum disorder has also been described for this gene (Strauss et al., 2014).

Although *Kcnh6* has shown strong association with the development of diabetes, *Kcnh7* has not yet been linked to T2D. However, *Kcnh7* transcripts were expressed in islets and INS-1 cells, along with *Kcnh6* (Mühlbauer et al., 2007). Therefore, the similar sequence homology and transcript expression of *Kcnh6* and *Kcnh7* could suggest that *Kcnh7* may have a yet undetermined potential role in the pathogenesis of T2D.

One of the 6 candidate genes is *Myh4*, which encodes for myosin heavy chain. Myosin is a motor protein that is actin binding and essential in muscle contraction (Schiaffino et al., 2015). *Myh4* mutations are associated with myosinopathies (Lindqvist et al., 2013). A mutation in this gene led to the development of skeletal muscle myofibrillar degeneration, with homozygotes developing hind limb paralysis within 2 weeks of birth (Kurapati et al., 2012). Although not

expressed in islets, *Myh4* was found to be upregulated in the skeletal muscles of T2D patients (Møller et al., 2017). However, there were no other studies reporting any further associations of *Myh4* and diabetes or glycaemic traits. Therefore, although the SIFT score for the SNP mutation in this gene predicted a deleterious phenotype, it is unlikely to be related to the development of diabetes in the O-NOD^{k} mice in this study.

The SIFT score for the 5th candidate gene *Ncor1*, was unavailable, therefore its phenotype could not be predicted as deleterious or benign. It is a transcriptional co-regulator linked with regulation of various pathways associated with insulin signaling and T2D such as PI3K signaling, cholesterol homeostasis and lipid transport (Furuya et al., 2007, Astapova et al., 2014, Ou-Yang et al., 2018). Targeted mutation of *Ncor1* in muscles increased muscle mass and mitochondrial activity, leading to enhanced exercise endurance in mice (Yamamoto et al., 2011). On the other hand, adipocyte-specific knockout of *Ncor1* led to increased obesity, but the mice had improved glucose tolerance and insulin sensitivity in peripheral tissues, and did not develop diabetes (Li et al., 2011). In the fasting state, *Ncor1* prevents hepatic lipid synthesis, whereas in the fed state, insulin phosphorylates *Ncor1*, inducing inhibition of PPARα transactivation in the liver. Ncor1- PPARα is then degraded by autophagy, thus regulating ketogenesis (Saito et al., 2019). Therefore, while loss of autophagy causes increased Ncor1 accumulation and defective lipid oxidation, liver-specific *Ncor1* knockout increases hepatic lipogenesis and oxidative metabolism (Jo et al., 2015, Saito et al., 2019).

Although *Ncor1* is known to be expressed in the pancreas, there is currently no research conducted on the role of *Ncor1* in the pancreas or islet, nor any pancreatic islet-specific *Ncor1* knockout mice studies. However, *Ncor1* knockout studies in the peripheral tissues and their association with diabetes suggest a potential role for this gene in the pathogenesis of diabetes.

Finally, the 6th candidate gene *Olfr954* is a member of the olfactory receptor (OLFR) family, which are GPCRs required for detection of odours (Shum et al., 2015). It is not expressed in the pancreas and current literature suggests that *Olfr954* has no known relationship with diabetes or glycaemic traits. Hence, this gene is unlikely to be causative of the T2D phenotype of the O-NOD^{k} mice when challenged by a HF diet.

Therefore, among the 6 candidate genes selected from the list of single nucleotide variants, *Atp13a3, Gpr125, Kcnh7 and Ncor1* present more promising associations with the diabetes phenotype in the O-NOD^{k} mice. However, since the WGS was only conducted on 2 mice per group, further Sanger sequencing for SNP validation in a greater number of mice is required.

A list of homozygous insertions and deletions present in the genome of HF-fed O-NOD^{k} mice was generated and pathway analysis was conducted using the Enrichr tool to highlight clusters of functionally linked genes among this list. The list of genes with insertions showed enrichment in pathways associated with pancreatic exocrine function and insulin secretion, where insertions were observed in the following genes: *Camk2b, Ryr2, Ppp2r5e, Gnaq, Cacna2d3, Cacna2d2, Prkca, Adcy1, Ppp2r3a, Plcb1, Cacng3, Slc8a1, Kcnma1* and *Kcnn2*. Validation of the presence of these insertions in the genomes of more O-NOD^{k} and RF-NOD^{k} mice is required in order to shortlist candidate genes associated with the diabetes phenotype in the O-NOD^{k} mice. Pathway analysis of genes with deletions did not present with pathways known to be associated with T2D. Therefore, further analysis and manual curation of the insertions and deletions is required in order to avoid overlooking any strong potential candidate genes.

It is also to be noted that certain regions of the genome may not have been completely and accurately aligned, since the reference mouse genome used was the C57BL/6J mouse, which is different from the NOD mouse genome. Strain-specific differences were observed when the

C57BL/6J mice genome was aligned to 16 widely used inbred mouse strains, including NOD/ShiLtJ, leading to gaps in the sequence (Lilue et al., 2018). However, since the full NOD reference genome library is not available, the well-characterized C57BL/6J mouse genome had to be used as a reference.

Finally, due to the small sample size used in this study, further analysis of the transcriptome in more mice would provide insights into the biological effects of these variants and supplement the observations made through WGS of the O-NOD^{k} and RF-NOD^{k} mice.

Chapter 7

Results

Transcriptomic alterations in the

O-NOD^{k} and RF-NOD^{k} mice

7.1 Introduction

High throughput whole transcriptome sequencing (RNA-seq) has been widely used for transcriptome profiling of specific tissues and cell types in an unbiased fashion, allowing identification and quantification of differentially expressed genes (DEGs) (Kratz and Carninci, 2014). Through transcriptome assembly and alignment of the RNA sequencing reads to a reference genome, it can also be used for identification of novel transcripts, alternative spliced isoforms, single nucleotide polymorphisms (SNPs) and indels (insertions and deletions). This technique also allows interpretation of the functional aspects of the genome and identification of biological pathways affected by changes in the genetic sequence. RNA-seq has been used for the identification of dysregulated genes and discovery of novel biomarkers associated with risk prediction for T2D (Christodoulou et al., 2019, Wu et al., 2017).

In the whole genome sequencing results described in chapter 6, SNPs in 6 candidate genes and over 500 indels (i.e. deletions, fusions and insertions) were observed in the genome of O-NOD^{k} mice, compared to RF-NOD^{k} mice. Therefore, the RNA-seq analysis was performed to investigate the whole transcriptome of the two NOD^{k} mice sub-strains in response to either NC or HF diet and provide further insights about exon areas that were of interest but did not map cleanly to the genome reference.

The aims of this chapter were: *i)* to conduct RNA-seq in islets of O-NOD^{k} and RF-NOD^{k} mice fed on either chow or HF diet, for identification of differential transcriptomic responses to diet stress between the two mice sub-strains that could be predisposing to T2D and *ii)* to provide additional sequencing information to resolve areas of the exon that were not clearly mapped in the whole genome sequencing, described in the previous chapter. Overall, it was expected that this approach would lead to the identification of genetic alterations that are translated into

functional modifications associated with T2D predisposition in the O-NOD^{k} mice and protection in the RF-NOD^{k} mice.

7.2 Experimental design

Age-matched male O-NOD^{k} and RF-NOD^{k} mice were placed on either normal chow (NC) or HF diet from 4 until 14 weeks of age (n=8/group). At the end of the study period, pancreatic islets were isolated for RNA extraction and subsequent sequencing using 150 bp paired end reads (n=4/group) was performed, as detailed in Chapter 2. Due to the costs involved in RNA sequencing, only 4 out of 8 mice were randomly selected across all groups to perform sequencing. The rest of the 4 mice islets were reserved for validation of gene expression in future studies. Transcriptome assembly was approached by alignment of the RNA sequencing reads to the reference genome (C57BL/6J) to construct transcripts, as depicted in Figure 44. In addition, *de novo* assembly to detect overlapping reads and creating a whole transcript is planned as future work (Figure 44). Details of RNA sequencing and bioinformatics analysis are described in Chapter 2.

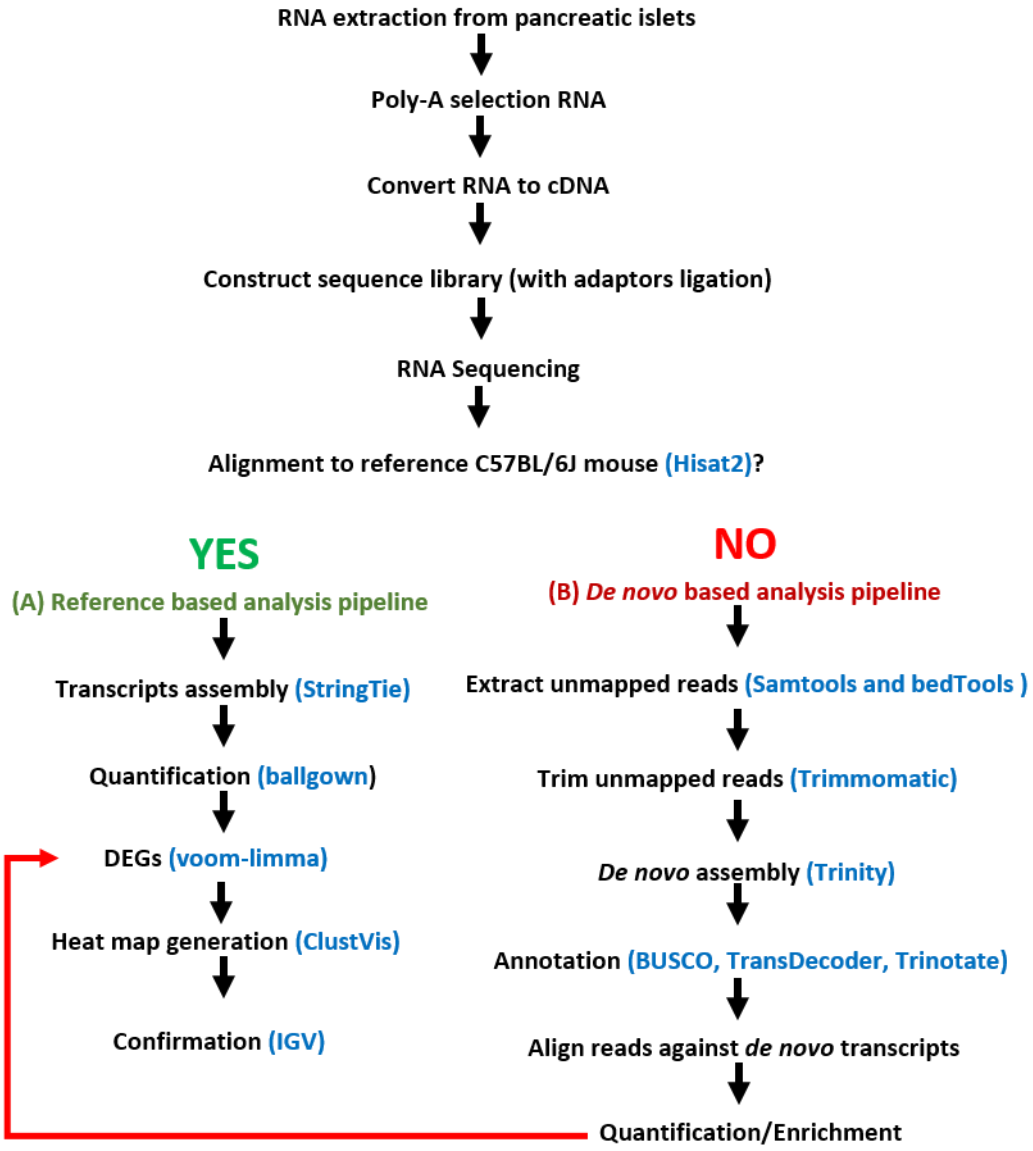

Figure 44: RNA sequencing data analysis workflow of the islet transcriptome of O-NOD^{k} and RF-NOD^{k} mice. Pancreatic islets were isolated from O-NOD^{k} and RF-NOD^{k} mice fed on chow or HF diet from 4-14 weeks of age, and used for RNA isolation. Following RNA quantification and quality determination, RNA sequencing was performed (n=4 per group). In this study, reads were mapped to a reference C57BL/6J mouse genome and gene expression levels were determined (workflow A). Pair-wise comparisons were conducted to screen for differentially expressed genes (DEGs) with voom-limma software and heat maps were generated using ClustVis. Sequences that did not align to the reference genome were assigned for *de novo* assembly (workflow B), in future studies.

7.3 Results

7.3.1 Mice sample data

In order to uncover genome-wide transcriptional changes associated with islet dysfunction prior to diabetes development, RNA-seq analysis was performed in islets isolated from O-NOD^{k} and RF-NOD^{k} mice, fed either NC or HF diet from 4-14 weeks of age. As previously observed, O-NOD^{k} mice on both diets displayed a progressive increase in body weight compared to RF-NOD^{k} mice, and by 14 weeks of age, HF-fed O-NOD^{k} mice were significantly heavier than HF-fed RF-NOD^{k} mice (42.0 ± 1.0 *vs* 35.9 ± 1.5 g, respectively at 14 weeks of age, $p<0.05$) (Table 11). The 10 weeks of HF-feeding did not result in development of moderate to severe hyperglycaemia in any mice, although two HF-fed O-NOD^{k} mice had mildly elevated blood glucose levels (7.7 mM and 8.7 mM) compared to other mice in this same group (5.9 mM and 7.0 mM) and the HF-fed RF-NOD^{k} group (5.9-7.0 mM) (Table 11).

Table 11: Body weight and non-fasting blood glucose levels of O-NOD^{k} and RF-NOD^{k} mice subjected to either NC or HF diet for 10 weeks, at the end of the study.

Strain	ID	Diet	Body weight (g)	Blood glucose (mM)	RNA RIN #
O-NOD^{k}	1	NC	33.98	5.6	9.0
O-NOD^{k}	2	NC	32.99	6.2	8.4
O-NOD^{k}	3	NC	34.47	7.2	8.7
O-NOD^{k}	4	NC	36.13	6.2	8.8
O-NOD^{k}	5	HF	42.63	7.0	8.9
O-NOD^{k}	6	HF	39.14	5.9	9.3
O-NOD^{k}	7	HF	46.01	8.7	8.7
O-NOD^{k}	8	HF	45.00	7.7	8.9
RF-NOD^{k}	9	NC	30.01	5.1	9.0
RF-NOD^{k}	10	NC	30.92	6.4	9.4
RF-NOD^{k}	11	NC	31.73	5.9	9.1
RF-NOD^{k}	12	NC	33.83	5.7	9.1
RF-NOD^{k}	13	HF	39.46	5.9	9.0
RF-NOD^{k}	14	HF	33.55	6.6	9.5
RF-NOD^{k}	15	HF	36.96	7.0	9.3
RF-NOD^{k}	16	HF	36.55	5.9	8.0

7.3.2 Read alignment accuracy

RNA-seq performed using the TruSeq Stranded mRNA by Illumina (150 bp paired end reads), yielded libraries with an average size of 23 million raw reads (Table 12). Of those, 45% of the reads (10.35 million) that aligned concordantly to both sides of the paired end reads of the C57BL/6J reference mice genome, were subjected to transcript assembly, using StringTie. The rest of the reads that either mapped to only one side of the paired end reads or did not map, which reflect inconsistencies between the NOD^{k} mice and the reference genome, were extracted for future analysis by *de novo* transcriptome analysis, as these reads may be useful for detection of big indels and/or structural rearrangements that could be associated with functional changes leading to T2D. Of note, due to the challenges imposed by the *de novo* assembly, including complexity and time-consumption, this study will focus only on the analysis of paired end reads with 100% concordance to the related reference genome.

Table 12: Summary of reads alignment concordance to the reference C57BL/6J mouse genome using Hisat2, following RNA-seq

Strain	Sample ID	Diet	# Reads paired	# Reads aligned concordantly exactly 1 time	
				# reads	% reads
O-NOD^{k}	1	NC	18,393,538	7,311,085	39.8
O-NOD^{k}	2	NC	23,108,731	9,386,403	40.6
O-NOD^{k}	3	NC	11,311,036	4,580,766	40.5
O-NOD^{k}	4	NC	25,699,036	11,676,013	45.4
O-NOD^{k}	5	HF	28,709,646	13,821,268	48.1
O-NOD^{k}	6	HF	23,054,829	9,762,648	42.4
O-NOD^{k}	7	HF	21,931,315	10,236,477	46.7
O-NOD^{k}	8	HF	26,037,157	12,479,432	47.9
RF-NOD^{k}	9	NC	26,023,744	13,454,058	51.7
RF-NOD^{k}	10	NC	21,396,506	10,944,497	51.2
RF-NOD^{k}	11	NC	25,242,438	11,130,590	44.1
RF-NOD^{k}	12	NC	25,872,184	12,482,889	48.3
RF-NOD^{k}	13	HF	23,973,900	10,632,942	44.4
RF-NOD^{k}	14	HF	31,631,314	12,655,266	40.0
RF-NOD^{k}	15	HF	28,664,189	14,085,556	49.1
RF-NOD^{k}	16	HF	22,089,264	10,120,376	45.8

7.3.3 Quality control (variabilities and outliers)

The characteristics of the RNA sequencing data generated in this study for the 16 different mice samples were visualized using multidimensional scaling analysis (MDS) plots based on gene expression data matrices (Figure 45A). Theoretically, samples with different gene expression profiles are expected to cluster in different areas of the plot. Interestingly, in this study, a clear cluster separation between O-NOD^{k} and RF-NOD^{k} mice sub-strains on both diets was not observed, as 12 of the 16 mice, irrespective of strain or diet clustered reasonably close together. Thus, for the most part, biological variations in mRNA expression within islets of the sub-strains is minimal, with little effect of diet. This could be due to the fact that both sub-strains of mice belong to the same NOD mouse strain.

Interestingly, the MDS plot analysis showed that two samples (i.e. #7 and 8) were clearly separated from the others. Of note, these samples were obtained from the two HF-fed O-NOD^{k} mice that had mildly elevated blood glucose levels. These results could be due to a glucose effect on the clustering of the samples which was seen with HF-feeding of the O-NOD^{k} mice only.

Additionally, the MDS plot showed that sample #1, obtained from a NC-fed O-NOD^{k} mouse, was also located apart from the other samples. In fact, the total number of reads and mappability obtained for this specific sample was reduced compared to the other sample libraries, thus indicating poor quality sequencing. Hence, this sample was classified as an outlier and conferred a lower sample weight in the subsequent adjustment steps to prevent skewing and misinterpretation of the RNA sequencing results (Figure 45B). Sample #9 a chow-fed RF-NOD^{k} mouse was also a possible outlier that was assigned a lower sample weight, although less so than for Sample #1. Finally, following quality control adjustments, 12,279 genes were identified and used for further analysis of differential gene expression.

As described in Table 12, only 4.5 million reads was obtained for sample # 3 compared to the rest of the samples analyzed. Therefore, it could be treated as an outlier and removed from the analysis or assigned a lower sample weight and be kept in the study. However, library size is only one of the many elements that are used to estimate sample quality and the quality of the reads of this sample was high enough to not be regarded as an outlier.

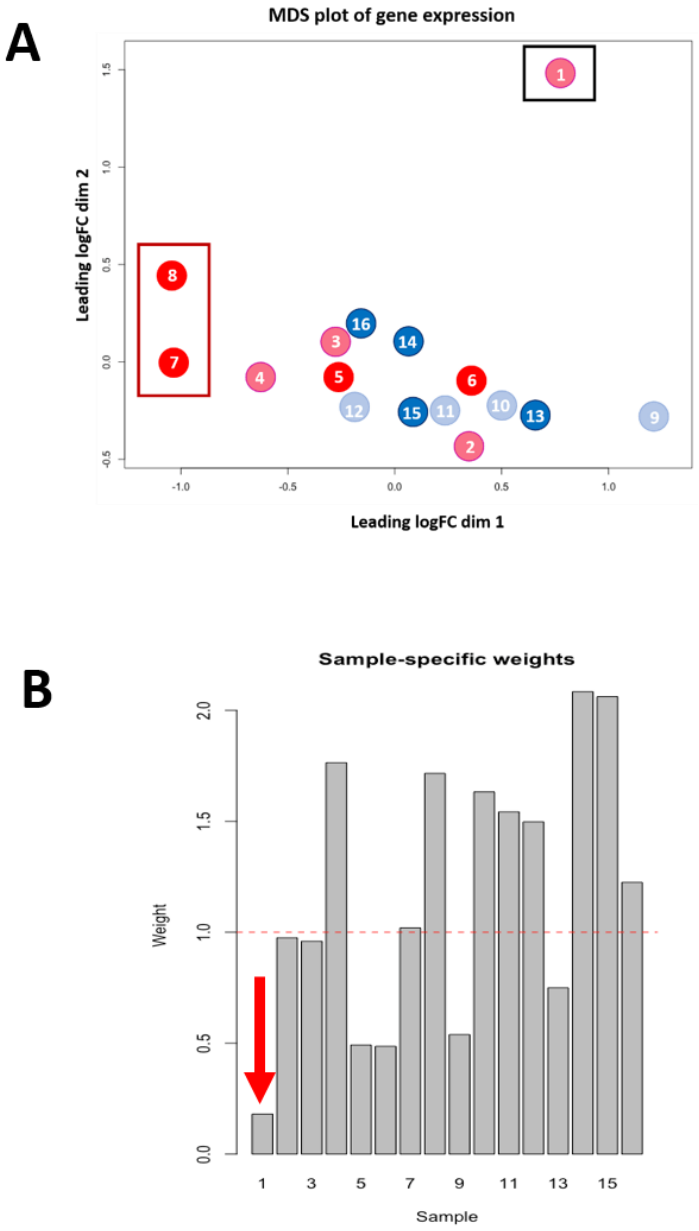

Figure 45: Multidimensional scaling analysis (MDS) plot of RNA-seq data and specific weight adjustment according to quality of the sequenced reads. MDS plot showing intra and inter-group sample variability and outliers. Each circle represents the islet sample from a single mouse with the colours representing mice groups (Dot colors, pink: O-NOD^{k}-NC (#1-4), red: O-NOD^{k}-HF (#5-8), light blue: RF-NOD^{k}-NC (#9-12), dark blue: RF-NOD^{k}-HF (#13-16), n=4/group). Sample #1 is identified as an outlier (black box), while samples #7 and #8 were observed to cluster separately from the other two mice of its group (red box) (A). Sample–specific weights graph depicting biological/technical outlier (red arrow) and possible outlier samples that were conferred a lower weight adjustment compared to the other samples to prevent skewing of results (B).

7.3.4 Differential expression analysis of O-NOD^k and RF-NOD^k mice

After pooling the data for both sub-strains, a three way differential gene expression analysis was performed, as summarized in Table 13. The approach used was a direct comparison between the two mice sub-strains (O-NOD^k and RF-NOD^k).

The 1st analysis was conducted regardless of diet (n=8 mice/ group), using adjusted p-value < 0.05 for significance (P_{adj} < 0.05); the gold standard for selection of differentially expressed genes (DEGs) of statistical significance. This analysis identified only 17 DEGS out of 12,278 genes, which includes one down-regulated gene and 16 up-regulated genes in the O-NOD^k mice compared to RF-NOD^k mice. Further comparisons investigating the diet effect also generated a very small number of DEGs, including 6 up-regulated DEGs for the NC-fed mice and 48 DEGs (1 down- and 47 up-regulated) for the HF diet-comparison (Table 13).

Table 13: Number of differentially expressed genes (DEGs) obtained with pair-wise comparisons of O-NOD^k mice *vs* RF-NOD^k mice, irrespective of diet (analysis #1), for mice on chow diet only (analysis #2), and for mice on HF diet only (analysis #3), with a selection criteria of $P_{adj.} < 0.05$.

Analysis #	Pair-wise comparison	DEGs $P_{adj} < 0.05$
1	O-NOD^k *vs* RF-NOD^k mice (n=8 mice/group)	17 (↓1 ↑16)
2	O-NOD^k *vs* RF-NOD^k mice Chow diet (n=4 mice/group)	6 (↑6)
3	O-NOD^k *vs* RF-NOD^k mice (HF diet) (n=4/group)	48 (↓1 ↑47)

Subsequent pair-wise comparisons were made using a selection criteria of $p < 0.05$ instead of *Padj* < 0.05, which was applied to all 3 analyses to generate a list with the top 20 genes putatively differentially expressed between the O-NOD^{k} and RF-NOD^{k} mice. For the first analysis (i.e., sub-strain comparison independent of dietary effect), Purkinje cell protein 4 (*Pcp4*), which has been linked to the calmodulin dependent kinase signaling pathway and regulation of neuronal differentiation (Mouton-Liger et al., 2011), was found to be down-regulated in the O-NOD^{k} mice (Table 14). The top 3 of the 19 up-regulated DEGs in the O-NOD^{k} mice include Syndecan 2 (*Sdc2*); which encodes for an integral membrane protein associated with cell adhesion and signaling, Succinate-CoA ligase GDP-forming subunit beta (*Suclg2*); linked to the tricarboxylic acid cycle and Carbonyl reductase 3 (*Cbr3*), a NADPH-dependent cytosolic enzyme involved in prostaglandin pathway and oxidative stress (Ebert et al., 2010, Choi et al., 2009).

Additionally, hierarchical clustering of the top 50 expressed genes ($p < 0.05$) between the two mice sub-strains was arranged as a heat map to allow visualization of inter-sample variations in gene expression for both O-NOD^{k} and RF-NOD^{k} mice (Figure 46). Even among the top 50 expressed genes, 94% of the genes were up-regulated in the O-NOD^{k} mice, compared to the RF-NOD^{k} mice. Of note, this heat map also illustrated the different transcriptome profile observed within the HF-fed O-NOD^{k} mice samples with the two mice that had mildly higher glycaemia, the 7th and 8th from the left-hand side, therefore indicating intra-group variation. Additionally, the first sample noted in this figure (left to right, NC-fed O-NOD^{k}), previously reported as a biological/technical outlier in Figure 45, was also observed to cluster differently and away from the rest of the O-NOD^{k} samples.

Table 14: Top 20 differentially expressed genes (p< 0.05) obtained through comparison between the O-NOD^{k} and the RF-NOD^{k} mice, independent of diet (n=8/ group). Altered genes classified as down-regulated (blue) and up-regulated (red) were ranked according to their respective p values.

Gene	Log Fold Change	P value	Adjusted p value (P_{adj})
Pcp4	-0.764	1.03E-07	4.23E-04
Sdc2	1.150	4.44E-14	5.46E-10
Suclg2	0.972	3.11E-12	1.91E-08
Cbr3	0.676	6.80E-07	2.09E-03
Gm15163	0.543	1.44E-06	3.54E-03
Aatk	0.527	2.20E-06	4.50E-03
Ifi27	0.512	4.32E-06	6.63E-03
Lxn	0.713	5.44E-06	7.42E-03
Dynlt1c	0.520	1.14E-05	1.40E-02
Lamc2	0.250	1.45E-05	1.49E-02
Dynlt1b	0.922	1.46E-05	1.49E-02
Smim1	0.324	2.48E-05	2.34E-02
C77080	0.316	3.23E-05	2.83E-02
Zfp26	0.329	4.92E-05	3.89E-02
Dusp26	0.403	5.07E-05	3.89E-02
Gm6485	0.367	5.53E-05	3.99E-02
Krt80	0.399	6.97E-05	4.75E-02
Gm10132	0.251	7.84E-05	5.07E-02
Tmem38b	0.370	1.07E-04	6.58E-02
Gm11423	0.300	1.14E-04	6.64E-02

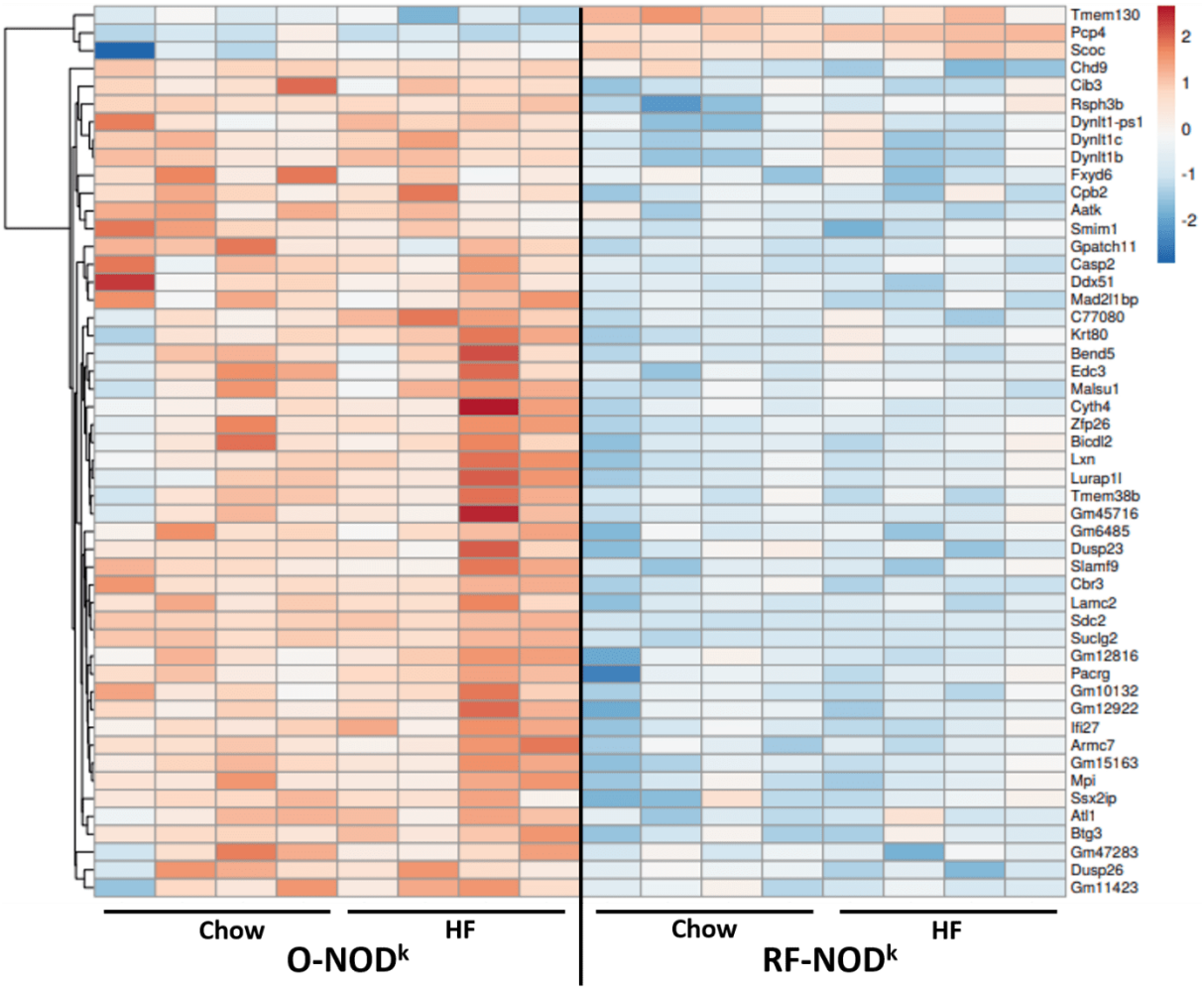

Figure 46: Visualization of gene clusters among O-NOD^k and RF-NOD^k mice. A heat map of the top 50 expressed genes ($p < 0.05$) showed that only 3 genes were down-regulated, whereas 47 others were up-regulated in the O-NOD^k mice compared to the RF-NOD^k mice.

7.3.5 Sub-strain effect on transcriptome of O-NOD^k and RF-NOD^k mice

A second set of pair-wise comparison was conducted between the NC-fed O-NOD^k and RF-NOD^k mice (n=4/group) to identify innate differences in the transcriptome of the two mice sub-strains, without the adjunct effects of HF-feeding.

As previously mentioned, this comparison only produced 6 DEGs ($q < 0.05$), which were all up-regulated in the NC-fed O-NOD^k mice compared to the NC-fed RF-NOD^k mice. The 6 DEGs identified included *Sdc2, Suclg2,* DNA-directed RNA polymerase II subunit RPB4 (*Polr2d*) responsible for encoding RNA Polymerase II, radial spoke head protein 3 homolog B (*Rsph3b*) which encodes a protein kinase A anchoring protein, metal regulatory transcription factor 1 (*Mtf1*) responsible for heavy metal homeostasis and FYVE and coiled-coil domain autophagy adaptor 1 (*Fyco1*) which is responsible for transport of autophagic vesicles (Jivan et al., 2009, Egli et al., 2003, Pankiv et al., 2010). Using a similar criteria of $p < 0.05$ as described in 7.3.4, a list containing the top 20 expressed genes with putative differential expression between the two mice sub-strains was obtained (Table 15). Only 2 out of the 20 genes were down-regulated in the NC-fed O-NOD^k mice compared to the NC-fed RF-NOD^k mice, which includes *Pcp4* and the decidual protein induced by progesterone autophagy regulator (*Depp1*), while the remaining 18 genes were up-regulated. Notably, most of these genes have a $\log_2$ fold change < 1, suggesting low inter-sub-strain transcriptomic differences between O-NOD^k and RF-NOD^k mice.

The heat map illustrating the hierarchical clustering of the top 50 expressed genes ($p < 0.05$) between the NC-fed mice sub-strains also showed that 47 out of the 50 genes were up-regulated in the NC-fed O-NOD^k mice compared to the NC-fed RF-NOD^k mice (Figure 47). Overall, NC-fed O-NOD^k mice do not have stark differences in gene expression when compared to the RF-NOD^k mice.

Table 15: Top 20 expressed genes (p<0.05) in NC-fed O-NOD^{k} mice *vs* RF-NOD^{k} mice (n=4/ group). Altered genes classified as down-regulated (blue) and up-regulated (red) were ranked according to their respective p values.

Gene	Log Fold Change	P value	Adjusted p value (P_{adj})
Pcp4	-0.530	1.8E-04	1.7E-01
Depp1	-0.765	3.8E-04	2.0E-01
Sdc2	1.181	2.2E-11	2.8E-07
Suclg2	1.036	1.6E-09	9.9E-06
Polr2d	0.481	2.0E-06	8.3E-03
Rsph3b	1.500	6.6E-06	2.0E-02
Mtf1	0.614	1.2E-05	2.9E-02
Fyco1	0.889	1.9E-05	4.0E-02
Gm13115	1.140	3.7E-05	6.5E-02
Gm15163	0.619	6.3E-05	9.7E-02
Aatk	0.548	8.6E-05	1.2E-01
Hba-a2	0.496	1.2E-04	1.4E-01
Fdx1	0.415	1.3E-04	1.4E-01
Pla2g16	0.396	1.7E-04	1.7E-01
Cx3cl1	0.384	2.0E-04	1.7E-01
Carhsp1	1.421	2.2E-04	1.7E-01
Cpsf7	0.959	2.2E-04	1.7E-01
Cbr3	0.567	2.7E-04	1.9E-01
Gpatch11	0.476	3.4E-04	2.0E-01
Lxn	0.689	3.8E-04	2.0E-01

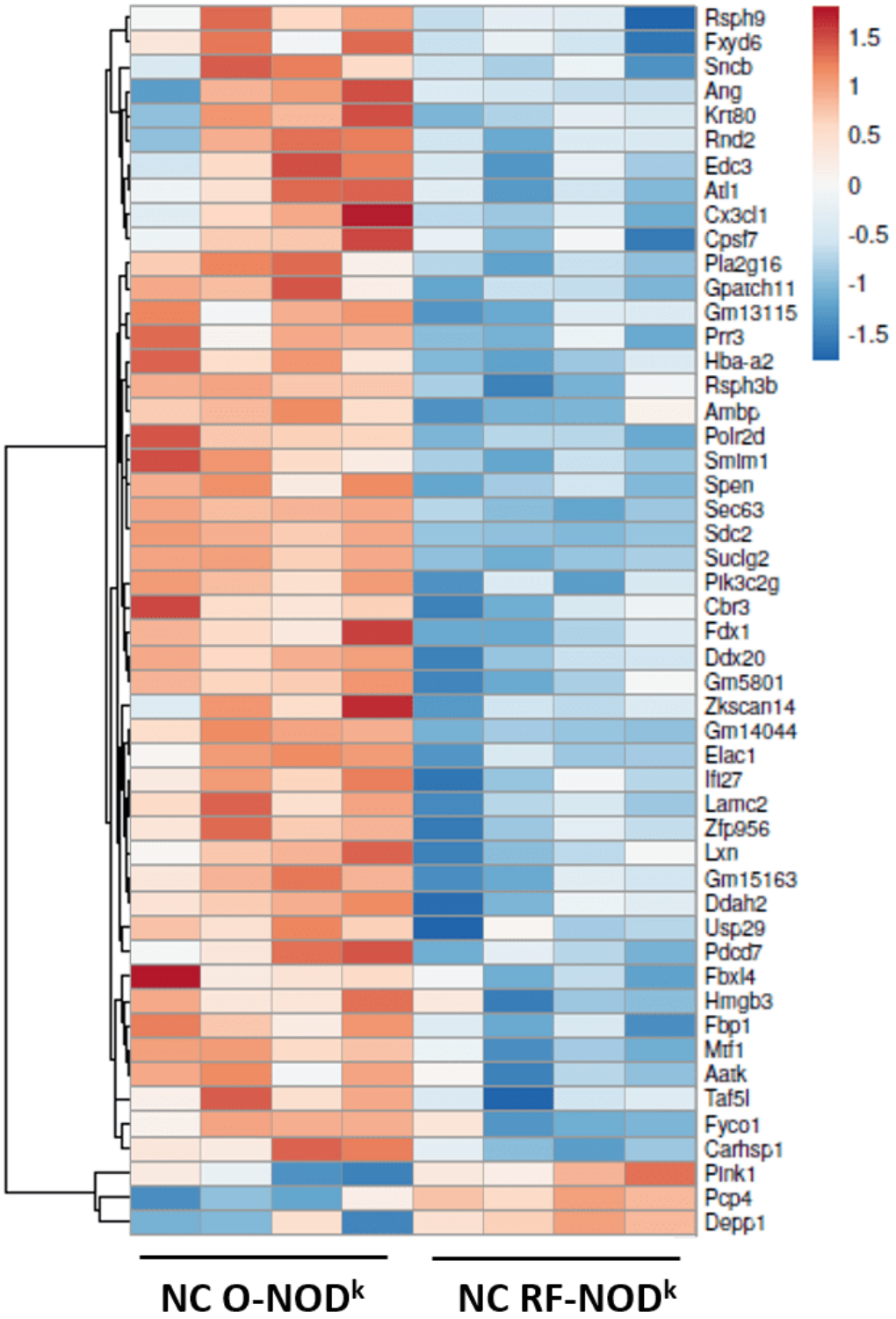

Figure 47: Heat map of the top 50 expressed genes (p< 0.05) with altered expression in NC-fed O-NOD^{k} and RF-NOD^{k} mice. 3 out of the top 50 genes (*Pink1*, *Pcp4* and *Depp1*) were down-regulated in the NC-fed O-NOD^{k} mice compared to RF-NOD^{k} mice, while the other genes were up-regulated.

7.3.6 HF-diet effect on transcriptome of O-NOD^{k} and RF-NOD^{k} mice

In the third pair-wise comparison, the transcriptome of HF-fed O-NOD^{k} mice was compared with HF-fed RF-NOD^{k} mice (n=4 mice/ group) to determine the effects of nutritional excess, on their gene expression.

A strict selection criteria of $P_{adj} < 0.05$ identified only 48 DEGs, of which only *Pcp4* was down-regulated in the HF-fed O-NOD^{k} mice, while the rest were up-regulated (Table 13). The top 20 DEGs in this pair-wise comparison also included some previously identified genes, including *Sdc2, Suclg2* and *Cbr3* (Table 16). HF-fed O-NOD^{k} mice also showed up-regulation in genes that were not differentially expressed in the NC-fed mice, such as interferon alpha inducible protein 27 (*Ifi27*) which is involved in apoptotic signaling pathways, P2X purinoreceptor 4 (*P2rx4*) associated with Ca^{2+} ion channel activity and guanylate cyclase 2 (*Gucy2c*) which is a transmembrane receptor involved in the regulation of intracellular cyclic guanosine monophosphate (cGMP) and KCl-induced insulin secretion (Wang et al., 2018, Egan and Khakh, 2004, Steinbrecher, 2014, Valentino et al., 2011, Kobayashi et al., 2016).

The heat map of the top 50 ranking expressed genes with $p<0.05$ in this pair-wise comparison between HF-fed mice showed great inter-group variation in the HF-fed O-NOD^{k} mice group, where 2 samples clearly clustered separately from the rest of the group (Figure 48). These two samples had a very different gene expression profile, including 38 up-regulated genes out of the top 50 having a higher log fold change in their expression compared to the rest of the group.

The differential expression pattern observed in these 2 HF-fed O-NOD^{k} mice could be due to differences in blood glucose levels and may not be related to inherent difference in the transcriptional pattern between the two sub-strains. Therefore, to better explore this possibility and also to prevent any confounding effects of glycaemia on gene expression profiles, the HF-fed O-NOD^{k} mice group was further stratified based on their blood glucose levels.

Table 16: Top 20 expressed genes (p<0.05) in HF-fed O-NOD^{k} mice *vs* RF-NOD^{k} mice (n=4/ group). Altered genes classified as down-regulated (blue) and up-regulated (red) were ranked according to their respective p values.

Gene	Log Fold Change	P value	Adjusted p value (P_{adj})
Pcp4	-0.986	3.48E-07	1.43E-03
Sdc2	1.226	8.89E-12	1.09E-07
Suclg2	1.033	1.30E-09	7.99E-06
Cbr3	0.912	1.66E-06	5.11E-03
Lxn	0.988	5.94E-06	1.46E-02
Gm7299	0.622	9.97E-06	1.82E-02
Ifi27	0.673	1.17E-05	1.82E-02
P2rx4	0.446	1.19E-05	1.82E-02
Gucy2c	0.995	2.50E-05	3.09E-02
C77080	0.406	2.52E-05	3.09E-02
Phkg2	0.583	2.77E-05	3.09E-02
Mgp	1.101	3.47E-05	3.33E-02
Dapl1	1.432	3.72E-05	3.33E-02
Abtb1	0.733	3.80E-05	3.33E-02
Gm15427	0.562	4.34E-05	3.34E-02
Tmem179	0.813	4.35E-05	3.34E-02
Gm15163	0.624	5.09E-05	3.68E-02
Cep63	0.444	6.36E-05	4.14E-02
Gm12922	0.451	7.35E-05	4.14E-02
Trpc4	0.364	7.38E-05	4.14E-02

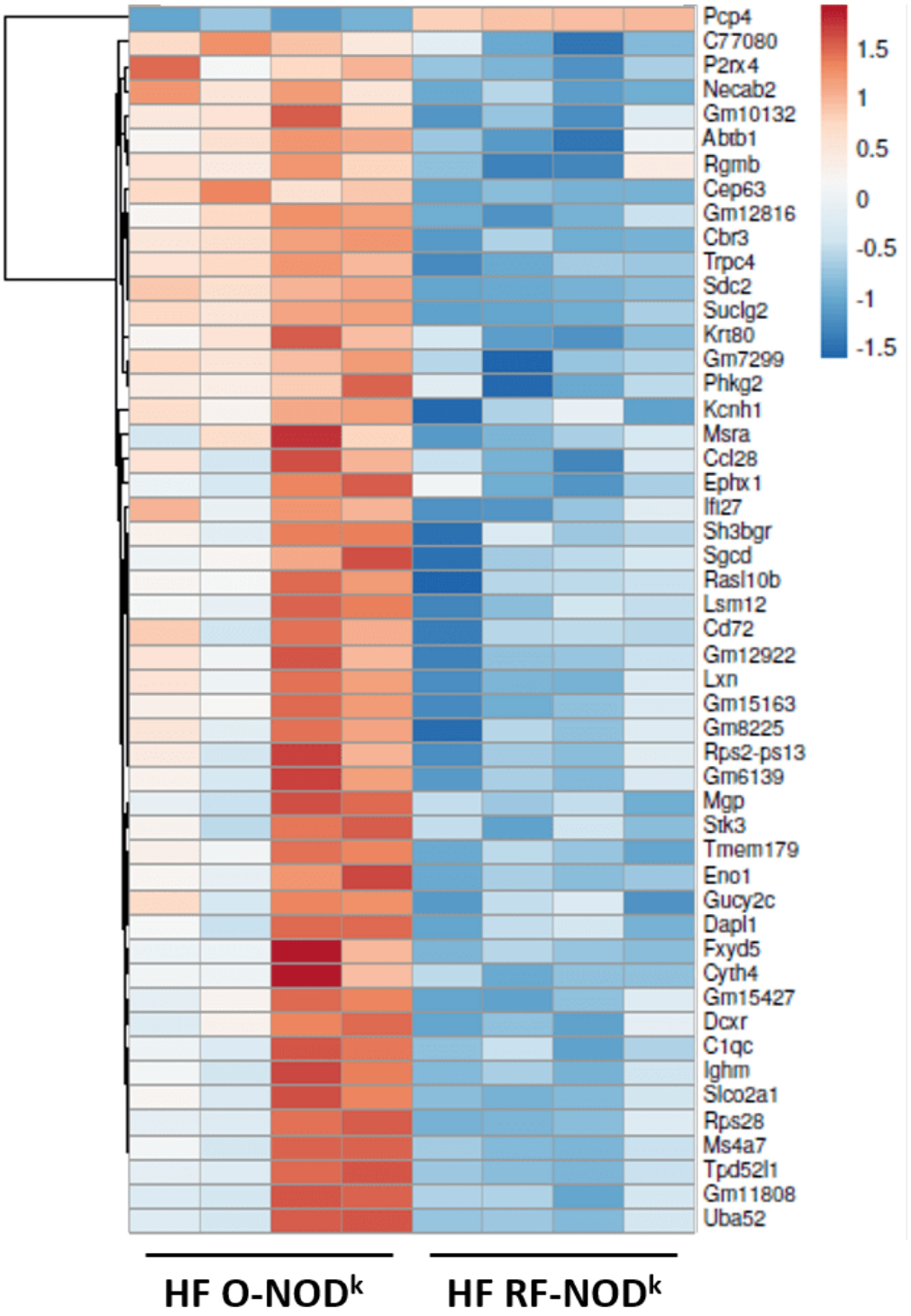

Figure 48: Heat map of the top 50 expressed genes (p< 0.05) with altered expression in HF-fed O-NOD^{k} and RF-NOD^{k} mice. 3 out of the top 50 genes (*Pink1*, *Pcp4* and *Depp1*) were down-regulated in the NC-fed O-NOD^{k} mice compared to the RF-NOD^{k} mice (A), whereas only 1 gene *Pcp4* was down-regulated in the HF-fed O-NOD^{k} mice compared to the RF-NOD^{k} mice (B).

Pair-wise comparisons were conducted between the two HF-fed O-NOD^{k} mice with lower glycaemia (n=2) and HF-fed RF-NOD^{k} mice (n=4). This comparison identified 161 DEGs with $P_{adj} < 0.05$, of which 49 were down-regulated and 112 were up-regulated in HF-fed O-NOD^{k} mice. There was up-regulation of previously observed genes in the HF-fed O-NOD^{k} mice such as *Sdc2, Suclg2* and *Cbr3*. Additionally, increased expression was also observed in ribosomal Protein S6 Kinase A2 (*Rps6ka2*), a protein serine/threonine kinase that regulates diverse cellular processes such as cellular growth, motility, survival and proliferation, PILR alpha associated neural protein (*Pianp*) which is a ligand for paired immunoglobulin-like type 2 receptor alpha (PILRA) involved in immune regulation and increased risk of Alzheimer's disease, and apoptosis associated tyrosine kinase (*Aatk*) in the HF-fed O-NOD^{k} mice, was also observed (Table 17) (Rathore et al., 2018).(Slattery et al., 2011, Milosevic et al., 2013)

On the other hand, genes involved in regulation of cell proliferation and apoptosis such as serine/threonine-protein phosphatase 4 regulatory subunit 3B (*Ppp4r3b*) and Cullin 4B (*Cul4b)* were down-regulated in HF-fed O-NOD^{k} mice. The heat map in Figure 49 also illustrates the clear difference in transcriptome of the HF-fed O-NOD^{k} mice which clustered differently than the HF-fed RF-NOD^{k} mice. Overall, HF-feeding led to a higher proportion of down-regulated genes (16 out of the top 50 genes) in HF-fed O-NOD^{k} mice compared to HF-fed RF-NOD^{k} mice.

Table 17: Top 20 differentially expressed genes in HF-fed O-NOD^{k} mice with lower glycaemia *vs* RF-NOD^{k} mice (n=2 *vs* 4/ group, respectively). Altered genes classified as down-regulated (blue) and up-regulated (red) were ranked according to their respective p values.

Gene	Log Fold Change	P value	Adjusted p value (P_{adj})
Pcp4	-0.943	1.56E-06	6.38E-03
Ppp4r3b	-0.728	6.04E-06	1.85E-02
Cul4b	-1.382	1.66E-05	4.09E-02
Sdc2	1.073	2.19E-10	2.69E-06
Suclg2	0.837	2.41E-08	1.48E-04
C77080	0.463	2.51E-05	5.14E-02
Cbr3	0.687	4.64E-05	7.12E-02
Pianp	0.324	4.55E-05	7.12E-02
Aatk	0.602	5.28E-05	7.21E-02
Cep63	0.491	6.13E-05	7.50E-02
Rps6ka2	0.37	6.72E-05	7.50E-02
Wbp1	1.522	8.94E-05	8.44E-02
Gm27533	1.064	8.79E-05	8.44E-02
Gm7299	0.514	1.38E-04	1.21E-01
Dynlt1b	1.131	2.28E-04	1.22E-01
Dynlt1c	0.635	1.91E-04	1.22E-01
Scamp4	0.611	2.19E-04	1.22E-01
Dusp26	0.524	1.55E-04	1.22E-01
P2rx4	-0.427	2.13E-04	1.22E-01
R3hdm4	-0.303	2.19E-04	1.22E-01

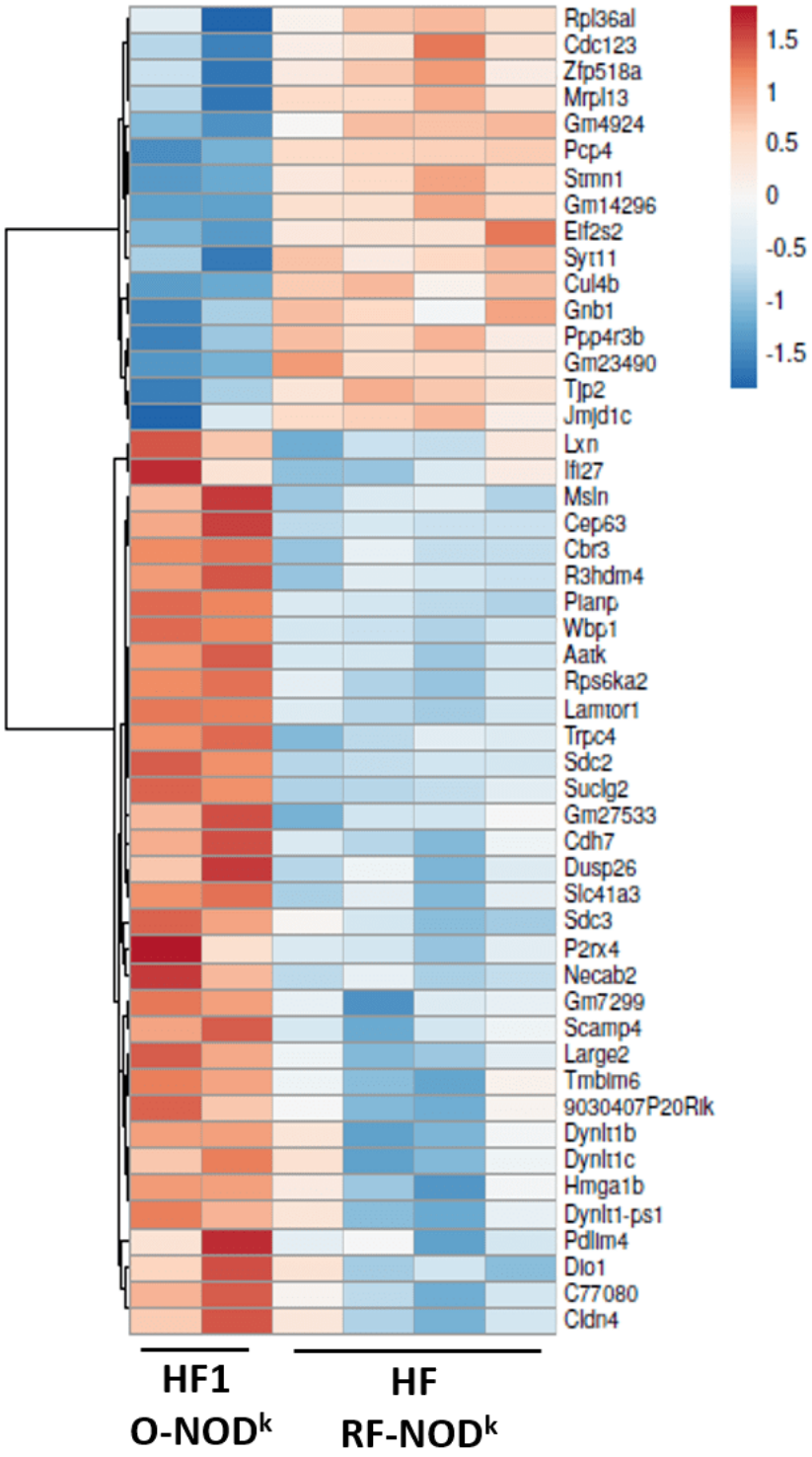

Figure 49: Heat map of the top 50 DEGs in HF-fed O-NOD^k and RF-NOD^k mice. Transcriptome of the HF-fed O-NOD^k mice with lower glycaemia (HF1) was compared to HF-fed RF-NOD^k mice to exclude the effects of hyperglycaemia on gene expression. 16 genes were down-regulated in the HF-fed O-NOD^k mice compared to the HF-fed RF-NOD^k mice with similar glucose levels.

Finally, the transcriptome of the two HF-fed O-NOD^{k} mice with mildly elevated glycaemia was compared to the HF-fed RF-NOD^{k} mice (n=4 mice/ group).

With a selection criteria of $P_{adj} < 0.05$, 5052 DEGs were identified, of which 231 genes were down-regulated and 4822 genes were up-regulated in the HF-fed O-NOD^{k} mice with mildly elevated glycaemia. Among the top 20 DEGs reported, once again, *Pcp4* was found to be down-regulated and *Sdc2* and *Suclg2* were up-regulated in the HF-fed O-NOD^{k} mice compared to RF-NODk mice. Other genes, such as matrix Gla protein (*Mgp)* and death associated protein like 1 (*Dapl1*), which are associated with inhibition of soft tissue calcification and epithelial differentiation and apoptosis, respectively, were also found to be highly expressed in the subgroup of HF-fed O-NOD^{k} mice (Table 18) (O'Young et al., 2011, Grassmann et al., 2015). Many of these genes had log fold expression change >1, which was also illustrated in the heat map showing close hierarchical clustering within the two mice groups (Figure 50).

Table 18: Top 20 differentially expressed genes (p<0.05) in HF-fed O-NOD^{k} mice with mildly elevated glycaemia *vs* RF-NOD^{k} mice (n=2 *vs* 4/ group). Altered genes classified as down-regulated (blue) and up-regulated (red) were ranked according to their respective p values.

Gene	Log Fold Change	P value	Adjusted p value (P_{adj})
Pcp4	-1.034	2.59E-07	1.59E-04
Sdc2	1.262	6.97E-12	8.55E-08
Mgp	1.403	2.48E-10	1.01E-06
Suclg2	1.091	2.10E-10	1.01E-06
Dapl1	1.790	6.39E-09	1.96E-05
Hmox1	0.848	9.96E-09	2.45E-05
Sord	0.911	2.79E-08	5.71E-05
Vgf	1.302	7.60E-08	9.56E-05
Sel1l3	1.036	5.49E-08	9.56E-05
Gm11808	0.620	7.61E-08	9.56E-05
Uba52	0.585	7.79E-08	9.56E-05
Ighm	2.423	1.60E-07	1.57E-04
Cd68	1.136	1.91E-07	1.57E-04
Ms4a7	1.036	1.76E-07	1.57E-04
Tpd52l1	0.701	1.90E-07	1.57E-04
Rps28	0.536	1.58E-07	1.57E-04
Cxcl13	1.661	2.36E-07	1.59E-04
Acp5	1.350	2.14E-07	1.59E-04
Pdlim1	1.027	2.54E-07	1.59E-04
Slfn2	0.807	2.24E-07	1.59E-04

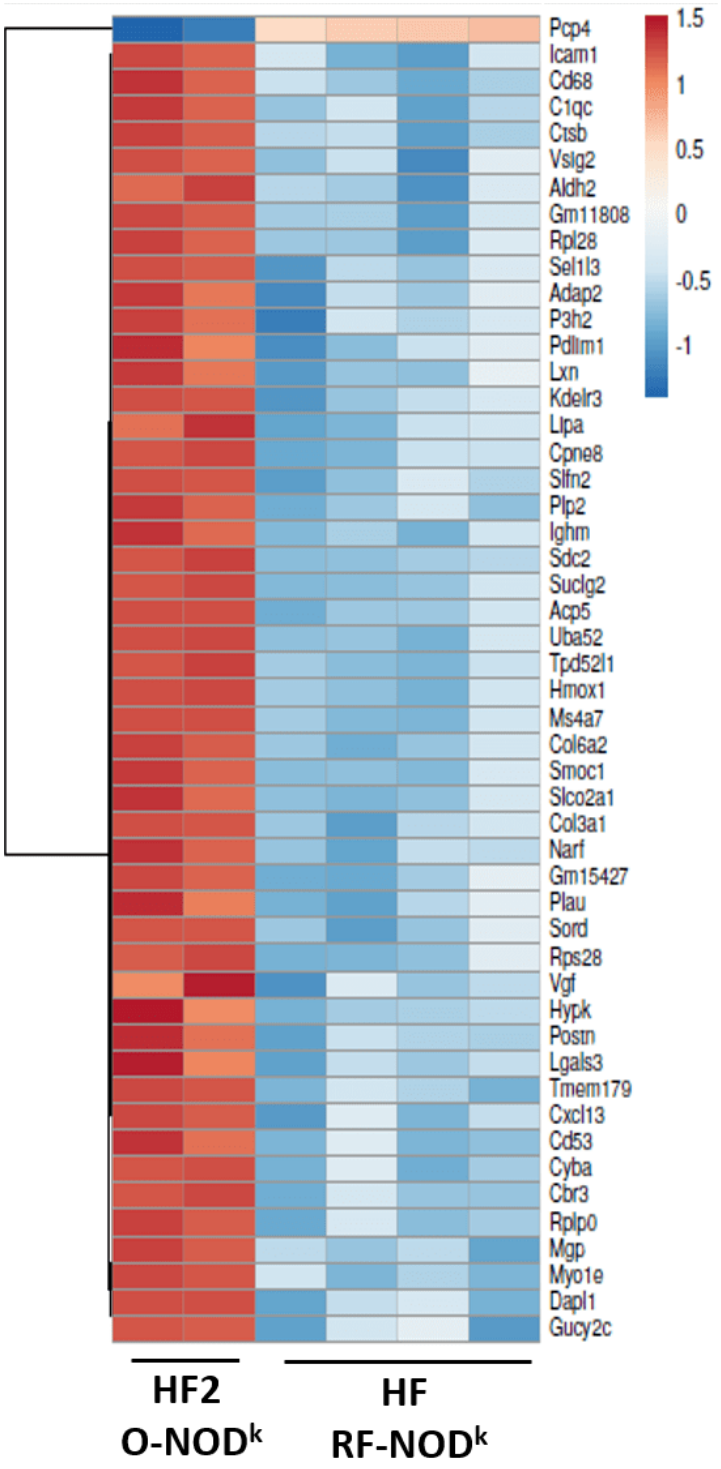

Figure 50: Heat map of the top 50 DEGs in HF-fed O-NOD^{k} mice with mildly elevated glycaemia and RF-NOD^{k} mice. Gene expression of the 2 HF-fed O-NOD^{k} mice with higher glycaemia was compared to HF-fed RF-NOD^{k} mice, which showed that only *Pcp4* was down-regulated in the O-NOD^{k} mice while the rest of the 49 genes were up-regulated.

7.3.7 Expression of genes associated with β-cell function

In addition to previous comparisons, the expression of hallmark genes associated with β-cell development and function, including hormones and transcription factors, lipid metabolism, oxidative stress, ER stress and inflammation were also evaluated between the two mice sub-strains, and illustrated as a heat map in Figure 51.

Similar to previous observations, inter-group variation among O-NOD^{k} mice was observed with no significant differences in gene expression among any of the mice groups. Interestingly, in the two HF-fed O-NOD^{k} mice with mild elevation in glucose, there was down-regulation of genes associated with β-cell function such as *MafA, Nkx6.1,* solute carrier family 2 member 2 (*Slc2a2*)/ *Glut2* and GLP-1 receptor (*Glp1r)* ($p<0.0001$) and *NeuroD1* and secretagogin (*Scgn*) ($p<0.01$) compared to all the other mice samples. These mice also had higher expression of p21 ($p<0.001$) and p53 ($p<0.01$), which are increased during dysregulated β-cell replication and activated by glucotoxicity (Tornovsky-Babeay et al., 2014).

Similarly, there was no marked clustering of the expression of islet β-cell hormones insulin (*Ins*) 1 and 2 among any of the groups. The expression of *Iapp* was up-regulated only in the HF-fed O-NOD^{k} mice ($p<0.05$). Of note, the expression of other islet hormones were also evaluated and only glucagon (data not shown) was down-regulated in all HF-fed mice from both sub-strains compared to the NC-fed mice.

The hierarchical clustering of the expression of genes associated with lipid metabolism showed upregulation of uncoupling protein 2 (*Ucp2*), adipose triglyceride lipase (*Atgl*) and hormone-sensitive lipase (*Hsl*) in the HF-fed O-NOD^{k} mice compared to the HF-fed RF-NOD^{k} mice, suggesting increased islet lipolysis ($p<0.05$). The two O-NOD^{k} mice with higher blood glucose levels had elevated expression of peroxisome proliferator-activated receptor gamma (*Pparg*)

and reduced expression of carnitine palmitoyltransferase 1 (*Cpt1*) compared to the rest of the mice ($p<0.05$).

There was similar expression of genes associated with oxidative stress, ER stress and inflammation among the NC-fed mice. However, remarkably the two HF-fed O-NOD^k mice with mildly elevated glycaemia displayed marked up-regulation in oxidative stress *catalase*, tribbles homolog 3 (*Trib3*), heme oxygenase 1 (*Ho-1*) and forkhead box protein O1 (*Foxo1*). Likewise, ER stress related genes C/EBP homologous protein (*CHOP*) and binding immunoglobulin protein (*Bip*), and inflammation genes CD68 and IL-22 were also up-regulated in these mice ($p<0.001$). Notably, the expression of IL-22 was increased in all HF-fed O-NOD^k mice compared to the HF-fed RF-NOD^k mice, suggesting the presence of an inflammatory environment in these mice.

Overall, there was no significant difference in the expression of genes associated with β-cell function and development between the two mice sub-strains. Up-regulation of genes involved in lipid metabolism such as *Ucp2*, *Atgl* and *Hsl* was observed in the HF-fed O-NOD^k mice compared to HF-fed RF-NOD^k mice. Interestingly, HF-feeding and increased glycaemia in the two HF-fed O-NOD^k mice was associated with down-regulation of transcription factors and genes involved in β-cell function and upregulation of cellular stress-related genes (oxidative and ER) and inflammation. This suggests that even with a mild elevation in blood glucose levels in response to HF-feeding, the O-NOD^k mice develop oxidative and ER stress along with elevation of some inflammatory markers.

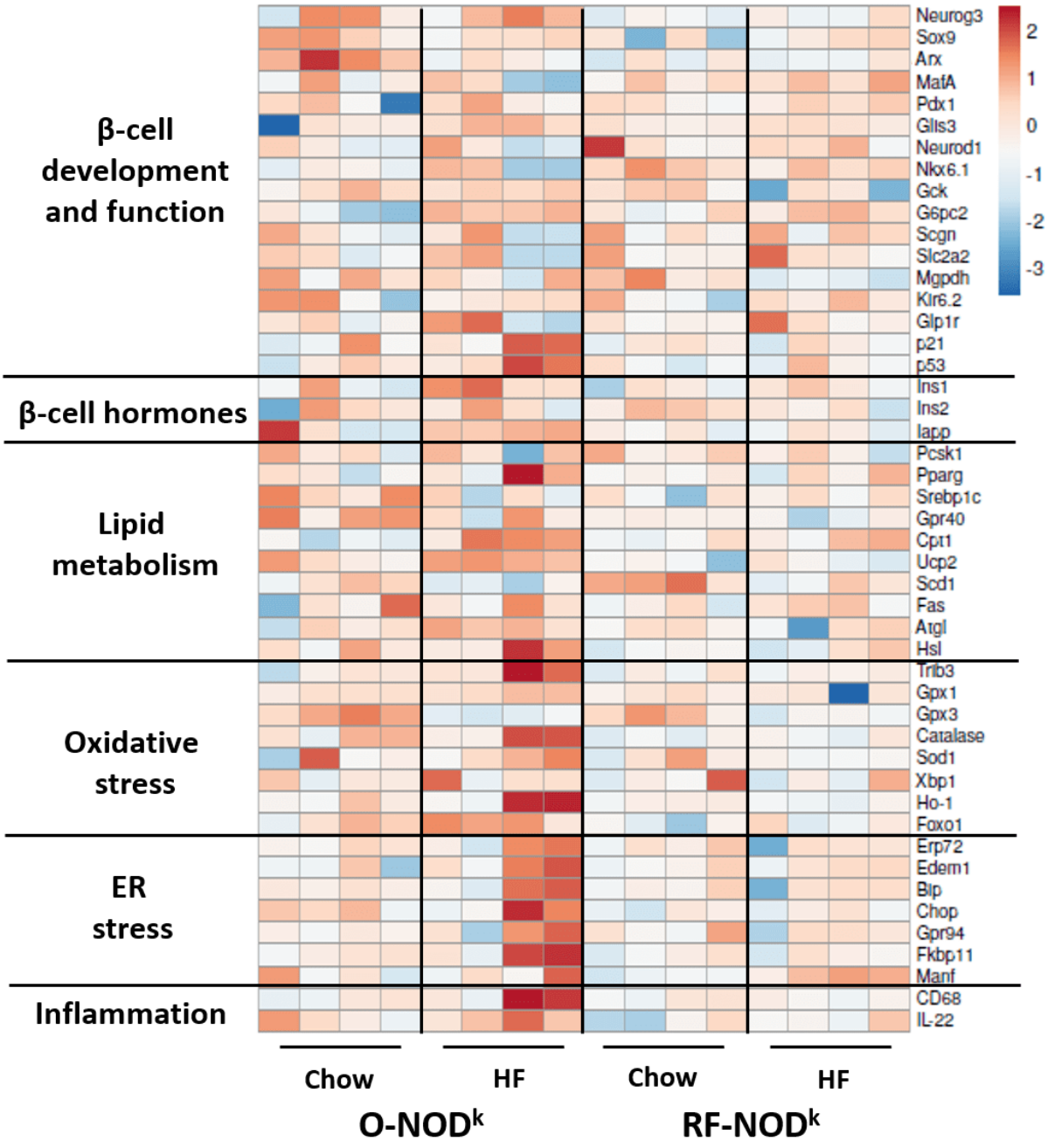

Figure 51: Heat map representing the expression of hallmark genes associated with β-cell function in O-NOD^k and RF-NOD^k mice. The log fold change in expression of genes associated with β-cell development and function including hormones and transcription factors, lipid metabolism, oxidative stress, ER stress and inflammation of the two mice sub-strains on NC and HF diet was visualized. There was no significant intra- or inter-group clustering of gene expression among both mice sub-strains on either diet. Of note, the two HF-fed O-NOD^k mice with mildly elevated blood glucose levels showed up-regulation of genes related to oxidative stress, ER stress and inflammation.

7.3.8 Pathway analysis of O-NOD^{k} and RF-NOD^{k} mice transcriptome

Pathway enrichment analysis of RNA-seq gene sets is useful to gain mechanistic insights into the association of DEGs with any biological process or molecular function in a more interpretable format. In order to successfully perform pathway analysis, a minimum of 100 DEGs is required for pathway analysis packages such as DAVID, Enrichr and KEGG. Unfortunately, in our study, the 3 pair-wise comparisons performed for O-NOD^{k} and RF-NOD^{k} mice only generated a very limited number of DEGs ($P_{adj} < 0.05$). Therefore, a different approach was applied consisting of a gene ranking system, where high inter-gene correlations (either positive or negative) were detected using the Camera R package (Wu and Smyth, 2012). This pathway analysis concept assumes that genes that are differentially expressed will move in the same direction (upregulation or downregulation) as other biologically related genes. Therefore, all the genes obtained from the RNA-seq were input into the linear model fitting object, and enriched pathways were subsequently obtained using the Hallmark database according to their correlation.

In the pair-wise comparison between NC-fed O-NOD^{k} mice and RF-NOD^{k} mice, the pathways with up-regulated enriched gene sets in the NC-fed O-NOD^{k} mice were related to pancreas β-cells, protein secretion, unfolded protein response and PI3k Akt mTOR signaling, whereas reactive oxygen species (ROS) pathway was down-regulated (Figure 52A). This suggests that the O-NOD^{k} mice may have higher functioning β-cells compared to the RF-NOD^{k} mice, as previously highlighted (Figure 51). The pathway analysis also suggests that unfolded protein response genes are highly expressed in the O-NOD^{k} mice and genes related to ROS formation are reduced. Although these results are interesting, caution is required in its interpretation since the p-values related to these pathways were not significant ($p > 0.05$). Therefore, the role of protein unfolding/ misfolding and ROS cannot be completely ruled out as an intrinsic characteristic of the O-NOD^{k} mice and requires further validation.

Similarly, when pathway analysis of expressed genes obtained from the pair-wise comparison of HF-fed O-NOD^{k} and RF-NOD^{k} mice was performed, enrichment of the pancreas β-cells genes, Hedgehog signaling, protein secretion and cholesterol homeostasis gene sets were found to be significantly upregulated in the HF-fed O-NOD^{k} mice (Figure 52B). There was also significant downregulation of genes associated with the epithelial mesenchymal transition pathway in the O-NOD^{k} mice.

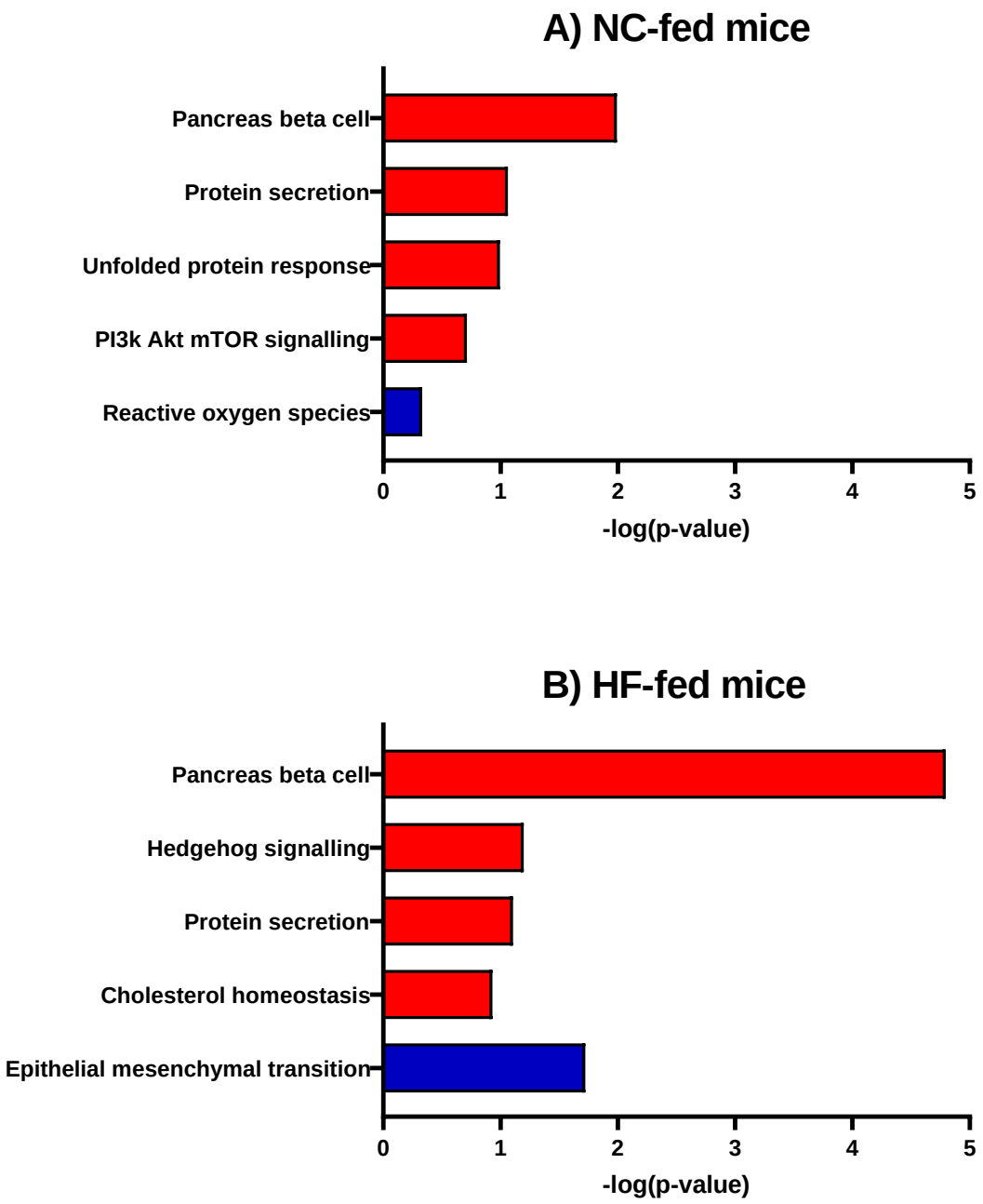

Figure 52: Enriched pathways associated with the pair-wise comparisons of O-NOD^{k} and RF-NOD^{k} mice. Pathway analysis was conducted on the genes obtained from the pair-wise comparisons of NC-fed O-NOD^{k} and RF-NOD^{k} mice (A) and HF-fed O-NOD^{k} and RF-NOD^{k} mice (B) to identify up-regulated (red) and down-regulated (blue) pathways in the O-NOD^{k} mice.

7.3.9 Candidate genes from whole genome sequencing study

The whole genome sequencing study in Chapter 6 identified 6 candidate genes with SNPs (*Atp13a3, Gpr125, Ncor1, Kcnh7, Myh4* and *Olfr954)* that could be associated with the diabetes phenotype in the HF-fed O-NOD^{k} mice. Since these genes could also result in altered transcriptional profiles in pancreatic islet, its expression was verified in the RNA-seq results. *Atp13a3, Gpr125* and *Ncor1* genes were expressed in both sub-strains of mice, but only *Atp13a3* was found at high levels in both NC and HF-fed O-NOD^{k} mice compared to respective RF-NOD^{k} mice, whereas no changes in gene expression of *Gpr125* and *Ncor1* were observed between the mice sub-strains (Figure 53).

The Interactive genomics viewer (IGV) confirmed that the expression of *Kcnh7* was variable and expressed at very low levels in both mice sub-strains in either of the diets, whereas *Myh4* and *Olfr954* were not detected in the islet transcript (Figure 54).

Nonetheless, since these results are only based on the gene expression obtained during RNA-seq analysis performed with 4 mice per group, further validation by qPCR with increased number of samples is required.

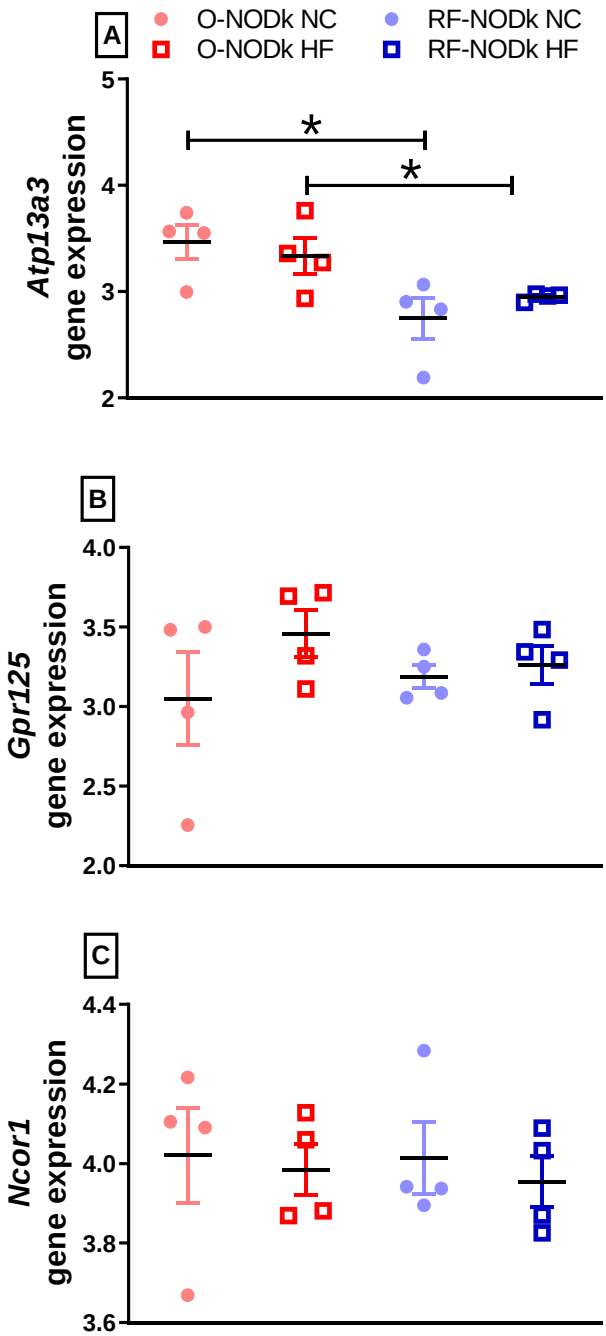

Figure 53: Expression of candidate genes obtained from the whole genome sequencing study in the RNA-seq sample data. While there was higher expression of *Atp13a3* in O-NOD^{k} mice on both NC and HF diet compared to respective RF-NOD^{k} mice counterparts, there was no difference in the expression of *Gpr125* and *Ncor1* among the mice groups. Data are means ± SEM for 4 mice per group. Two-way ANOVA with Bonferroni post-hoc test, *p<0.05.

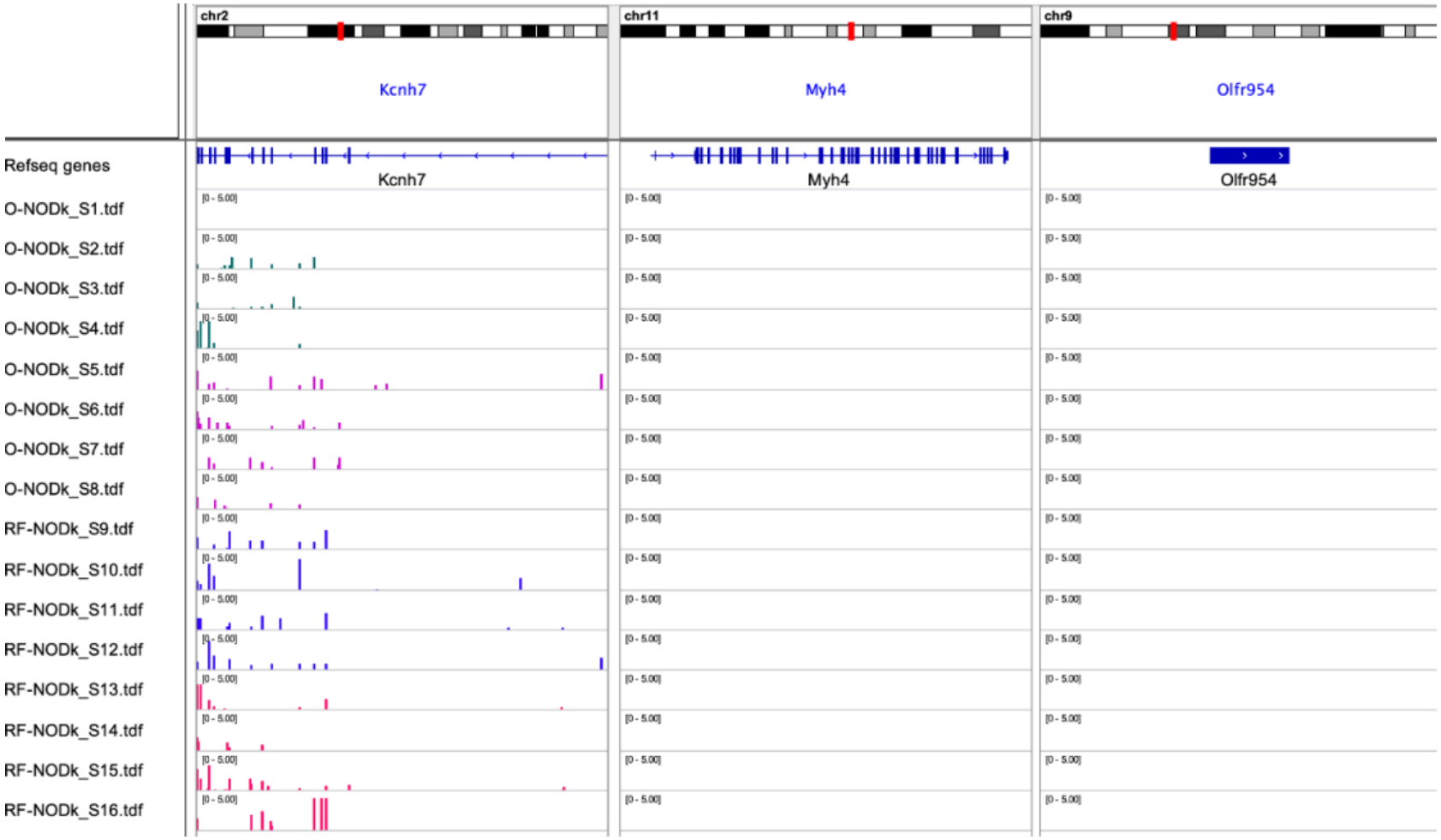

Figure 54: Visualization of the expression of candidate genes in the islet transcriptome of O-NOD^{k} and RF-NOD^{k} mice, fed on NC and HF diet on interactive genomics viewer (IGV). The expression of *Kcnh7* was variable between the two mice groups, while *Myh4* and *Olfr954* were not expressed in the islets of both mice sub-strains.

7.4 Discussion

In this chapter, the transcriptome of pancreatic islets from 2 different mice sub-strains, the O-NOD^{k} (diabetes-prone) and RF-NOD^{k} (diabetes-resistant) mice fed on NC and HF diet, was evaluated to provide additional information to the whole genome sequencing results described in chapter 6, in an attempt to identify SNPs involved in the development of T2D.

This strategy yielded libraries with over 23 million raw reads, of which only around 45% aligned concordantly exactly one time to the reference transcriptome. The low mapping percentage obtained was almost certainly due to difference between NOD and reference (C57BL/6J) genomes, in addition to the transcriptome of the NOD^{k} mice being a mix of two different mouse strains (NOD/MrkTacfBR (NOD) and B10.BR/SgSnJ), as well as the presence of pseudogenes and paralogous genes. Thus, only 10.35 million concordantly aligned reads obtained per sample were used for determination of differential expression of genes between the different mice groups, which is lower in numbers compared to similar studies performed by others (Fadista et al., 2014, Bonnycastle et al., 2019). The rest of the unmapped reads was set aside to undergo *de novo* transcript assembly, for detection of overlaps between reads to obtain the full NOD^{k} specific mouse transcripts. However, *de novo* transcriptomics is a very computer-intensive and time-consuming technique, which unfortunately was not possible to be fully addressed during this study period. Therefore, this chapter limits its analysis to transcriptomes that perfectly aligned to the reference mouse. Thus, the workflow proposed in this chapter aimed to provide further support to the findings obtained from the WGS experiments (chapter 6), plus identification of altered genes and pathways associated with diabetes.

The first approach assessed transcriptome differences between O-NOD^{k} and RF- NOD^{k} mice independent of diet, whereas the 2nd and 3rd analysis investigated the dietary effects. Interestingly, all these 3 different analyses resulted in the identification of 4 differentially

expressed genes, including *Pcp4* (down-regulated), *Sdc2*, *Suclg2* and *Cbr3* (up-regulated) in the O-NOD^{k} mice.

Pcp4 also known as brain-specific polypeptide 19 (*Pep19*), encodes a calmodulin calcium binding protein, which has a protective role in the central nervous system against cellular degeneration and apoptosis. Reduced expression levels of this molecule in the brain have been associated with Alzheimer's disease, Huntington's disease, and alcoholism (Kanazawa et al., 2008, Harashima et al., 2011). *Pcp4* modulates the binding of Ca^{2+} to calmodulin (CaM), activating the Ca^{2+}/CaM-dependent kinase II (CaMKII) pathway which stimulates insulin secretion from β-cells (Norling et al., 1994, Wang and Putkey, 2016). Inhibition of this pathway reduces GSIS and Ca^{2+} influx into islet β-cells (Dadi et al., 2014). Furthermore, *Pcp4* has an anti-apoptotic role since it protects cortical neurons from Ca^{2+} overload, and also sensitizes HeLa cells ATP-dependent Ca^{2+} efflux, increasing the frequency of Ca^{2+} oscillations (Wang et al., 2013, Kanazawa et al., 2008). Some studies have even proposed *Pcp4* and Pcp4-like protein 1 (*Pcp4l1*), the closest related protein to *Pcp4*, as possible candidate genes with a possible protective role against T2D and β-cell failure (Kluth et al., 2015, Stancill et al., 2017).

Reduced *Pcp4* expression, as observed in the O-NOD^{k} mice, would seem to favour reduced rather than increased GSIS based on its known interactions with CaMKII. However, if it has anti-apoptotic effects, or like Pcp4-like protein 1, protects against β-cell failure, its lower expression in O-NOD^{k} mice may be involved in the propensity of this sub-strain to develop diabetes. Thus, when *Pcp4* is down-regulated as is seen in the O-NOD^{k} mouse islets, it is possible that this predisposes the β-cells to apoptosis under conditions of nutrient-induced cell stress.

Sdc2 is the gene that encodes for the protein syndecan 2, also known as cell surface-associated heparan sulfate proteoglycan 1 (HSPG1), a member of a transmembrane proteoglycan family

to which chondroitin sulfate or heparan sulfate chains are attached. In vertebrates, 4 different genes encode for syndecans and its corresponding proteins (SDC1, SDC2, SDC3 and SDC4) (Chakravarti and Adams, 2006). It is associated with cell adhesion, motility and signaling (Choi et al., 2009). Many studies have highlighted the involvement of heparan sulfate and *Sdc1* in islet β-cell survival and its importance as an early marker for diabetes nephropathy and T1D (Svennevig et al., 2006, Simeonovic et al., 2018, Ziolkowski et al., 2012). Reductions in SDC4 within endothelial cells and impaired angiogenesis have been shown in diabetic mice and human umbilical vein endothelial cells cultured in high glucose conditions (Li et al., 2016a). SDC2 has been associated with amyloid plaque formation in the brain in Alzheimer's disease (van Horssen et al., 2001). Since accumulation of islet amyloid has been reported in human T2D (Haataja et al., 2008), and *Iapp* expression was increased in the HF-fed O-NOD^{k} mice, it is possible that increased SCD2 could be interacting with IAPP to alter extracellular matrix protein accumulation to cause islet damage in these mice. Against this possibility, islet amyloid accumulation is a clinical feature found only in human T2D and rodent *Iapp* is non-amyloidogenic (Höppener et al., 2008). It is unclear, therefore, how increased *Sdc2* expression could be associated with the pathogenesis of diabetes in the O-NOD^{k} mice and this deserve further investigation.

The other significantly up-regulated gene in the O-NOD^{k} mice was *Suclg2*, which encodes the GTP-specific beta subunit of succinyl-CoA synthase, a mitochondrial enzyme involved in the reversible formation of succinyl-CoA and succinate in the Krebs cycle (Kacso et al., 2016). Succinyl-CoA formation generates the energy-rich nucleotide GTP, which is further used for ATP synthesis. Thus, increased expression of *Suclg2* could be indicative of increased succinyl-CoA synthase activity and be associated with elevated ATP synthesis and augmented insulin secretion at all times in the O-NOD^{k} mice. This could lead to increased demand for insulin synthesis causing ER stress and possible cell death, principally in conditions involving nutrient

excess. In fact, a genetic mapping study conducted in European and African-American populations have identified *Suclg2* as a neighbouring gene to a T2D susceptibility locus (Lau et al., 2017). Therefore, assessments of islet ATP production and succinyl-CoA synthase activity are essential to confirm the possible link of *Suclg2* to T2D.

Another gene linked to diabetes that was found up-regulated in the O-NOD^{k} mice is *Cbr3*, a NADPH-dependent cytosolic enzyme that has high sequence similarity with T1D gene-associated *Cbr1* (Bergholdt et al., 2005). Interestingly, *Cbr3* and *Cbr1* are adjoining genes that are believed to replace each other in particular biological functions (Bergholdt et al., 2007). Rashid *et al* have shown that knock down of *Cbr1* in pancreatic cell lines by siRNA causes lipid deposition, increases ROS production and cellular death, and reduces insulin secretion when the cells are stimulated with LXR/FXR agonist, therefore highlighting the importance of *Cbr1* in lipid detoxification (Rashid et al., 2010). Additionally, SNPs in *Cbr3* are associated with increased risk of T2D and insulin resistance, possibly due to enhanced adipogenesis and a consequent effect on insulin sensitivity (Chang et al., 2012). Furthermore, *Cbr3* expression was found to be regulated by nuclear factor-erythroid 2 related factor 2 (Nrf2) which is associated with the cellular response to oxidative stress (Rashid et al., 2010, Ebert et al., 2010). Thus, due to its similarity to *Cbr1*, interchangeable function and highest tissue expression in the pancreas, it is possible that *Cbr3* could be linked to T2D development (Miura et al., 2008).

When comparing differences in hallmark β-cell genes between the two mice sub-strains, *Foxo1* and *Neurog3* were found to be up-regulated in the O-NOD^{k} mice compared to the RF-NOD^{k} mice. Interestingly, transgenic mice over-expressing *Foxo1* develop the same features observed in the HF-fed O-NOD^{k} mice, including obesity, development of glucose intolerance, insulin resistance, loss of β-cell mass and diabetes (Kikuchi et al., 2012, Kim et al., 2012). Although overexpression of *Foxo1* is associated with reduced *Pdx-1* and *NeuroD1* expression, in our

mouse model, these genes were down-regulated only in the two HF-fed O-NOD^{k} mice with higher blood glucose levels. In these same mice, we also observed upregulation of genes associated with oxidative and ER stress, suggesting that the enhanced insulin processing demand imposed by HF-feeding could be causing cellular stress and consequent β-cell death in these mice. There was also reduced expression of several β-cell development and function genes in the two mildly hyperglycaemic HF-fed O-NOD^{k} mice (*MafA, Neurod1, Nkx6.1, Scgn, Slc2a2* and *Glp1r*) suggesting some dedifferentiation of β-cells in this mice. Although this proposition is supported by the observation of increased islet cell apoptosis in HF-fed O-NOD^{k} mice during the histological analyses (described in Chapter 3), further validation of stress and apoptosis-related genes, as well as β-cell development and function genes, in a larger sample size is required.

Lastly, of some interest is *Scgn* which was downregulated in the two 2 HF-fed O-NOD^{k} mice with higher glycaemia. *Scgn* encodes for secretagogin, a sensor calcium-binding protein. Its expression is modulated by insulin and glucose (Maj et al., 2012). It acts as a Ca^{2+} sensor and increases insulin secretion by interacting with the actin cytoskeleton in the plasma membrane and with synaptosome-associated protein 25 (SNAP-25), which is part of the soluble N-ethylmaleimide sensitive factor attachment protein receptor (SNARE) complex responsible for insulin exocytosis from the β-cells (Rogstam et al., 2007, Yang et al., 2016). Furthermore, it is also associated with β-cell differentiation since it inactivates the 26S proteasome thereby preventing *Pdx*-1 degradation (Malenczyk et al., 2018). Recently, reduced *Scgn* expression has been linked to increased ER-stress and apoptosis in the Min6 β-cell line (Wu et al., 2020). Due to the negative correlation of its expression in islets with T2D, it has been identified as a biomarker and therapeutic target for diabetes (Malenczyk et al., 2017).

It is also important to note that since the HF-fed O-NOD^{k} mice group was further stratified due to the increased glucose levels in 2 mice, pair-wise comparison between the HF-fed mice was conducted in 2 mice from the O-NOD^{k} group. Furthermore, the transcriptome of the two HF-fed O-NOD^{k} mice with lower blood glucose was also compared to the two HF-fed O-NOD^{k} mice with higher blood glucose levels. Although a large number of differentially expressed genes were identified, due to the small sample size of n=2, definite conclusions of transcriptomic alterations with statistical significance cannot be drawn from this analysis. Ideally, another islet RNA-seq study will be required to increase the number of samples obtained from mice with similar glycaemic levels to reinforce the observations made in this study. Increase the sample size for HF-fed O-NOD^{k} mice with higher blood glucose levels also would allow identification of transcripts associated with hyperglycaemia, which could then be excluded from the list of candidate genes. It may also be worthwhile to perform single cell RNA-seq by isolating β-cells to determine specific cells transcriptome profiles of the different endocrine islet cells (Segerstolpe et al., 2016, Dorrell et al., 2011).

In summary, transcriptome analysis of the islets of O-NOD^{k} and RF-NOD^{k} mice suggest that the O-NOD^{k} mice may have inherent up-regulation of genes associated with Ca^{2+}/CaMKII pathway, heparan sulfate chains, Krebs cycle and Ca^{2+} sensing in the β-cells, which could lead to increase ER stress and apoptosis, and consequently T2D. Additionally, the 2 HF-fed O-NOD^{k} mice with higher glucose levels also had reduced expression of some key islet β-cell development and function genes and increased expression of oxidative and ER stress-related genes and pro-inflammatory markers, which could either be causative of the higher glucose levels in these mice or be a consequence of it.

Chapter 8

Final Discussion and Conclusion

8.1 Final discussion

T2D is a chronic metabolic disorder characterized by persistent hyperglycaemia due to inadequate insulin secretion (β-cell dysfunction) and/or impaired insulin action (insulin resistance). Although β-cell dysfunction is recognized as an early feature of T2D, increasing evidence from genetic studies suggest that it is a pre-requisite and more likely a determinant of T2D than insulin resistance (Dupuis et al., 2010, Lyssenko et al., 2005). Whilst there are several proposed mechanisms involved in the development of impaired β-cell function such as gluco/lipo-toxicity, oxidative and ER stress and inflammation, the exact triggering factor(s) causing β-cell dysfunction and T2D is still unknown.

The T1D-resistant O-NOD^{k} mouse sub-strain (created from the T1D-prone NOD mice through replacement of the Idd1-H2^{g7} with Idd-H2^{k}) develops T2D when fed a HF diet, which makes this sub-strain an excellent mouse model to study non-immune susceptibility factors associated with the pathogenesis of both T1D and T2D. Through routine colony refreshment, our lab developed another sub-strain of NOD^{k} mice, the RF-NOD^{k} mice, which are resistant to HF diet-induced T2D. Since both O-NOD^{k} and RF-NOD^{k} mice colonies have been maintained in the same animal facility under similar environmental conditions, it is believed that T2D predisposition in the O-NOD^{k} mice is genetic in its origin. Therefore, these two NOD^{k} mice sub-strains, with different metabolic phenotypes provide a great opportunity to explore the genetic factors involved in T2D development and potentially uncover novel mutations in genes that have not yet been associated with T2D. Based on this, the aim of this thesis was to characterize the phenotype and genotype of these two mice sub-strains, in order to determine the genetic factor(s) responsible for the development of T2D in the HF-fed O-NOD^{k} mice.

A long-term study (from 4-24 weeks of age) was designed to monitor physiological changes in these two mice sub-strains in response to diet challenge (Chapter 3). This study revealed that

O-NOD^{k} mice have accelerated body weight gain on both NC and HF diets compared to RF-NOD^{k} mice. Prolonged HF-feeding also leads to the development of impaired glucose tolerance, which is accompanied by a complete lack of 1st phase insulin response, thus suggesting β-cell dysfunction. The great majority of HF-fed O-NOD^{k} mice develop progressive hyperglycaemia and ultimately diabetes. Most interestingly, the development of diabetes in the O-NOD^{k} mice is accompanied by markedly elevated levels of plasma insulin.

As reported in several mouse models of obesity-induced T2D, increased weight gain in response to HF diet could be mainly attributed to an increased storage of nutrients in fat depots possibly resulting from imbalance between food intake and energy expenditure (Della Vedova et al., 2016). Additionally, this excessive fat accumulation could be potentially leading to ectopic fat spill-over in other tissues such as liver, skeletal muscle and pancreas, and be associated with development of insulin resistance and β-cell dysfunction (Almandoz et al., 2013). Unfortunately, due to a lack of equipment in our institution, body mass composition (lean and fat mass), food intake and energy expenditure were not assessed in this study. However, fat depots weights (SAT and VAT), as well as plasma TG and FFA, revealed that both mice sub-strains had similar responses to HF diet and presented positive energy storage. Of note, an increase in relative liver weight and augmented hepatic TG deposition was observed in the HF-fed O-NOD^{k} mice only, corroborating the presence of ectopic lipid deposition and possible hepatic insulin resistance.

The development of global insulin resistance in the HF-fed O-NOD^{k} mice was confirmed based on the increased HOMA-IR, which is a highly used index for determination of insulin resistance in human studies. As HOMA-IR has not been completely validated for use in mice, proper investigation of *in vivo* insulin sensitivity through the use of the gold standard hyperinsulinaemic-euglycaemic clamps, will be required.

Strikingly, O-NOD^k mice developed marked hyperinsulinaemia compared to RF-NOD^k mice in response to NC or HF diets, which was observed in both fasting and fed states and during ipGTT. Islet β-cell function assessed *in vitro* by static insulin secretion assays showed that O-NOD^k mice challenged by chronic HF-feeding secrete more insulin than RF-NOD^k mice when stimulated by glucose and fatty acids. Similar observations were also made when islets were stimulated by glucose and the insulin secretagogue IBMX, therefore indicating that the O-NOD^k mice may have an inherent predisposition to insulin hypersecretion. This observation was further supported by the higher plasma proinsulin and c-peptide levels observed in the HF-fed O-NOD^k mice compared to the HF-fed RF-NOD^k mice.

Since HF-fed O-NOD^k mice were observed to have higher insulin processing than the HF-fed RF-NOD^k mice, but similar delayed insulin clearance, it is plausible to believe that the increased insulin response of the O-NOD^k mice could be driving their predisposition to diabetes. Interestingly, while the *in vitro* study confirms an increased insulin responsiveness of the β-cells of HF-fed O-NOD^k mice to nutrient excess, this effect was not observed during the ipGTT. This suggests that there may be other factors outside the β-cell that may be inhibiting *in vivo* glucose-stimulated insulin secretion.

As described by others, exposure to HF diet resulted in increased β-cell mass in HF-fed RF-NOD^k mice, whereas no changes were observed in the HF-fed O-NOD^k mice. However, after stratification based on glycaemic levels showed that non-diabetic mice had increased β-cell mass, whereas HF-fed O-NOD^k mice with T2D (non-fasting glucose ≥ 12 mM) had reduced β-cell mass. Evidence of apoptosis was also observed in the islets of HF-fed O-NOD^k mice, suggesting the presence of T2D-associated β-cell death, as reported in literature (Butler et al., 2003, Federici et al., 2001). However, this needs to be verified with further dual immunohistochemistry for insulin and activated caspase-3.

In parallel to phenotypic characterization, we also conducted genotypic characterization of both O-NOD^k and RF-NOD^k mice. Selective breeding studies revealed that the allele(s) responsible for diabetes susceptibility in the O-NOD^k mice follow Mendelian laws of inheritance and it is possibly caused by an allele that is homozygous recessive.

This information was subsequently used as a selection criterion for whole genome sequencing analysis. After alignment of DNA libraries to a reference mouse genome, SNPs, insertions, and deletions present in the O-NOD^k mice but absent in the RF-NOD^k mice were selected. Using various filters such as SIFT score, homozygosity, novel/ rare SNPs and non-synonymous change, 6 candidate genes with SNPs in the O-NOD^k mice were obtained, of which *Atp13a3, Kcnh7, Gpr125,* and *Ncor1* were predicted to be the strongest candidates. Although the function of *Atp13a3* is not well-characterized compared to the rest of the ATPase family, it is assumed to play a role as a transmembrane cation transporter (Axelsen and Palmgren, 1998). However, due to its expression in the pancreas and its unknown substrate specificity, it could potentially function as a modulator of insulin secretion in the β-cells in a similar manner as the other ATPase channels (ATP-sensitive K^+ and voltage-dependent Ca^{2+} channel). Additionally, the second candidate gene *Kcnh7* is a part of the voltage-gated K^+ channel, which has high sequence similarity and transcript expression to *Kcnh6* (Mühlbauer et al., 2007). *Kcnh6* is associated with regulation of intracellular Ca^{2+} and GSIS, as well as loss of β-cell mass and ER stress in the islets (Yang et al., 2018). Therefore, *Kcnh7* may also have a prospective role in modulation of insulin secretion in the β-cells.

The 3rd candidate gene *Gpr125* is also incompletely characterized and proposed to function as a cell surface receptor for transmembrane receptor signaling. Interestingly, reduced *Gpr125* expression was associated with increased HbA_1c levels in patients with T2D post 2 years follow up (Slieker et al., 2018). This proffers a yet undetermined link of this gene to the pathogenesis of T2D. Finally, the co-transcriptional regulator *Ncor1* gene has been associated with insulin

signaling and T2D through regulation of various signaling pathways (Furuya et al., 2007, Astapova et al., 2014, Ou-Yang et al., 2018). Targeted knockout of *Ncor1* in the liver, adipose tissue and skeletal muscles establish its role in the development of peripheral tissue insulin resistance and T2D (Li et al., 2011, Yamamoto et al., 2011, Saito et al., 2019). Although there is no current research describing its function in the β-cells, there is still likelihood of its relation to the pathogenesis of T2D.

Apart from the SNPs detected in these candidate genes, over 1200 homozygous insertions and deletions were also observed in the O-NOD^{k} mice. Gene insertions were enriched in pathway gene sets associated with pancreatic exocrine function and insulin secretion, while genes with deletions did not show known links to T2D pathogenesis. It is highly possible that the genetic factor(s) associated with diabetes could be one of these structural variants, particularly among the homozygous insertions. However, the bioinformatics analyses of these insertions and deletions are outside the scope of this study and will be further investigated in future studies.

Furthermore, there is also a possibility that the HF diet could be aggravating T2D in the O-NOD^{k} mice due to epigenetic modifications such as DNA methylation or histone acetylation/deacetylation. Recent studies have shown that epigenetic modulations dysregulating signalling pathways are associated with T2D pathogenesis and related complications (Khullar et al., 2017, Xu et al., 2017, Li et al., 2016b). Thus, such modifications could result in gene expression alterations, mostly modulated through the action of transcriptional corepressors and coactivators (Mottis et al., 2013). Of interest, the corepressor *Ncor1*, which is required for the activity of histone deacetylase 3 (HDAC3) (You et al., 2013) was one of the candidate genes identified during the whole genome sequencing study in Chapter 6. One strategy to remove any effects of HF diet on the epigenome and analyse the effects of only the genetic factors, would be to perform the WGS in chow-fed mice from both O-NOD^{k} and RF-NOD^{k} colonies. Comparison of their genome sequences may be able to determine

inherent genetic mutations or polymorphisms that could be contributing to the HF diet induced T2D observed in the O-NOD^{k} mice, without the confounding effects of epigenetic modifications. However, since the genetic alteration is not fully penetrant as observed in the long term study in Chapter 3, it would be difficult to identify which mice would develop hyperglycaemia when stressed with HF diet, if they were only studied in normal chow diet conditions

Finally, RNA sequencing analysis of the O-NOD^{k} and RF-NOD^{k} mice for transcriptomic profiling revealed high genome similarity between the two mice sub-strains, and consequently a reduced number of differentially expressed genes were identified in pair-wise comparisons. Despite this issue, 4 differentially expressed genes were identified in this study, including *Pcp4, Sdc2, Suclg2 and Cbr3*. Through intense literature review, *Pcp4* and *Suclg2* gene were selected as strong candidate genes that could be playing a role in the β-cell insulin hyper-responsiveness observed in the O-NOD^{k} mice. As mentioned in chapter 7, *Suclg2* encodes the GTP-specific beta subunit of succinyl-CoA synthase, a mitochondrial enzyme involved in the reversible conversion of succinyl-CoA and succinate in the Krebs cycle. If confirmed that O-NOD^{k} mice have augmented succinyl-CoA synthase activity, this would lead to increased production of GTP and subsequently ATP. Increased ATP/ADP ratio would promote closure of K_{ATP}-dependent channels and opening of the voltage dependent calcium channels leading to increased influx of intracellular Ca^{2+}, resulting in increased insulin secretion. However, if O-NOD^{k} mice also have reduced levels of Pcp4, a calmodulin-calcium binding molecule with protective function against high Ca^{2+} levels, this would result in over-activation of the Ca^{2+}-calmodulin pathway and consequent augmented insulin release. Such alterations would not be a problem when the O-NOD^{k} mice is fed NC diet, however, when on HF diet it would lead to further requirement for insulin processing, therefore imposing a greater level of stress to the ER, resulting in β-cell apoptosis if not resolved by the UPR-response. This hypothesis is further

supported by high expression of genes related to oxidative and ER-stress observed in the HF-fed O-NOD^{k} mice, but it needs to be considered with caution, as further experiments (another RNA-seq and further validation by qPCR) with increased sample size is required. Additionally, the role of the other genes need further investigation.

8.2 Limitations of the study

Increased weight gain was observed with HF-feeding in the O-NOD^{k} mice compared to the HF-fed RF-NOD^{k} mice. This could be attributed to an imbalance in the energy flux (energy intake and expenditure) in these mice. Thus, differences in food intake, physical activity and energy expenditure between the two mice sub-strain could be contributing to weight gain, as described in other studies (Bachmanov et al., 2002). Attempts were made to assess food intake by measuring food consumption in normal ventilated cages over a 72 hour period, every fortnight. Unfortunately, food consumption could not be measured accurately since the HF diet pellets have a soft consistency and were prone to crumbling.

Finally, the RNA-seq study was performed in 4 groups of mice (n=4 mice/ group), in both O-NOD^{k} and RF-NOD^{k} mice fed on NC and HF diet. The selection of the samples for this study was completely unbiased and not based on blood glucose levels since all mice were not diabetic at the harvesting time. Unexpectedly, the results obtained from this analysis clearly showed different clustering in two HF-fed O-NOD^{k} mice which also presented different transcriptomic profiles compared to the rest of the group. These results were assumed to be resulting from their slightly higher blood glucose levels compared to the other samples in this group. The altered transcriptomic profile were consistent with these two mice having altered lipid metabolism, increased oxidative and ER stress and some β-cell dedifferentiation. This inter-group disparity in the transcriptomic profile suggests that there may be a sub-group within the O-NOD^{k} mice group, in which the genes are expressed differentially, leading to faster and more severe susceptibility to T2D. This was also observed in the long-term study (described in chapter 3), where 5 out of 12 HF-fed O-NOD^{k} mice had to be culled prior to the end of the experimental period due to development of overt diabetes (BGL > 20mM).

Another rationale for the differential hierarchical clustering of the two HF-fed O-NOD^{k} mice could be a consequence of the higher circulating blood glucose levels in these mice since glucose can affect the expression of multiple genes involved in insulin secretion (Schuit et al., 2002). Therefore, sample stratification based on blood glucose levels was performed to avoid the confounding effects of higher glycaemia on gene expression profile, which caused a reduction in the sample numbers available for analysis (2 normoglycaemic HF-fed O-NOD^{k} mice to the 4 HF-fed RF-NOD^{k} mice). This reduced the statistical power and the strength of the results.

However, this could also potentially allow identification of alterations in the transcriptome associated with hyperglycaemia. The results obtained in the RNA-seq analysis revealed particularly interesting results that a small increase in blood glucose levels in the two HF-fed O-NOD^{k} mice led to a significant change in the transcriptomic landscape of the islets. Similar to our observations, various studies have observed that even a mild elevation in glucose levels can change the expression of genes and transcription factors associated with β-cell function and identity, including *Pdx1*, *Nkx6-1*, *Foxo1*, insulin gene enhancer protein (*Isl*), *Pax6* and regulatory factor X6 (*Rfx6*) (Ebrahimi et al., 2020, Ottosson-Laakso et al., 2017). Therefore, this mouse model could be used to identify genes that are altered during prediabetes, which could then be targeted to delay the development of diabetes.

In order to avoid the effects of hyperglycaemia on the transcriptomic landscape of the mice, RNA-seq could be performed at an earlier age. This would also allow us to observe differences in gene expression that occurs independent of the environment, which are not associated with a comorbidity under normal conditions, but could potentially lead to a comorbidity when β-cell compensation is required under stressed conditions (such as HF diet). However, there is also the possibility that at an earlier age, HF diet may not have stressed the islets for long enough to cause any alterations in gene expression. Therefore, the transcriptome of the HF-fed and NC-

fed mice may be similar at that early point. Additionally, the required qPCR validation of results have not yet been performed, which limits the complete interpretation of the results. Therefore, qPCR experiments with increased number of samples are required to increase the strength of the RNA-seq data. Another limitation in the RNA-seq analyses is the low level of alignment concordance (~45%) to the C57BL/6J library. Further analysis using a more complex *de novo* analysis pipeline is required which is beyond the scope of this thesis.

Finally, a recurrent limitation of this study was the low sample size of the experimental mice. Power calculations for the long term study (Chapter 3), *in vitro* GSIS study (Chapter 4) and the selective breeding study (Chapter 5) mice numbers used showed that the studies had achieved 90% power with a statistical significance of $p<0.05$. However, for the whole genome sequencing study (Chapter 6), at least a sample size of 6 mice per group would have significantly improved the accuracy and reliability of the study. Similarly, for the RNA-seq study, islets were isolated from 8 mice per group. However, due to financial constraints, only 4 mice per group were analysed for RNA-seq. Sequencing the transcriptome of all 8 mice in each experimental group would have increased the power of the differentially expressed genes obtained from this study and would have allowed improved comparison of the transcriptome of the HF-fed and chow-fed mice. Alternative strategies to increase the power of the genetic findings (i.e. WGS and RNA-seq) would include performing Sanger sequencing and later qPCR validation in more samples to strengthen the observations

8.3 Conclusion

In conclusion, when challenged by HF diet, O-NOD^{k} mice develop obesity, T2D and hyperinsulinaemia. These mice are more susceptible to increased insulin production and secretion compared to the RF-NOD^{k} mice. Defective insulin clearance may also be contributing to the high circulating insulin levels in the HF-fed O-NOD^{k} mice, although it is unlikely to be the cause of the diabetes phenotype. *In vitro*, islets of the HF-fed O-NOD^{k} mice are very insulin responsive to fuel (glucose and fatty acids) and non-fuel (IBMX) stimuli, whereas *in vivo* insulin secretion does not seem to be modulated by glucose as late ipGTT shows a lack of 1st phase insulin secretion. Therefore, the O-NOD^{k} mice may be predisposed to increased β-cell function, which is further augmented with chronic HF-feeding. This could be leading to the development of β-cell dysfunction and loss of β-cell mass, ultimately causing cell death.

The whole genome and RNA-seq studies show alterations in the gene sequence and transcription of certain genes that are associated with calcium binding and signaling. Thus, the postulated homozygous recessive genetic factor(s) causing diabetes susceptibility in the O-NOD^{k} mice may be associated with high calcium ion influx and increased signaling across the plasma membranes of the β-cells, leading to insulin hypersecretion. Furthermore, since T2D is a polygenic disorder, mutations in more than one gene could be responsible for diabetes susceptibility in the O-NOD^{k} mice. Nonetheless, further analysis of the sequencing data and confirmation of gene expression of candidate genes would provide strength and more insights into the mechanisms by which O-NOD^{k} mice are predisposed to developing diabetes when subjected to HF diet.

8.4 Future directions

Although extensive phenotypic and genotypic characterization of O-NOD^{k} and RF-NOD^{k} mice has been conducted in this thesis, further experiments are still required for validation of observations made in this study.

During the histological analysis of the pancreas sections of both O-NOD^{k} and RF-NOD^{k} mice, evidence of islet cell apoptosis was observed in some islets of HF-fed O-NOD^{k} mice. However, since the tissue was not double stained for insulin and activated caspase-3, it is impossible to ascertain that HF-feeding is leading to β-cell death in the O-NOD^{k} mice. Therefore, quantitative assessment of islet β-cell apoptosis needs to be conducted in pancreatic sections through dual immunohistochemistry for insulin and activated caspase-3 for precise assessment of β-cell apoptosis.

Analysis of the whole genome of the O-NOD^{k} and RF-NOD^{k} mice generated 4 strong candidate genes *Atp13a3, Gpr125, Kcnh7* and *Ncor1* with SNPs leading to a deleterious phenotype following an amino acid change. Since the whole genome sequencing study was only conducted on 2 mice per group, Sanger sequencing will be required for confirmation of SNPs in these candidate genes in more mice. Additionally, it will also be particularly interesting to evaluate if any of these SNPs are present in the single anomalous diabetic HF-fed RF-NOD^{k} mouse identified in the long-term phenotyping study described in Chapter 3. Further analysis and validation of the insertions, deletions and gene translocations identified during WGS will also be required to generate another list of more candidate genes that could be associated with the diabetes phenotype in the HF-fed O-NOD^{k} mice.

RNA-seq analysis showed differential expression of genes such as *Sdc2, Sucgl2, Cbr3* and *Pcp4* in the O-NOD^{k} mice compared to the RF-NOD^{k} mice. This needs to be further validated in more mice (n=8 mice per group) through qPCR to increase the strength of the data. As

previously mentioned, only an average of 45% of all RNA-Seq reads mapped concordantly to the reference genome. Therefore, the unmapped reads will need to be manually overlapped through *de novo* transcript assembly using Trinity software. This will provide a more complete transcriptomic profile of the O-NOD^{k} and RF-NOD^{k} mice, which will be useful for additional identification of DEGs and enriched pathways that could be involved in the predisposition of T2D.

Further analysis and validation of the whole genome sequencing and RNA-seq data allow determination of the genetic factor(s) associated with the development of diabetes in the HF-fed O-NOD^{k} mice. The role of this selected genetic mutation in the pathogenesis of diabetes will be further examined by creating a CRISPR/Cas9 mouse model with the same genetic mutation in the RF-NOD^{k} mice. Development of diabetes in the CRISPR/Cas9 RF-NOD^{k} mice will confirm this mutation as the primary cause of diabetes in the O-NOD^{k} mice. The generated mouse model will also allow further investigation of the mechanisms involved in T2D pathogenesis, particularly if it is a novel mutation in a gene not yet associated with diabetes.

Identification of the genetic factor(s) causing the diabetes phenotype in the HF-fed O-NOD^{k} mice may not only be relevant to the pathogenesis of human T2D, but could also be related to non-immune islet β-cell susceptibility factors in T1D. This would allow novel therapeutic targets to preserve and protect functional islet β-cells, and consequently prevent or treat T2D. Furthermore, it could also unlock novel preventative and therapeutic strategies for T2D.

In this study, the hyper-responsiveness of NOD^{k} islet β-cells to metabolic excess make them vulnerable to β-cell injury. Similarly to the O-NOD^{k} mouse model, Indigenous and Torres Strait Islander people in Australia also have higher rates of obesity, extreme insulin resistance and have higher circulating insulin levels from very early on, with increased prevalence of T2D in youth (Valery et al., 2009, Titmuss et al., 2019, Burrow and Ride, 2016). Hospitalization and

mortality rates associated with T2D are also quite high in this population group compared to non-indigenous Australians (Australian Institute of Health and Welfare, 2015). Therefore, by studying the mechanisms of diabetes development in the O-NOD^{k} mice and the associated genetic factors, we could potently find candidate genes that could be predisposing these individuals to T2D. This would allow the development of targeted gene therapy for treatment of diabetes and its comorbidities, and even delay disease progression if identified earlier.

References

ADEYEMO, A. A., ZAGHLOUL, N. A., CHEN, G., DOUMATEY, A. P., LEITCH, C. C., HOSTELLEY, T. L., NESMITH, J. E., ZHOU, J., BENTLEY, A. R., SHRINER, D., FASANMADE, O., OKAFOR, G., EGHAN, B., JR., AGYENIM-BOATENG, K., CHANDRASEKHARAPPA, S., ADELEYE, J., BALOGUN, W., OWUSU, S., AMOAH, A., ACHEAMPONG, J., JOHNSON, T., OLI, J., ADEBAMOWO, C., COLLINS, F., DUNSTON, G. & ROTIMI, C. N. 2019. ZRANB3 is an African-specific type 2 diabetes locus associated with beta-cell mass and insulin response. *Nat Commun,* 10**,** 3195.

ADIELS, M., OLOFSSON, S. O., TASKINEN, M. R. & BOREN, J. 2008. Overproduction of very low-density lipoproteins is the hallmark of the dyslipidemia in the metabolic syndrome. *Arterioscler Thromb Vasc Biol,* 28**,** 1225-36.

AHLKVIST, L., BROWN, K. & AHREN, B. 2013. Upregulated insulin secretion in insulin-resistant mice: evidence of increased islet GLP1 receptor levels and GPR119-activated GLP1 secretion. *Endocr Connect,* 2**,** 69-78.

AHLOULAY, M., SCHMITT, F., DECHAUX, M. & BANKIR, L. 1999. Vasopressin and urinary concentrating activity in diabetes mellitus. *Diabetes Metab,* 25**,** 213-22.

ALARCON, C., BOLAND, B. B., UCHIZONO, Y., MOORE, P. C., PETERSON, B., RAJAN, S., RHODES, O. S., NOSKE, A. B., HAATAJA, L., ARVAN, P., MARSH, B. J., AUSTIN, J. & RHODES, C. J. 2016. Pancreatic β-Cell Adaptive Plasticity in Obesity Increases Insulin Production but Adversely Affects Secretory Function. *Diabetes,* 65**,** 438-50.

ALARCÓN, C., LEAHY, J. L., SCHUPPIN, G. T. & RHODES, C. J. 1995. Increased secretory demand rather than a defect in the proinsulin conversion mechanism causes hyperproinsulinemia in a glucose-infusion rat model of non-insulin-dependent diabetes mellitus. *J Clin Invest,* 95**,** 1032-9.

ALMANDOZ, J. P., SINGH, E., HOWELL, L. A., GROTHE, K., VLAZNY, D. T., SMAILOVIC, A., IRVING, B. A., NELSON, R. H. & MILES, J. M. 2013. Spillover of Fatty acids during dietary fat storage in type 2 diabetes: relationship to body fat depots and effects of weight loss. *Diabetes,* 62**,** 1897-1903.

ALONSO, N., JULIAN, M. T., CARRASCAL, J., COLOBRAN, R., PUJOL-AUTONELL, I., RODRIGUEZ-FERNANDEZ, S., TENIENTE, A., FERNANDEZ, M. A., MINARRO, A., RUIZ DE VILLA, M. C., VIVES-PI, M. & PUIG-DOMINGO, M. 2015. Type 1 Diabetes Prevention in NOD Mice by Targeting DPPIV/CD26 Is Associated with Changes in CD8(+)T Effector Memory Subset. *PLoS One,* 10**,** e0142186.

ALQUIER, T., PEYOT, M. L., LATOUR, M. G., KEBEDE, M., SORENSEN, C. M., GESTA, S., RONALD KAHN, C., SMITH, R. D., JETTON, T. L., METZ, T. O., PRENTKI, M. & POITOUT, V. 2009. Deletion of GPR40 impairs glucose-induced insulin secretion in vivo in mice without affecting intracellular fuel metabolism in islets. *Diabetes,* 58**,** 2607-15.

ALTSHULER, D., HIRSCHHORN, J. N., KLANNEMARK, M., LINDGREN, C. M., VOHL, M. C., NEMESH, J., LANE, C. R., SCHAFFNER, S. F., BOLK, S., BREWER, C., TUOMI, T., GAUDET, D., HUDSON, T. J., DALY, M., GROOP, L. & LANDER, E. S. 2000. The common PPARgamma Pro12Ala polymorphism is associated with decreased risk of type 2 diabetes. *Nat Genet,* 26**,** 76-80.

AMERICAN DIABETES, A. 2011. Diagnosis and classification of diabetes mellitus. *Diabetes care,* 34 Suppl 1**,** S62-S69.

ANDERSON, C. A., PETTERSSON, F. H., BARRETT, J. C., ZHUANG, J. J., RAGOUSSIS, J., CARDON, L. R. & MORRIS, A. P. 2008. Evaluating the effects of imputation on the power, coverage, and cost efficiency of genome-wide SNP platforms. *American journal of human genetics,* 83**,** 112-119.

ANDREWS, T. D., WHITTLE, B., FIELD, M. A., BALAKISHNAN, B., ZHANG, Y., SHAO, Y., CHO, V., KIRK, M., SINGH, M., XIA, Y., HAGER, J., WINSLADE, S., SJOLLEMA, G., BEUTLER, B., ENDERS, A. & GOODNOW, C. C. 2012. Massively parallel sequencing of

the mouse exome to accurately identify rare, induced mutations: an immediate source for thousands of new mouse models. *Open biology,* 2**,** 120061-120061.
ARAFAT, H. A., KATAKAM, A. K., CHIPITSYNA, G., GONG, Q., VANCHA, A. R., GABBETA, J. & DAFOE, D. C. 2007. Osteopontin protects the islets and beta-cells from interleukin-1 beta-mediated cytotoxicity through negative feedback regulation of nitric oxide. *Endocrinology,* 148**,** 575-84.
ARIF, S., TREE, T. I., ASTILL, T. P., TREMBLE, J. M., BISHOP, A. J., DAYAN, C. M., ROEP, B. O. & PEAKMAN, M. 2004. Autoreactive T cell responses show proinflammatory polarization in diabetes but a regulatory phenotype in health. *J Clin Invest,* 113**,** 451-63.
ASAKAWA, A., INUI, A., KAGA, T., KATSUURA, G., FUJIMIYA, M., FUJINO, M. A. & KASUGA, M. 2003a. Antagonism of ghrelin receptor reduces food intake and body weight gain in mice. *Gut,* 52**,** 947-52.
ASAKAWA, A., INUI, A., YUZURIHA, H., UENO, N., KATSUURA, G., FUJIMIYA, M., FUJINO, M. A., NIIJIMA, A., MEGUID, M. M. & KASUGA, M. 2003b. Characterization of the effects of pancreatic polypeptide in the regulation of energy balance. *Gastroenterology,* 124**,** 1325-36.
ASHCROFT, F. M., HARRISON, D. E. & ASHCROFT, S. J. 1984. Glucose induces closure of single potassium channels in isolated rat pancreatic beta-cells. *Nature,* 312**,** 446-8.
ASHCROFT, F. M. & RORSMAN, P. 1989. Electrophysiology of the pancreatic beta-cell. *Prog Biophys Mol Biol,* 54**,** 87-143.
ASTAPOVA, I., RAMADOSS, P., COSTA-E-SOUSA, R. H., YE, F., HOLTZ, K. A., LI, Y., NIEPEL, M. W., COHEN, D. E. & HOLLENBERG, A. N. 2014. Hepatic nuclear corepressor 1 regulates cholesterol absorption through a TRβ1-governed pathway. *J Clin Invest,* 124**,** 1976-86.
ATKINSON, M. A., EISENBARTH, G. S. & MICHELS, A. W. 2014. Type 1 diabetes. *Lancet (London, England),* 383**,** 69-82.
ATLANTIS, E., MARTIN, S. A., HAREN, M. T., TAYLOR, A. W. & WITTERT, G. A. 2009. Inverse associations between muscle mass, strength, and the metabolic syndrome. *Metabolism,* 58**,** 1013-22.
ATTANÉ, C., PEYOT, M.-L., LUSSIER, R., ZHANG, D., JOLY, E., MADIRAJU, S. R. M. & PRENTKI, M. 2016. Differential Insulin Secretion of High-Fat Diet-Fed C57BL/6NN and C57BL/6NJ Mice: Implications of Mixed Genetic Background in Metabolic Studies. *PloS one,* 11**,** e0159165-e0159165.
ATTIE, A. D., CHURCHILL, G. A. & NADEAU, J. H. 2017. How mice are indispensable for understanding obesity and diabetes genetics. *Curr Opin Endocrinol Diabetes Obes,* 24**,** 83-91.
AUSTRALIAN INSTITUTE OF HEALTH AND WELFARE, A. 2015. The health and welfare of Australia's Aboriginal an Torres Strait Islander Peoples. *AIHW Canberra*.
AXELSEN, K. B. & PALMGREN, M. G. 1998. Evolution of substrate specificities in the P-type ATPase superfamily. *J Mol Evol,* 46**,** 84-101.
AZIZ, S., SHEIKH GHADZI, S. M., ABIDIN, N. E., TANGIISURAN, B., ZAINAL, H., LOOI, I., IBRAHIM, K. A., SIDEK, N. N., WEI, L. K., KENG YEE, L., ABDUL AZIZ, Z. & HARUN, S. N. 2019. Gender Differences and Risk Factors of Recurrent Stroke in Type 2 Diabetic Malaysian Population with History of Stroke: The Observation from Malaysian National Neurology Registry. *J Diabetes Res,* 2019**,** 1794267.
BACHAR, E., ARIAV, Y., KETZINEL-GILAD, M., CERASI, E., KAISER, N. & LEIBOWITZ, G. 2009. Glucose amplifies fatty acid-induced endoplasmic reticulum stress in pancreatic beta-cells via activation of mTORC1. *PLoS One,* 4**,** e4954.
BACHMANOV, A. A., REED, D. R., BEAUCHAMP, G. K. & TORDOFF, M. G. 2002. Food intake, water intake, and drinking spout side preference of 28 mouse strains. *Behavior genetics,* 32**,** 435-443.
BALENT, B., GOSWAMI, G., GOODLOE, G., ROGATSKY, E., RAUTA, O., NEZAMI, R., MINTS, L., ANGELETTI, R. H. & STEIN, D. T. 2002. Acute elevation of NEFA causes hyperinsulinemia without effect on insulin secretion rate in healthy human subjects. *Ann N Y Acad Sci,* 967**,** 535-43.

BANTING, F. G., BEST, C. H., COLLIP, J. B., CAMPBELL, W. R. & FLETCHER, A. A. 1922. Pancreatic Extracts in the Treatment of Diabetes Mellitus. *Can Med Assoc J,* 12**,** 141-6.
BARRIO, R., BELLANNÉ-CHANTELOT, C., MORENO, J. C., MOREL, V., CALLE, H., ALONSO, M. & MUSTIELES, C. 2002. Nine novel mutations in maturity-onset diabetes of the young (MODY) candidate genes in 22 Spanish families. *J Clin Endocrinol Metab,* 87**,** 2532-9.
BEDROOD, S., LI, Y., ISAS, J. M., HEGDE, B. G., BAXA, U., HAWORTH, I. S. & LANGEN, R. 2012. Fibril structure of human islet amyloid polypeptide. *J Biol Chem,* 287**,** 5235-41.
BEER, S. F., HEATON, D. A., ALBERTI, K. G., PYKE, D. A. & LESLIE, R. D. 1990. Impaired glucose tolerance precedes but does not predict insulin-dependent diabetes mellitus: a study of identical twins. *Diabetologia,* 33**,** 497-502.
BEIGREZAEI, S., GHIASVAND, R., FEIZI, A. & IRAJ, B. 2019. Relationship between Dietary Patterns and Incidence of Type 2 Diabetes. *International journal of preventive medicine,* 10**,** 122-122.
BELLOU, V., BELBASIS, L., TZOULAKI, I. & EVANGELOU, E. 2018. Risk factors for type 2 diabetes mellitus: An exposure-wide umbrella review of meta-analyses. *PLoS One,* 13**,** e0194127.
BENJAMIN, D., SATO, T., CIBULSKIS, K., GETZ, G., STEWART, C. & LICHTENSTEIN, L. 2019. Calling Somatic SNVs and Indels with Mutect2. *bioRxiv***,** 861054.
BENNER, C., VAN DER MEULEN, T., CACÉRES, E., TIGYI, K., DONALDSON, C. J. & HUISING, M. O. 2014. The transcriptional landscape of mouse beta cells compared to human beta cells reveals notable species differences in long non-coding RNA and protein-coding gene expression. *BMC Genomics,* 15**,** 620.
BERGHOLDT, R., KARLSEN, A. E., HAGEDORN, P. H., AALUND, M., NIELSEN, J. H., KRUHØFFER, M., ORNTOFT, T., WANG, H., WOLLHEIM, C. B., NERUP, J. & POCIOT, F. 2007. Transcriptional profiling of type 1 diabetes genes on chromosome 21 in a rat beta-cell line and human pancreatic islets. *Genes Immun,* 8**,** 232-8.
BERGHOLDT, R., NERUP, J. & POCIOT, F. 2005. Fine mapping of a region on chromosome 21q21.11-q22.3 showing linkage to type 1 diabetes. *J Med Genet,* 42**,** 17-25.
BETSHOLTZ, C., CHRISTMANSSON, L., ENGSTRÖM, U., RORSMAN, F., SVENSSON, V., JOHNSON, K. H. & WESTERMARK, P. 1989. Sequence divergence in a specific region of islet amyloid polypeptide (IAPP) explains differences in islet amyloid formation between species. *FEBS Lett,* 251**,** 261-4.
BHATNAGAR, A., MILBURN, P. J., LOBIGS, M., BLANDEN, R. V. & GAUTAM, A. M. 2001. Nonobese diabetic mice display elevated levels of class II-associated invariant chain peptide associated with I-Ag7 on the cell surface. *J Immunol,* 166**,** 4490-7.
BI, Y., WANG, J. L., LI, M. L., ZHOU, J. & SUN, X. L. 2019. The association between pancreas steatosis and metabolic syndrome: A systematic review and meta-analysis. *Diabetes Metab Res Rev,* 35**,** e3142.
BLACK, M. H., WATANABE, R. M., TRIGO, E., TAKAYANAGI, M., LAWRENCE, J. M., BUCHANAN, T. A. & XIANG, A. H. 2013. High-fat diet is associated with obesity-mediated insulin resistance and β-cell dysfunction in Mexican Americans. *J Nutr,* 143**,** 479-85.
BLAIR, D. R., LYTTLE, C. S., MORTENSEN, J. M., BEARDEN, C. F., JENSEN, A. B., KHIABANIAN, H., MELAMED, R., RABADAN, R., BERNSTAM, E. V., BRUNAK, S., JENSEN, L. J., NICOLAE, D., SHAH, N. H., GROSSMAN, R. L., COX, N. J., WHITE, K. P. & RZHETSKY, A. 2013. A nondegenerate code of deleterious variants in Mendelian loci contributes to complex disease risk. *Cell,* 155**,** 70-80.
BOCK, T., PAKKENBERG, B. & BUSCHARD, K. 2003. Increased islet volume but unchanged islet number in ob/ob mice. *Diabetes,* 52**,** 1716-22.
BOCK, T., PAKKENBERG, B. & BUSCHARD, K. 2005. Genetic Background Determines the Size and Structure of the Endocrine Pancreas. *Diabetes,* 54**,** 133-137.
BÖNI-SCHNETZLER, M., BOLLER, S., DEBRAY, S., BOUZAKRI, K., MEIER, D. T., PRAZAK, R., KERR-CONTE, J., PATTOU, F., EHSES, J. A., SCHUIT, F. C. & DONATH, M. Y. 2009. Free fatty acids induce a proinflammatory response in islets via the abundantly expressed interleukin-1 receptor I. *Endocrinology,* 150**,** 5218-29.

BÖNI-SCHNETZLER, M., THORNE, J., PARNAUD, G., MARSELLI, L., EHSES, J. A., KERR-CONTE, J., PATTOU, F., HALBAN, P. A., WEIR, G. C. & DONATH, M. Y. 2008. Increased interleukin (IL)-1beta messenger ribonucleic acid expression in beta -cells of individuals with type 2 diabetes and regulation of IL-1beta in human islets by glucose and autostimulation. *J Clin Endocrinol Metab,* 93**,** 4065-74.

BONNYCASTLE, L. L., GILDEA, D. E., YAN, T., NARISU, N., SWIFT, A. J., WOLFSBERG, T. G., ERDOS, M. R. & COLLINS, F. S. 2019. Single-cell transcriptomics from human pancreatic islets: sample preparation matters. *Biology Methods and Protocols,* 4.

BOSCO, D., ARMANET, M., MOREL, P., NICLAUSS, N., SGROI, A., MULLER, Y. D., GIOVANNONI, L., PARNAUD, G. & BERNEY, T. 2010. Unique arrangement of alpha- and beta-cells in human islets of Langerhans. *Diabetes,* 59**,** 1202-10.

BRIANT, L. J. B., REINBOTHE, T. M. & SPILIOTIS, I. 2018. delta-cells and beta-cells are electrically coupled and regulate alpha-cell activity via somatostatin. 596**,** 197-215.

BRIAUD, I., HARMON, J. S., KELPE, C. L., SEGU, V. B. & POITOUT, V. 2001. Lipotoxicity of the pancreatic beta-cell is associated with glucose-dependent esterification of fatty acids into neutral lipids. *Diabetes,* 50**,** 315-21.

BRISSOVA, M., FOWLER, M. J., NICHOLSON, W. E., CHU, A., HIRSHBERG, B., HARLAN, D. M. & POWERS, A. C. 2005. Assessment of human pancreatic islet architecture and composition by laser scanning confocal microscopy. *J Histochem Cytochem,* 53**,** 1087-97.

BRUN, T., ROCHE, E., ASSIMACOPOULOS-JEANNET, F., CORKEY, B. E., KIM, K. H. & PRENTKI, M. 1996. Evidence for an anaplerotic/malonyl-CoA pathway in pancreatic beta-cell nutrient signaling. *Diabetes,* 45**,** 190-8.

BRUNO, G., RUNZO, C., CAVALLO-PERIN, P., MERLETTI, F., RIVETTI, M., PINACH, S., NOVELLI, G., TROVATI, M., CERUTTI, F. & PAGANO, G. 2005. Incidence of type 1 and type 2 diabetes in adults aged 30-49 years: the population-based registry in the province of Turin, Italy. *Diabetes Care,* 28**,** 2613-9.

BUNN, H. F., HANEY, D. N., KAMIN, S., GABBAY, K. H. & GALLOP, P. M. 1976. The biosynthesis of human hemoglobin A1c. Slow glycosylation of hemoglobin in vivo. *J Clin Invest,* 57**,** 1652-9.

BURROW, S. & RIDE, K. 2016. Review of diabetes among Aboriginal and Torres Strait Islander people. *Australian Indigenous HealthInfoNet*.

BUTLER, A. E., JANSON, J., BONNER-WEIR, S., RITZEL, R., RIZZA, R. A. & BUTLER, P. C. 2003. Beta-cell deficit and increased beta-cell apoptosis in humans with type 2 diabetes. *Diabetes,* 52**,** 102-10.

CABRERA, O., BERMAN, D. M., KENYON, N. S., RICORDI, C., BERGGREN, P. O. & CAICEDO, A. 2006. The unique cytoarchitecture of human pancreatic islets has implications for islet cell function. *Proc Natl Acad Sci U S A,* 103**,** 2334-9.

CADENAS, E. & DAVIES, K. J. 2000. Mitochondrial free radical generation, oxidative stress, and aging. *Free Radic Biol Med,* 29**,** 222-30.

CADET, J., DAVIES, K. J. A., MEDEIROS, M. H., DI MASCIO, P. & WAGNER, J. R. 2017. Formation and repair of oxidatively generated damage in cellular DNA. *Free Radic Biol Med,* 107**,** 13-34.

CALFON, M., ZENG, H., URANO, F., TILL, J. H., HUBBARD, S. R., HARDING, H. P., CLARK, S. G. & RON, D. 2002. IRE1 couples endoplasmic reticulum load to secretory capacity by processing the XBP-1 mRNA. *Nature,* 415**,** 92-6.

CARRERO, J. A., CALDERON, B., TOWFIC, F., ARTYOMOV, M. N. & UNANUE, E. R. 2013. Defining the transcriptional and cellular landscape of type 1 diabetes in the NOD mouse. *PLoS One,* 8**,** e59701.

CATALANO, K. J., MADDUX, B. A., SZARY, J., YOUNGREN, J. F., GOLDFINE, I. D. & SCHAUFELE, F. 2014. Insulin resistance induced by hyperinsulinemia coincides with a persistent alteration at the insulin receptor tyrosine kinase domain. *PloS one,* 9**,** e108693-e108693.

CAUCHI, S., EZZIDI, I., EL ACHHAB, Y., MTIRAOUI, N., CHAIEB, L., SALAH, D., NEJJARI, C., LABRUNE, Y., YENGO, L., BEURY, D., VAXILLAIRE, M., MAHJOUB, T., CHIKRI,

M. & FROGUEL, P. 2012. European genetic variants associated with type 2 diabetes in North African Arabs. *Diabetes Metab,* 38**,** 316-23.
CEN, J., SARGSYAN, E. & BERGSTEN, P. 2016. Fatty acids stimulate insulin secretion from human pancreatic islets at fasting glucose concentrations via mitochondria-dependent and -independent mechanisms. *Nutrition & metabolism,* 13**,** 59-59.
CHAKRAVARTI, R. & ADAMS, J. C. 2006. Comparative genomics of the syndecans defines an ancestral genomic context associated with matrilins in vertebrates. *BMC Genomics,* 7**,** 83.
CHANG, Y. C., LIU, P. H., TSAI, Y. C., CHIU, Y. F., SHIH, S. R., HO, L. T., LEE, W. J., LU, C. H., QUERTERMOUS, T., CURB, J. D., LEE, W. J., LEE, P. C., HE, Y. H., YEH, J. I., HWANG, J. J., TSAI, S. H. & CHUANG, L. M. 2012. Genetic variation in the carbonyl reductase 3 gene confers risk of type 2 diabetes and insulin resistance: a potential regulator of adipogenesis. *J Mol Med (Berl),* 90**,** 847-58.
CHEN, X., SCHULZ-TRIEGLAFF, O., SHAW, R., BARNES, B., SCHLESINGER, F., KÄLLBERG, M., COX, A. J., KRUGLYAK, S. & SAUNDERS, C. T. 2016. Manta: rapid detection of structural variants and indels for germline and cancer sequencing applications. *Bioinformatics,* 32**,** 1220-2.
CHIU, C. C., SINGH, S. & DE PABLO, J. J. 2013. Effect of proline mutations on the monomer conformations of amylin. *Biophys J,* 105**,** 1227-35.
CHOI, S., KIM, Y., PARK, H., HAN, I. O., CHUNG, E., LEE, S. Y., KIM, Y. B., LEE, J. W., OH, E. S. & YI, J. Y. 2009. Syndecan-2 overexpression regulates adhesion and migration through cooperation with integrin alpha2. *Biochem Biophys Res Commun,* 384**,** 231-5.
CHRISTODOULOU, M.-I., AVGERIS, M., KOKKINOPOULOU, I., MARATOU, E., MITROU, P., KONTOS, C. K., PAPPAS, E., BOUTATI, E., SCORILAS, A. & FRAGOULIS, E. G. 2019. Blood-based analysis of type-2 diabetes mellitus susceptibility genes identifies specific transcript variants with deregulated expression and association with disease risk. *Scientific Reports,* 9**,** 1512.
CINTI, F., BOUCHI, R., KIM-MULLER, J. Y., OHMURA, Y., SANDOVAL, P. R., MASINI, M., MARSELLI, L., SULEIMAN, M., RATNER, L. E., MARCHETTI, P. & ACCILI, D. 2016. Evidence of beta-Cell Dedifferentiation in Human Type 2 Diabetes. *J Clin Endocrinol Metab,* 101**,** 1044-54.
CNOP, M., ABDULKARIM, B., BOTTU, G., CUNHA, D. A., IGOILLO-ESTEVE, M., MASINI, M., TURATSINZE, J. V., GRIEBEL, T., VILLATE, O., SANTIN, I., BUGLIANI, M., LADRIERE, L., MARSELLI, L., MCCARTHY, M. I., MARCHETTI, P., SAMMETH, M. & EIZIRIK, D. L. 2014. RNA sequencing identifies dysregulation of the human pancreatic islet transcriptome by the saturated fatty acid palmitate. *Diabetes,* 63**,** 1978-93.
CNOP, M., LADRIERE, L., HEKERMAN, P., ORTIS, F., CARDOZO, A. K., DOGUSAN, Z., FLAMEZ, D., BOYCE, M., YUAN, J. & EIZIRIK, D. L. 2007. Selective inhibition of eukaryotic translation initiation factor 2 alpha dephosphorylation potentiates fatty acid-induced endoplasmic reticulum stress and causes pancreatic beta-cell dysfunction and apoptosis. *J Biol Chem,* 282**,** 3989-97.
CONCANNON, P., CHEN, W. M., JULIER, C., MORAHAN, G., AKOLKAR, B., ERLICH, H. A., HILNER, J. E., NERUP, J., NIERRAS, C., POCIOT, F., TODD, J. A. & RICH, S. S. 2009. Genome-wide scan for linkage to type 1 diabetes in 2,496 multiplex families from the Type 1 Diabetes Genetics Consortium. *Diabetes,* 58**,** 1018-22.
CONCANNON, P., ERLICH, H. A., JULIER, C., MORAHAN, G., NERUP, J., POCIOT, F., TODD, J. A. & RICH, S. S. 2005. Type 1 diabetes: evidence for susceptibility loci from four genome-wide linkage scans in 1,435 multiplex families. *Diabetes,* 54**,** 2995-3001.
COOPER, G. J., WILLIS, A. C., CLARK, A., TURNER, R. C., SIM, R. B. & REID, K. B. 1987. Purification and characterization of a peptide from amyloid-rich pancreases of type 2 diabetic patients. *Proc Natl Acad Sci U S A,* 84**,** 8628-32.
CORKEY, B. E. 2012. Diabetes: Have We Got It All Wrong? *Insulin hypersecretion and food additives: cause of obesity and diabetes?,* 35**,** 2432-2437.
CRESCENZO, R., BIANCO, F., FALCONE, I., COPPOLA, P., LIVERINI, G. & IOSSA, S. 2013. Increased hepatic de novo lipogenesis and mitochondrial efficiency in a model of obesity induced by diets rich in fructose. *Eur J Nutr,* 52**,** 537-45.

CROPANO, C., SANTORO, N., GROOP, L., DALLA MAN, C., COBELLI, C., GALDERISI, A., KURSAWE, R., PIERPONT, B., GOFFREDO, M. & CAPRIO, S. 2017. The rs7903146 Variant in the TCF7L2 Gene Increases the Risk of Prediabetes/Type 2 Diabetes in Obese Adolescents by Impairing β-Cell Function and Hepatic Insulin Sensitivity. *Diabetes Care,* 40**,** 1082-1089.

CUCAK, H., GRUNNET, L. G. & ROSENDAHL, A. 2014. Accumulation of M1-like macrophages in type 2 diabetic islets is followed by a systemic shift in macrophage polarization. *J Leukoc Biol,* 95**,** 149-60.

CUNHA, D. A., HEKERMAN, P., LADRIERE, L., BAZARRA-CASTRO, A., ORTIS, F., WAKEHAM, M. C., MOORE, F., RASSCHAERT, J., CARDOZO, A. K., BELLOMO, E., OVERBERGH, L., MATHIEU, C., LUPI, R., HAI, T., HERCHUELZ, A., MARCHETTI, P., RUTTER, G. A., EIZIRIK, D. L. & CNOP, M. 2008. Initiation and execution of lipotoxic ER stress in pancreatic beta-cells. *J Cell Sci,* 121**,** 2308-18.

CURRY, D. L., BENNETT, L. L. & GRODSKY, G. M. 1968. Dynamics of insulin secretion by the perfused rat pancreas. *Endocrinology,* 83**,** 572-84.

DADI, P. K., VIERRA, N. C., USTIONE, A., PISTON, D. W., COLBRAN, R. J. & JACOBSON, D. A. 2014. Inhibition of pancreatic β-cell Ca2+/calmodulin-dependent protein kinase II reduces glucose-stimulated calcium influx and insulin secretion, impairing glucose tolerance. *The Journal of biological chemistry,* 289**,** 12435-12445.

DAIMON, M., JI, G., SAITOH, T., OIZUMI, T., TOMINAGA, M., NAKAMURA, T., ISHII, K., MATSUURA, T., INAGEDA, K., MATSUMINE, H., KIDO, T., HTAY, L., KAMATANI, N., MURAMATSU, M. & KATO, T. 2003. Large-scale search of SNPs for type 2 DM susceptibility genes in a Japanese population. *Biochem Biophys Res Commun,* 302**,** 751-8.

DE KONING, E. J., BODKIN, N. L., HANSEN, B. C. & CLARK, A. 1993. Diabetes mellitus in Macaca mulatta monkeys is characterised by islet amyloidosis and reduction in beta-cell population. *Diabetologia,* 36**,** 378-84.

DECHECCHI, M. C., TAMANINI, A. & CABRINI, G. 2018. Molecular basis of cystic fibrosis: from bench to bedside. *Annals of translational medicine,* 6**,** 334-334.

DEL GUERRA, S., LUPI, R., MARSELLI, L., MASINI, M., BUGLIANI, M., SBRANA, S., TORRI, S., POLLERA, M., BOGGI, U., MOSCA, F., DEL PRATO, S. & MARCHETTI, P. 2005. Functional and molecular defects of pancreatic islets in human type 2 diabetes. *Diabetes,* 54**,** 727-35.

DELLA VEDOVA, M. C., MUÑOZ, M. D., SANTILLAN, L. D., PLATEO-PIGNATARI, M. G., GERMANÓ, M. J., RINALDI TOSI, M. E., GARCIA, S., GOMEZ, N. N., FORNES, M. W., GOMEZ MEJIBA, S. E. & RAMIREZ, D. C. 2016. A Mouse Model of Diet-Induced Obesity Resembling Most Features of Human Metabolic Syndrome. *Nutrition and metabolic insights,* 9**,** 93-102.

DEMAY, Y., PEROCHON, J., SZUPLEWSKI, S., MIGNOTTE, B. & GAUMER, S. 2014. The PERK pathway independently triggers apoptosis and a Rac1/Slpr/JNK/Dilp8 signaling favoring tissue homeostasis in a chronic ER stress Drosophila model. *Cell Death & Disease,* 5**,** e1452-e1452.

DEMINE, S., SCHIAVO, A. A., MARIN-CANAS, S., MARCHETTI, P., CNOP, M. & EIZIRIK, D. L. 2020. Pro-inflammatory cytokines induce cell death, inflammatory responses, and endoplasmic reticulum stress in human iPSC-derived beta cells. *Stem Cell Res Ther,* 11**,** 7.

DENG, S., VATAMANIUK, M., HUANG, X., DOLIBA, N., LIAN, M. M., FRANK, A., VELIDEDEOGLU, E., DESAI, N. M., KOEBERLEIN, B., WOLF, B., BARKER, C. F., NAJI, A., MATSCHINSKY, F. M. & MARKMANN, J. F. 2004. Structural and functional abnormalities in the islets isolated from type 2 diabetic subjects. *Diabetes,* 53**,** 624-32.

DO, O. H., GUNTON, J. E., GAISANO, H. Y. & THORN, P. 2016. Changes in beta cell function occur in prediabetes and early disease in the Lepr (db) mouse model of diabetes. *Diabetologia,* 59**,** 1222-30.

DODSON, G. & STEINER, D. 1998. The role of assembly in insulin's biosynthesis. *Curr Opin Struct Biol,* 8**,** 189-94.

DOLENŠEK, J., RUPNIK, M. S. & STOŽER, A. 2015. Structural similarities and differences between the human and the mouse pancreas. *Islets,* 7**,** e1024405-e1024405.

DOOLEY, J., TIAN, L., SCHONEFELDT, S., DELGHINGARO-AUGUSTO, V., GARCIA-PEREZ, J. E., PASCIUTO, E., DI MARINO, D., CARR, E. J., OSKOLKOV, N., LYSSENKO, V., FRANCKAERT, D., LAGOU, V., OVERBERGH, L., VANDENBUSSCHE, J., ALLEMEERSCH, J., CHABOT-ROY, G., DAHLSTROM, J. E., LAYBUTT, D. R., PETROVSKY, N., SOCHA, L., GEVAERT, K., JETTEN, A. M., LAMBRECHTS, D., LINTERMAN, M. A., GOODNOW, C. C., NOLAN, C. J., LESAGE, S., SCHLENNER, S. M. & LISTON, A. 2016. Genetic predisposition for beta cell fragility underlies type 1 and type 2 diabetes. *Nat Genet,* 48**,** 519-27.

DORRELL, C., SCHUG, J., LIN, C. F., CANADAY, P. S., FOX, A. J., SMIRNOVA, O., BONNAH, R., STREETER, P. R., STOECKERT, C. J., JR., KAESTNER, K. H. & GROMPE, M. 2011. Transcriptomes of the major human pancreatic cell types. *Diabetologia,* 54**,** 2832-2844.

DOU, H., WANG, C., WU, X., YAO, L., ZHANG, X., TENG, S., XU, H., LIU, B., WU, Q., ZHANG, Q., HU, M., WANG, Y., WANG, L., WU, Y., SHANG, S., KANG, X., ZHENG, L., ZHANG, J., RAOUX, M., LANG, J., LI, Q., SU, J., YU, X., CHEN, L. & ZHOU, Z. 2015. Calcium influx activates adenylyl cyclase 8 for sustained insulin secretion in rat pancreatic beta cells. *Diabetologia,* 58**,** 324-33.

DRUCE, M. R., WREN, A. M., PARK, A. J., MILTON, J. E., PATTERSON, M., FROST, G., GHATEI, M. A., SMALL, C. & BLOOM, S. R. 2005. Ghrelin increases food intake in obese as well as lean subjects. *Int J Obes (Lond),* 29**,** 1130-6.

DRUCKER, D. J. 2013. Incretin action in the pancreas: potential promise, possible perils, and pathological pitfalls. *Diabetes,* 62**,** 3316-3323.

DRUCKER, D. J., PHILIPPE, J., MOJSOV, S., CHICK, W. L. & HABENER, J. F. 1987. Glucagon-like peptide I stimulates insulin gene expression and increases cyclic AMP levels in a rat islet cell line. *Proc Natl Acad Sci U S A,* 84**,** 3434-8.

DUCA, L. M., REBOUSSIN, B. A., PIHOKER, C., IMPERATORE, G., SAYDAH, S., MAYER-DAVIS, E., REWERS, A. & DABELEA, D. 2019. Diabetic ketoacidosis at diagnosis of type 1 diabetes and glycemic control over time: The SEARCH for diabetes in youth study. *Pediatr Diabetes,* 20**,** 172-179.

DUDEK, N. L., THOMAS, H. E., MARIANA, L., SUTHERLAND, R. M., ALLISON, J., ESTELLA, E., ANGSTETRA, E., TRAPANI, J. A., SANTAMARIA, P., LEW, A. M. & KAY, T. W. 2006. Cytotoxic T-cells from T-cell receptor transgenic NOD8.3 mice destroy beta-cells via the perforin and Fas pathways. *Diabetes,* 55**,** 2412-8.

DUPUIS, J., LANGENBERG, C., PROKOPENKO, I., SAXENA, R., SORANZO, N., JACKSON, A. U., WHEELER, E., GLAZER, N. L., BOUATIA-NAJI, N., GLOYN, A. L., LINDGREN, C. M., MAGI, R., MORRIS, A. P., RANDALL, J., JOHNSON, T., ELLIOTT, P., RYBIN, D., THORLEIFSSON, G., STEINTHORSDOTTIR, V., HENNEMAN, P., GRALLERT, H., DEHGHAN, A., HOTTENGA, J. J., FRANKLIN, C. S., NAVARRO, P., SONG, K., GOEL, A., PERRY, J. R., EGAN, J. M., LAJUNEN, T., GRARUP, N., SPARSO, T., DONEY, A., VOIGHT, B. F., STRINGHAM, H. M., LI, M., KANONI, S., SHRADER, P., CAVALCANTI-PROENCA, C., KUMARI, M., QI, L., TIMPSON, N. J., GIEGER, C., ZABENA, C., ROCHELEAU, G., INGELSSON, E., AN, P., O'CONNELL, J., LUAN, J., ELLIOTT, A., MCCARROLL, S. A., PAYNE, F., ROCCASECCA, R. M., PATTOU, F., SETHUPATHY, P., ARDLIE, K., ARIYUREK, Y., BALKAU, B., BARTER, P., BEILBY, J. P., BEN-SHLOMO, Y., BENEDIKTSSON, R., BENNETT, A. J., BERGMANN, S., BOCHUD, M., BOERWINKLE, E., BONNEFOND, A., BONNYCASTLE, L. L., BORCH-JOHNSEN, K., BOTTCHER, Y., BRUNNER, E., BUMPSTEAD, S. J., CHARPENTIER, G., CHEN, Y. D., CHINES, P., CLARKE, R., COIN, L. J., COOPER, M. N., CORNELIS, M., CRAWFORD, G., CRISPONI, L., DAY, I. N., DE GEUS, E. J., DELPLANQUE, J., DINA, C., ERDOS, M. R., FEDSON, A. C., FISCHER-ROSINSKY, A., FOROUHI, N. G., FOX, C. S., FRANTS, R., FRANZOSI, M. G., GALAN, P., GOODARZI, M. O., GRAESSLER, J., GROVES, C. J., GRUNDY, S., GWILLIAM, R., GYLLENSTEN, U., HADJADJ, S., et al. 2010. New genetic loci implicated in fasting glucose homeostasis and their impact on type 2 diabetes risk. *Nat Genet,* 42**,** 105-16.

DYACHOK, O., IDEVALL-HAGREN, O., SÅGETORP, J., TIAN, G., WUTTKE, A., ARRIEUMERLOU, C., AKUSJÄRVI, G., GYLFE, E. & TENGHOLM, A. 2008. Glucose-induced cyclic AMP oscillations regulate pulsatile insulin secretion. *Cell Metab,* 8**,** 26-37.

DYBALA, M. P. & HARA, M. 2019. Heterogeneity of the Human Pancreatic Islet. *Diabetes,* 68**,** 1230-1239.

EBBERT, M. T. W., WADSWORTH, M. E., STALEY, L. A., HOYT, K. L., PICKETT, B., MILLER, J., DUCE, J., KAUWE, J. S. K., RIDGE, P. G. & FOR THE ALZHEIMER'S DISEASE NEUROIMAGING, I. 2016. Evaluating the necessity of PCR duplicate removal from next-generation sequencing data and a comparison of approaches. *BMC Bioinformatics,* 17**,** 239.

EBERT, B., KISIELA, M., MALÁTKOVÁ, P., EL-HAWARI, Y. & MASER, E. 2010. Regulation of human carbonyl reductase 3 (CBR3; SDR21C2) expression by Nrf2 in cultured cancer cells. *Biochemistry,* 49**,** 8499-511.

EBRAHIMI, A. G., HOLLISTER-LOCK, J., SULLIVAN, B. A., TSUCHIDA, R., BONNER-WEIR, S. & WEIR, G. C. 2020. Beta cell identity changes with mild hyperglycemia: Implications for function, growth, and vulnerability. *Molecular Metabolism,* 35**,** 100959.

ECHOUFFO-TCHEUGUI, J. B., SHORT, M. I., XANTHAKIS, V., FIELD, P., SPONHOLTZ, T. R., LARSON, M. G. & VASAN, R. S. 2019. Natural History of Obesity Subphenotypes: Dynamic Changes Over Two Decades and Prognosis in the Framingham Heart Study. *J Clin Endocrinol Metab,* 104**,** 738-752.

EGAN, T. M. & KHAKH, B. S. 2004. Contribution of Calcium Ions to P2X Channel Responses. *The Journal of Neuroscience,* 24**,** 3413-3420.

EGLI, D., SELVARAJ, A., YEPISKOPOSYAN, H., ZHANG, B., HAFEN, E., GEORGIEV, O. & SCHAFFNER, W. 2003. Knockout of 'metal-responsive transcription factor' MTF-1 in Drosophila by homologous recombination reveals its central role in heavy metal homeostasis. *Embo j,* 22**,** 100-8.

EHSES, J. A., PERREN, A., EPPLER, E., RIBAUX, P., POSPISILIK, J. A., MAOR-CAHN, R., GUERIPEL, X., ELLINGSGAARD, H., SCHNEIDER, M. K., BIOLLAZ, G., FONTANA, A., REINECKE, M., HOMO-DELARCHE, F. & DONATH, M. Y. 2007. Increased number of islet-associated macrophages in type 2 diabetes. *Diabetes,* 56**,** 2356-70.

EINARSON, T. R., ACS, A., LUDWIG, C. & PANTON, U. H. 2018. Prevalence of cardiovascular disease in type 2 diabetes: a systematic literature review of scientific evidence from across the world in 2007-2017. *Cardiovascular diabetology,* 17**,** 83-83.

EIZIRIK, D. L., PIPELEERS, D. G., LING, Z., WELSH, N., HELLERSTRÖM, C. & ANDERSSON, A. 1994. Major species differences between humans and rodents in the susceptibility to pancreatic beta-cell injury. *Proceedings of the National Academy of Sciences of the United States of America,* 91**,** 9253-9256.

EL-AZZOUNY, M., EVANS, C. R., TREUTELAAR, M. K., KENNEDY, R. T. & BURANT, C. F. 2014. Increased glucose metabolism and glycerolipid formation by fatty acids and GPR40 receptor signaling underlies the fatty acid potentiation of insulin secretion. *J Biol Chem,* 289**,** 13575-88.

ERLICH, H., VALDES, A. M., NOBLE, J., CARLSON, J. A., VARNEY, M., CONCANNON, P., MYCHALECKYJ, J. C., TODD, J. A., BONELLA, P., FEAR, A. L., LAVANT, E., LOUEY, A. & MOONSAMY, P. 2008. HLA DR-DQ haplotypes and genotypes and type 1 diabetes risk: analysis of the type 1 diabetes genetics consortium families. *Diabetes,* 57**,** 1084-92.

ESENSTEN, J. H., LEE, M. R., GLIMCHER, L. H. & BLUESTONE, J. A. 2009. T-bet-deficient NOD mice are protected from diabetes due to defects in both T cell and innate immune system function. *J Immunol,* 183**,** 75-82.

EVANS, C. C., LEPARD, K. J., KWAK, J. W., STANCUKAS, M. C., LASKOWSKI, S., DOUGHERTY, J., MOULTON, L., GLAWE, A., WANG, Y., LEONE, V., ANTONOPOULOS, D. A., SMITH, D., CHANG, E. B. & CIANCIO, M. J. 2014. Exercise prevents weight gain and alters the gut microbiota in a mouse model of high fat diet-induced obesity. *PLoS One,* 9**,** e92193.

EVLIYAOĞLU, O., ERCAN, O., ATAOĞLU, E., ZÜBARIOĞLU, Ü., ÖZCABı, B., DAĞDEVIREN, A., ERDOĞAN, H., DE FRANCO, E. & ELLARD, S. 2018. Neonatal Diabetes: Two Cases with Isolated Pancreas Agenesis due to Homozygous PTF1A Enhancer

Mutations and One with Developmental Delay, Epilepsy, and Neonatal Diabetes Syndrome due to KCNJ11 Mutation. *Journal of clinical research in pediatric endocrinology,* 10**,** 168-174.

FABBRINI, E., MAGKOS, F., MOHAMMED, B. S., PIETKA, T., ABUMRAD, N. A., PATTERSON, B. W., OKUNADE, A. & KLEIN, S. 2009. Intrahepatic fat, not visceral fat, is linked with metabolic complications of obesity. *Proceedings of the National Academy of Sciences,* 106**,** 15430-15435.

FADISTA, J., VIKMAN, P., LAAKSO, E. O., MOLLET, I. G., ESGUERRA, J. L., TANEERA, J., STORM, P., OSMARK, P., LADENVALL, C., PRASAD, R. B., HANSSON, K. B., FINOTELLO, F., UVEBRANT, K., OFORI, J. K., DI CAMILLO, B., KRUS, U., CILIO, C. M., HANSSON, O., ELIASSON, L., ROSENGREN, A. H., RENSTRÖM, E., WOLLHEIM, C. B. & GROOP, L. 2014. Global genomic and transcriptomic analysis of human pancreatic islets reveals novel genes influencing glucose metabolism. *Proceedings of the National Academy of Sciences,* 111**,** 13924-13929.

FAHIM, A. T., DAIGER, S. P. & WELEBER, R. G. 1993. Nonsyndromic Retinitis Pigmentosa Overview. *In:* ADAM, M. P., ARDINGER, H. H., PAGON, R. A., WALLACE, S. E., BEAN, L. J. H., STEPHENS, K. & AMEMIYA, A. (eds.) *GeneReviews(®).* Seattle (WA): University of Washington, Seattle

FARHAT, B., ALMELKAR, A., RAMACHANDRAN, K., WILLIAMS, S. J., HUANG, H.-H., ZAMIEROWKSI, D., NOVIKOVA, L. & STEHNO-BITTEL, L. 2013. Small human islets comprised of more β-cells with higher insulin content than large islets. *Islets,* 5**,** 87-94.

FARRELL, G. C., MRIDHA, A. R., YEH, M. M., ARSOV, T., VAN ROOYEN, D. M., BROOLING, J., NGUYEN, T., HEYDET, D., DELGHINGARO-AUGUSTO, V., NOLAN, C. J., SHACKEL, N. A., MCLENNAN, S. V., TEOH, N. C. & LARTER, C. Z. 2014. Strain dependence of diet-induced NASH and liver fibrosis in obese mice is linked to diabetes and inflammatory phenotype. *Liver International,* 34**,** 1084-1093.

FAVARETTO, F., MILAN, G., COLLIN, G. B., MARSHALL, J. D., STASI, F., MAFFEI, P., VETTOR, R. & NAGGERT, J. K. 2014. GLUT4 defects in adipose tissue are early signs of metabolic alterations in Alms1GT/GT, a mouse model for obesity and insulin resistance. *PloS one,* 9**,** e109540-e109540.

FEDERICI, M., HRIBAL, M., PEREGO, L., RANALLI, M., CARADONNA, Z., PEREGO, C., USELLINI, L., NANO, R., BONINI, P., BERTUZZI, F., MARLIER, L. N. J. L., DAVALLI, A. M., CARANDENTE, O., PONTIROLI, A. E., MELINO, G., MARCHETTI, P., LAURO, R., SESTI, G. & FOLLI, F. 2001. High Glucose Causes Apoptosis in Cultured Human Pancreatic Islets of Langerhans. *A Potential Role for Regulation of Specific Bcl Family Genes Toward an Apoptotic Cell Death Program,* 50**,** 1290-1301.

FILHOULAUD, G., BENHAMED, F., PAGESY, P., BONNER, C., FARDINI, Y., ILIAS, A., MOVASSAT, J., BURNOL, A. F., GUILMEAU, S., KERR-CONTE, J., PATTOU, F., ISSAD, T. & POSTIC, C. 2019. O-GlcNacylation Links TxNIP to Inflammasome Activation in Pancreatic β Cells. *Front Endocrinol (Lausanne),* 10**,** 291.

FISHER, E., NITZ, I., LINDNER, I., RUBIN, D., BOEING, H., MÖHLIG, M., HAMPE, J., SCHREIBER, S., SCHREZENMEIR, J. & DÖRING, F. 2007. Candidate gene association study of type 2 diabetes in a nested case-control study of the EPIC-Potsdam cohort - role of fat assimilation. *Mol Nutr Food Res,* 51**,** 185-91.

FLOREZ, H., PAN, Q., ACKERMANN, R. T., MARRERO, D. G., BARRETT-CONNOR, E., DELAHANTY, L., KRISKA, A., SAUDEK, C. D., GOLDBERG, R. B. & RUBIN, R. R. 2012. Impact of lifestyle intervention and metformin on health-related quality of life: the diabetes prevention program randomized trial. *J Gen Intern Med,* 27**,** 1594-601.

FOLEY, S. B., RIOS, J. J., MGBEMENA, V. E., ROBINSON, L. S., HAMPEL, H. L., TOLAND, A. E., DURHAM, L. & ROSS, T. S. 2015. Use of Whole Genome Sequencing for Diagnosis and Discovery in the Cancer Genetics Clinic. *EBioMedicine,* 2**,** 74-81.

FRANSSON, U., ROSENGREN, A. H., SCHUIT, F. C., RENSTRÖM, E. & MULDER, H. 2006. Anaplerosis via pyruvate carboxylase is required for the fuel-induced rise in the ATP:ADP ratio in rat pancreatic islets. *Diabetologia,* 49**,** 1578-86.

FREDRIKSSON, R., LAGERSTRÖM, M. C., LUNDIN, L. G. & SCHIÖTH, H. B. 2003. The G-protein-coupled receptors in the human genome form five main families. Phylogenetic analysis, paralogon groups, and fingerprints. *Mol Pharmacol,* 63**,** 1256-72.

FU, J. F., YEN, T. H., CHEN, Y., HUANG, Y. J., HSU, C. L., LIANG, D. C. & SHIH, L. Y. 2013. Involvement of Gpr125 in the myeloid sarcoma formation induced by cooperating MLL/AF10(OM-LZ) and oncogenic KRAS in a mouse bone marrow transplantation model. *Int J Cancer,* 133**,** 1792-802.

FUKUSHIMA, M., USAMI, M., IKEDA, M., NAKAI, Y., TANIGUCHI, A., MATSUURA, T., SUZUKI, H., KUROSE, T., YAMADA, Y. & SEINO, Y. 2004. Insulin secretion and insulin sensitivity at different stages of glucose tolerance: a cross-sectional study of Japanese type 2 diabetes. *Metabolism - Clinical and Experimental,* 53**,** 831-835.

FURUTA, M., ZHOU, A., WEBB, G., CARROLL, R., RAVAZZOLA, M., ORCI, L. & STEINER, D. F. 2001. Severe defect in proglucagon processing in islet A-cells of prohormone convertase 2 null mice. *J Biol Chem,* 276**,** 27197-202.

FURUYA, F., GUIGON, C. J., ZHAO, L., LU, C., HANOVER, J. A. & CHENG, S.-Y. 2007. Nuclear receptor corepressor is a novel regulator of phosphatidylinositol 3-kinase signaling. *Molecular and cellular biology,* 27**,** 6116-6126.

GALDERISI, A., POLIDORI, D., WEISS, R., GIANNINI, C., PIERPONT, B., TRICO, D. & CAPRIO, S. 2019. Lower Insulin Clearance Parallels a Reduced Insulin Sensitivity in Obese Youths and Is Associated With a Decline in beta-Cell Function Over Time. *Diabetes,* 68**,** 2074-2084.

GAO, Y., SARTORI, D. J., LI, C., YU, Q. C., KUSHNER, J. A., SIMON, M. C. & DIEHL, J. A. 2012. PERK is required in the adult pancreas and is essential for maintenance of glucose homeostasis. *Mol Cell Biol,* 32**,** 5129-39.

GEDULIN, B. R., JODKA, C. M., HERRMANN, K. & YOUNG, A. A. 2006. Role of endogenous amylin in glucagon secretion and gastric emptying in rats demonstrated with the selective antagonist, AC187. *Regul Pept,* 137**,** 121-7.

GEERLINGS, S. E. & HOEPELMAN, A. I. 1999. Immune dysfunction in patients with diabetes mellitus (DM). *FEMS Immunol Med Microbiol,* 26**,** 259-65.

GEIGER, M. A., GUILLAUMON, A. T., PANENI, F., MATTER, C. M. & STEIN, S. 2020. Role of the Nuclear Receptor Corepressor 1 (NCOR1) in Atherosclerosis and Associated Immunometabolic Diseases. *Front Immunol,* 11**,** 569358.

GEMBAL, M., GILON, P. & HENQUIN, J. C. 1992. Evidence that glucose can control insulin release independently from its action on ATP-sensitive K+ channels in mouse B cells. *J Clin Invest,* 89**,** 1288-95.

GERST, F., SINGER, C., NOACK, K., GRAF, D., KAISER, G., PANSE, M., KOVAROVA, M., SCHLEICHER, E., HÄRING, H. U., DREWS, G. & ULLRICH, S. 2019. Glucose Responsiveness of β-Cells Depends on Fatty Acids. *Exp Clin Endocrinol Diabetes*.

GHIASI, S. M., DAHLBY, T., HEDE ANDERSEN, C., HAATAJA, L., PETERSEN, S., OMAR-HMEADI, M., YANG, M., PIHL, C., BRESSON, S. E., KHILJI, M. S., KLINDT, K., CHETA, O., PERONE, M. J., TYRBERG, B., PRATS, C., BARG, S., TENGHOLM, A., ARVAN, P., MANDRUP-POULSEN, T. & MARZEC, M. T. 2019. Endoplasmic Reticulum Chaperone Glucose-Regulated Protein 94 Is Essential for Proinsulin Handling. *Diabetes,* 68**,** 747-760.

GLOYN, A. L., WEEDON, M. N., OWEN, K. R., TURNER, M. J., KNIGHT, B. A., HITMAN, G., WALKER, M., LEVY, J. C., SAMPSON, M., HALFORD, S., MCCARTHY, M. I., HATTERSLEY, A. T. & FRAYLING, T. M. 2003. Large-Scale Association Studies of Variants in Genes Encoding the Pancreatic β-Cell K+ATP Channel Subunits Kir6.2 (KCNJ11) and SUR1 (ABCC8) Confirm That the KCNJ11/E23K Variant Is Associated With Type 2 Diabetes. *Diabetes,* 52**,** 568-572.

GODSLAND, I. F., JEFFS, J. A. R. & JOHNSTON, D. G. 2004. Loss of beta cell function as fasting glucose increases in the non-diabetic range. *Diabetologia,* 47**,** 1157-1166.

GONEN, M. S., ARIKOGLU, H., ERKOC KAYA, D., OZDEMIR, H., IPEKCI, S. H., ARSLAN, A., KAYIS, S. A. & GOGEBAKAN, B. 2012. Effects of single nucleotide polymorphisms in K(ATP) channel genes on type 2 diabetes in a Turkish population. *Arch Med Res,* 43**,** 317-23.
GOOSSENS, G. H. 2017. The Metabolic Phenotype in Obesity: Fat Mass, Body Fat Distribution, and Adipose Tissue Function. *Obesity facts,* 10**,** 207-215.
GOTO, Y., SUZUKI, K., ONO, T., SASAKI, M. & TOYOTA, T. 1988. Development of diabetes in the non-obese NIDDM rat (GK rat). *Adv Exp Med Biol,* 246**,** 29-31.
GRÄF, S., HAIMEL, M., BLEDA, M., HADINNAPOLA, C., SOUTHGATE, L., LI, W., HODGSON, J., LIU, B., SALMON, R. M., SOUTHWOOD, M., MACHADO, R. D., MARTIN, J. M., TREACY, C. M., YATES, K., DAUGHERTY, L. C., SHAMARDINA, O., WHITEHORN, D., HOLDEN, S., ALDRED, M., BOGAARD, H. J., CHURCH, C., COGHLAN, G., CONDLIFFE, R., CORRIS, P. A., DANESINO, C., EYRIES, M., GALL, H., GHIO, S., GHOFRANI, H. A., GIBBS, J. S. R., GIRERD, B., HOUWELING, A. C., HOWARD, L., HUMBERT, M., KIELY, D. G., KOVACS, G., MACKENZIE ROSS, R. V., MOLEDINA, S., MONTANI, D., NEWNHAM, M., OLSCHEWSKI, A., OLSCHEWSKI, H., PEACOCK, A. J., PEPKE-ZABA, J., PROKOPENKO, I., RHODES, C. J., SCELSI, L., SEEGER, W., SOUBRIER, F., STEIN, D. F., SUNTHARALINGAM, J., SWIETLIK, E. M., TOSHNER, M. R., VAN HEEL, D. A., VONK NOORDEGRAAF, A., WAISFISZ, Q., WHARTON, J., WORT, S. J., OUWEHAND, W. H., SORANZO, N., LAWRIE, A., UPTON, P. D., WILKINS, M. R., TREMBATH, R. C. & MORRELL, N. W. 2018. Identification of rare sequence variation underlying heritable pulmonary arterial hypertension. *Nat Commun,* 9**,** 1416.
GRASSMANN, F., FRIEDRICH, U., FAUSER, S., SCHICK, T., MILENKOVIC, A., SCHULZ, H. L., VON STRACHWITZ, C. N., BETTECKEN, T., LICHTNER, P., MEITINGER, T., AREND, N., WOLF, A., HARITOGLOU, C., RUDOLPH, G., CHAKRAVARTHY, U., SILVESTRI, G., MCKAY, G. J., FREITAG-WOLF, S., KRAWCZAK, M., SMITH, R. T., MERRIAM, J. C., MERRIAM, J. E., ALLIKMETS, R., HEID, I. M. & WEBER, B. H. 2015. A Candidate Gene Association Study Identifies DAPL1 as a Female-Specific Susceptibility Locus for Age-Related Macular Degeneration (AMD). *Neuromolecular Med,* 17**,** 111-20.
GRAVENA, C., MATHIAS, P. & ASHCROFT, S. 2002. Acute effects of fatty acids on insulin secretion from rat and human islets of Langerhans. 173**,** 73.
GRODSKY, G. M. 1972. A threshold distribution hypothesis for packet storage of insulin and its mathematical modeling. *J Clin Invest,* 51**,** 2047-59.
GUAN, W., PLUZHNIKOV, A., COX, N. J., BOEHNKE, M. & INTERNATIONAL TYPE 2 DIABETES LINKAGE ANALYSIS, C. 2008. Meta-analysis of 23 type 2 diabetes linkage studies from the International Type 2 Diabetes Linkage Analysis Consortium. *Human heredity,* 66**,** 35-49.
GUPTA, D., JETTON, T., LAROCK, K., MONGA, N., SATISH, B., LAUSIER, J., PESHAVARIA, M. & LEAHY, J. 2017. Temporal Characterization of β-cell Adaptive and Maladaptive Mechanisms During Chronic High Fat Feeding in C57BL/6NTac Mice. *Journal of Biological Chemistry,* 292**,** jbc.M117.781047.
GUPTA, S., MCGRATH, B. & CAVENER, D. R. 2010. PERK (EIF2AK3) regulates proinsulin trafficking and quality control in the secretory pathway. *Diabetes,* 59**,** 1937-47.
GURGUL, E., LORTZ, S., TIEDGE, M., JÖRNS, A. & LENZEN, S. 2004. Mitochondrial catalase overexpression protects insulin-producing cells against toxicity of reactive oxygen species and proinflammatory cytokines. *Diabetes,* 53**,** 2271-80.
HAATAJA, L., GURLO, T., HUANG, C. J. & BUTLER, P. C. 2008. Islet amyloid in type 2 diabetes, and the toxic oligomer hypothesis. *Endocr Rev,* 29**,** 303-16.
HABTEMICHAEL, N. & KOVACS, G. 2002. Cloning the AFURS1 gene which is up-regulated in senescent human parenchymal kidney cells. *Gene,* 283**,** 271-275.
HAGE HASSAN, R., PACHECO DE SOUSA, A. C., MAHFOUZ, R., HAINAULT, I., BLACHNIO-ZABIELSKA, A., BOURRON, O., KOSKAS, F., GÓRSKI, J., FERRÉ, P., FOUFELLE, F. & HAJDUCH, E. 2016. Sustained Action of Ceramide on the Insulin Signaling Pathway in Muscle Cells: Implication of the double-stranded RNA-activated protein kinase. *J Biol Chem,* 291**,** 3019-29.

HAGMAN, D. K., HAYS, L. B., PARAZZOLI, S. D. & POITOUT, V. 2005. Palmitate inhibits insulin gene expression by altering PDX-1 nuclear localization and reducing MafA expression in isolated rat islets of Langerhans. *J Biol Chem,* 280**,** 32413-8.
HAIST, R. E. 1971. Functions of the islets of Langerhans. *Canadian Medical Association journal,* 105**,** 956-passim.
HALL, E., DEKKER NITERT, M., VOLKOV, P., MALMGREN, S., MULDER, H., BACOS, K. & LING, C. 2018. The effects of high glucose exposure on global gene expression and DNA methylation in human pancreatic islets. *Mol Cell Endocrinol,* 472**,** 57-67.
HALL, E., VOLKOV, P., DAYEH, T., BACOS, K., RÖNN, T., NITERT, M. D. & LING, C. 2014. Effects of palmitate on genome-wide mRNA expression and DNA methylation patterns in human pancreatic islets. *BMC Medicine,* 12**,** 103.
HAMANN, A., FLIER, J. S. & LOWELL, B. B. 1996. Decreased brown fat markedly enhances susceptibility to diet-induced obesity, diabetes, and hyperlipidemia. *Endocrinology,* 137**,** 21-9.
HAN, X., ZHOU, J., ZHANG, P., SONG, F., JIANG, R., LI, M., XIA, F. & GUO, F. J. 2013. IRE1alpha dissociates with BiP and inhibits ER stress-mediated apoptosis in cartilage development. *Cell Signal,* 25**,** 2136-46.
HANLEY, A. J. G., D'AGOSTINO, R., WAGENKNECHT, L. E., SAAD, M. F., SAVAGE, P. J., BERGMAN, R. & HAFFNER, S. M. 2002. Increased Proinsulin Levels and Decreased Acute Insulin Response Independently Predict the Incidence of Type 2 Diabetes in the Insulin Resistance Atherosclerosis Study. *Diabetes,* 51**,** 1263-1270.
HARASHIMA, S., WANG, Y., HORIUCHI, T., SEINO, Y. & INAGAKI, N. 2011. Purkinje cell protein 4 positively regulates neurite outgrowth and neurotransmitter release. *J Neurosci Res,* 89**,** 1519-30.
HARDMAN, R. M. & FORSYTHE, I. D. 2009. Ether-à-go-go-related gene K+ channels contribute to threshold excitability of mouse auditory brainstem neurons. *J Physiol,* 587**,** 2487-97.
HAYNES, C. M., TITUS, E. A. & COOPER, A. A. 2004. Degradation of misfolded proteins prevents ER-derived oxidative stress and cell death. *Mol Cell,* 15**,** 767-76.
HE, M.-Q., WANG, J.-Y., WANG, Y., SUI, J., ZHANG, M., DING, X., ZHAO, Y., CHEN, Z.-Y., REN, X.-X. & SHI, B.-Y. 2020. High-fat diet-induced adipose tissue expansion occurs prior to insulin resistance in C57BL/6J mice. *Chronic Diseases and Translational Medicine,* 6**,** 198-207.
HELLMAN, B., IDAHL, L. A., LERNMARK, A. & TÄLJEDAL, I. B. 1974. The pancreatic beta-cell recognition of insulin secretagogues: does cyclic AMP mediate the effect of glucose? *Proc Natl Acad Sci U S A,* 71**,** 3405-9.
HEMMINGSEN, B., GIMENEZ-PEREZ, G., MAURICIO, D., ROQUÉ, I. F. M., METZENDORF, M. I. & RICHTER, B. 2017. Diet, physical activity or both for prevention or delay of type 2 diabetes mellitus and its associated complications in people at increased risk of developing type 2 diabetes mellitus. *Cochrane Database Syst Rev,* 12**,** Cd003054.
HENDERSON, J. R. & MOSS, M. C. 1985. A morphometric study of the endocrine and exocrine capillaries of the pancreas. *Q J Exp Physiol,* 70**,** 347-56.
HENQUIN, J.-C. 2019. The challenge of correctly reporting hormones content and secretion in isolated human islets. *Molecular metabolism,* 30**,** 230-239.
HENQUIN, J. C., DUFRANE, D., KERR-CONTE, J. & NENQUIN, M. 2015. Dynamics of glucose-induced insulin secretion in normal human islets. *Am J Physiol Endocrinol Metab,* 309**,** E640-50.
HERMANS, M. P. & VALENSI, P. 2018. Elevated triglycerides and low high-density lipoprotein cholesterol level as marker of very high risk in type 2 diabetes. *Curr Opin Endocrinol Diabetes Obes,* 25**,** 118-129.
HERNANDEZ, L. & BRIESE, E. 1972. Analysis of diabetic hyperphagia and polydipsia. *Physiol Behav,* 9**,** 741-6.
HERRERO, L., RUBÍ, B., SEBASTIÁN, D., SERRA, D., ASINS, G., MAECHLER, P., PRENTKI, M. & HEGARDT, F. G. 2005. Alteration of the malonyl-CoA/carnitine palmitoyltransferase I interaction in the beta-cell impairs glucose-induced insulin secretion. *Diabetes,* 54**,** 462-71.
HOLST, J. J. 2019. The incretin system in healthy humans: The role of GIP and GLP-1. *Metabolism,* 96**,** 46-55.

HOMO-DELARCHE, F., CALDERARI, S., IRMINGER, J.-C., GANGNERAU, M.-N., COULAUD, J., RICKENBACH, K., DOLZ, M., HALBAN, P., PORTHA, B. & SERRADAS, P. 2006. Islet Inflammation and Fibrosis in a Spontaneous Model of Type 2 Diabetes, the GK Rat. *Diabetes,* 55**,** 1625-1633.

HÖPPENER, J. W. M., JACOBS, H. M., WIERUP, N., SOTTHEWES, G., SPRONG, M., DE VOS, P., BERGER, R., SUNDLER, F. & AHRÉN, B. 2008. Human islet amyloid polypeptide transgenic mice: in vivo and ex vivo models for the role of hIAPP in type 2 diabetes mellitus. *Experimental diabetes research,* 2008**,** 697035-697035.

HOSHIYAMA, M., LI, B., YAO, J., HARADA, T., MORIOKA, T. & OITE, T. 2003. Effect of high glucose on nitric oxide production and endothelial nitric oxide synthase protein expression in human glomerular endothelial cells. *Nephron Exp Nephrol,* 95**,** e62-8.

HOWE, H. R., 3RD, HEIDAL, K., CHOI, M. D., KRAUS, R. M., BOYLE, K. & HICKNER, R. C. 2011. Increased adipose tissue lipolysis after a 2-week high-fat diet in sedentary overweight/obese men. *Metabolism: clinical and experimental,* 60**,** 976-981.

HRYTSENKO, O., WRIGHT, J. R., MORRISON, C. M. & POHAJDAK, B. 2007. Insulin expression in the brain and pituitary cells of tilapia (Oreochromis niloticus). *Brain research,* 1135**,** 31-40.

HUANG, C. J., LIN, C. Y., HAATAJA, L., GURLO, T., BUTLER, A. E., RIZZA, R. A. & BUTLER, P. C. 2007. High expression rates of human islet amyloid polypeptide induce endoplasmic reticulum stress mediated beta-cell apoptosis, a characteristic of humans with type 2 but not type 1 diabetes. *Diabetes,* 56**,** 2016-27.

HUANG, X. F. & ARVAN, P. 1995. Intracellular transport of proinsulin in pancreatic beta-cells. Structural maturation probed by disulfide accessibility. *J Biol Chem,* 270**,** 20417-23.

HULL, R. L., ANDRIKOPOULOS, S., VERCHERE, C. B., VIDAL, J., WANG, F., CNOP, M., PRIGEON, R. L. & KAHN, S. E. 2003. Increased dietary fat promotes islet amyloid formation and beta-cell secretory dysfunction in a transgenic mouse model of islet amyloid. *Diabetes,* 52**,** 372-9.

HULL, R. L., KODAMA, K., UTZSCHNEIDER, K. M., CARR, D. B., PRIGEON, R. L. & KAHN, S. E. 2005. Dietary-fat-induced obesity in mice results in beta cell hyperplasia but not increased insulin release: evidence for specificity of impaired beta cell adaptation. *Diabetologia,* 48**,** 1350-8.

HULL, R. L., WILLARD, J. R., STRUCK, M. D., BARROW, B. M., BRAR, G. S., ANDRIKOPOULOS, S. & ZRAIKA, S. 2017. High fat feeding unmasks variable insulin responses in male C57BL/6 mouse substrains. *The Journal of endocrinology,* 233**,** 53-64.

HUSAIN, S. & THROWER, E. 2009. Molecular and cellular regulation of pancreatic acinar cell function. *Current opinion in gastroenterology,* 25**,** 466-471.

IKEGAMI, H., MAKINO, S., YAMATO, E., KAWAGUCHI, Y., UEDA, H., SAKAMOTO, T., TAKEKAWA, K. & OGIHARA, T. 1995. Identification of a new susceptibility locus for insulin-dependent diabetes mellitus by ancestral haplotype congenic mapping. *J Clin Invest,* 96**,** 1936-42.

IKEZAWA, Y., YAMATANI, K., OHNUMA, H., DAIMON, M., MANAKA, H. & SASAKI, H. 2003. Glucagon-like peptide-1 inhibits glucagon-induced glycogenolysis in perivenous hepatocytes specifically. *Regul Pept,* 111**,** 207-10.

INABA, K., MASUI, S., IIDA, H., VAVASSORI, S., SITIA, R. & SUZUKI, M. 2010. Crystal structures of human Ero1alpha reveal the mechanisms of regulated and targeted oxidation of PDI. *Embo j,* 29**,** 3330-43.

INTERNATIONAL DIABETES FEDERATION 2017. Recommendations For Managing Type 2 Diabetes In Primary Care.

INTERNATIONAL DIABETES FEDERATION 2019. IDF Diabetes Atlas, 9th edn. Brussels,

Belgium: International Diabetes Federation.

IOZZO, P., HALLSTEN, K., OIKONEN, V., VIRTANEN, K. A., KEMPPAINEN, J., SOLIN, O., FERRANNINI, E., KNUUTI, J. & NUUTILA, P. 2003. Insulin-mediated hepatic glucose uptake is impaired in type 2 diabetes: evidence for a relationship with glycemic control. *J Clin Endocrinol Metab,* 88**,** 2055-60.

IVARSSON, R., QUINTENS, R., DEJONGHE, S., TSUKAMOTO, K., IN 'T VELD, P., RENSTRÖM, E. & SCHUIT, F. C. 2005. Redox control of exocytosis: regulatory role of NADPH, thioredoxin, and glutaredoxin. *Diabetes,* 54**,** 2132-42.
IWAWAKI, T., AKAI, R., KOHNO, K. & MIURA, M. 2004. A transgenic mouse model for monitoring endoplasmic reticulum stress. *Nat Med,* 10**,** 98-102.
JACKSON, G. R., SCOTT, I. U., QUILLEN, D. A., WALTER, L. E. & GARDNER, T. W. 2012. Inner retinal visual dysfunction is a sensitive marker of non-proliferative diabetic retinopathy. *Br J Ophthalmol,* 96**,** 699-703.
JACQUEMINET, S., BRIAUD, I., ROUAULT, C., REACH, G. & POITOUT, V. 2000. Inhibition of insulin gene expression by long-term exposure of pancreatic beta cells to palmitate is dependent on the presence of a stimulatory glucose concentration. *Metabolism,* 49**,** 532-6.
JANSSEN, S. W., HERMUS, A. R., LANGE, W. P., KNIJNENBURG, Q., VAN DER LAAK, J. A., SWEEP, C. G., MARTENS, G. J. & VERHOFSTAD, A. A. 2001. Progressive histopathological changes in pancreatic islets of Zucker Diabetic Fatty rats. *Exp Clin Endocrinol Diabetes,* 109**,** 273-82.
JARURATANASIRIKUL, S., THAMMARATCHUCHAI, S., PUWANANT, M., MO-SUWAN, L. & SRIPLUNG, H. 2016. Progression from impaired glucose tolerance to type 2 diabetes in obese children and adolescents: a 3-6-year cohort study in southern Thailand. *J Pediatr Endocrinol Metab,* 29**,** 1267-1275.
JETTON, T. L., LAUSIER, J., LAROCK, K., TROTMAN, W. E., LARMIE, B., HABIBOVIC, A., PESHAVARIA, M. & LEAHY, J. L. 2005. Mechanisms of compensatory beta-cell growth in insulin-resistant rats: roles of Akt kinase. *Diabetes,* 54**,** 2294-304.
JIVAN, A., EARNEST, S., JUANG, Y. C. & COBB, M. H. 2009. Radial spoke protein 3 is a mammalian protein kinase A-anchoring protein that binds ERK1/2. *J Biol Chem,* 284**,** 29437-45.
JO, Y. S., RYU, D., MAIDA, A., WANG, X., EVANS, R. M., SCHOONJANS, K. & AUWERX, J. 2015. Phosphorylation of the nuclear receptor corepressor 1 by protein kinase B switches its corepressor targets in the liver in mice. *Hepatology (Baltimore, Md.),* 62**,** 1606-1618.
JORNAYVAZ, F. R., BIRKENFELD, A. L., JURCZAK, M. J., KANDA, S., GUIGNI, B. A., JIANG, D. C., ZHANG, D., LEE, H.-Y., SAMUEL, V. T. & SHULMAN, G. I. 2011. Hepatic insulin resistance in mice with hepatic overexpression of diacylglycerol acyltransferase 2. *Proceedings of the National Academy of Sciences,* 108**,** 5748-5752.
JUN, D. W., HAN, J. H., KIM, S. H., JANG, E. C., KIM, N. I., LEE, J. S., SONG, M. H., KIM, S. H., JO, Y. J. & PARK, Y. S. 2008. Association between low thigh fat and non-alcoholic fatty liver disease. *J Gastroenterol Hepatol,* 23**,** 888-93.
JUSTER-SWITLYK, K. & SMITH, A. G. 2016. Updates in diabetic peripheral neuropathy. *F1000Research,* 5**,** F1000 Faculty Rev-738.
KACSO, G., RAVASZ, D., DOCZI, J., NÉMETH, B., MADGAR, O., SAADA, A., ILIN, P., MILLER, C., OSTERGAARD, E., IORDANOV, I., ADAMS, D., VARGEDO, Z., ARAKI, M., ARAKI, K., NAKAHARA, M., ITO, H., GÁL, A., MOLNÁR, M. J., NAGY, Z., PATOCS, A., ADAM-VIZI, V. & CHINOPOULOS, C. 2016. Two transgenic mouse models for β-subunit components of succinate-CoA ligase yielding pleiotropic metabolic alterations. *The Biochemical journal,* 473**,** 3463-3485.
KAIHARA, K. A., DICKSON, L. M., JACOBSON, D. A., TAMARINA, N., ROE, M. W., PHILIPSON, L. H. & WICKSTEED, B. 2013. β-Cell-specific protein kinase A activation enhances the efficiency of glucose control by increasing acute-phase insulin secretion. *Diabetes,* 62**,** 1527-36.
KALLIOKOSKI, O., JACOBSEN, K. R., DARUSMAN, H. S., HENRIKSEN, T., WEIMANN, A., POULSEN, H. E., HAU, J. & ABELSON, K. S. P. 2013. Mice do not habituate to metabolism cage housing--a three week study of male BALB/c mice. *PloS one,* 8**,** e58460-e58460.
KANAT, M., NORTON, L., WINNIER, D., JENKINSON, C., DEFRONZO, R. A. & ABDUL-GHANI, M. A. 2011. Impaired early- but not late-phase insulin secretion in subjects with impaired fasting glucose. *Acta Diabetol,* 48**,** 209-17.
KANAZAWA, Y., MAKINO, M., MORISHIMA, Y., YAMADA, K., NABESHIMA, T. & SHIRASAKI, Y. 2008. Degradation of PEP-19, a calmodulin-binding protein, by calpain is

implicated in neuronal cell death induced by intracellular Ca2+ overload. *Neuroscience,* 154**,** 473-81.
KANHERE, A., HERTWECK, A., BHATIA, U., GÖKMEN, M. R., PERUCHA, E., JACKSON, I., LORD, G. M. & JENNER, R. G. 2012. T-bet and GATA3 orchestrate Th1 and Th2 differentiation through lineage-specific targeting of distal regulatory elements. *Nat Commun,* 3**,** 1268.
KARASKOV, E., SCOTT, C., ZHANG, L., TEODORO, T., RAVAZZOLA, M. & VOLCHUK, A. 2006. Chronic palmitate but not oleate exposure induces endoplasmic reticulum stress, which may contribute to INS-1 pancreatic beta-cell apoptosis. *Endocrinology,* 147**,** 3398-407.
KARVONEN, M., VIIK-KAJANDER, M., MOLTCHANOVA, E., LIBMAN, I., LAPORTE, R. & TUOMILEHTO, J. 2000. Incidence of childhood type 1 diabetes worldwide. Diabetes Mondiale (DiaMond) Project Group. *Diabetes Care,* 23**,** 1516-26.
KASHYAP, S., BELFORT, R., GASTALDELLI, A., PRATIPANAWATR, T., BERRIA, R., PRATIPANAWATR, W., BAJAJ, M., MANDARINO, L., DEFRONZO, R. & CUSI, K. 2003. A sustained increase in plasma free fatty acids impairs insulin secretion in nondiabetic subjects genetically predisposed to develop type 2 diabetes. *Diabetes,* 52**,** 2461-74.
KATAOKA, K., HAN, S. I., SHIODA, S., HIRAI, M., NISHIZAWA, M. & HANDA, H. 2002. MafA is a glucose-regulated and pancreatic beta-cell-specific transcriptional activator for the insulin gene. *J Biol Chem,* 277**,** 49903-10.
KAUFMAN, R. J. 2011. Beta-cell failure, stress, and type 2 diabetes. *N Engl J Med,* 365**,** 1931-3.
KAZMIERCZAK, M., ZHANG, X., CHEN, B., MULKEY, D. K., SHI, Y., WAGNER, P. G., PIVAROFF-WARD, K., SASSIC, J. K., BAYLISS, D. A. & JEGLA, T. 2013. External pH modulates EAG superfamily K+ channels through EAG-specific acidic residues in the voltage sensor. *The Journal of general physiology,* 141**,** 721-735.
KEBEDE, M., ALQUIER, T., LATOUR, M. G., SEMACHE, M., TREMBLAY, C. & POITOUT, V. 2008. The fatty acid receptor GPR40 plays a role in insulin secretion in vivo after high-fat feeding. *Diabetes,* 57**,** 2432-7.
KEHM, R., KÖNIG, J., NOWOTNY, K., JUNG, T., DEUBEL, S., GOHLKE, S., SCHULZ, T. J. & HÖHN, A. 2018. Age-related oxidative changes in pancreatic islets are predominantly located in the vascular system. *Redox biology,* 15**,** 387-393.
KEILDSON, S., FADISTA, J., LADENVALL, C., HEDMAN, A. K., ELGZYRI, T., SMALL, K. S., GRUNDBERG, E., NICA, A. C., GLASS, D., RICHARDS, J. B., BARRETT, A., NISBET, J., ZHENG, H. F., RONN, T., STROM, K., ERIKSSON, K. F., PROKOPENKO, I., SPECTOR, T. D., DERMITZAKIS, E. T., DELOUKAS, P., MCCARTHY, M. I., RUNG, J., GROOP, L., FRANKS, P. W., LINDGREN, C. M. & HANSSON, O. 2014. Expression of phosphofructokinase in skeletal muscle is influenced by genetic variation and associated with insulin sensitivity. *Diabetes,* 63**,** 1154-65.
KELLER, M. P., GATTI, D. M., SCHUELER, K. L., RABAGLIA, M. E., STAPLETON, D. S., SIMECEK, P., VINCENT, M., ALLEN, S., BROMAN, A. T., BACHER, R., KENDZIORSKI, C., BROMAN, K. W., YANDELL, B. S., CHURCHILL, G. A. & ATTIE, A. D. 2018. Genetic Drivers of Pancreatic Islet Function. *Genetics,* 209**,** 335-356.
KELLER, M. P., RABAGLIA, M. E., SCHUELER, K. L., STAPLETON, D. S., GATTI, D. M., VINCENT, M., MITOK, K. A., WANG, Z., ISHIMURA, T., SIMONETT, S. P., EMFINGER, C. H., DAS, R., BECK, T., KENDZIORSKI, C., BROMAN, K. W., YANDELL, B. S., CHURCHILL, G. A. & ATTIE, A. D. 2019. Gene loci associated with insulin secretion in islets from non-diabetic mice. *The Journal of clinical investigation,* 129**,** 4419-4432.
KELLEY, D. E. & MANDARINO, L. J. 2000. Fuel selection in human skeletal muscle in insulin resistance: a reexamination. *Diabetes,* 49**,** 677-83.
KHALDI, M. Z., GUIOT, Y., GILON, P., HENQUIN, J. C. & JONAS, J. C. 2004. Increased glucose sensitivity of both triggering and amplifying pathways of insulin secretion in rat islets cultured for 1 wk in high glucose. *Am J Physiol Endocrinol Metab,* 287**,** E207-17.
KHULLAR, M., CHEEMA, B. S. & RAUT, S. K. 2017. Emerging Evidence of Epigenetic Modifications in Vascular Complication of Diabetes. *Frontiers in Endocrinology,* 8.

KIKUCHI, O., KOBAYASHI, M., AMANO, K., SASAKI, T., KITAZUMI, T., KIM, H. J., LEE, Y. S., YOKOTA-HASHIMOTO, H., KITAMURA, Y. I. & KITAMURA, T. 2012. FoxO1 gain of function in the pancreas causes glucose intolerance, polycystic pancreas, and islet hypervascularization. *PLoS One,* 7**,** e32249.

KILIMNIK, G., ZHAO, B., JO, J., PERIWAL, V., WITKOWSKI, P., MISAWA, R. & HARA, M. 2011. Altered islet composition and disproportionate loss of large islets in patients with type 2 diabetes. *PLoS One,* 6**,** e27445.

KIM, A., MILLER, K., JO, J., KILIMNIK, G., WOJCIK, P. & HARA, M. 2009a. Islet architecture: A comparative study. *Islets,* 1**,** 129-36.

KIM, D., PAGGI, J. M., PARK, C., BENNETT, C. & SALZBERG, S. L. 2019. Graph-based genome alignment and genotyping with HISAT2 and HISAT-genotype. *Nature Biotechnology,* 37**,** 907-915.

KIM, H. J., KOBAYASHI, M., SASAKI, T., KIKUCHI, O., AMANO, K., KITAZUMI, T., LEE, Y. S., YOKOTA-HASHIMOTO, H., SUSANTI, V. Y., KITAMURA, Y. I., NAKAE, J. & KITAMURA, T. 2012. Overexpression of FoxO1 in the hypothalamus and pancreas causes obesity and glucose intolerance. *Endocrinology,* 153**,** 659-71.

KIM, J. W., YOU, Y. H., HAM, D. S., CHO, J. H., KO, S. H., SONG, K. H., SON, H. Y., SUH-KIM, H., LEE, I. K. & YOON, K. H. 2009b. Suppression of peroxisome proliferator-activated receptor gamma-coactivator-1alpha normalizes the glucolipotoxicity-induced decreased BETA2/NeuroD gene transcription and improved glucose tolerance in diabetic rats. *Endocrinology,* 150**,** 4074-83.

KIM, J. Y., NASR, A., TFAYLI, H., BACHA, F., MICHALISZYN, S. F. & ARSLANIAN, S. 2017. Increased Lipolysis, Diminished Adipose Tissue Insulin Sensitivity, and Impaired β-Cell Function Relative to Adipose Tissue Insulin Sensitivity in Obese Youth With Impaired Glucose Tolerance. *Diabetes,* 66**,** 3085-3090.

KIM, N. H., KIM, D. L., CHOI, K. M., BAIK, S. H. & CHOI, D. S. 2000. Serum insulin, proinsulin and proinsulin/insulin ratio in type 2 diabetic patients: as an index of beta-cell function or insulin resistance. *The Korean journal of internal medicine,* 15**,** 195-201.

KIMPIMAKI, T., KUPILA, A., HAMALAINEN, A. M., KUKKO, M., KULMALA, P., SAVOLA, K., SIMELL, T., KESKINEN, P., ILONEN, J., SIMELL, O. & KNIP, M. 2001. The first signs of beta-cell autoimmunity appear in infancy in genetically susceptible children from the general population: the Finnish Type 1 Diabetes Prediction and Prevention Study. *J Clin Endocrinol Metab,* 86**,** 4782-8.

KLEC, C., ZIOMEK, G., PICHLER, M., MALLI, R. & GRAIER, W. F. 2019. Calcium Signaling in ß-cell Physiology and Pathology: A Revisit. *International journal of molecular sciences,* 20**,** 6110.

KLUTH, O., MATZKE, D., KAMITZ, A., JÄHNERT, M., VOGEL, H., SCHERNECK, S., SCHULZE, M., STAIGER, H., MACHICAO, F., HÄRING, H.-U., JOOST, H.-G. & SCHÜRMANN, A. 2015. Identification of Four Mouse Diabetes Candidate Genes Altering β-Cell Proliferation. *PLOS Genetics,* 11**,** e1005506.

KNIP, M., VIRTANEN, S. M., SEPPA, K., ILONEN, J., SAVILAHTI, E., VAARALA, O., REUNANEN, A., TERAMO, K., HAMALAINEN, A. M., PARONEN, J., DOSCH, H. M., HAKULINEN, T. & AKERBLOM, H. K. 2010. Dietary intervention in infancy and later signs of beta-cell autoimmunity. *N Engl J Med,* 363**,** 1900-8.

KNOWLER, W. C., BARRETT-CONNOR, E., FOWLER, S. E., HAMMAN, R. F., LACHIN, J. M., WALKER, E. A. & NATHAN, D. M. 2002. Reduction in the incidence of type 2 diabetes with lifestyle intervention or metformin. *N Engl J Med,* 346**,** 393-403.

KOBAYASHI, M., YAMATO, E., TANABE, K., TASHIRO, F., MIYAZAKI, S. & MIYAZAKI, J. 2016. Functional Analysis of Novel Candidate Regulators of Insulin Secretion in the MIN6 Mouse Pancreatic β Cell Line. *PLoS One,* 11**,** e0151927.

KOMATSU, M., SATO, Y., YAMADA, S., YAMAUCHI, K., HASHIZUME, K. & AIZAWA, T. 2002. Triggering of Insulin Release by a Combination of cAMP Signal and Nutrients. *Diabetes,* 51**,** S29-S32.

KOMATSU, M., YAJIMA, H., YAMADA, S., KANEKO, T., SATO, Y., YAMAUCHI, K., HASHIZUME, K. & AIZAWA, T. 1999. Augmentation of Ca2+-stimulated insulin release by

glucose and long-chain fatty acids in rat pancreatic islets: free fatty acids mimic ATP-sensitive K+ channel-independent insulinotropic action of glucose. *Diabetes,* 48**,** 1543-9.
KOSKA, J., DELPARIGI, A., DE COURTEN, B., WEYER, C. & TATARANNI, P. A. 2004. Pancreatic Polypeptide Is Involved in the Regulation of Body Weight in Pima Indian Male Subjects. *Diabetes,* 53**,** 3091-3096.
KOTRONEN, A., JUURINEN, L., TIIKKAINEN, M., VEHKAVAARA, S. & YKI-JARVINEN, H. 2008. Increased liver fat, impaired insulin clearance, and hepatic and adipose tissue insulin resistance in type 2 diabetes. *Gastroenterology,* 135**,** 122-30.
KOTRONEN, A., VEHKAVAARA, S., SEPPALA-LINDROOS, A., BERGHOLM, R. & YKI-JARVINEN, H. 2007. Effect of liver fat on insulin clearance. *Am J Physiol Endocrinol Metab,* 293**,** E1709-15.
KRAEGEN, E. W., CLARK, P. W., JENKINS, A. B., DALEY, E. A., CHISHOLM, D. J. & STORLIEN, L. H. 1991. Development of muscle insulin resistance after liver insulin resistance in high-fat-fed rats. *Diabetes,* 40**,** 1397-403.
KRATZ, A. & CARNINCI, P. 2014. The devil in the details of RNA-seq. *Nat Biotechnol,* 32**,** 882-4.
KÜHLBRANDT, W. 2004. Biology, structure and mechanism of P-type ATPases. *Nature Reviews Molecular Cell Biology,* 5**,** 282-295.
KURAPATI, R., MCKENNA, C., LINDQVIST, J., WILLIAMS, D., SIMON, M., LEPROUST, E., BAKER, J., CHEESEMAN, M., CARROLL, N., DENNY, P., LAVAL, S., LOCHMÜLLER, H., OCHALA, J. & BLANCO, G. 2012. Myofibrillar myopathy caused by a mutation in the motor domain of mouse MyHC IIb. *Hum Mol Genet,* 21**,** 1706-24.
LAKHTAKIA, R. 2013. The history of diabetes mellitus. *Sultan Qaboos University medical journal,* 13**,** 368-370.
LAU, W., ANDREW, T. & MANIATIS, N. 2017. High-Resolution Genetic Maps Identify Multiple Type 2 Diabetes Loci at Regulatory Hotspots in African Americans and Europeans. *Am J Hum Genet,* 100**,** 803-816.
LAUENBORG, J., JØRGENSEN, M. K., DAMM, P., MAJOR-PEDERSEN, A., EIBERG, H., URHAMMER, S., PEDERSEN, O. & HANSEN, T. 2011. The influence of parental history of diabetes and offspring birthweight on offspring glucose metabolism in adulthood. *Acta Obstet Gynecol Scand,* 90**,** 1357-63.
LAW, C. W., ALHAMDOOSH, M., SU, S., DONG, X., TIAN, L., SMYTH, G. K. & RITCHIE, M. E. 2016. RNA-seq analysis is easy as 1-2-3 with limma, Glimma and edgeR. *F1000Research,* 5**,** ISCB Comm J-1408.
LAW, C. W., CHEN, Y., SHI, W. & SMYTH, G. K. 2014. voom: precision weights unlock linear model analysis tools for RNA-seq read counts. *Genome Biology,* 15**,** R29.
LAYBUTT, D. R., KANETO, H., HASENKAMP, W., GREY, S., JONAS, J.-C., SGROI, D. C., GROFF, A., FERRAN, C., BONNER-WEIR, S., SHARMA, A. & WEIR, G. C. 2002. Increased Expression of Antioxidant and Antiapoptotic Genes in Islets That May Contribute to β-Cell Survival During Chronic Hyperglycemia. *Diabetes,* 51**,** 413-423.
LAYBUTT, D. R., PRESTON, A. M., AKERFELDT, M. C., KENCH, J. G., BUSCH, A. K., BIANKIN, A. V. & BIDEN, T. J. 2007. Endoplasmic reticulum stress contributes to beta cell apoptosis in type 2 diabetes. *Diabetologia,* 50**,** 752-63.
LAZO-DE-LA-VEGA-MONROY, M.-L. & FERNANDEZ-MEJIA, C. 2011. Beta-Cell Function and Failure in Type 1 Diabetes. *Type 1 Diabetes - Pathogenesis, Genetics and Immunotherapy.*
LEE, C. M., COLAGIURI, R., MAGLIANO, D. J., CAMERON, A. J., SHAW, J., ZIMMET, P. & COLAGIURI, S. 2013. The cost of diabetes in adults in Australia. *Diabetes Res Clin Pract,* 99**,** 385-90.
LEE, E., RYU, G. R., KO, S. H., AHN, Y. B., YOON, K. H., HA, H. & SONG, K. H. 2011. Antioxidant treatment may protect pancreatic beta cells through the attenuation of islet fibrosis in an animal model of type 2 diabetes. *Biochem Biophys Res Commun,* 414**,** 397-402.
LEE, J., KIM, D. & KIM, C. 2017. Resistance Training for Glycemic Control, Muscular Strength, and Lean Body Mass in Old Type 2 Diabetic Patients: A Meta-Analysis. *Diabetes Ther,* 8**,** 459-473.
LEE, J. S., KIM, S. H., JUN, D. W., HAN, J. H., JANG, E. C., PARK, J. Y., SON, B. K., KIM, S. H., JO, Y. J., PARK, Y. S. & KIM, Y. S. 2009. Clinical implications of fatty pancreas:

correlations between fatty pancreas and metabolic syndrome. *World J Gastroenterol,* 15**,** 1869-75.

LEES-MILLER, J. P., GUO, J., SOMERS, J. R., ROACH, D. E., SHELDON, R. S., RANCOURT, D. E. & DUFF, H. J. 2003. Selective knockout of mouse ERG1 B potassium channel eliminates I(Kr) in adult ventricular myocytes and elicits episodes of abrupt sinus bradycardia. *Mol Cell Biol,* 23**,** 1856-62.

LEGCHENKO, E., LIU, B., WEST, J., VANGHELUWE, P., UPTON, P. & MORRELL, N. 2020. Protein truncating mutations in ATP13A3 promote pulmonary arterial hypertension in mice. *ERJ Open Research,* 6**,** 83.

LEMAIRE, K., RAVIER, M. A., SCHRAENEN, A., CREEMERS, J. W., VAN DE PLAS, R., GRANVIK, M., VAN LOMMEL, L., WAELKENS, E., CHIMIENTI, F., RUTTER, G. A., GILON, P., IN'T VELD, P. A. & SCHUIT, F. C. 2009. Insulin crystallization depends on zinc transporter ZnT8 expression, but is not required for normal glucose homeostasis in mice. *Proc Natl Acad Sci U S A,* 106**,** 14872-7.

LENZEN, S., DRINKGERN, J. & TIEDGE, M. 1996. Low antioxidant enzyme gene expression in pancreatic islets compared with various other mouse tissues. *Free Radic Biol Med,* 20**,** 463-6.

LEVETAN, C. 2010. Distinctions between islet neogenesis and β-cell replication: Implications for reversal of Type 1 and 2 diabetes. *Journal of Diabetes,* 2**,** 76-84.

LI, H. & DURBIN, R. 2009. Fast and accurate short read alignment with Burrows–Wheeler transform. *Bioinformatics,* 25**,** 1754-1760.

LI, H., HANDSAKER, B., WYSOKER, A., FENNELL, T., RUAN, J., HOMER, N., MARTH, G., ABECASIS, G. & DURBIN, R. 2009. The Sequence Alignment/Map format and SAMtools. *Bioinformatics,* 25**,** 2078-9.

LI, J., HOUSEKNECHT, K. L., STENBIT, A. E., KATZ, E. B. & CHARRON, M. J. 2000a. Reduced glucose uptake precedes insulin signaling defects in adipocytes from heterozygous GLUT4 knockout mice. *Faseb j,* 14**,** 1117-25.

LI, M., BAUMEISTER, P., ROY, B., PHAN, T., FOTI, D., LUO, S. & LEE, A. S. 2000b. ATF6 as a transcription activator of the endoplasmic reticulum stress element: thapsigargin stress-induced changes and synergistic interactions with NF-Y and YY1. *Molecular and cellular biology,* 20**,** 5096-5106.

LI, P., FAN, W., XU, J., LU, M., YAMAMOTO, H., AUWERX, J., SEARS, D. D., TALUKDAR, S., OH, D., CHEN, A., BANDYOPADHYAY, G., SCADENG, M., OFRECIO, J. M., NALBANDIAN, S. & OLEFSKY, J. M. 2011. Adipocyte NCoR knockout decreases PPARγ phosphorylation and enhances PPARγ activity and insulin sensitivity. *Cell,* 147**,** 815-26.

LI, R., XIE, J., WU, H., LI, G., CHEN, J., CHEN, Q., WANG, L. & XU, B. 2016a. Syndecan-4 shedding impairs macrovascular angiogenesis in diabetes mellitus. *Biochem Biophys Res Commun,* 474**,** 15-21.

LI, X., LI, C. & SUN, G. 2016b. Histone Acetylation and Its Modifiers in the Pathogenesis of Diabetic Nephropathy. *Journal of Diabetes Research,* 2016**,** 4065382.

LI, X., ROSZKO, I., SEPICH, D. S., NI, M., HAMM, H. E., MARLOW, F. L. & SOLNICA-KREZEL, L. 2013. Gpr125 modulates Dishevelled distribution and planar cell polarity signaling. *Development,* 140**,** 3028-39.

LI, Y., JIANG, W., NIU, Q., SUN, Y., MENG, C., TAN, L., SONG, C., QIU, X., LIAO, Y. & DING, C. 2019. eIF2α-CHOP-BCl-2/JNK and IRE1α-XBP1/JNK signaling promote apoptosis and inflammation and support the proliferation of Newcastle disease virus. *Cell Death & Disease,* 10**,** 891.

LIANG, J. Q., TEOH, N., XU, L., POK, S., LI, X., CHU, E. S. H., CHIU, J., DONG, L., ARFIANTI, E., HAIGH, W. G., YEH, M. M., IOANNOU, G. N., SUNG, J. J. Y., FARRELL, G. & YU, J. 2018. Dietary cholesterol promotes steatohepatitis related hepatocellular carcinoma through dysregulated metabolism and calcium signaling. *Nature Communications,* 9**,** 4490.

LIBERZON, A., BIRGER, C., THORVALDSDÓTTIR, H., GHANDI, M., MESIROV, J. P. & TAMAYO, P. 2015. The Molecular Signatures Database (MSigDB) hallmark gene set collection. *Cell systems,* 1**,** 417-425.

LICHOLAI, J. A., NGUYEN, K. P., FOBBS, W. C., SCHUSTER, C. J., ALI, M. A. & KRAVITZ, A. V. 2018. Why Do Mice Overeat High-Fat Diets? How High-Fat Diet Alters the Regulation of Daily Caloric Intake in Mice. *Obesity (Silver Spring, Md.),* 26**,** 1026-1033.

LIGHT, P. E., MANNING FOX, J. E., RIEDEL, M. J. & WHEELER, M. B. 2002. Glucagon-like peptide-1 inhibits pancreatic ATP-sensitive potassium channels via a protein kinase A- and ADP-dependent mechanism. *Mol Endocrinol,* 16**,** 2135-44.

LILUE, J., DORAN, A. G., FIDDES, I. T., ABRUDAN, M., ARMSTRONG, J., BENNETT, R., CHOW, W., COLLINS, J., COLLINS, S., CZECHANSKI, A., DANECEK, P., DIEKHANS, M., DOLLE, D.-D., DUNN, M., DURBIN, R., EARL, D., FERGUSON-SMITH, A., FLICEK, P., FLINT, J., FRANKISH, A., FU, B., GERSTEIN, M., GILBERT, J., GOODSTADT, L., HARROW, J., HOWE, K., IBARRA-SORIA, X., KOLMOGOROV, M., LELLIOTT, C. J., LOGAN, D. W., LOVELAND, J., MATHEWS, C. E., MOTT, R., MUIR, P., NACHTWEIDE, S., NAVARRO, F. C. P., ODOM, D. T., PARK, N., PELAN, S., PHAM, S. K., QUAIL, M., REINHOLDT, L., ROMOTH, L., SHIRLEY, L., SISU, C., SJOBERG-HERRERA, M., STANKE, M., STEWARD, C., THOMAS, M., THREADGOLD, G., THYBERT, D., TORRANCE, J., WONG, K., WOOD, J., YALCIN, B., YANG, F., ADAMS, D. J., PATEN, B. & KEANE, T. M. 2018. Sixteen diverse laboratory mouse reference genomes define strain-specific haplotypes and novel functional loci. *Nature Genetics,* 50**,** 1574-1583.

LIM, S., BAE, J. H., CHUN, E. J., KIM, H., KIM, S. Y., KIM, K. M., CHOI, S. H., PARK, K. S., FLOREZ, J. C. & JANG, H. C. 2014. Differences in pancreatic volume, fat content, and fat density measured by multidetector-row computed tomography according to the duration of diabetes. *Acta Diabetol,* 51**,** 739-48.

LINDQVIST, J., IWAMOTO, H., BLANCO, G. & OCHALA, J. 2013. The fraction of strongly bound cross-bridges is increased in mice that carry the myopathy-linked myosin heavy chain mutation MYH4L342Q. *Dis Model Mech,* 6**,** 834-40.

LIPSON, K. L., FONSECA, S. G., ISHIGAKI, S., NGUYEN, L. X., FOSS, E., BORTELL, R., ROSSINI, A. A. & URANO, F. 2006. Regulation of insulin biosynthesis in pancreatic beta cells by an endoplasmic reticulum-resident protein kinase IRE1. *Cell Metab,* 4**,** 245-54.

LIPSON, K. L., GHOSH, R. & URANO, F. 2008. The role of IRE1alpha in the degradation of insulin mRNA in pancreatic beta-cells. *PLoS One,* 3**,** e1648.

LIU, B., LEGCHENKO, E., WEST, J. A., HAMOUDA, N., VANGHELUWE, P., UPTON, P. D. & MORRELL, N. A. 2019. ATP13A3 Loss of Function Disrupts Polyamine Homeostasis in Pulmonary Arterial Endothelial Cells. *Circulation,* 140**,** A14378-A14378.

LIU, R., HOLIK, A. Z., SU, S., JANSZ, N., CHEN, K., LEONG, H. S., BLEWITT, M. E., ASSELIN-LABAT, M.-L., SMYTH, G. K. & RITCHIE, M. E. 2015. Why weight? Modelling sample and observational level variability improves power in RNA-seq analyses. *Nucleic Acids Research,* 43**,** e97-e97.

LIU, Y. L., SEMJONOUS, N. M., MURPHY, K. G., GHATEI, M. A. & BLOOM, S. R. 2008. The effects of pancreatic polypeptide on locomotor activity and food intake in mice. *Int J Obes (Lond),* 32**,** 1712-5.

LIU, Y. Q., HAN, J., EPSTEIN, P. N. & LONG, Y. S. 2005. Enhanced rat beta-cell proliferation in 60% pancreatectomized islets by increased glucose metabolic flux through pyruvate carboxylase pathway. *Am J Physiol Endocrinol Metab,* 288**,** E471-8.

LIU, Y. Q., JETTON, T. L. & LEAHY, J. L. 2002. β-Cell Adaptation to Insulin Resistance: INCREASED PYRUVATE CARBOXYLASE AND MALATE-PYRUVATE SHUTTLE ACTIVITY IN ISLETS OF NONDIABETIC ZUCKER FATTY RATS. *Journal of Biological Chemistry,* 277**,** 39163-39168.

LONGNECKER, D. 2014. Anatomy and Histology of the Pancreas. *Pancreapedia: Exocrine Pancreas Knowledge Base***,** 1-26.

LUPI, R., DOTTA, F., MARSELLI, L., DEL GUERRA, S., MASINI, M., SANTANGELO, C., PATANÉ, G., BOGGI, U., PIRO, S., ANELLO, M., BERGAMINI, E., MOSCA, F., DI MARIO, U., DEL PRATO, S. & MARCHETTI, P. 2002. Prolonged exposure to free fatty acids has cytostatic and pro-apoptotic effects on human pancreatic islets: evidence that beta-

cell death is caspase mediated, partially dependent on ceramide pathway, and Bcl-2 regulated. *Diabetes,* 51**,** 1437-42.
LYSSENKO, V., ALMGREN, P., ANEVSKI, D., PERFEKT, R., LAHTI, K., NISSEN, M., ISOMAA, B., FORSEN, B., HOMSTROM, N., SALORANTA, C., TASKINEN, M. R., GROOP, L. & TUOMI, T. 2005. Predictors of and longitudinal changes in insulin sensitivity and secretion preceding onset of type 2 diabetes. *Diabetes,* 54**,** 166-74.
MACDONALD, P. E. & RORSMAN, P. 2006. Oscillations, Intercellular Coupling, and Insulin Secretion in Pancreatic β Cells. *PLOS Biology,* 4**,** e49.
MACK, C., WILSON, J., ATHANACIO, J., REYNOLDS, J., LAUGERO, K., GUSS, S., VU, C., ROTH, J. & PARKES, D. 2007. Pharmacological actions of the peptide hormone amylin in the long-term regulation of food intake, food preference, and body weight. *Am J Physiol Regul Integr Comp Physiol,* 293**,** R1855-63.
MADAN, M., PATEL, A., SKRUBER, K., GEERTS, D., ALTOMARE, D. A. & IV, O. P. 2016. ATP13A3 and caveolin-1 as potential biomarkers for difluoromethylornithine-based therapies in pancreatic cancers. *Am J Cancer Res,* 6**,** 1231-52.
MAECHLER, P. & WOLLHEIM, C. B. 1999. Mitochondrial glutamate acts as a messenger in glucose-induced insulin exocytosis. *Nature,* 402**,** 685-9.
MAEDLER, K., OBERHOLZER, J., BUCHER, P., SPINAS, G. A. & DONATH, M. Y. 2003. Monounsaturated fatty acids prevent the deleterious effects of palmitate and high glucose on human pancreatic beta-cell turnover and function. *Diabetes,* 52**,** 726-33.
MAEDLER, K., SERGEEV, P., RIS, F., OBERHOLZER, J., JOLLER-JEMELKA, H. I., SPINAS, G. A., KAISER, N., HALBAN, P. A. & DONATH, M. Y. 2002. Glucose-induced beta cell production of IL-1beta contributes to glucotoxicity in human pancreatic islets. *J Clin Invest,* 110**,** 851-60.
MAHAJAN, A., GO, M. J., ZHANG, W., BELOW, J. E., GAULTON, K. J., FERREIRA, T., HORIKOSHI, M., JOHNSON, A. D., NG, M. C. Y., PROKOPENKO, I., SALEHEEN, D., WANG, X., ZEGGINI, E., ABECASIS, G. R., ADAIR, L. S., ALMGREN, P., ATALAY, M., AUNG, T., BALDASSARRE, D., BALKAU, B., BAO, Y., BARNETT, A. H., BARROSO, I., BASIT, A., BEEN, L. F., BEILBY, J., BELL, G. I., BENEDIKTSSON, R., BERGMAN, R. N., BOEHM, B. O., BOERWINKLE, E., BONNYCASTLE, L. L., BURTT, N., CAI, Q., CAMPBELL, H., CAREY, J., CAUCHI, S., CAULFIELD, M., CHAN, J. C. N., CHANG, L.-C., CHANG, T.-J., CHANG, Y.-C., CHARPENTIER, G., CHEN, C.-H., CHEN, H., CHEN, Y.-T., CHIA, K.-S., CHIDAMBARAM, M., CHINES, P. S., CHO, N. H., CHO, Y. M., CHUANG, L.-M., COLLINS, F. S., CORNELIS, M. C., COUPER, D. J., CRENSHAW, A. T., VAN DAM, R. M., DANESH, J., DAS, D., DE FAIRE, U., DEDOUSSIS, G., DELOUKAS, P., DIMAS, A. S., DINA, C., DONEY, A. S. F., DONNELLY, P. J., DORKHAN, M., VAN DUIJN, C., DUPUIS, J., EDKINS, S., ELLIOTT, P., EMILSSON, V., ERBEL, R., ERIKSSON, J. G., ESCOBEDO, J., ESKO, T., EURY, E., FLOREZ, J. C., FONTANILLAS, P., FOROUHI, N. G., FORSEN, T., FOX, C., FRASER, R. M., FRAYLING, T. M., FROGUEL, P., FROSSARD, P., GAO, Y., GERTOW, K., GIEGER, C., GIGANTE, B., GRALLERT, H., GRANT, G. B., GROOP, L. C., GROVES, C. J., GRUNDBERG, E., GUIDUCCI, C., HAMSTEN, A., HAN, B.-G., HARA, K., HASSANALI, N., et al. 2014. Genome-wide trans-ancestry meta-analysis provides insight into the genetic architecture of type 2 diabetes susceptibility. *Nature Genetics,* 46**,** 234-244.
MAHENDRAN, Y., CEDERBERG, H., VANGIPURAPU, J., KANGAS, A. J., SOININEN, P., KUUSISTO, J., UUSITUPA, M., ALA-KORPELA, M. & LAAKSO, M. 2013. Glycerol and fatty acids in serum predict the development of hyperglycemia and type 2 diabetes in Finnish men. *Diabetes Care,* 36**,** 3732-8.
MAJ, M., MILENKOVIC, I., BAUER, J., BERGGÅRD, T., VEIT, M., ILHAN-MUTLU, A., WAGNER, L. & TRETTER, V. 2012. Novel insights into the distribution and functional aspects of the calcium binding protein secretagogin from studies on rat brain and primary neuronal cell culture. *Front Mol Neurosci,* 5**,** 84.
MAKINO, S., KUNIMOTO, K., MURAOKA, Y., MIZUSHIMA, Y., KATAGIRI, K. & TOCHINO, Y. 1980. Breeding of a non-obese, diabetic strain of mice. *Jikken Dobutsu,* 29**,** 1-13.

MALENCZYK, K., GIRACH, F., SZODORAI, E., STORM, P., SEGERSTOLPE, Å., TORTORIELLO, G., SCHNELL, R., MULDER, J., ROMANOV, R. A., BORÓK, E., PISCITELLI, F., DI MARZO, V., SZABÓ, G., SANDBERG, R., KUBICEK, S., LUBEC, G., HÖKFELT, T., WAGNER, L., GROOP, L. & HARKANY, T. 2017. A TRPV1-to-secretagogin regulatory axis controls pancreatic β-cell survival by modulating protein turnover. *Embo j,* 36**,** 2107-2125.

MALENCZYK, K., SZODORAI, E., SCHNELL, R., LUBEC, G., SZABÓ, G., HÖKFELT, T. & HARKANY, T. 2018. Secretagogin protects Pdx1 from proteasomal degradation to control a transcriptional program required for β cell specification. *Molecular metabolism,* 14**,** 108-120.

MARCHETTI, P., BUGLIANI, M., LUPI, R., MARSELLI, L., MASINI, M., BOGGI, U., FILIPPONI, F., WEIR, G. C., EIZIRIK, D. L. & CNOP, M. 2007. The endoplasmic reticulum in pancreatic beta cells of type 2 diabetes patients. *Diabetologia,* 50**,** 2486-94.

MARTINDALE, J. J., FERNANDEZ, R., THUERAUF, D., WHITTAKER, R., GUDE, N., SUSSMAN, M. A. & GLEMBOTSKI, C. C. 2006. Endoplasmic reticulum stress gene induction and protection from ischemia/reperfusion injury in the hearts of transgenic mice with a tamoxifen-regulated form of ATF6. *Circ Res,* 98**,** 1186-93.

MATHUR, A., MARINE, M., LU, D., SWARTZ-BASILE, D. A., SAXENA, R., ZYROMSKI, N. J. & PITT, H. A. 2007. Nonalcoholic fatty pancreas disease. *HPB,* 9**,** 312-318.

MCCLELLAN, J. & KING, M.-C. 2010. Genetic Heterogeneity in Human Disease. *Cell,* 141**,** 210-217.

MCCULLOCH, L. J., VAN DE BUNT, M., BRAUN, M., FRAYN, K. N., CLARK, A. & GLOYN, A. L. 2011. GLUT2 (SLC2A2) is not the principal glucose transporter in human pancreatic beta cells: implications for understanding genetic association signals at this locus. *Mol Genet Metab,* 104**,** 648-53.

MCKENNA, A., HANNA, M., BANKS, E., SIVACHENKO, A., CIBULSKIS, K., KERNYTSKY, A., GARIMELLA, K., ALTSHULER, D., GABRIEL, S., DALY, M. & DEPRISTO, M. A. 2010. The Genome Analysis Toolkit: a MapReduce framework for analyzing next-generation DNA sequencing data. *Genome research,* 20**,** 1297-1303.

MCKENZIE, M. D., JAMIESON, E., JANSEN, E. S., SCOTT, C. L., HUANG, D. C., BOUILLET, P., ALLISON, J., KAY, T. W., STRASSER, A. & THOMAS, H. E. 2010. Glucose induces pancreatic islet cell apoptosis that requires the BH3-only proteins Bim and Puma and multi-BH domain protein Bax. *Diabetes,* 59**,** 644-52.

MEIGS, J. B., CUPPLES, L. A. & WILSON, P. W. 2000. Parental transmission of type 2 diabetes: the Framingham Offspring Study. *Diabetes,* 49**,** 2201-7.

MEIJSSEN, S., CABEZAS, M. C., BALLIEUX, C. G. M., DERKSEN, R. J., BILECEN, S. & ERKELENS, D. W. 2001. Insulin Mediated Inhibition of Hormone Sensitive Lipase Activity in Vivo in Relation to Endogenous Catecholamines in Healthy Subjects. *The Journal of Clinical Endocrinology & Metabolism,* 86**,** 4193-4197.

MELLOUL, D., MARSHAK, S. & CERASI, E. 2002. Regulation of insulin gene transcription. *Diabetologia,* 45**,** 309-26.

METSALU, T. & VILO, J. 2015. ClustVis: a web tool for visualizing clustering of multivariate data using Principal Component Analysis and heatmap. *Nucleic Acids Research,* 43**,** W566-W570.

MICHALSKA, M., WOLF, G., WALTHER, R. & NEWSHOLME, P. 2010. Effects of pharmacological inhibition of NADPH oxidase or iNOS on pro-inflammatory cytokine, palmitic acid or H2O2-induced mouse islet or clonal pancreatic β-cell dysfunction. *Biosci Rep,* 30**,** 445-53.

MIKI, A., RICORDI, C., SAKUMA, Y., YAMAMOTO, T., MISAWA, R., MITA, A., MOLANO, R. D., VAZIRI, N. D., PILEGGI, A. & ICHII, H. 2018. Divergent antioxidant capacity of human islet cell subsets: A potential cause of beta-cell vulnerability in diabetes and islet transplantation. *PLoS One,* 13**,** e0196570.

MILOSEVIC, N., KÜHNEMUTH, B., MÜHLBERG, L., RIPKA, S., GRIESMANN, H., LÖLKES, C., BUCHHOLZ, M., AUST, D., PILARSKY, C., KRUG, S., GRESS, T. & MICHL, P. 2013. Synthetic lethality screen identifies RPS6KA2 as modifier of epidermal growth factor receptor activity in pancreatic cancer. *Neoplasia (New York, N.Y.),* 15**,** 1354-1362.

MINGES, K. E., ZIMMET, P., MAGLIANO, D. J., DUNSTAN, D. W., BROWN, A. & SHAW, J. E. 2011. Diabetes prevalence and determinants in Indigenous Australian populations: A systematic review. *Diabetes Res Clin Pract,* 93**,** 139-149.

MINN, A. H., HAFELE, C. & SHALEV, A. 2005. Thioredoxin-interacting protein is stimulated by glucose through a carbohydrate response element and induces beta-cell apoptosis. *Endocrinology,* 146**,** 2397-405.

MIRZAEI, H., AKRAMI, S. M., GOLMOHAMMADI, T., DOOSTI, M., HESHMAT, R., NAKHJAVANI, M. & AMIRI, P. 2009. Polymorphism of Pro12Ala in the peroxisome proliferator-activated receptor gamma2 gene in Iranian diabetic and obese subjects. *Metab Syndr Relat Disord,* 7**,** 453-8.

MITOK, K. A., FREIBERGER, E. C., SCHUELER, K. L., RABAGLIA, M. E., STAPLETON, D. S., KWIECIEN, N. W., MALEC, P. A., HEBERT, A. S., BROMAN, A. T., KENNEDY, R. T., KELLER, M. P., COON, J. J. & ATTIE, A. D. 2018. Islet proteomics reveals genetic variation in dopamine production resulting in altered insulin secretion. *J Biol Chem,* 293**,** 5860-5877.

MIURA, T., NISHINAKA, T. & TERADA, T. 2008. Different functions between human monomeric carbonyl reductase 3 and carbonyl reductase 1. *Mol Cell Biochem,* 315**,** 113-21.

MIZUKAMI, H., TAKAHASHI, K., INABA, W., OSONOI, S., KAMATA, K., TSUBOI, K. & YAGIHASHI, S. 2014. Age-associated changes of islet endocrine cells and the effects of body mass index in Japanese. *Journal of diabetes investigation,* 5**,** 38-47.

MOLINA, J., RODRIGUEZ-DIAZ, R., FACHADO, A., JACQUES-SILVA, M. C., BERGGREN, P.-O. & CAICEDO, A. 2014. Control of insulin secretion by cholinergic signaling in the human pancreatic islet. *Diabetes,* 63**,** 2714-2726.

MØLLER, A. B., KAMPMANN, U., HEDEGAARD, J., THORSEN, K., NORDENTOFT, I., VENDELBO, M. H., MØLLER, N. & JESSEN, N. 2017. Altered gene expression and repressed markers of autophagy in skeletal muscle of insulin resistant patients with type 2 diabetes. *Scientific Reports,* 7**,** 43775.

MORA, C., WONG, F. S., CHANG, C. H. & FLAVELL, R. A. 1999. Pancreatic infiltration but not diabetes occurs in the relative absence of MHC class II-restricted CD4 T cells: studies using NOD/CIITA-deficient mice. *J Immunol,* 162**,** 4576-88.

MOTTIS, A., MOUCHIROUD, L. & AUWERX, J. 2013. Emerging roles of the corepressors NCoR1 and SMRT in homeostasis. *Genes Dev,* 27**,** 819-35.

MOUTON-LIGER, F., THOMAS, S., RATTENBACH, R., MAGNOL, L., LARIGALDIE, V., LEDRU, A., HERAULT, Y., VERNEY, C. & CRÉAU, N. 2011. PCP4 (PEP19) overexpression induces premature neuronal differentiation associated with Ca(2+) /calmodulin-dependent kinase II-δ activation in mouse models of Down syndrome. *J Comp Neurol,* 519**,** 2779-802.

MUGABO, Y., ZHAO, S., LAMONTAGNE, J., AL-MASS, A., PEYOT, M. L., CORKEY, B. E., JOLY, E., MADIRAJU, S. R. M. & PRENTKI, M. 2017. Metabolic fate of glucose and candidate signaling and excess-fuel detoxification pathways in pancreatic β-cells. *J Biol Chem,* 292**,** 7407-7422.

MUGABO, Y., ZHAO, S., SEIFRIED, A., GEZZAR, S., AL-MASS, A., ZHANG, D., LAMONTAGNE, J., ATTANE, C., POURSHARIFI, P., IGLESIAS, J., JOLY, E., PEYOT, M. L., GOHLA, A., MADIRAJU, S. R. & PRENTKI, M. 2016. Identification of a mammalian glycerol-3-phosphate phosphatase: Role in metabolism and signaling in pancreatic β-cells and hepatocytes. *Proc Natl Acad Sci U S A,* 113**,** E430-9.

MÜHLBAUER, E., BAZWINSKY, I., WOLGAST, S., KLEMENZ, A. & PESCHKE, E. 2007. Circadian changes of ether-a-go-go-related-gene (Erg) potassium channel transcripts in the rat pancreas and beta-cell. *Cell Mol Life Sci,* 64**,** 768-80.

MULLER, L. M., GORTER, K. J., HAK, E., GOUDZWAARD, W. L., SCHELLEVIS, F. G., HOEPELMAN, A. I. & RUTTEN, G. E. 2005. Increased risk of common infections in patients with type 1 and type 2 diabetes mellitus. *Clin Infect Dis,* 41**,** 281-8.

MURANO, I., BARBATELLI, G., PARISANI, V., LATINI, C., MUZZONIGRO, G., CASTELLUCCI, M. & CINTI, S. 2008. Dead adipocytes, detected as crown-like structures, are prevalent in visceral fat depots of genetically obese mice. *J Lipid Res,* 49**,** 1562-8.

NAGAO, M., ASAI, A., KAWAHARA, M., NAKAJIMA, Y., SATO, Y., TANIMURA, K., OKAJIMA, F., TAKAYA, M., SUDO, M., TAKEMITSU, S., HARADA, T., SUGIHARA, H. & OIKAWA, S. 2012. Selective breeding of mice for different susceptibilities to high fat diet-induced glucose intolerance: Development of two novel mouse lines, Selectively bred Diet-induced Glucose intolerance-Prone and -Resistant. *Journal of diabetes investigation,* 3**,** 245-251.

NAJA, F., HWALLA, N., ITANI, L., SALEM, M., AZAR, S. T., ZEIDAN, M. N. & NASREDDINE, L. 2012. Dietary patterns and odds of Type 2 diabetes in Beirut, Lebanon: a case-control study. *Nutr Metab (Lond),* 9**,** 111.

NAJJAR, S. M. & PERDOMO, G. 2019. Hepatic Insulin Clearance: Mechanism and Physiology. *Physiology (Bethesda),* 34**,** 198-215.

NAKAMURA, A., MIYOSHI, H., UKAWA, S., NAKAMURA, K., NAKAGAWA, T., TERAUCHI, Y., TAMAKOSHI, A. & ATSUMI, T. 2020. Proinsulin is sensitive to reflect glucose intolerance. *J Diabetes Investig,* 11**,** 75-79.

NAM, J. S., HAN, J. W., LEE, S. B., YOU, J. H., KIM, M. J., KANG, S., PARK, J. S. & AHN, C. W. 2018. Calpain-10 and Adiponectin Gene Polymorphisms in Korean Type 2 Diabetes Patients. *Endocrinology and metabolism (Seoul, Korea),* 33**,** 364-371.

NAUCK, M. A., HOMBERGER, E., SIEGEL, E. G., ALLEN, R. C., EATON, R. P., EBERT, R. & CREUTZFELDT, W. 1986. Incretin effects of increasing glucose loads in man calculated from venous insulin and C-peptide responses. *J Clin Endocrinol Metab,* 63**,** 492-8.

NCD RISK FACTOR COLLABORATION 2016. Worldwide trends in diabetes since 1980: a pooled analysis of 751 population-based studies with 4.4 million participants. *Lancet,* 387**,** 1513-1530.

NEUENSCHWANDER, M., BALLON, A., WEBER, K. S., NORAT, T., AUNE, D., SCHWINGSHACKL, L. & SCHLESINGER, S. 2019. Role of diet in type 2 diabetes incidence: umbrella review of meta-analyses of prospective observational studies. *BMJ,* 366**,** l2368.

NG, P. C. & HENIKOFF, S. 2001. Predicting deleterious amino acid substitutions. *Genome Res,* 11**,** 863-74.

NG, P. C. & HENIKOFF, S. 2003. SIFT: Predicting amino acid changes that affect protein function. *Nucleic acids research,* 31**,** 3812-3814.

NICOLSON, T. J., BELLOMO, E. A., WIJESEKARA, N., LODER, M. K., BALDWIN, J. M., GYULKHANDANYAN, A. V., KOSHKIN, V., TARASOV, A. I., CARZANIGA, R., KRONENBERGER, K., TANEJA, T. K., DA SILVA XAVIER, G., LIBERT, S., FROGUEL, P., SCHARFMANN, R., STETSYUK, V., RAVASSARD, P., PARKER, H., GRIBBLE, F. M., REIMANN, F., SLADEK, R., HUGHES, S. J., JOHNSON, P. R., MASSEBOEUF, M., BURCELIN, R., BALDWIN, S. A., LIU, M., LARA-LEMUS, R., ARVAN, P., SCHUIT, F. C., WHEELER, M. B., CHIMIENTI, F. & RUTTER, G. A. 2009. Insulin storage and glucose homeostasis in mice null for the granule zinc transporter ZnT8 and studies of the type 2 diabetes-associated variants. *Diabetes,* 58**,** 2070-83.

NIKITIN, A. G., POTAPOV, V. Y., BROVKINA, O. I., KOKSHAROVA, E. O., KHODYREV, D. S., PHILIPPOV, Y. I., MICHUROVA, M. S., SHAMKHALOVA, M. S., VIKULOVA, O. K., SMETANINA, S. A., SUPLOTOVA, L. A., KONONENKO, I. V., KALASHNIKOV, V. Y., SMIRNOVA, O. M., MAYOROV, A. Y., NOSIKOV, V. V., AVERYANOV, A. V. & SHESTAKOVA, M. V. 2017. Association of polymorphic markers of genes FTO, KCNJ11, CDKAL1, SLC30A8, and CDKN2B with type 2 diabetes mellitus in the Russian population. *PeerJ,* 5**,** e3414.

NOBLE, J. A., VALDES, A. M., VARNEY, M. D., CARLSON, J. A., MOONSAMY, P., FEAR, A. L., LANE, J. A., LAVANT, E., RAPPNER, R., LOUEY, A., CONCANNON, P., MYCHALECKYJ, J. C. & ERLICH, H. A. 2010. HLA class I and genetic susceptibility to type 1 diabetes: results from the Type 1 Diabetes Genetics Consortium. *Diabetes,* 59**,** 2972-9.

NODA, M., KOMATSU, M. & SHARP, G. W. G. 1996. The βHC-9 Pancreatic β-Cell Line Preserves the Characteristics of Progenitor Mouse Islets. *Diabetes,* 45**,** 1766-1773.

NOLAN, C. J., LEAHY, J. L., DELGHINGARO-AUGUSTO, V., MOIBI, J., SONI, K., PEYOT, M. L., FORTIER, M., GUAY, C., LAMONTAGNE, J., BARBEAU, A., PRZYBYTKOWSKI,

E., JOLY, E., MASIELLO, P., WANG, S., MITCHELL, G. A. & PRENTKI, M. 2006a. Beta cell compensation for insulin resistance in Zucker fatty rats: increased lipolysis and fatty acid signalling. *Diabetologia,* 49**,** 2120-30.

NOLAN, C. J., MADIRAJU, M. S. R., DELGHINGARO-AUGUSTO, V., PEYOT, M.-L. & PRENTKI, M. 2006b. Fatty Acid Signaling in the β-Cell and Insulin Secretion. *Diabetes,* 55**,** S16-S23.

NOLAN, C. J. & PRENTKI, M. 2019. Insulin resistance and insulin hypersecretion in the metabolic syndrome and type 2 diabetes: Time for a conceptual framework shift. *Diab Vasc Dis Res,* 16**,** 118-127.

NOORCHASHM, H., NOORCHASHM, N., KERN, J., ROSTAMI, S. Y., BARKER, C. F. & NAJI, A. 1997. B-cells are required for the initiation of insulitis and sialitis in nonobese diabetic mice. *Diabetes,* 46**,** 941-6.

NORDMANN, T. M., DROR, E., SCHULZE, F., TRAUB, S., BERISHVILI, E., BARBIEUX, C., BÖNI-SCHNETZLER, M. & DONATH, M. Y. 2017. The Role of Inflammation in β-cell Dedifferentiation. *Sci Rep,* 7**,** 6285.

NORLING, L. L., COLCA, J. R., KELLY, P. T., MCDANIEL, M. L. & LANDT, M. 1994. Activation of calcium and calmodulin dependent protein kinase II during stimulation of insulin secretion. *Cell Calcium,* 16**,** 137-50.

NSEIR, W., NASSAR, F. & ASSY, N. 2010. Soft drinks consumption and nonalcoholic fatty liver disease. *World J Gastroenterol,* 16**,** 2579-88.

NYAGA, D. M., VICKERS, M. H., JEFFERIES, C., PERRY, J. K. & O'SULLIVAN, J. M. 2018. Type 1 Diabetes Mellitus-Associated Genetic Variants Contribute to Overlapping Immune Regulatory Networks. *Frontiers in Genetics,* 9.

NYE, C. K., HANSON, R. W. & KALHAN, S. C. 2008. Glyceroneogenesis is the dominant pathway for triglyceride glycerol synthesis in vivo in the rat. *The Journal of biological chemistry,* 283**,** 27565-27574.

O'YOUNG, J., LIAO, Y., XIAO, Y., JALKANEN, J., LAJOIE, G., KARTTUNEN, M., GOLDBERG, H. A. & HUNTER, G. K. 2011. Matrix Gla Protein Inhibits Ectopic Calcification by a Direct Interaction with Hydroxyapatite Crystals. *Journal of the American Chemical Society,* 133**,** 18406-18412.

OKUN, M. M. & SHIELDS, D. 1992. Translocation of preproinsulin across the endoplasmic reticulum membrane. The relationship between nascent polypeptide size and extent of signal recognition particle-mediated inhibition of protein synthesis. *J Biol Chem,* 267**,** 11476-82.

OLOFSSON, S. O., STILLEMARK-BILLTON, P. & ASP, L. 2000. Intracellular assembly of VLDL: two major steps in separate cell compartments. *Trends Cardiovasc Med,* 10**,** 338-45.

OLSON, L. K., REDMON, J. B., TOWLE, H. C. & ROBERTSON, R. P. 1993. Chronic exposure of HIT cells to high glucose concentrations paradoxically decreases insulin gene transcription and alters binding of insulin gene regulatory protein. *J Clin Invest,* 92**,** 514-9.

OTTOSSON-LAAKSO, E., KRUS, U., STORM, P., PRASAD, R. B., OSKOLKOV, N., AHLQVIST, E., FADISTA, J., HANSSON, O., GROOP, L. & VIKMAN, P. 2017. Glucose-Induced Changes in Gene Expression in Human Pancreatic Islets: Causes or Consequences of Chronic Hyperglycemia. *Diabetes,* 66**,** 3013-3028.

OU-YANG, Q., LIN, X.-M., ZHU, Y.-J., ZHENG, B., LI, L., YANG, Y.-C., HOU, G.-J., CHEN, X., LUO, G.-J., HUO, F., LENG, Q.-B., GONZALEZ, F. J., JIANG, X.-Q., WANG, H.-Y. & CHEN, L. 2018. Distinct role of nuclear receptor corepressor 1 regulated de novo fatty acids synthesis in liver regeneration and hepatocarcinogenesis in mice. *Hepatology (Baltimore, Md.),* 67**,** 1071-1087.

OYADOMARI, S., KOIZUMI, A., TAKEDA, K., GOTOH, T., AKIRA, S., ARAKI, E. & MORI, M. 2002. Targeted disruption of the Chop gene delays endoplasmic reticulum stress-mediated diabetes. *J Clin Invest,* 109**,** 525-32.

OZAKI, N., SHIBASAKI, T., KASHIMA, Y., MIKI, T., TAKAHASHI, K., UENO, H., SUNAGA, Y., YANO, H., MATSUURA, Y., IWANAGA, T., TAKAI, Y. & SEINO, S. 2000. cAMP-GEFII is a direct target of cAMP in regulated exocytosis. *Nat Cell Biol,* 2**,** 805-11.

OZAWA, S., KATSUTA, H., SUZUKI, K., TAKAHASHI, K., TANAKA, T., SUMITANI, Y., NISHIDA, S., YOSHIMOTO, K. & ISHIDA, H. 2014. Estimated proinsulin processing

activity of prohormone convertase (PC) 1/3 rather than PC2 is decreased in pancreatic β-cells of type 2 diabetic patients. *Endocr J,* 61**,** 607-14.
PALMGREN, M. G. & NISSEN, P. 2011. P-Type ATPases. *Annual Review of Biophysics,* 40**,** 243-266.
PANAGIOTAKOS, D. B., TZIMA, N., PITSAVOS, C., CHRYSOHOOU, C., PAPAKONSTANTINOU, E., ZAMPELAS, A. & STEFANADIS, C. 2005. The relationship between dietary habits, blood glucose and insulin levels among people without cardiovascular disease and type 2 diabetes; the ATTICA study. *Rev Diabet Stud,* 2**,** 208-15.
PANKIV, S., ALEMU, E. A., BRECH, A., BRUUN, J.-A., LAMARK, T., ØVERVATN, A., BJØRKØY, G. & JOHANSEN, T. 2010. FYCO1 is a Rab7 effector that binds to LC3 and PI3P to mediate microtubule plus end–directed vesicle transport. *Journal of Cell Biology,* 188**,** 253-269.
PATANÈ, G., PIRO, S., RABUAZZO, A. M., ANELLO, M., VIGNERI, R. & PURRELLO, F. 2000. Metformin restores insulin secretion altered by chronic exposure to free fatty acids or high glucose: a direct metformin effect on pancreatic beta-cells. *Diabetes,* 49**,** 735-40.
PEARSON, J. A., WONG, F. S. & WEN, L. 2016a. The importance of the Non Obese Diabetic (NOD) mouse model in autoimmune diabetes. *J Autoimmun,* 66**,** 76-88.
PEARSON, T., WATTIS, J. A. D., KING, J. R., MACDONALD, I. A. & MAZZATTI, D. J. 2016b. The Effects of Insulin Resistance on Individual Tissues: An Application of a Mathematical Model of Metabolism in Humans. *Bulletin of mathematical biology,* 78**,** 1189-1217.
PERTEA, M., KIM, D., PERTEA, G. M., LEEK, J. T. & SALZBERG, S. L. 2016. Transcript-level expression analysis of RNA-seq experiments with HISAT, StringTie and Ballgown. *Nature Protocols,* 11**,** 1650-1667.
PETERSEN, K. F., DUFOUR, S., SAVAGE, D. B., BILZ, S., SOLOMON, G., YONEMITSU, S., CLINE, G. W., BEFROY, D., ZEMANY, L., KAHN, B. B., PAPADEMETRIS, X., ROTHMAN, D. L. & SHULMAN, G. I. 2007. The role of skeletal muscle insulin resistance in the pathogenesis of the metabolic syndrome. *Proc Natl Acad Sci U S A,* 104**,** 12587-94.
PFEIFER, C. R., SHOMORONY, A., ARONOVA, M. A., ZHANG, G., CAI, T., XU, H., NOTKINS, A. L. & LEAPMAN, R. D. 2015. Quantitative analysis of mouse pancreatic islet architecture by serial block-face SEM. *J Struct Biol,* 189**,** 44-52.
PFÜTZNER, A. & FORST, T. 2011. Elevated intact proinsulin levels are indicative of Beta-cell dysfunction, insulin resistance, and cardiovascular risk: impact of the antidiabetic agent pioglitazone. *Journal of diabetes science and technology,* 5**,** 784-793.
PODOLIN, P. L., PRESSEY, A., DELARATO, N. H., FISCHER, P. A., PETERSON, L. B. & WICKER, L. S. 1993. I-E+ nonobese diabetic mice develop insulitis and diabetes. *J Exp Med,* 178**,** 793-803.
POITOUT, V., OLSON, L. K. & ROBERTSON, R. P. 1996. Chronic exposure of betaTC-6 cells to supraphysiologic concentrations of glucose decreases binding of the RIPE3b1 insulin gene transcription activator. *J Clin Invest,* 97**,** 1041-6.
PORTE, D., JR. & PUPO, A. A. 1969. Insulin responses to glucose: evidence for a two pool system in man. *J Clin Invest,* 48**,** 2309-19.
PRENTKI, M., CORKEY, B. E. & MADIRAJU, S. R. M. 2020. Lipid-associated metabolic signalling networks in pancreatic beta cell function. *Diabetologia,* 63**,** 10-20.
PRENTKI, M., JOLY, E., EL-ASSAAD, W. & RODUIT, R. 2002. Malonyl-CoA signaling, lipid partitioning, and glucolipotoxicity: role in beta-cell adaptation and failure in the etiology of diabetes. *Diabetes,* 51 Suppl 3**,** S405-13.
PRENTKI, M., MATSCHINSKY, F. M. & MADIRAJU, S. R. 2013. Metabolic signaling in fuel-induced insulin secretion. *Cell Metab,* 18**,** 162-85.
PRESTON, A. M., GURISIK, E., BARTLEY, C., LAYBUTT, D. R. & BIDEN, T. J. 2009. Reduced endoplasmic reticulum (ER)-to-Golgi protein trafficking contributes to ER stress in lipotoxic mouse beta cells by promoting protein overload. *Diabetologia,* 52**,** 2369-2373.
PULJUNG, M., VEDOVATO, N., USHER, S. & ASHCROFT, F. 2019. Activation mechanism of ATP-sensitive K(+) channels explored with real-time nucleotide binding. *Elife,* 8.

PURI, V., KONDA, S., RANJIT, S., AOUADI, M., CHAWLA, A., CHOUINARD, M., CHAKLADAR, A. & CZECH, M. P. 2007. Fat-specific protein 27, a novel lipid droplet protein that enhances triglyceride storage. *J Biol Chem,* 282**,** 34213-8.

QIU, X., HILL, A., PACKER, J., LIN, D., MA, Y.-A. & TRAPNELL, C. 2017. Single-cell mRNA quantification and differential analysis with Census. *Nature methods,* 14**,** 309-315.

QU, X., SEALE, J. P. & DONNELLY, R. 1999. Tissue and isoform-selective activation of protein kinase C in insulin-resistant obese Zucker rats - effects of feeding. *J Endocrinol,* 162**,** 207-14.

QUICLET, C., DITTBERNER, N., GÄSSLER, A., STADION, M., GERST, F., HELMS, A., BAUMEIER, C., SCHULZ, T. J. & SCHÜRMANN, A. 2019. Pancreatic adipocytes mediate hypersecretion of insulin in diabetes-susceptible mice. *Metabolism,* 97**,** 9-17.

RABIEE, A., GALIATSATOS, P., SALAS-CARRILLO, R., THOMPSON, M. J., ANDERSEN, D. K. & ELAHI, D. 2011. Pancreatic Polypeptide Administration Enhances Insulin Sensitivity and Reduces the Insulin Requirement of Patients on Insulin Pump Therapy. *Journal of Diabetes Science and Technology,* 5**,** 1521-1528.

RACHDAOUI, N., POLO-PARADA, L. & ISMAIL-BEIGI, F. 2019. Prolonged Exposure to Insulin Inactivates Akt and Erk1/2 and Increases Pancreatic Islet and INS1E beta-Cell Apoptosis. *J Endocr Soc,* 3**,** 69-90.

RADHA, V., VIMALESWARAN, K. S., BABU, H. N., ABATE, N., CHANDALIA, M., SATIJA, P., GRUNDY, S. M., GHOSH, S., MAJUMDER, P. P., DEEPA, R., RAO, S. M. & MOHAN, V. 2006. Role of genetic polymorphism peroxisome proliferator-activated receptor-gamma2 Pro12Ala on ethnic susceptibility to diabetes in South-Asian and Caucasian subjects: Evidence for heterogeneity. *Diabetes Care,* 29**,** 1046-51.

RAO, P., ZHOU, Y., GE, S.-Q., WANG, A.-X., YU, X.-W., ALZAIN, M. A., VERONICA, A. K., QIU, J., SONG, M.-S., ZHANG, J., WANG, H., FANG, H.-H., GAO, Q., WANG, Y.-X. & WANG, W. 2016. Validation of Type 2 Diabetes Risk Variants Identified by Genome-Wide Association Studies in Northern Han Chinese. *International journal of environmental research and public health,* 13**,** 863.

RASHID, M. A., LEE, S., TAK, E., LEE, J., CHOI, T. G., LEE, J. W., KIM, J. B., YOUN, J. H., KANG, I., HA, J. & KIM, S. S. 2010. Carbonyl reductase 1 protects pancreatic β-cells against oxidative stress-induced apoptosis in glucotoxicity and glucolipotoxicity. *Free Radic Biol Med,* 49**,** 1522-33.

RATHORE, N., RAMANI, S. R., PANTUA, H., PAYANDEH, J., BHANGALE, T., WUSTER, A., KAPOOR, M., SUN, Y., KAPADIA, S. B., GONZALEZ, L., ZARRIN, A. A., GOATE, A., HANSEN, D. V., BEHRENS, T. W. & GRAHAM, R. R. 2018. Paired Immunoglobulin-like Type 2 Receptor Alpha G78R variant alters ligand binding and confers protection to Alzheimer's disease. *PLoS Genet,* 14**,** e1007427.

REBELATO, E., SANTOS, L. R., CARPINELLI, A. R., RORSMAN, P. & ABDULKADER, F. 2018. Short-term high glucose culture potentiates pancreatic beta cell function. *Scientific Reports,* 8**,** 13061.

REICH, E. P., VON GRAFENSTEIN, H., BARLOW, A., SWENSON, K. E., WILLIAMS, K. & JANEWAY, C. A., JR. 1994. Self peptides isolated from MHC glycoproteins of non-obese diabetic mice. *J Immunol,* 152**,** 2279-88.

REIMER, M. K. & AHRÉN, B. 2002. Altered β-Cell Distribution of pdx-1 and GLUT-2 After a Short-Term Challenge With a High-Fat Diet in C57BL/6J Mice. *Diabetes,* 51**,** S138-S143.

REWERS, M. & LUDVIGSSON, J. 2016. Environmental risk factors for type 1 diabetes. *Lancet,* 387**,** 2340-2348.

RISSO, D., SCHWARTZ, K., SHERLOCK, G. & DUDOIT, S. 2011. GC-content normalization for RNA-Seq data. *BMC Bioinformatics,* 12**,** 480.

RITCHIE, M. E., PHIPSON, B., WU, D., HU, Y., LAW, C. W., SHI, W. & SMYTH, G. K. 2015. limma powers differential expression analyses for RNA-sequencing and microarray studies. *Nucleic Acids Res,* 43**,** e47.

ROAT, R., RAO, V., DOLIBA, N. M., MATSCHINSKY, F. M., TOBIAS, J. W., GARCIA, E., AHIMA, R. S. & IMAI, Y. 2014. Alterations of Pancreatic Islet Structure, Metabolism and Gene Expression in Diet-Induced Obese C57BL/6J Mice. *PLOS ONE,* 9**,** e86815.

ROBINSON, J. T., THORVALDSDÓTTIR, H., TURNER, D. & MESIROV, J. P. 2020. igv.js: an embeddable JavaScript implementation of the Integrative Genomics Viewer (IGV). *bioRxiv*, 2020.05.03.075499.
ROBINSON, M. D. & OSHLACK, A. 2010. A scaling normalization method for differential expression analysis of RNA-seq data. *Genome Biol,* 11**,** R25.
ROCHE, E., FARFARI, S., WITTERS, L. A., ASSIMACOPOULOS-JEANNET, F., THUMELIN, S., BRUN, T., CORKEY, B. E., SAHA, A. K. & PRENTKI, M. 1998. Long-term exposure of beta-INS cells to high glucose concentrations increases anaplerosis, lipogenesis, and lipogenic gene expression. *Diabetes,* 47**,** 1086-94.
ROCKETTE-WAGNER, B., EDELSTEIN, S., VENDITTI, E. M., REDDY, D., BRAY, G. A., CARRION-PETERSEN, M. L., DABELEA, D., DELAHANTY, L. M., FLOREZ, H., FRANKS, P. W., MONTEZ, M. G., RUBIN, R., KRISKA, A. M. & DIABETES PREVENTION PROGRAM RESEARCH, G. 2015. The impact of lifestyle intervention on sedentary time in individuals at high risk of diabetes. *Diabetologia,* 58**,** 1198-1202.
RODUIT, R., NOLAN, C., ALARCON, C., MOORE, P., BARBEAU, A., DELGHINGARO-AUGUSTO, V., PRZYBYKOWSKI, E., MORIN, J., MASSÉ, F., MASSIE, B., RUDERMAN, N., RHODES, C., POITOUT, V. & PRENTKI, M. 2004. A Role for the Malonyl-CoA/Long-Chain Acyl-CoA Pathway of Lipid Signaling in the Regulation of Insulin Secretion in Response to Both Fuel and Nonfuel Stimuli. *Diabetes,* 53**,** 1007-1019.
ROGSTAM, A., LINSE, S., LINDQVIST, A., JAMES, P., WAGNER, L. & BERGGÅRD, T. 2007. Binding of calcium ions and SNAP-25 to the hexa EF-hand protein secretagogin. *Biochem J,* 401**,** 353-63.
RORSMAN, P. & ASHCROFT, F. M. 2018. Pancreatic β-Cell Electrical Activity and Insulin Secretion: Of Mice and Men. *Physiological reviews,* 98**,** 117-214.
RORSMAN, P. & TRUBE, G. 1985. Glucose dependent K+-channels in pancreatic beta-cells are regulated by intracellular ATP. *Pflugers Arch,* 405**,** 305-9.
ROSENBAUM, D. M., RASMUSSEN, S. G. F. & KOBILKA, B. K. 2009. The structure and function of G-protein-coupled receptors. *Nature,* 459**,** 356-363.
ROUILLE, Y., WESTERMARK, G., MARTIN, S. K. & STEINER, D. F. 1994. Proglucagon is processed to glucagon by prohormone convertase PC2 in alpha TC1-6 cells. *Proc Natl Acad Sci U S A,* 91**,** 3242-6.
RUMALA, C. Z., LIU, J., LOCASALE, J. W., CORKEY, B. E., DEENEY, J. T. & RAMEH, L. E. 2020. Exposure of Pancreatic β-Cells to Excess Glucose Results in Bimodal Activation of mTORC1 and mTOR-Dependent Metabolic Acceleration. *iScience,* 23**,** 100858.
SAISHO, Y., BUTLER, A. E., MEIER, J. J., MONCHAMP, T., ALLEN-AUERBACH, M., RIZZA, R. A. & BUTLER, P. C. 2007. Pancreas volumes in humans from birth to age one hundred taking into account sex, obesity, and presence of type-2 diabetes. *Clin Anat,* 20**,** 933-42.
SAITO, K. E. N., IWAMA, N. & TAKAHASHI, T. 1978. Morphometrical Analysis on Topographical Difference in Size Distribution, Number and Volume of Islets in the Human Pancreas. *The Tohoku Journal of Experimental Medicine,* 124**,** 177-186.
SAITO, T., KUMA, A., SUGIURA, Y., ICHIMURA, Y., OBATA, M., KITAMURA, H., OKUDA, S., LEE, H. C., IKEDA, K., KANEGAE, Y., SAITO, I., AUWERX, J., MOTOHASHI, H., SUEMATSU, M., SOGA, T., YOKOMIZO, T., WAGURI, S., MIZUSHIMA, N. & KOMATSU, M. 2019. Autophagy regulates lipid metabolism through selective turnover of NCoR1. *Nat Commun,* 10**,** 1567.
SAKAI, K., MATSUMOTO, K., NISHIKAWA, T., SUEFUJI, M., NAKAMARU, K., HIRASHIMA, Y., KAWASHIMA, J., SHIROTANI, T., ICHINOSE, K., BROWNLEE, M. & ARAKI, E. 2003. Mitochondrial reactive oxygen species reduce insulin secretion by pancreatic beta-cells. *Biochem Biophys Res Commun,* 300**,** 216-22.
SAKURABA, H., MIZUKAMI, H., YAGIHASHI, N., WADA, R., HANYU, C. & YAGIHASHI, S. 2002. Reduced beta-cell mass and expression of oxidative stress-related DNA damage in the islet of Japanese Type II diabetic patients. *Diabetologia,* 45**,** 85-96.
SALAS-SALVADÓ, J., GUASCH-FERRÉ, M., LEE, C.-H., ESTRUCH, R., CLISH, C. B. & ROS, E. 2015. Protective Effects of the Mediterranean Diet on Type 2 Diabetes and Metabolic Syndrome. *The Journal of nutrition,* 146**,** 920S-927S.

SALGIN, B., ONG, K. K., THANKAMONY, A., EMMETT, P., WAREHAM, N. J. & DUNGER, D. B. 2012. Higher fasting plasma free fatty acid levels are associated with lower insulin secretion in children and adults and a higher incidence of type 2 diabetes. *J Clin Endocrinol Metab,* 97**,** 3302-9.

SCHERER, P. E. 2019. The many secret lives of adipocytes: implications for diabetes. *Diabetologia,* 62**,** 223-232.

SCHEUNER, D., VANDER MIERDE, D., SONG, B., FLAMEZ, D., CREEMERS, J. W., TSUKAMOTO, K., RIBICK, M., SCHUIT, F. C. & KAUFMAN, R. J. 2005. Control of mRNA translation preserves endoplasmic reticulum function in beta cells and maintains glucose homeostasis. *Nat Med,* 11**,** 757-64.

SCHIAFFINO, S., ROSSI, A. C., SMERDU, V., LEINWAND, L. A. & REGGIANI, C. 2015. Developmental myosins: expression patterns and functional significance. *Skeletal Muscle,* 5**,** 22.

SCHORK, N. J., MURRAY, S. S., FRAZER, K. A. & TOPOL, E. J. 2009. Common vs. rare allele hypotheses for complex diseases. *Curr Opin Genet Dev,* 19**,** 212-9.

SCHRIER, R. W., ESTACIO, R. O., ESLER, A. & MEHLER, P. 2002. Effects of aggressive blood pressure control in normotensive type 2 diabetic patients on albuminuria, retinopathy and strokes. *Kidney Int,* 61**,** 1086-97.

SCHUIT, F., FLAMEZ, D., DE VOS, A. & PIPELEERS, D. 2002. Glucose-Regulated Gene Expression Maintaining the Glucose-Responsive State of β-Cells. *Diabetes,* 51**,** S326-S332.

SCHULTHEIS, P. J., HAGEN, T. T., O'TOOLE, K. K., TACHIBANA, A., BURKE, C. R., MCGILL, D. L., OKUNADE, G. W. & SHULL, G. E. 2004. Characterization of the P5 subfamily of P-type transport ATPases in mice. *Biochem Biophys Res Commun,* 323**,** 731-8.

SCHWENK, R. W., BAUMEIER, C., FINAN, B., KLUTH, O., BRAUER, C., JOOST, H. G., DIMARCHI, R. D., TSCHÖP, M. H. & SCHÜRMANN, A. 2015. GLP-1-oestrogen attenuates hyperphagia and protects from beta cell failure in diabetes-prone New Zealand obese (NZO) mice. *Diabetologia,* 58**,** 604-14.

SEGERSTOLPE, Å., PALASANTZA, A., ELIASSON, P., ANDERSSON, E.-M., ANDRÉASSON, A.-C., SUN, X., PICELLI, S., SABIRSH, A., CLAUSEN, M., BJURSELL, M. K., SMITH, D. M., KASPER, M., ÄMMÄLÄ, C. & SANDBERG, R. 2016. Single-Cell Transcriptome Profiling of Human Pancreatic Islets in Health and Type 2 Diabetes. *Cell metabolism,* 24**,** 593-607.

SEPE, P. S., OHRI, A., SANAKA, S., BERZIN, T. M., SEKHON, S., BENNETT, G., MEHTA, G., CHUTTANI, R., KANE, R., PLESKOW, D. & SAWHNEY, M. S. 2011. A prospective evaluation of fatty pancreas by using EUS. *Gastrointest Endosc,* 73**,** 987-93.

SHAH, P., VELLA, A., BASU, A., BASU, R., SCHWENK, W. F. & RIZZA, R. A. 2000. Lack of suppression of glucagon contributes to postprandial hyperglycemia in subjects with type 2 diabetes mellitus. *J Clin Endocrinol Metab,* 85**,** 4053-9.

SHAH, S. S., RAMIREZ, C. E., POWERS, A. C., YU, C., SHIBAO, C. A. & LUTHER, J. M. 2016. Hyperglycemic clamp-derived disposition index is negatively associated with metabolic syndrome severity in obese subjects. *Metabolism: clinical and experimental,* 65**,** 835-842.

SHARMA, A., MOORE, M., MARCORA, E., LEE, J. E., QIU, Y., SAMARAS, S. & STEIN, R. 1999. The NeuroD1/BETA2 sequences essential for insulin gene transcription colocalize with those necessary for neurogenesis and p300/CREB binding protein binding. *Mol Cell Biol,* 19**,** 704-13.

SHAW, J. E., SICREE, R. A. & ZIMMET, P. Z. 2010. Global estimates of the prevalence of diabetes for 2010 and 2030. *Diabetes Res Clin Pract,* 87**,** 4-14.

SHERRY, S. T., WARD, M. H., KHOLODOV, M., BAKER, J., PHAN, L., SMIGIELSKI, E. M. & SIROTKIN, K. 2001. dbSNP: the NCBI database of genetic variation. *Nucleic acids research,* 29**,** 308-311.

SHI, H., KOKOEVA, M. V., INOUYE, K., TZAMELI, I., YIN, H. & FLIER, J. S. 2006. TLR4 links innate immunity and fatty acid-induced insulin resistance. *J Clin Invest,* 116**,** 3015-25.

SHIBASAKI, T., SUNAGA, Y., FUJIMOTO, K., KASHIMA, Y. & SEINO, S. 2004. Interaction of ATP sensor, cAMP sensor, Ca2+ sensor, and voltage-dependent Ca2+ channel in insulin granule exocytosis. *J Biol Chem,* 279**,** 7956-61.

SHIMABUKURO, M., ZHOU, Y. T., LEVI, M. & UNGER, R. H. 1998. Fatty acid-induced beta cell apoptosis: a link between obesity and diabetes. *Proceedings of the National Academy of Sciences of the United States of America,* 95**,** 2498-2502.

SHIOTA, C., LARSSON, O., SHELTON, K. D., SHIOTA, M., EFANOV, A. M., HOY, M., LINDNER, J., KOOPTIWUT, S., JUNTTI-BERGGREN, L., GROMADA, J., BERGGREN, P. O. & MAGNUSON, M. A. 2002. Sulfonylurea receptor type 1 knock-out mice have intact feeding-stimulated insulin secretion despite marked impairment in their response to glucose. *J Biol Chem,* 277**,** 37176-83.

SHUM, E. Y., ESPINOZA, J. L., RAMAIAH, M. & WILKINSON, M. F. 2015. Identification of novel post-transcriptional features in olfactory receptor family mRNAs. *Nucleic acids research,* 43**,** 9314-9326.

SIMECEK, P., CHURCHILL, G. A., YANG, H., ROWE, L. B., HERBERG, L., SERREZE, D. V. & LEITER, E. H. 2015. Genetic Analysis of Substrain Divergence in Non-Obese Diabetic (NOD) Mice. *G3 (Bethesda),* 5**,** 771-5.

SIMEONOVIC, C. J., POPP, S. K., STARRS, L. M., BROWN, D. J., ZIOLKOWSKI, A. F., LUDWIG, B., BORNSTEIN, S. R., WILSON, J. D., PUGLIESE, A., KAY, T. W. H., THOMAS, H. E., LOUDOVARIS, T., CHOONG, F. J., FREEMAN, C. & PARISH, C. R. 2018. Loss of intra-islet heparan sulfate is a highly sensitive marker of type 1 diabetes progression in humans. *PloS one,* 13**,** e0191360-e0191360.

SJOHOLM, A. 2019. Ketosis-Prone Type 2 Diabetes: A Case Series. *Front Endocrinol (Lausanne),* 10**,** 684.

SKOWRONSKI, A. A., RAVUSSIN, Y., LEIBEL, R. L. & LEDUC, C. A. 2017. Energy homeostasis in leptin deficient Lepob/ob mice. *PLoS One,* 12**,** e0189784.

SLATTERY, M. L., LUNDGREEN, A., HERRICK, J. S. & WOLFF, R. K. 2011. Genetic variation in RPS6KA1, RPS6KA2, RPS6KB1, RPS6KB2, and PDK1 and risk of colon or rectal cancer. *Mutat Res,* 706**,** 13-20.

SLEPCHENKO, K. G., CORBIN, K. L. & NUNEMAKER, C. S. 2019. Comparing methods to normalize insulin secretion shows the process may not be needed. *J Endocrinol*.

SLIEKER, R. C., VAN DER HEIJDEN, A. A. W. A., VAN LEEUWEN, N., MEI, H., NIJPELS, G., BEULENS, J. W. J. & 'T HART, L. M. 2018. HbA1c is associated with altered expression in blood of cell cycle- and immune response-related genes. *Diabetologia,* 61**,** 138-146.

SMITH, G. I., SHANKARAN, M., YOSHINO, M., SCHWEITZER, G. G., CHONDRONIKOLA, M., BEALS, J. W., OKUNADE, A. L., PATTERSON, B. W., NYANGAU, E., FIELD, T., SIRLIN, C. B., TALUKDAR, S., HELLERSTEIN, M. K. & KLEIN, S. 2020. Insulin resistance drives hepatic de novo lipogenesis in nonalcoholic fatty liver disease. *The Journal of Clinical Investigation,* 130**,** 1453-1460.

SOARES, M. B., SCHON, E., HENDERSON, A., KARATHANASIS, S. K., CATE, R., ZEITLIN, S., CHIRGWIN, J. & EFSTRATIADIS, A. 1985. RNA-mediated gene duplication: the rat preproinsulin I gene is a functional retroposon. *Mol Cell Biol,* 5**,** 2090-103.

SOLOMON, T. P., KNUDSEN, S. H., KARSTOFT, K., WINDING, K., HOLST, J. J. & PEDERSEN, B. K. 2012. Examining the effects of hyperglycemia on pancreatic endocrine function in humans: evidence for in vivo glucotoxicity. *J Clin Endocrinol Metab,* 97**,** 4682-91.

SONE, H. & KAGAWA, Y. 2005. Pancreatic beta cell senescence contributes to the pathogenesis of type 2 diabetes in high-fat diet-induced diabetic mice. *Diabetologia,* 48**,** 58-67.

SØRENSEN, D. M., BUCH-PEDERSEN, M. J. & PALMGREN, M. G. 2010. Structural divergence between the two subgroups of P5 ATPases. *Biochimica et Biophysica Acta (BBA) - Bioenergetics,* 1797**,** 846-855.

SOWERS, C. R., WANG, R., BOURNE, R. A., MCGRATH, B. C., HU, J., BEVILACQUA, S. C., PATON, J. C., PATON, A. W., COLLARDEAU-FRACHON, S., NICOLINO, M. & CAVENER, D. R. 2018. The protein kinase PERK/EIF2AK3 regulates proinsulin processing not via protein synthesis but by controlling endoplasmic reticulum chaperones. *J Biol Chem,* 293**,** 5134-5149.

SPEAKMAN, J. R. 2019. Use of high-fat diets to study rodent obesity as a model of human obesity. *International Journal of Obesity,* 43**,** 1491-1492.

SRIKANTHAN, P., HEVENER, A. L. & KARLAMANGLA, A. S. 2010. Sarcopenia exacerbates obesity-associated insulin resistance and dysglycemia: findings from the National Health and Nutrition Examination Survey III. *PLoS One,* 5**,** e10805.

SRIKANTHAN, P. & KARLAMANGLA, A. S. 2011. Relative Muscle Mass Is Inversely Associated with Insulin Resistance and Prediabetes. Findings from The Third National Health and Nutrition Examination Survey. *The Journal of Clinical Endocrinology & Metabolism,* 96**,** 2898-2903.

SRINIVASAN, S., BERNAL-MIZRACHI, E., OHSUGI, M. & PERMUTT, M. A. 2002. Glucose promotes pancreatic islet beta-cell survival through a PI 3-kinase/Akt-signaling pathway. *Am J Physiol Endocrinol Metab,* 283**,** E784-93.

STANCILL, J. S., CARTAILLER, J.-P., CLAYTON, H. W., O'CONNOR, J. T., DICKERSON, M. T., DADI, P. K., OSIPOVICH, A. B., JACOBSON, D. A. & MAGNUSON, M. A. 2017. Chronic β-Cell Depolarization Impairs β-Cell Identity by Disrupting a Network of Ca(2+)-Regulated Genes. *Diabetes,* 66**,** 2175-2187.

STECK, A. K., JOHNSON, K., BARRIGA, K. J., MIAO, D., YU, L., HUTTON, J. C., EISENBARTH, G. S. & REWERS, M. J. 2011. Age of islet autoantibody appearance and mean levels of insulin, but not GAD or IA-2 autoantibodies, predict age of diagnosis of type 1 diabetes: diabetes autoimmunity study in the young. *Diabetes Care,* 34**,** 1397-9.

STEINBRECHER, K. A. 2014. The multiple roles of guanylate cyclase C, a heat stable enterotoxin receptor. *Current Opinion in Gastroenterology,* 30**,** 1-6.

STENE, L. C., OIKARINEN, S., HYOTY, H., BARRIGA, K. J., NORRIS, J. M., KLINGENSMITH, G., HUTTON, J. C., ERLICH, H. A., EISENBARTH, G. S. & REWERS, M. 2010. Enterovirus infection and progression from islet autoimmunity to type 1 diabetes: the Diabetes and Autoimmunity Study in the Young (DAISY). *Diabetes,* 59**,** 3174-80.

STICKLE, D. F., REYNOLDS, M. A., MORRIS, M. D. & QUON, M. J. 1999. Dynamic changes in plasma proinsulin/insulin ratio during insulin secretion influence correlation between radioimmunoassay (RIA) and IMX measurements of insulin. *Clin Chim Acta,* 284**,** 1-13.

STRAUSS, K. A., MARKX, S., GEORGI, B., PAUL, S. M., JINKS, R. N., HOSHI, T., MCDONALD, A., FIRST, M. B., LIU, W., BENKERT, A. R., HEAPS, A. D., TIAN, Y., CHAKRAVARTI, A., BUCAN, M. & PUFFENBERGER, E. G. 2014. A population-based study of KCNH7 p.Arg394His and bipolar spectrum disorder. *Hum Mol Genet,* 23**,** 6395-406.

SU, S., LAW, C. W., AH-CANN, C., ASSELIN-LABAT, M. L., BLEWITT, M. E. & RITCHIE, M. E. 2017. Glimma: interactive graphics for gene expression analysis. *Bioinformatics,* 33**,** 2050-2052.

SUCCURRO, E., MARINI, M. A., FRONTONI, S., HRIBAL, M. L., ANDREOZZI, F., LAURO, R., PERTICONE, F. & SESTI, G. 2008. Insulin secretion in metabolically obese, but normal weight, and in metabolically healthy but obese individuals. *Obesity (Silver Spring),* 16**,** 1881-6.

SVENNEVIG, K., KOLSET, S. O. & BANGSTAD, H. J. 2006. Increased syndecan-1 in serum is related to early nephropathy in type 1 diabetes mellitus patients. *Diabetologia,* 49**,** 2214-2216.

SWALLOW, J. G. & GARLAND, T., JR. 2005. Selection Experiments as a Tool in Evolutionary and Comparative Physiology: Insights into Complex Traits—an Introduction to the Symposium1. *Integrative and Comparative Biology,* 45**,** 387-390.

TAKAHASHI, H. 1984. Scanning electron microscopy of the rat exocrine pancreas. *Arch Histol Jpn,* 47**,** 387-404.

TAKAHASHI, H., SHIBASAKI, T., PARK, J. H., HIDAKA, S., TAKAHASHI, T., ONO, A., SONG, D. K. & SEINO, S. 2015. Role of Epac2A/Rap1 signaling in interplay between incretin and sulfonylurea in insulin secretion. *Diabetes,* 64**,** 1262-72.

TANG, C., YEUNG, L. S. N., KOULAJIAN, K., ZHANG, L., TAI, K., VOLCHUK, A. & GIACCA, A. 2018. Glucose-Induced β-Cell Dysfunction In Vivo: Evidence for a Causal Role of C-jun N-terminal Kinase Pathway. *Endocrinology,* 159**,** 3643-3654.

TENGHOLM, A. 2012. Cyclic AMP dynamics in the pancreatic β-cell. *Upsala journal of medical sciences,* 117**,** 355-369.

TENGHOLM, A. & GYLFE, E. 2017. cAMP signalling in insulin and glucagon secretion. *Diabetes Obes Metab,* 19 Suppl 1**,** 42-53.

THANOPOULOU, A. C., KARAMANOS, B. G., ANGELICO, F. V., ASSAAD-KHALIL, S. H., BARBATO, A. F., DEL BEN, M. P., DJORDJEVIC, P. B., DIMITRIJEVIC-SRECKOVIC, V. S., GALLOTTI, C. A., KATSILAMBROS, N. L., MIGDALIS, I. N., MRABET, M. M., PETKOVA, M. K., ROUSSI, D. P. & TENCONI, M. T. 2003. Dietary fat intake as risk factor for the development of diabetes: multinational, multicenter study of the Mediterranean Group for the Study of Diabetes (MGSD). *Diabetes Care,* 26**,** 302-7.

THIEBAUD, D., JACOT, E., DEFRONZO, R. A., MAEDER, E., JEQUIER, E. & FELBER, J. P. 1982. The effect of graded doses of insulin on total glucose uptake, glucose oxidation, and glucose storage in man. *Diabetes,* 31**,** 957-63.

THOMAS, C., MACKEY, M. M., DIAZ, A. A. & COX, D. P. 2009. Hydroxyl radical is produced via the Fenton reaction in submitochondrial particles under oxidative stress: implications for diseases associated with iron accumulation. *Redox Rep,* 14**,** 102-8.

THORENS, B., CHENG, Z. Q., BROWN, D. & LODISH, H. F. 1990. Liver glucose transporter: a basolateral protein in hepatocytes and intestine and kidney cells. *Am J Physiol,* 259**,** C279-85.

THUNANDER, M., PETERSSON, C., JONZON, K., FORNANDER, J., OSSIANSSON, B., TORN, C., EDVARDSSON, S. & LANDIN-OLSSON, M. 2008. Incidence of type 1 and type 2 diabetes in adults and children in Kronoberg, Sweden. *Diabetes Res Clin Pract,* 82**,** 247-55.

TITMUSS, A., DAVIS, E. A., BROWN, A. & MAPLE-BROWN, L. J. 2019. Emerging diabetes and metabolic conditions among Aboriginal and Torres Strait Islander young people. *Medical Journal of Australia,* 210**,** 111-113.e1.

TONG, X., KONO, T. & EVANS-MOLINA, C. 2015. Nitric oxide stress and activation of AMP-activated protein kinase impair β-cell sarcoendoplasmic reticulum calcium ATPase 2b activity and protein stability. *Cell death & disease,* 6**,** e1790-e1790.

TORNOVSKY-BABEAY, S., DADON, D., ZIV, O., TZIPILEVICH, E., KADOSH, T., SCHYR-BEN HAROUSH, R., HIJA, A., STOLOVICH-RAIN, M., FURTH-LAVI, J., GRANOT, Z., PORAT, S., PHILIPSON, L. H., HEROLD, K. C., BHATTI, T. R., STANLEY, C., ASHCROFT, F. M., IN'T VELD, P., SAADA, A., MAGNUSON, M. A., GLASER, B. & DOR, Y. 2014. Type 2 diabetes and congenital hyperinsulinism cause DNA double-strand breaks and p53 activity in β cells. *Cell Metab,* 19**,** 109-21.

TRIVEDI, P., GRAHAM, K. L., KRISHNAMURTHY, B., FYNCH, S., SLATTERY, R. M., KAY, T. W. & THOMAS, H. E. 2016. Perforin facilitates beta cell killing and regulates autoreactive CD8+ T-cell responses to antigen in mouse models of type 1 diabetes. *Immunol Cell Biol,* 94**,** 334-41.

TU, B. P. & WEISSMAN, J. S. 2004. Oxidative protein folding in eukaryotes: mechanisms and consequences. *J Cell Biol,* 164**,** 341-6.

TUO, Y., FENG, D. D., WANG, D. F., SUN, J., LI, S. B. & CHEN, C. 2012. Long-term in vitro treatment of INS-1 rat pancreatic β-cells by unsaturated free fatty acids protects cells against gluco- and lipotoxicities via activation of GPR40 receptors. *Clin Exp Pharmacol Physiol,* 39**,** 423-8.

TYRBERG, B., ANDERSSON, A. & BORG, L. A. 2001. Species differences in susceptibility of transplanted and cultured pancreatic islets to the beta-cell toxin alloxan. *Gen Comp Endocrinol,* 122**,** 238-51.

UEMURA, A., OKU, M., MORI, K. & YOSHIDA, H. 2009. Unconventional splicing of XBP1 mRNA occurs in the cytoplasm during the mammalian unfolded protein response. *J Cell Sci,* 122**,** 2877-86.

UNGER, R. H. & GRUNDY, S. 1985. Hyperglycaemia as an inducer as well as a consequence of impaired islet cell function and insulin resistance: implications for the management of diabetes. *Diabetologia,* 28**,** 119-21.

USUI, R., YABE, D., FAUZI, M., GOTO, H., BOTAGAROVA, A., TOKUMOTO, S., TATSUOKA, H., TAHARA, Y., KOBAYASHI, S., MANABE, T., BABA, Y., KUROSAKI, T., HERRERA, P. L., OGURA, M., NAGASHIMA, K. & INAGAKI, N. 2019. GPR40 activation initiates store-operated Ca2+ entry and potentiates insulin secretion via the IP3R1/STIM1/Orai1 pathway in pancreatic β-cells. *Scientific Reports,* 9**,** 15562.

UWAIFO, G. I., PARIKH, S. J., KEIL, M., ELBERG, J., CHIN, J. & YANOVSKI, J. A. 2002. Comparison of insulin sensitivity, clearance, and secretion estimates using euglycemic and hyperglycemic clamps in children. *J Clin Endocrinol Metab,* 87**,** 2899-905.
VAGIN, O., DENEVICH, S., MUNSON, K. & SACHS, G. 2002. SCH28080, a K+-Competitive Inhibitor of the Gastric H,K-ATPase, Binds Near the M5−6 Luminal Loop, Preventing K+ Access to the Ion Binding Domain. *Biochemistry,* 41**,** 12755-12762.
VALENTINO, M. A., LIN, J. E., SNOOK, A. E., LI, P., KIM, G. W., MARSZALOWICZ, G., MAGEE, M. S., HYSLOP, T., SCHULZ, S. & WALDMAN, S. A. 2011. A uroguanylin-GUCY2C endocrine axis regulates feeding in mice. *J Clin Invest,* 121**,** 3578-88.
VALERY, P. C., MOLONEY, A., COTTERILL, A., HARRIS, M., SINHA, A. K. & GREEN, A. C. 2009. Prevalence of obesity and metabolic syndrome in Indigenous Australian youths. *Obesity Review,* 10**,** 255-61.
VAN CITTERS, G. W., KABIR, M., KIM, S. P., MITTELMAN, S. D., DEA, M. K., BRUBAKER, P. L. & BERGMAN, R. N. 2002. Elevated glucagon-like peptide-1-(7-36)-amide, but not glucose, associated with hyperinsulinemic compensation for fat feeding. *J Clin Endocrinol Metab,* 87**,** 5191-8.
VAN DAM, R. M., WILLETT, W. C., RIMM, E. B., STAMPFER, M. J. & HU, F. B. 2002. Dietary Fat and Meat Intake in Relation to Risk of Type 2 Diabetes in Men. *Diabetes Care,* 25**,** 417-424.
VAN DE GIESSEN, E., LA FLEUR, S. E., DE BRUIN, K., VAN DEN BRINK, W. & BOOIJ, J. 2012. Free-choice and no-choice high-fat diets affect striatal dopamine D2/3 receptor availability, caloric intake, and adiposity. *Obesity (Silver Spring),* 20**,** 1738-40.
VAN DER AUWERA, G. A., CARNEIRO, M. O., HARTL, C., POPLIN, R., DEL ANGEL, G., LEVY-MOONSHINE, A., JORDAN, T., SHAKIR, K., ROAZEN, D., THIBAULT, J., BANKS, E., GARIMELLA, K. V., ALTSHULER, D., GABRIEL, S. & DEPRISTO, M. A. 2013. From FastQ data to high confidence variant calls: the Genome Analysis Toolkit best practices pipeline. *Curr Protoc Bioinformatics,* 43**,** 11.10.1-11.10.33.
VAN DIJK, P. J. & ELLIS, T. H. 2016. The Full Breadth of Mendel's Genetics. *Genetics,* 204**,** 1327-1336.
VAN HORSSEN, J., OTTE-HÖLLER, I., DAVID, G., MAAT-SCHIEMAN, M. L., VAN DEN HEUVEL, L. P., WESSELING, P., DE WAAL, R. M. & VERBEEK, M. M. 2001. Heparan sulfate proteoglycan expression in cerebrovascular amyloid beta deposits in Alzheimer's disease and hereditary cerebral hemorrhage with amyloidosis (Dutch) brains. *Acta Neuropathol,* 102**,** 604-14.
VAN LOON, L. J., KOOPMAN, R., STEGEN, J. H., WAGENMAKERS, A. J., KEIZER, H. A. & SARIS, W. H. 2003. Intramyocellular lipids form an important substrate source during moderate intensity exercise in endurance-trained males in a fasted state. *J Physiol,* 553**,** 611-25.
VÉRET, J., COANT, N., BERDYSHEV, E. V., SKOBELEVA, A., THERVILLE, N., BAILBÉ, D., GORSHKOVA, I., NATARAJAN, V., PORTHA, B. & LE STUNFF, H. 2011. Ceramide synthase 4 and de novo production of ceramides with specific N-acyl chain lengths are involved in glucolipotoxicity-induced apoptosis of INS-1 β-cells. *Biochem J,* 438**,** 177-89.
VERGARI, E., KNUDSEN, J. G., RAMRACHEYA, R. & SALEHI, A. 2019. Insulin inhibits glucagon release by SGLT2-induced stimulation of somatostatin secretion. 10**,** 139.
VOGT, C., ARDEHALI, H., IOZZO, P., YKI-JARVINEN, H., KOVAL, J., MAEZONO, K., PENDERGRASS, M., PRINTZ, R., GRANNER, D., DEFRONZO, R. & MANDARINO, L. 2000. Regulation of hexokinase II expression in human skeletal muscle in vivo. *Metabolism,* 49**,** 814-8.
VON HERRATH, M., SANDA, S. & HEROLD, K. 2007. Type 1 diabetes as a relapsing-remitting disease? *Nat Rev Immunol,* 7**,** 988-94.
VON MERING, J. & MINKOWSKI, O. 1890. Diabetes mellitus nach Pankreasexstirpation. *Archiv für experimentelle Pathologie und Pharmakologie,* 26**,** 371- 387.
VROEGRIJK, I. O., VAN KLINKEN, J. B., VAN DIEPEN, J. A., VAN DEN BERG, S. A., FEBBRAIO, M., STEINBUSCH, L. K., GLATZ, J. F., HAVEKES, L. M., VOSHOL, P. J.,

RENSEN, P. C., VAN DIJK, K. W. & VAN HARMELEN, V. 2013. CD36 is important for adipocyte recruitment and affects lipolysis. *Obesity (Silver Spring),* 21**,** 2037-45.
WANG, H., MAECHLER, P., RITZ-LASER, B., HAGENFELDT, K. A., ISHIHARA, H., PHILIPPE, J. & WOLLHEIM, C. B. 2001. Pdx1 level defines pancreatic gene expression pattern and cell lineage differentiation. *J Biol Chem,* 276**,** 25279-86.
WANG, H., QIU, X., LIN, S., CHEN, X., WANG, T. & LIAO, T. 2018. Knockdown of IFI27 inhibits cell proliferation and invasion in oral squamous cell carcinoma. *World Journal of Surgical Oncology,* 16**,** 64.
WANG, J., CHEN, Y., YUAN, Q., TANG, W., ZHANG, X. & OSEI, K. 2011. Control of precursor maturation and disposal is an early regulative mechanism in the normal insulin production of pancreatic beta-cells. *PLoS One,* 6**,** e19446.
WANG, J. & SEVIER, C. S. 2016. Formation and Reversibility of BiP Protein Cysteine Oxidation Facilitate Cell Survival during and post Oxidative Stress. *J Biol Chem,* 291**,** 7541-57.
WANG, L., LIU, Q., KITAMOTO, T., HOU, J., QIN, J. & ACCILI, D. 2019. Identification of Insulin-Responsive Transcription Factors That Regulate Glucose Production by Hepatocytes. *Diabetes,* 68**,** 1156-1167.
WANG, Q. & BRUBAKER, P. L. 2002. Glucagon-like peptide-1 treatment delays the onset of diabetes in 8 week-old db/db mice. *Diabetologia,* 45**,** 1263-73.
WANG, Q., ZHANG, H., ZHAO, B. & FEI, H. 2009. IL-1beta caused pancreatic beta-cells apoptosis is mediated in part by endoplasmic reticulum stress via the induction of endoplasmic reticulum Ca2+ release through the c-Jun N-terminal kinase pathway. *Mol Cell Biochem,* 324**,** 183-90.
WANG, Q., ZHANG, M., XU, M., GU, W., XI, Y., QI, L., LI, B. & WANG, W. 2015. Brown adipose tissue activation is inversely related to central obesity and metabolic parameters in adult human. *PLoS One,* 10**,** e0123795.
WANG, X. & PUTKEY, J. A. 2016. PEP-19 modulates calcium binding to calmodulin by electrostatic steering. *Nature communications,* 7**,** 13583-13583.
WANG, X., XIONG, L. W., EL AYADI, A., BOEHNING, D. & PUTKEY, J. A. 2013. The calmodulin regulator protein, PEP-19, sensitizes ATP-induced Ca2+ release. *The Journal of biological chemistry,* 288**,** 2040-2048.
WATERSTON, R. H., LINDBLAD-TOH, K., BIRNEY, E., ROGERS, J., ABRIL, J. F., AGARWAL, P., AGARWALA, R., AINSCOUGH, R., ALEXANDERSSON, M., AN, P., ANTONARAKIS, S. E., ATTWOOD, J., BAERTSCH, R., BAILEY, J., BARLOW, K., BECK, S., BERRY, E., BIRREN, B., BLOOM, T., BORK, P., BOTCHERBY, M., BRAY, N., BRENT, M. R., BROWN, D. G., BROWN, S. D., BULT, C., BURTON, J., BUTLER, J., CAMPBELL, R. D., CARNINCI, P., CAWLEY, S., CHIAROMONTE, F., CHINWALLA, A. T., CHURCH, D. M., CLAMP, M., CLEE, C., COLLINS, F. S., COOK, L. L., COPLEY, R. R., COULSON, A., COURONNE, O., CUFF, J., CURWEN, V., CUTTS, T., DALY, M., DAVID, R., DAVIES, J., DELEHAUNTY, K. D., DERI, J., DERMITZAKIS, E. T., DEWEY, C., DICKENS, N. J., DIEKHANS, M., DODGE, S., DUBCHAK, I., DUNN, D. M., EDDY, S. R., ELNITSKI, L., EMES, R. D., ESWARA, P., EYRAS, E., FELSENFELD, A., FEWELL, G. A., FLICEK, P., FOLEY, K., FRANKEL, W. N., FULTON, L. A., FULTON, R. S., FUREY, T. S., GAGE, D., GIBBS, R. A., GLUSMAN, G., GNERRE, S., GOLDMAN, N., GOODSTADT, L., GRAFHAM, D., GRAVES, T. A., GREEN, E. D., GREGORY, S., GUIGÓ, R., GUYER, M., HARDISON, R. C., HAUSSLER, D., HAYASHIZAKI, Y., HILLIER, L. W., HINRICHS, A., HLAVINA, W., HOLZER, T., HSU, F., HUA, A., HUBBARD, T., HUNT, A., JACKSON, I., JAFFE, D. B., JOHNSON, L. S., JONES, M., JONES, T. A., JOY, A., KAMAL, M., KARLSSON, E. K., et al. 2002. Initial sequencing and comparative analysis of the mouse genome. *Nature,* 420**,** 520-62.
WEIR, G. C. & BONNER-WEIR, S. 2004. Five stages of evolving beta-cell dysfunction during progression to diabetes. *Diabetes,* 53 Suppl 3**,** S16-21.
WEISBERG, S. P., MCCANN, D., DESAI, M., ROSENBAUM, M., LEIBEL, R. L. & FERRANTE, A. W., JR. 2003. Obesity is associated with macrophage accumulation in adipose tissue. *J Clin Invest,* 112**,** 1796-808.

WEISS, R., CAPRIO, S., TROMBETTA, M., TAKSALI, S. E., TAMBORLANE, W. V. & BONADONNA, R. 2005. Beta-cell function across the spectrum of glucose tolerance in obese youth. *Diabetes,* 54**,** 1735-43.
WEKSLER-ZANGEN, S., RAZ, I., LENZEN, S., JÖRNS, A., EHRENFELD, S., AMIR, G., OPRESCU, A., YAGIL, Y., YAGIL, C., ZANGEN, D. H. & KAISER, N. 2008. Impaired Glucose-Stimulated Insulin Secretion Is Coupled With Exocrine Pancreatic Lesions in the Cohen Diabetic Rat. *Diabetes,* 57**,** 279-287.
WENTWORTH, B. M., SCHAEFER, I. M., VILLA-KOMAROFF, L. & CHIRGWIN, J. M. 1986. Characterization of the two nonallelic genes encoding mouse preproinsulin. *J Mol Evol,* 23**,** 305-12.
WESTERLUND, J. & BERGSTEN, P. 2001. Glucose Metabolism and Pulsatile Insulin Release From Isolated Islets. *Diabetes,* 50**,** 1785-1790.
WESTERMARK, P., WERNSTEDT, C., WILANDER, E. & SLETTEN, K. 1986. A novel peptide in the calcitonin gene related peptide family as an amyloid fibril protein in the endocrine pancreas. *Biochem Biophys Res Commun,* 140**,** 827-31.
WEYER, C., BOGARDUS, C., MOTT, D. M. & PRATLEY, R. E. 1999. The natural history of insulin secretory dysfunction and insulin resistance in the pathogenesis of type 2 diabetes mellitus. *J Clin Invest,* 104**,** 787-94.
WILLEMSEN, G., WARD, K. J., BELL, C. G., CHRISTENSEN, K., BOWDEN, J., DALGÅRD, C., HARRIS, J. R., KAPRIO, J., LYLE, R., MAGNUSSON, P. K., MATHER, K. A., ORDOŇANA, J. R., PEREZ-RIQUELME, F., PEDERSEN, N. L., PIETILÄINEN, K. H., SACHDEV, P. S., BOOMSMA, D. I. & SPECTOR, T. 2015. The Concordance and Heritability of Type 2 Diabetes in 34,166 Twin Pairs From International Twin Registers: The Discordant Twin (DISCOTWIN) Consortium. *Twin Res Hum Genet,* 18**,** 762-71.
WILLIAMS, R., KARURANGA, S., MALANDA, B., SAEEDI, P., BASIT, A., BESANÇON, S., BOMMER, C., ESTEGHAMATI, A., OGURTSOVA, K., ZHANG, P. & COLAGIURI, S. 2020. Global and regional estimates and projections of diabetes-related health expenditure: Results from the International Diabetes Federation Diabetes Atlas, 9th edition. *Diabetes Res Clin Pract,* 162**,** 108072.
WORLD HEALTH ORGANIZATION 2017. Obesity and overweight fact sheet [Internet]. Available from http://www.who.int/dietphysicalactivity/media/en/gsfs_obesity.pdf. Accessed April 2017.
WORLD HEALTH ORGANIZATION 2019. Classification of Diabetes Mellitus. World Heath Organization, Geneva.
WU, C., CHEN, X., SHU, J. & LEE, C. T. 2017. Whole-genome expression analyses of type 2 diabetes in human skin reveal altered immune function and burden of infection. *Oncotarget,* 8**,** 34601-34609.
WU, D. & SMYTH, G. K. 2012. Camera: a competitive gene set test accounting for inter-gene correlation. *Nucleic Acids Research,* 40**,** e133-e133.
WU, L., LV, Y., LV, Y., XIANG, S., ZHAO, Z., TANG, Z., OU, L., YAN, B., XIAO, X., WEN, G., CAO, R. & YANG, J. 2020. A novel secretagogin/ATF4 pathway is involved in oxidized LDL-induced endoplasmic reticulum stress and islet β-cell apoptosis. *Acta Biochimica et Biophysica Sinica*.
WU, Y., CHEN, W., GONG, L., KE, C., WANG, H. & CAI, Y. 2018. Elevated G-Protein Receptor 125 (GPR125) Expression Predicts Good Outcomes in Colorectal Cancer and Inhibits Wnt/β-Catenin Signaling Pathway. *Med Sci Monit,* 24**,** 6608-6616.
XIAO, K., SUN, Z., JIN, X., MA, W., SONG, Y., LAI, S., CHEN, Q., FAN, M., ZHANG, J., YUE, W. & HUANG, Z. 2018. ERG3 potassium channel-mediated suppression of neuronal intrinsic excitability and prevention of seizure generation in mice. *J Physiol,* 596**,** 4729-4752.
XU, Z., TONG, Q., ZHANG, Z., WANG, S., ZHENG, Y., LIU, Q., QIAN, L. B., CHEN, S. Y., SUN, J. & CAI, L. 2017. Inhibition of HDAC3 prevents diabetic cardiomyopathy in OVE26 mice via epigenetic regulation of DUSP5-ERK1/2 pathway. *Clin Sci (Lond),* 131**,** 1841-1857.
XUE, A., WU, Y., ZHU, Z., ZHANG, F., KEMPER, K. E., ZHENG, Z., YENGO, L., LLOYD-JONES, L. R., SIDORENKO, J., WU, Y., MCRAE, A. F., VISSCHER, P. M., ZENG, J. &

YANG, J. 2018. Genome-wide association analyses identify 143 risk variants and putative regulatory mechanisms for type 2 diabetes. *Nat Commun,* 9**,** 2941.
YAGIHASHI, S. 2017. Diabetes and pancreas size, does it matter? *Journal of diabetes investigation,* 8**,** 413-415.
YAMAMOTO, H., WILLIAMS, E. G., MOUCHIROUD, L., CANTÓ, C., FAN, W., DOWNES, M., HÉLIGON, C., BARISH, G. D., DESVERGNE, B., EVANS, R. M., SCHOONJANS, K. & AUWERX, J. 2011. NCoR1 is a conserved physiological modulator of muscle mass and oxidative function. *Cell,* 147**,** 827-39.
YAMAZAKI, H., TSUBOYA, T., KATANUMA, A., KODAMA, Y., TAUCHI, S., DOHKE, M. & MAGUCHI, H. 2016. Lack of Independent Association Between Fatty Pancreas and Incidence of Type 2 Diabetes: 5-Year Japanese Cohort Study. *Diabetes Care,* 39**,** 1677-83.
YANG, J. K., LU, J., YUAN, S. S., ASAN, CAO, X., QIU, H. Y., SHI, T. T., YANG, F. Y., LI, Q., LIU, C. P., WU, Q., WANG, Y. H., HUANG, H. X., KAYOUMU, A., FENG, J. P., XIE, R. R., ZHU, X. R., LIU, C., YANG, G. R., ZHANG, M. R., XIE, C. L., CHEN, C., ZHANG, B., LIU, G., ZHANG, X. Q. & XU, A. 2018. From Hyper- to Hypoinsulinemia and Diabetes: Effect of KCNH6 on Insulin Secretion. *Cell Rep,* 25**,** 3800-3810.e6.
YANG, S.-Y., LEE, J.-J., LEE, J.-H., LEE, K., OH, S. H., LIM, Y.-M., LEE, M.-S. & LEE, K.-J. 2016. Secretagogin affects insulin secretion in pancreatic β-cells by regulating actin dynamics and focal adhesion. *The Biochemical journal,* 473**,** 1791-1803.
YANO, B. L., HAYDEN, D. W. & JOHNSON, K. H. 1981. Feline insular amyloid: association with diabetes mellitus. *Vet Pathol,* 18**,** 621-7.
YATES, T., HENSON, J., EDWARDSON, C., DUNSTAN, D., BODICOAT, D. H., KHUNTI, K. & DAVIES, M. J. 2015. Objectively measured sedentary time and associations with insulin sensitivity: Importance of reallocating sedentary time to physical activity. *Prev Med,* 76**,** 79-83.
YONEDA, S., UNO, S., IWAHASHI, H., FUJITA, Y., YOSHIKAWA, A., KOZAWA, J., OKITA, K., TAKIUCHI, D., EGUCHI, H., NAGANO, H., IMAGAWA, A. & SHIMOMURA, I. 2013. Predominance of beta-cell neogenesis rather than replication in humans with an impaired glucose tolerance and newly diagnosed diabetes. *J Clin Endocrinol Metab,* 98**,** 2053-61.
YOON, K. H., KO, S. H., CHO, J. H., LEE, J. M., AHN, Y. B., SONG, K. H., YOO, S. J., KANG, M. I., CHA, B. Y., LEE, K. W., SON, H. Y., KANG, S. K., KIM, H. S., LEE, I. K. & BONNER-WEIR, S. 2003. Selective beta-cell loss and alpha-cell expansion in patients with type 2 diabetes mellitus in Korea. *J Clin Endocrinol Metab,* 88**,** 2300-8.
YOU, S. H., LIM, H. W., SUN, Z., BROACHE, M., WON, K. J. & LAZAR, M. A. 2013. Nuclear receptor co-repressors are required for the histone-deacetylase activity of HDAC3 in vivo. *Nat Struct Mol Biol,* 20**,** 182-7.
YU, C., CHEN, Y., CLINE, G. W., ZHANG, D., ZONG, H., WANG, Y., BERGERON, R., KIM, J. K., CUSHMAN, S. W., COONEY, G. J., ATCHESON, B., WHITE, M. F., KRAEGEN, E. W. & SHULMAN, G. I. 2002. Mechanism by which fatty acids inhibit insulin activation of insulin receptor substrate-1 (IRS-1)-associated phosphatidylinositol 3-kinase activity in muscle. *J Biol Chem,* 277**,** 50230-6.
ZHANG, F. & TZANAKAKIS, E. S. 2017. Optogenetic regulation of insulin secretion in pancreatic β-cells. *Scientific Reports,* 7**,** 9357.
ZHANG, M., WANG, S., GUO, B., MENG, G., SHU, C., MAI, W., ZHENG, Q., CHEN, X., WU, Y. & WANG, L. 2019. An altered CD8(+) T cell epitope of insulin prevents type 1 diabetes in humanized NOD mice. *Cell Mol Immunol,* 16**,** 590-601.
ZHENG, X., ZHENG, X., WANG, X., MA, Z., GUPTA SUNKARI, V., BOTUSAN, I., TAKEDA, T., BJÖRKLUND, A., INOUE, M., CATRINA, S. B., BRISMAR, K., POELLINGER, L. & PEREIRA, T. S. 2012. Acute hypoxia induces apoptosis of pancreatic β-cell by activation of the unfolded protein response and upregulation of CHOP. *Cell death & disease,* 3**,** e322-e322.
ZIOLKOWSKI, A. F., POPP, S. K., FREEMAN, C., PARISH, C. R. & SIMEONOVIC, C. J. 2012. Heparan sulfate and heparanase play key roles in mouse β cell survival and autoimmune diabetes. *J Clin Invest,* 122**,** 132-41.

Appendix

Solutions:

Preparation of solutions mentioned in Chapter 2 (Materials and Methods) are shown below.

Sodium Phosphate Buffer

- 0.025 M Ethylenediaminotetra acetic acid (EDTA)
- 0.05 M Sodium phosphate monobasic
- 0.01% Thimerosal

The pH was adjusted to 7.5 with NaOH (10N), solution was topped up with Milli-Q water and sterile-filtered using 0.22 µm filter (Millipore Corporation, MA, USA) and stored at 4^{o}C.

BSA-Sodium Phosphate Buffer- 1 L solution

- 10 g of BSA- RIA grade
- 1000 mL of Sodium phosphate buffer

The solution was wrapped in aluminum foil and stored at 4^{o}C.

PEG- Sodium Phosphate Buffer- 1 L solution

- 30 g of PEG 8000
- 1000 mL of phosphate buffer

The solution was wrapped in aluminum foil and stored at 4^{o}C.

KOH (Potassium Hydroxide)

- 0.5 M KOH

The solution was topped up with 95% ethanol.

$MgSO_4$ (Magnesium Sulphate)

- 0.15 M $MgSO_4.7H_20$

The solution was topped up with Milli-Q water.

3,3'- Diaminobenzidine (DAB) solution

- 1 set of 2 DAB tablets
- 10 mL deionized Milli Q water

HEPES (1M)- 1 L solution

- 238.4 g of 4-*(2-hydroxyethyl)-1*-piperazineethanesulfonic acid (HEPES)
- 0.1 g of Thimerosal (0.01%)
- 1000 mL of Milli-Q water

The pH of the solution was adjusted to 7.4, filtered using 0.22 µm filter and stored at 4°C.

Enzymatic pancreas inflation solution

- 10x Hanks Balanced Salt Solution (HBSS)
- 20 mM HEPES, pH 7.4
- 0.1 mg/mL liberase
- 0.0067 mg/mL of DNase I

HBSS-1% BSA *Wash buffer solution- 1 L solution*

- 100 mL HBSS 10x
- 20 mL HEPES 1M, pH 7.4
- 0.2 g BSA-fraction V

The solution was topped up with Milli-Q water and stored at 4°C.

Roswell Park Memorial Institute (RPMI) Complete medium

- 10% FBS
- 1% HEPES 100x
- 1% Sodium pyruvate
- 1% Glutamine 100x
- 1% Antibiotics (penicillin/streptomycin)

The solution was topped up with RPMI-1640 medium and stored at 4^{o}C.

Glutamine 100X (MW= 146.14)

- 205 mM L-glutamine.
- Warm RPMI 1640

The solution was filtered using 0.22 µm filter and stored at -20^{o}C.

HEPES 100X (1M) (MW=238.3)

- 1M HEPES
- RPMI 1640 medium

The pH of the solution was adjusted to 7.3, filtered using 0.22 µm filter and stored at 4^{o}C.

Na-Pyruvate 100X (MW=110.04)

- 0.01 M Sodium pyruvate
- RPMI 1640 medium

The solution was filtered using 0.22 µm filter and stored at -20^{o}C.

5x Krebs Ringer Bicarbonate Buffer (KRB)

- 675 mM Sodium Chloride (NaCl)
- 18 mM Potassium Chloride (KCl)
- 2.5 mM Sodium phosphate (NaH_2PO_4)
- 2.5 mM Magnesium Chloride ($MgCl_2$)
- 7.5 mM Calcium Chloride ($CaCl_2$)

KRB + HEPES (KRBH) solution- 1 L solution

- 200 mL of 5x Krebs Ringer Buffer **(**KRB)
- 20 mL of $NaHCO_3$ 50x
- 10 mL of HEPES 1M pH 7.4

The pH of the solution was adjusted to 7.4, topped up with Milli-Q water and incubated at 37ºC with 5% CO_2 for 1 hour.

KRBH wash buffer- 1 L solution

- 1L of KRBH solution
- 3 mM of 1M glucose
- 0.07% of BSA- Heat shock fraction (A7888)

KRBH-5% BSA fatty acid free *solution-1 L solution*

- 1 L of KRBH solution
- 5% BSA fatty acid free

The solution was filtered using 0.22 µm filter and stored overnight at 4ºC.

4 mM Palmitate solution

- 200 mg of Sodium palmitate
- 30 mL of KRBH solution supplemented by 5% BSA Fatty acid free

Nitrogen gas was added to the solution and sealed for overnight (16 hours) incubation at 37ºC on a rocker/shaker. On the following day, the solution was sterile-filtered through a 0.22 µm filter and stored at -20ºC for future use.

4 mM Oleate solution

- 40 mg of Sodium oleate
- 20 mL of KRBH solution supplemented by 5% BSA Fatty acid free

After addition of Nitrogen gas, the solution was sealed and incubated overnight on a rocker/shaker at 37^{o}C. On the next day, the solution was sterile-filtered and stored at -20^{o}C.

Islet Protein lysis buffer

- 50 mM Tris pH 8.0 (1M)
- 100 mM EDTA
- 0.5% Sodium dodecyl sulfate (SDS)

The solution was topped up with Milli-Q water.

Appendix Table 1: Scoring criteria for H&E-stained pancreas sections

Scoring parameter	Scores
Pancreas fat	0= none 1: infrequent 2= mild (some) 3= moderate 4=severe
Acute inflammation	0= none 1: minimal 2= mild 3= moderate 4=severe
Chronic inflammation	0= none 1: minimal 2= mild 3= moderate 4=severe
Main location of inflammation	1= lobule 2= peri-ductal 3= peri-islet 4= lobule + peri-duct 5= peri-duct + peri-islet 6= all
Ducts affected by inflammation	1= <10% 2= 10-50% 3= >50%
Islet cell apoptosis	0= absent 1= present

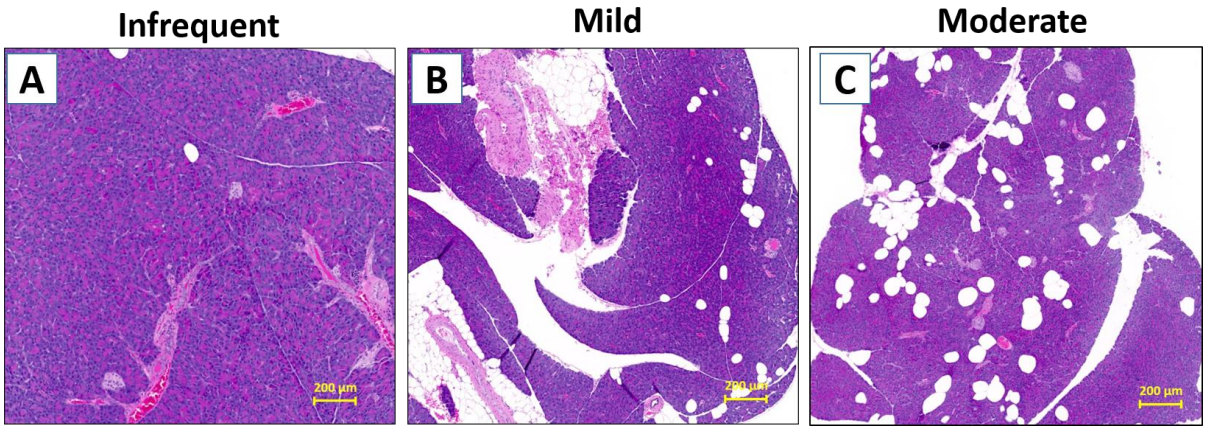

Figure 55: Representative images of scoring for fat infiltration in the pancreas of O-NOD^{k} and RF-NOD^{k} mice, fed on NC and HF diet. Pancreas section were cut and stained with H&E. Qualitative analysis was performed to determine the severity of pancreatic fat infiltration, with sections scored as minimal to infrequent with very few adipocytes (A), mild (B) and moderate (C). There were no samples with severe fat infiltration.